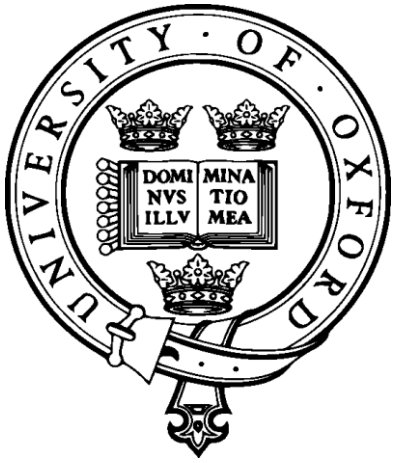
Developing Ways of Implementing Biocatalytic Hydrogenation Reactions in Flow

Barnabas Poznansky

St Hugh's College
University of Oxford



A thesis submitted for the degree of

Doctor of Philosophy

Trinity 2021

Acknowledgments

First, I would like to thank my academic supervisors Prof. Kylie Vincent and Dr Holly Reeve for their incredible supervision over the last four years. They are both greatly inspirational and have provided me with exceptional guidance throughout. Among other things, Kylie has frequently come up with thought provoking and exciting ideas and solutions with regard to my work. Holly has motivated me to constantly aim for more through her passion and deep knowledge of the subject. I am extremely grateful to my industrial supervisors Dr Sarah Warren and Dr Matthew Bycroft. Sarah provided brilliant guidance in the early part of my PhD and I am hugely grateful for her training and supervision during my industrial placement in 2019. Matt has been a brilliant supervisor during the last few years of my PhD, constantly providing industrial insight and ideas, as well as support. I also thank the wider team at Dr Reddy's Laboratories Ltd (Cambridge) for their input and support throughout, especially during my industrial placement, and I am incredibly grateful to the company as a whole for their partnership.

I would like to thank Dr Lisa Thompson, my Post-Doc supervisor in the early part of my PhD for her fantastic training, guidance and support, I was very lucky to learn from the best. I am grateful to Dr Jack Rowbotham for his project support, ideas and friendship throughout my PhD, he made every day fun and I wish him and his tuck shop all the best in the future. I am very appreciative of the very hard work by the Part II student, Hannah Taylor, who managed to achieve a great amount during a very difficult pandemic hit year. I will forever be indebted to Dr Miguel Ramirez Hernandez for his incredible support throughout and for preparing many of the enzymes that I used in this work. I would like to thank everyone else in the Vincent group, past and present, including Koji, Tim, Sarah,

Michael, Justin, Xu, Jiaao and Simone. You were all a fantastic bunch of people to work with.

There are many great people I have become friends with during my 4 years in Oxford, who have made the whole process so much more fulfilling and enjoyable. Rex and Chris have been there since day 1 and I enjoyed every second we spent together. To the rest of the Glanville road support team: Solo, George, Atti, Ellie, Mike and Caz, thank you for inviting me so openly into your family, your support has been amazing. I have been lucky enough to play football with some brilliant people in the MCR and the Uni Broncos during my PhD, ultimately building some great friendships along the way: Joey, Ace, Zac, Louis, Tomás, Jorich, Roma (Yarma), to name but a few. Likewise, in the St Hugh's College MCR, it has been a pleasure meeting so many brilliant people on incredible paths in life.

Special thank you to Joshua and Mark for your help proof-reading this Thesis.

Finally, and most importantly, I would like to thank all of my amazing family, whom without, none of this would have been possible. Mum, Mark, Dad, Joshua, Sebastian, Harriet, Frederica, Gabriella, Theodore, Grandma Sylvia, Grandpa Jack and all the rest, your support throughout has been beyond measure.

This thesis is dedicated to my late grandma, Professor Dulcie Coleman, who inspired me to become a scientist.

Abstract

The use of enzymes as catalysts is becoming more common, in part due to their high selectivity under mild reaction conditions. However, many redox enzymes require cofactors (NADH or NADPH) as an electron source to operate. Due to the high cost of NAD(P)H, cofactor regeneration systems have been developed, which often involve addition of a second enzyme and/or a sacrificial reductant. Furthermore, the enzymes can be difficult to recover from solution, which can inhibit the uptake of biocatalytic processes. Immobilising enzymes on a support allows for easier recovery and re-use of the biocatalyst, lowering the cost of the process, however, no enzyme immobilisation system has found ubiquity. Flow chemistry is a technique that has seen an increase in research and industrial implementation in recent years, for its greener and more efficient chemical production. Supported biocatalysts are suited to use in flow reactors, where the catalyst is retained within the reactor and substrates are continuously pumped through. The work in this Thesis seeks to address the challenges associated with using immobilised redox enzymes for chemical synthesis in continuous flow. First, the translation of industry standard cofactor recycling systems (FDH–formate and ADH–IPA) onto a simple carbon particle support and into flow was studied. The continuous synthesis of industrially relevant enantiomerically pure molecules was demonstrated for both systems. Next, work focused on translating a H_2-driven cofactor recycling system into continuous flow. The H_2-driven 'HydRegen' system uses a robust hydrogenase and NAD^+ reductase immobilised onto an electron conducting carbon support to regenerate NADH. Application of the H_2-driven cofactor regeneration system in a commercially available hydrogenation flow reactor demonstrated high turnover frequencies of 85,200 h^{-1} and the production of an industrially relevant molecule.

Collaborations and assistance

Some of the enzymes used in this Thesis were kindly prepared and provided by other Vincent group members or collaborators. I am grateful to Dr Miguel Hernandez Ramirez (Vincent group) for preparation of the SH, I64A, Hyd1 and AtQR samples and for performing the SDS-PAGE experiment discussed in Section 6.1. I would also like to thank Johnson Matthey PLC for providing the ADH-19, ADH-20, ADH-61, ADH-101, ADH-105 and FDH samples. Finally, I am very grateful to Dr Reddy's Laboratories Ltd. for providing me with the ADH-1001, KRED-NADH-101 and KRED.

I am extremely grateful to ThalesNano Inc., Chemistry Department Teaching Laboratory and Dr Reddy's Laboratories for loaning me the use of an H-Cube reactor at various points throughout this study, without this generosity a large amount of the research would not have been possible.

The experiments in Chapter 5 and Chapter 6 (up to Figure 6-10) were conducted in collaboration with a Part II (4^{th} year MChem project) student who was under my supervision. For each experiment, I developed the methodology and either performed the experiment with the student shadowing me, jointly with the student or by aiding the student through the work remotely. The experiments were performed during the 2020/2021 academic year, where Covid-19 laboratory restrictions led to limited lab time, making a joint DPhil/Part II more feasible than training a Part II for a completely separate project.

Publications

1. Poznansky, B., Thompson, L.A., Warren, S.A., Reeve, H.A., Vincent, K.A., ‘Carbon as a Simple Support for Redox Biocatalysis in Continuous Flow’, *Organic Process Research and Development*, 2020, **24** (10), 2281-2287.

2. Poznansky, B., Cleary, S.E.,Thompson, L.A., Reeve, H.A., Vincent, K.A., ‘Boosting the Productivity of H_2-Driven Biocatalysis in a Commercial Hydrogenation Flow Reactor Using H_2 From Water Electrolysis’, *Frontiers in Chemical Engineering*, 2021, **3**, 35, DOI: 10.3389/fceng.2021.718257.

Covid-19 impact statement

On Thursday 19th March 2020, the Inorganic Chemistry Laboratory (Department of Chemistry, University of Oxford) where I conduct my laboratory research, was shut down because of the Covid-19 pandemic. I was able to return to laboratory-based work on Monday 13th July 2020 under strict departmental restrictions, such as laboratory occupancy levels and opening times. The laboratory occupancy restrictions meant that between July 2020 to June 2021, I was able to attend the laboratory for 2.5 days per week on average, this was because of the high number of Vincent group members (25+ researchers) in comparison to our allowed Covid-19 laboratory occupancy level (~8-10 researchers). During this period from March 2020 to June 2021, I estimate that I was not able to attend the laboratory for a cumulative total of 8 months (overall DPhil research project = 44 months). To mitigate the impact of the Covid-19 pandemic on my research, I used the time working-from-home to analyse data and write-up my Thesis, as well as completing my Confirmation of Status one term early. This mitigation allowed me to work for a longer period of time in the laboratory when restrictions began to ease in June 2021. However, it is reasonable to suggest that due to the timing of the pandemic (3rd/4th year of DPhil project) that the full scope of my research project was not able to be explored, instead focusing on achieving complete laboratory projects.

Abbreviations

ADH	alcohol dehydrogenase
AH	asymmetric hydrogenation
API	active pharmaceutical ingredient
ATH	asymmetric transfer hydrogenation
BINAP	(2,2'-bis(diphenylphosphino)-1,1'-binaphthyl)
BP	black pearls
c	concentration
C=X	double bonded carbon and heteroatom (O, N, C etc.)
CD	cinchonidine
CLEA	cross-linked enzyme aggregates
DMSO	dimethylsulfoxide
E factor	environmental factor
E. coli	*Escherichia coli*
e.e.	enantiomeric excess
FDA	food and drug administration
FDH	formate dehydrogenase
GC	gas chromatography
GDH	glucose dehydrogenase
HOMO	highest occupied molecular orbital
HPLC	high-performance liquid chromatography
Hyd1	*Escherichia coli* Hydrogenase 1
i.d.	inner diameter
I64A	NAD^+ reductase
IPA	isopropyl alcohol
KPB	potassium phosphate buffer
LCA	life cycle assessment
LC-MS	liquid chromatography coupled with mass spectrometry
LUMO	lowest unoccupied molecular orbital
MW	molecular weight
NAD^+	nicotinamide adenine dinucleotide (oxidised)
NADH	nicotinamide adenine dinucleotide hydride (reduced)
$NADP^+$	nicotinamide adenine dinucleotide phosphate (oxidised)
NADPH	nicotinamide adenine dinucleotide phosphate hydride (reduced)
NMR/^{1}H-NMR	^{1}H nuclear magnetic resonance spectroscopy
PBR	packed-bed reactor
ppm	parts per million
PTFE	polytetrafluoroethylene
PVA	polyvinylalcohol
R. eutropha	*Ralstonia eutropha* H16
R^2	coefficient of determination

rpm	revolutions per minute
SDS-PAGE	sodium dodecyl sulphate - polyacrylamide gel electrophoresis
SH	soluble hydrogenase
STY	space-time yield
THF	tetrahydrofuran
TiTR	tube-in-tube reactor
TN	turnover number (moles product generated per mole cofactor used)
TOF	turnover frequency (number of product generated per minute per enzyme)
t_{Res}	residence time
Tris-HCl	tris(hydroxymethyl)aminomethane buffered with concentrated HCl
TsDPEN	*N*-tosylated 1,2-diphenyl-1,2-ethylenediamine
TTN	total turnover number (moles product generated per mole enzyme)
U	units = µmole min^{-1}
UV-Vis	ultraviolet-visible
v/v%	volume/volume percentage
ε	extinction coefficient

Table of contents

Acknowledgments i

Abstract iv

Collaborations and assistance vi

Publications vii

Covid-19 impact statement viii

Abbreviations ix

Table of contents xi

1 Introduction 1

1.1 Traditional methods for ketone reduction 7

1.1.1 Traditional hydrogenation 7

1.1.2 Ketone reduction 7

1.1.3 Stoichiometric reduction 8

1.1.4 Metal-catalysed asymmetric hydrogenation of ketones 10

1.2 Towards green hydrogenation chemistry 16

1.3 Biocatalysis 20

1.3.1 Enzyme immobilisation 22

1.4 Cofactor recycling 24

1.4.1 Alcohol Dehydrogenase 27

1.4.2 Glucose Dehydrogenase 28

1.4.3 Formate Dehydrogenase 28

1.4.4 Phosphite Dehydrogenase 29

1.5 H_2-driven cofactor recycling 29

1.6 Flow chemistry 32

1.7 Biocatalysis in continuous flow 33

1.8 Continuous flow reaction design with immobilised biocatalysts 35

1.9 Redox biocatalysis in flow with immobilised enzymes 38

1.9.1 Immobilised GDH–glucose cofactor recycling system in continuous flow 39

1.9.2 Immobilised FDH–formate cofactor recycling system in continuous flow 41

1.9.3 Immobilised ADH–IPA substrate-coupled cofactor recycling system in continuous flow 42
1.10 H_2-driven cofactor recycling in flow 45
1.11 Aims and structure of this thesis 47
2 General Methods and Theory 50
2.1 Flow Chemistry 50
2.1.1 Immobilised biocatalysts in packed-bed-reactors 50
2.1.2 Residence time and PBRs 51
2.1.3 Additional flow equipment 52
2.2 Ultraviolet-visible spectroscopy 53
2.2.1 Determination of concentration using UV-Vis 55
2.2.2 Protein concentration calibration curves 56
2.3 Gas chromatography 57
2.4 Nuclear magnetic resonance spectroscopy 59
2.5 In-line benchtop flow NMR 59
2.6 High performance liquid chromatography 60
2.7 Enzyme samples 60
2.7.1 NAD^+-reducing enzymes 60
2.7.2 Hydrogenase enzymes 61
2.7.3 Cofactor-dependent enzymes 61
2.7.4 Immobilising enzymes onto carbon particles 61
2.8 Chemicals and buffers 62
2.8.1 Buffers 62
2.8.2 Cofactors 63
2.8.3 Other reagents 63
2.9 General Procedures 63
2.9.1 Biocataltyic ADH-IPA driven NADH generation in batch, for Chapters 5 and 6 64
2.9.2 Biocataltyic ADH-driven ketone reduction in batch for Chapters 5 and 6 64
2.9.3 Biocatalytic ketone reduction with ADH-IPA driven cofactor recycling in batch for Chapters 5 and 6 65
2.9.4 Continuous flow ketone reduction reaction conditions for Chapters 5 and 6 66

2.9.5 General procedure for the specific activity of SH free in solution in batch for Chapters 7 and 8 66
2.9.6 General procedure for the specific activity of SH immobilised onto carbon in batch for Chapters 7 and 8 67
2.9.7 General preparation of CatCart biocatalyst cartridges for H-Cube reactor experiments in Chapters 7 and 8 67
2.9.8 General procedure for H_2-powered biocatalytic cofactor reduction in the H-Cube flow reactor for Chapters 7 and 8 68
2.9.9 General procedure for H_2-powered biocatalytic ketone reduction in the H-Cube flow reactor for Chapters 7 and 8 68
3 Immobilising FDH and LDH onto carbon for biocatalysis with cofactor recycling in continuous flow 71
3.1.1 NADH-dependent biocatalytic pyruvate reduction 72
3.1.2 Product analysis 72
3.2 Biocatalytic conversion of pyruvate to lactate in batch 73
3.2.1 General immobilisation procedure for FDH and LDH onto carbon particles 73
3.2.2 Conversion of pyruvate to lactate with FDH and LDH in solution or immobilised, under batch conditions 74
3.2.3 Determining the carbon type for enzyme immobilisation 74
3.2.4 Immobilisation studies for FDH and LDH on BP2000 carbon particles 76
3.2.5 Specific activity of LDH in solution and immobilised onto BP2000 in batch 78
3.2.6 The specific activity of FDH in solution and immobilised onto BP2000 in batch 81
3.3 Biocatalytic conversion of pyruvate to lactate in continuous flow 83
3.3.1 Continuous flow equipment set-up 83
3.3.2 FDH and LDH leaching studies in continuous flow 84
3.3.3 Conversion of pyruvate to lactate with FDH and LDH immobilised onto BP2000 in a continuous PBR 88
3.3.4 Initial continuous flow reactions 88
3.3.5 Seven-day continuous run 90
3.4 Optimisation of the immobilised FDH/LDH system in continuous flow 92
3.4.1 Variation in t_{Res} 93
3.4.2 Variation of NAD^+ mol% 95
3.4.3 Varying the number of equivalents of formate 96
3.4.4 Varying the concentration of Tris-HCl 97
3.5 Additional process optimisation metrics 99

3.5.1 Analysis of system STY 99
3.5.2 Analysis of system E-factor 101
3.5.3 Overall system analysis for multi-target optimisation 102
3.6 JMP modelling 104
3.7 Operational viability 107
3.7.1 The activity of FDH and LDH in continuous flow 107
3.7.2 Catalyst reusability in flow 108
3.7.3 Longer-term operation 109
3.8 Summary 111
4 Immobilising FDH and ketoreductase enzymes onto carbon for industrially relevant biocatalysis in continuous flow 114
4.1 Introduction 114
4.2 Biocatalytic synthesis of API precursor molecules with FDH recycling 114
4.2.1 Ticagrelor 114
4.2.2 Synthesis of the starting material 2-chloro-1-(3,4-difluorophenyl)ethan-1-one 115
4.2.3 Enzyme screening for ketone reduction of 2-chloro-1-(3,4-difluorophenyl)ethan-1-one, in solution 116
4.2.4 Biocatalytic ketone reduction of 2-chloro-1-(3,4-difluorophenyl)ethan-1-one, with enzymes immobilised onto BP2000 118
4.2.5 Aprepitant 120
4.2.6 Enzyme screening for ketone reduction of 1-(3,5-bis(trifluoromethyl)phenyl)ethan-1-one, in solution 120
4.2.7 Biocatalytic ketone reduction 1-(3,5-bis(trifluoromethyl)phenyl)ethan-1-one, with enzymes immobilised onto BP2000 122
4.2.8 Biocatalytic conversion of 1-(3,5-bis(trifluoromethyl) phenyl)ethan-1-one to (*R*)-1-(3,5-bis(trifluoromethyl) phenyl)ethan-1-ol in continuous flow 126
4.3 Biocatalytic conversion of 3-quinuclidinone to (*R*)-3-quinuclidinol in with FDH–formate cofactor recycling in continuous flow 132
4.4 Summary 136
5 Immobilising ADH onto carbon for ketone reduction and IPA-driven cofactor recycling in batch and continuous flow 138
5.1 Introduction 138
5.2 Immobilisation studies for ADH-101 and ADH-105 onto activated charcoal 140
5.3 ADH-101 and ADH-105 for the ‘forward’ ketone reduction reaction in batch 142

5.4 ADH-101 and ADH-105 for the ‘backward’ IPA-driven NAD(P)$^+$ reduction reaction in batch 148

5.5 Full cycle: ketone reduction and substrate coupled IPA-driven cofactor recycling with ADH-101 and ADH-105 in batch 155

5.5.1 Full cycle: reduction of 1-(5-pyrimidinyl)ethenone with IPA-driven cofactor recycling by ADH-101 in batch 156

5.5.2 Full cycle: reduction of acetophenone with IPA-driven cofactor recycling by ADH-105 in batch 159

5.6 Translation from batch into continuous flow 161

5.6.1 Full cycle: reduction of 1-(5-pyrimidinyl)ethenone with IPA-driven cofactor recycling by ADH-101 in continuous flow 162

5.6.2 Full cycle: reduction of acetophenone with IPA-driven cofactor recycling by ADH-105 in continuous flow 163

5.7 Troubleshooting poor continuous flow performance of ADH-101 and ADH-105 immobilised on activated charcoal 166

5.7.1 Forward ketone reduction catalysed by ADH-101 or ADH-105 in continuous flow 166

5.7.2 ADH-101 and ADH-105 for the backward IPA-driven NAD(P)$^+$ reduction reaction in continuous flow 171

5.7.3 ADH-101 and ADH-105 leaching studies in continuous flow 174

5.7.4 Exploring the presence of NAD(P)H oxidase in the crude ADH-101 and ADH-105 enzymes 176

5.8 Summary 179

6 Immobilising ADH-1001 onto carbon for synthesis of an API precursor with IPA-driven cofactor recycling in batch and continuous flow 182

6.1 Introduction 182

6.1.1 Immobilisation of ADH-1001 onto activated charcoal 183

6.2 ADH-1001 for the ‘forward’ ketone reduction of ethyl 4-chloroacetoacetate in batch 184

6.3 ADH-1001 for the ‘backward’ IPA-driven NAD$^+$ reduction reaction in batch 187

6.4 Full cycle: ketone reduction of ethyl 4-chloroacetoacetate and substrate coupled IPA-driven cofactor recycling with ADH-1001 in batch 190

6.5 Translation of ADH-1001 full cycle system from batch into continuous flow 193

6.5.1 ADH-1001 leaching study in continuous flow 193

6.5.2 Full cycle: reduction of ethyl 4-chloroacetoacetate with IPA-driven cofactor recycling by ADH-1001 in continuous flow 195

6.5.3 Increasing the substrate concentration to 50 mM 197
6.5.4 Increasing the substrate concentration to 100 mM 199
6.5.5 Increasing the substrate to NAD^+ molar ratio to 1000:1 by decreasing NAD^+ to 0.1 mM 200
6.6 Studying the continuous flow reaction with in-line benchtop flow NMR 202
6.6.1 Comparing with GC analysis 204
6.6.2 Variation of reaction buffer solution 207
6.6.3 Stabilising the ADH-1001 with zinc sulphate 210
6.6.4 Increasing the catalyst loading in the PBR 213
6.7 Summary 217
7 H_2-driven NAD^+ reduction in the H-Cube flow reactor 221
7.1 Introduction 221
7.2 Immobilisation studies for SH, I64A and Hyd1 onto activated charcoal 222
7.2.1 Immobilisation efficiency of for SH, I64A and Hyd1 onto activated charcoal 223
7.2.2 Batch specific activity of the enzymes in solution and immobilised onto activated charcoal 224
7.3 NAD^+ reduction with SH/C in the H-Cube reactor 227
7.3.1 H-Cube reactor flow set-up 227
7.3.2 Initial SH/C H-Cube reactor results 229
7.3.3 Increasing the cofactor throughput over the SH/C in the H-Cube reactor 231
7.3.4 Varying the H_2 flow rate in the H-Cube to determine the effect on SH activity 233
7.3.5 Temperature stability of SH/C in the H-Cube 235
7.3.6 Activity lifetime of SH/C in the H-Cube 237
7.3.7 Leaching study of SH/C in the H-Cube 242
7.4 NAD^+ reduction with HydRegen enzymes immobilised onto activated charcoal in the H-Cube reactor 245
7.4.1 Activity lifetime of SH+Hyd1/C in the H-Cube 246
7.4.2 Temperature stability of SH+Hyd1/C in the H-Cube 252
7.4.3 Stability of SH+Hyd1/C in alternative buffer systems 257
7.4.4 Establishing SH and Hyd1 activity when co-immobilised onto alternative carbon types in the H-Cube 259
7.4.5 Preliminary test of I64A+Hyd1/C in the H-Cube 261
7.5 Summary 263
8 Biocatalytic ketone reductions with H_2-driven cofactor recycling in the H-Cube reactor 265

8.1 Introduction 265

8.2 Biocatalytic conversion of pyruvate to lactate in the H-Cube reactor 266

8.2.1 Implementation of SH+LDH/C in the H-Cube reactor 266

8.2.2 Specific activity of SH+LDH/C for the conversion of pyruvate to lactate in the H-Cube 269

8.2.3 Activity lifetime of SH+LDH/C for the conversion of pyruvate to lactate in the H-Cube 271

8.2.4 Activity lifetime of SH+Hyd1+LDH/C for the conversion of pyruvate to lactate in the H-Cube 274

8.2.5 Closed loop, multi pass continuous flow with SH+Hyd1+LDH/C for the conversion of pyruvate to lactate in the H-Cube 279

8.2.6 Preliminary test of I64A+Hyd1+LDH/C for the conversion of pyruvate to lactate in the H-Cube 281

8.3 Biocatalytic ketone reduction of ethyl 4-chloroacetoacetate with H_2-driven cofactor recycling by ADH-1001 in the H-Cube 282

8.4 Summary 285

9 Summary and Comparison 288

10 Outlook and Future Work 295

References 298

Appendices 310

A. NMR spectra for pyruvate to lactate 310

B. GC traces 312

C. GC calibration curves 315

D. HPLC traces 316

E. Friedel-Crafts preparation of 2-chloro-1-(3,4-difluorophenyl)ethan-1-one in Section 4.2.2 317

F. Benchtop NMR spectra and calibration curves 318

G. Protein concentration calibration curves 318

1 Introduction

In 2011, leaders of the top pharmaceutical and fine-chemical companies assembled for a round-table discussion to identify the key areas of focus for future sustainable manufacturing.[1] From the ten areas identified, the top two highest ranked were bioprocesses and continuous production. This thesis is focused on the application of redox biocatalysis to continuous flow technology for a more sustainable method of chemical synthesis.

The ability to achieve a high level of chirality in chemical transformations is of great importance to the pharmaceutical and fine chemicals industry.[2,3] Different enantiomers of the same compound can be distinguishable by living organisms. This leads to differing properties displayed by enantiomers, for example different smell and taste.[4] For the pharmaceutical industry, enantiomers can have varying pharmacokinetics, which has an impact on the safety and the efficacy of the drugs.[5,6] This was highlighted in the 1950's by the drug thalidomide, which was sold as racemic mixture and prescribed as a treatment for morning sickness in pregnant woman.[7] Although the (*R*)-enantiomer of thalidomide does have a sedative quality, devastatingly, the (*S*)-enantiomer caused severe birth defects in the unborn children. In 2015, 17 out of the 18 small-molecule active pharmaceutical ingredients (APIs) that were approved by the U.S. Food and Drug Administration (FDA) with chiral centres were enantiomerically pure,[8] highlighting the large requirement for asymmetric chemical synthetic routes.

Biocatalysis involves the use of enzymes to catalyse chemical transformations. The use of this bioprocess is a rapidly growing sector, as enzymes have been shown to carry out highly specific asymmetric transformations with high efficiency under mild reaction

conditions. [9–16] Biocatalysis is inherently a multidisciplinary field, comprising of skilled biologists, chemists and chemical engineers, the diverse knowledge of whom offers benefits. Compared with traditional metal catalysis, biocatalytic equivalent transformations have been shown to decrease process waste, energy consumption and costs at large scales.[17–19] There has been rapid recent progress in enzyme engineering and intensification of enzyme production, making biocatalysis an increasingly more viable option for use in large-scale chemical production. In 2018, Frances Arnold was awarded a Nobel Prize in Chemistry for her work on the directed evolution of enzymes.[20–22] This field of work has broad scope[23,24] in areas such as materials[25] and medical science[26–28]and a large impact has been felt in the field of biocatalysis.[29,30] Progress in directed evolution means that it is now possible to custom-design enzymes to meet a set of specific requirements,[31] such as increasing substrate specificity or inversely increasing substrate scope, increasing enantioselectivity, swapping enantioselectivity, increasing specific activity and improving enzyme stability.[32–40] A successful pharmaceutical application of this technique was demonstrated by Merck and Codexis who synthesized sitagliptin for the anti-diabetic medicine marketed as Januvia, which is Merck's biggest product in terms of volume sold and sales.[41–43] In one year, a transaminase enzyme was developed by directed evolution for the selective reduction of a non-natural ketone, in the key stereoselective step of the synthesis. A single enantiomer of the desired amine in >99.95% enantiomeric excess (e.e.) was formed. This bioprocess outperformed the ruthenium-based hydrogenation step, leading Merck to re-file the manufacturing process with the regulatory agencies immediately.[44]

Continuous flow is simply the performance of a general range of chemical processes and transformations in pipes or tubes, in contrast to in a traditional batch stirred vessel. A

flow reaction involves the continuous pumping of a starting material through a 'reaction zone', for example, a packed-bed reactor (PBR) containing a heterogeneous catalyst or an area of tubing penetrated with light for a photochemical reaction.[45] Flow chemistry intrinsically enables stricter control of reaction conditions over batch due to the higher ratio of surface area to volume of the tubing compared with a batch vessel.[46] This added control can lead to improved safety and reaction selectivity.[47] As a result, continuous flow technology is increasingly being deployed in the pharmaceutical and fine-chemical industry because it has also been shown to reduce waste, reduce costs and accelerate scale-up compared with batch manufacturing, all achieved with a smaller footprint.[47–54] Flow chemistry is inherently modular—different pumps, tubing, reaction zones, separators, in-line analysis and purification technology can all be combined depending on the desired reaction. This makes flow ideal for rapid reaction optimisation. It is also being used at the forefront of reaction discovery and optimisation in combination with artificial intelligence and machine learning techniques.[55–57]

In 2016, Adamo and co-workers developed a modular system that used state-of-the-art technology to manufacture multiple APIs, including diphenhydramine hydrochloride (anti-histamine) and diazepam (anxiolytic) to the quality and safety of U.S. Pharmacopeia standards.[58] The end-to-end synthesis of these small molecules was achieved on a fully continuous and automated platform that included multiple upstream reactor types and downstream purification, separation and analysis. The plug-and-play system, which was the size of a refrigerator, was demonstrated for the synthesis and purification of diazepam at a scale of approximately 3,000 doses per day (5 mg dose size).

Recently, considerable progress has been made in translating biocatalysis to continuous flow systems.[59–65] Enzymes have regularly been deployed in solution through flow

systems; however, in many recent examples the enzymes are immobilised onto solid supports, and these heterogeneous biocatalysts are then amenable for use in PBRs. The use of immobilised enzymes has been found to improve the stability and increase the lifetime of the enzyme.[66–68] Moreover, the benefit of the high catalyst-to-substrate ratio that is achievable in continuous flow when using packed bed reactors can often enable shorter reaction times and improvements in yield compared with batch. The inherent continuous removal of the reaction solution seen in continuous flow systems can also help to overcome substrate or product inhibition of the enzyme, which is a common problem in biocatalysis. Recent advances in enzyme immobilisation have used techniques such as HaloTag[69] and histidine tagging of proteins, as well as using a range of support materials.[70–72] However, many of these enzyme-immobilisation techniques often require expensive supports and modification of the support and/or enzyme. The immobilisation protocol is often lengthy and can sometimes cause a loss of enzyme activity when compared with the free enzyme in solution.

In 2020, Paradisi and co-workers demonstrated the benefits of biocatalysis in flow by performing a dual-enzyme cascade synthesis of L-pipecolic acid—a precursor of several APIs, including the antitumor drug swainsonine (Figure 1-1).[73]

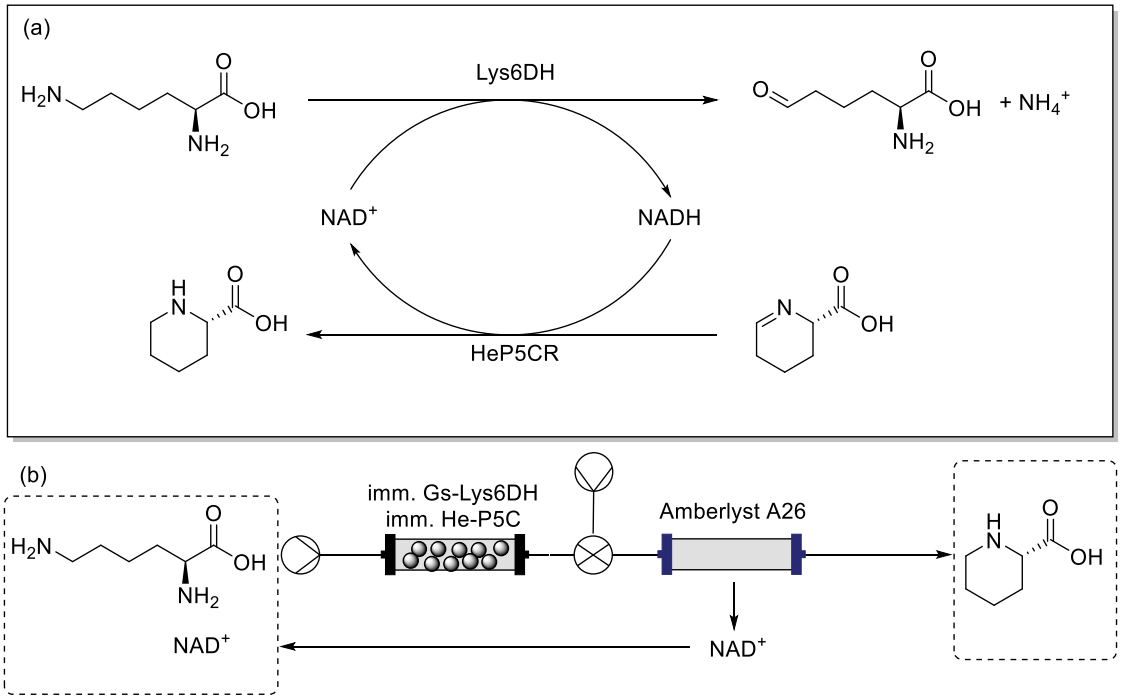


Figure 1-1: (a) Continuous dual-enzyme cascade flow production of L-pipecolic acid. (b) The first packed-bed-reactor contains immobilised (imm.) lysine dehydrogenase (Gs-Lys6DH) and imm. Pyrroline-5-carboxylate reductase (He-P5C). The second PBR enables in-line recovery and reuse of expensive NAD^+ using a product catch and release strategy with a Amberlyst A26 scavenger.[73]

The redox enzyme lysine dehydrogenase and a pyrroline-5-carboxylate reductase were immobilised onto agarose microbeads and loaded into a PBR volume. The experiment achieved a L-pipecolic acid molar conversion of >99% and the process resulted in an increase of almost tenfold in the total turnover number (TTN, number of product per enzyme) for each enzyme compared with the free enzyme in solution used in batch.[73] This example also highlights a key limitation of the use of redox enzymes in batch and flow—the lysine dehydrogenase is dependent on a stoichiometric reductant, in this case, the reduced form of the cofactor nicotinamide adenine dinucleotide hydride (NADH). The NADH is oxidised to nicotinamide adenine dinucleotide (NAD^+). Most biocatalytic redox enzymes are dependent on a stoichiometric cofactor, which is currently a major drawback for the application of redox enzymes in industry because the cofactors required,

such as NADH, are very expensive. To decrease the requirement for large amounts of cofactor, recycling systems have been developed. However, the widely adopted methods are not very atom efficient, generating large amounts of carbon waste. For large-scale use in industry, this can complicate the equation, raising environmental and economic concerns.

This Thesis will address the existing drawbacks of the application of redox biocatalysis in flow. Carbon is used as a simple immobilisation support to facilitate transformations with traditional cofactor recycling techniques, with a focus of improving the environmental factor (*E* factor[74]) metrics of these systems. A cofactor regeneration approach, which uses enzymes immobilised on carbon and H_2 as a clean reducing equivalent, is also applied to flow with the aim of showing enhanced productivity and green credentials over the existing methods. Work in collaboration with Dr Reddy's Laboratories Ltd, will also see this clean approach applied to the synthesis of APIs, to overcome the previous limitations of the approach for use on an industrial scale.

In this introduction, traditional chemical reduction methods will be discussed followed by an analysis of enzyme catalysis in this area. A particular focus will be placed on the immobilisation of chemoreduction and bioreduction catalysts, before a discussion of flow chemistry and the use of these immobilised catalysts in this field. The majority of the experimental work described in this thesis focuses on the reduction of ketones to alcohols; a substantial part of the introduction therefore shares this focus, with references to pharmaceutical examples.

1.1 Traditional methods for ketone reduction

1.1.1 Traditional hydrogenation

Hydrogenation reactions involve the addition of H_2 across a double or triple bond. It is estimated that 10–20% of all reactions performed to produce chemicals are hydrogenation reactions.[75] A number of chemical methods are available for hydrogenation reactions using sacrificial hydride donor chemicals; however, it is widely acknowledged that hydrogenation reactions that use H_2 gas are greener approaches.[76] Heterogeneous and homogeneous transition metal catalysts have had an essential role in hydrogenation chemistry, in both academic research and industrial chemical synthesis, since their first demonstration in the 19th century.[77] However, these methods often use expensive rare heavy transition metals and can require high temperatures and pressures to achieve appreciable rates.[78] It can also prove difficult to achieve good chemoselectivity and enantioselectivity, although a number of enantioselective catalysts have been designed for specific reactions. Thus, while Sabatier[79], Knowles[80] and Noyori[81] have all been awarded Nobel Prizes for their work on hydrogenation chemistry, it is clear that there are still challenges to be overcome and new hydrogenation methods to be developed. In this section, the theory of asymmetric ketone reductions will be briefly introduced, followed by a limited review of the history and recent literature of traditional hydrogenation catalysts. The end of the section focuses on the development of heterogeneous metal hydrogenation catalysts.

1.1.2 Ketone reduction

A ketone reduction reaction consists of reducing the oxidation state of an sp^2 hybridised ketone (3 σ-bonds and 1 π-bond) to an sp^3 functionalised group (4 σ-bonds) such as an alcohol or an amine.[82] A C=O double bond is planar; due to the difference in

electronegativity of carbon and oxygen atoms, the electron density from the π-bond is situated closer to the O atom than the C atom (Figure 1-2). This polarity is exploited in hydrogenation reactions, which can be simplified as a hydride being added to the partial positive charged carbon and a proton being added to the partial negative charged oxygen.[82]

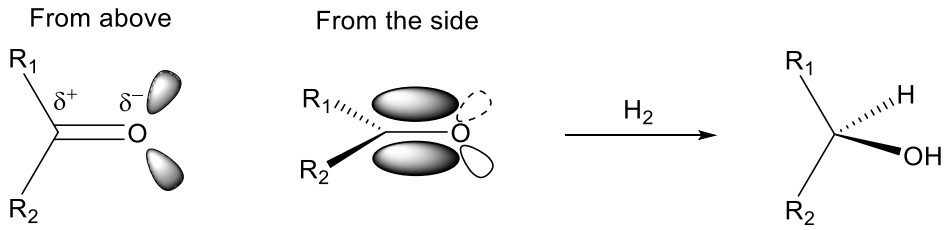


Figure 1-2: Structure of a ketone and the alcohol product from hydrogenation.

If R_1 and R_2 are non-equivalent (pro-chiral) this transformation presents an opportunity to add ever important chirality. Diastereoselectivity can be achieved if R_1 or R_2 themselves are chiral. The R_1 and R_2 groups have a role in the equilibrium constant of a ketone reduction transformation. If R_1 and R_2 are electron donating, this stabilises the ketone. For ketone conversion to alcohols, bulky R_1 and R_2 will also decrease the stability of the alcohol product.[82] Ketone reductions are therefore often less favourable than aldehyde reductions (R_1 = H). It is common in the pharmaceutical industry to approach target compounds through a 'reduce the oxidation state down approach', rather than by oxidising up, owing to safety concerns (explosivity) and the toxicity of the stoichiometric oxidants required.[83,84] Asymmetric alcohols themselves are key precursors for the synthesis of pharmaceuticals, flavours and fragrances.[85,86]

1.1.3 Stoichiometric reduction

There are a number of reagents that are used for ketone reduction that require stoichiometric addition. The reagents that are most commonly turned to are $LiAlH_4$ and

$NaBH_4$, as they can be implemented with relative ease for the reduction of carbonyl bonds; $LiAlH_4$ is the more reactive of the two. A hydride from the highly polarised aluminium–hydrogen bonds can attack the C=O bond, with stabilisation of the carbonyl oxygen by the Li^+ cation. The lithium alkoxide tetrahedral intermediate then coordinates from its nucleophilic oxygen with the AlH_3 Lewis acid metal ion, increasing the polarisation across the C=O bond. After a proton transfer work-up, the alcohol product is irreversibly formed. Although the high reactivity of $LiAlH_4$ can be beneficial, it also raises a number of issues. It enables very limited control of the chemoselectivity, simply diminishing in the order of functional group electrophilicity (aldehyde > ketone > ester > carboxylate), leading to over-reductions of the starting material. Furthermore, $LiAlH_4$ is highly flammable and reacts violently with water, requiring strict control of reaction conditions[84]—a drawback for its use in industry. Although it is less reactive, $NaBH_4$ is often the preferred ketone and aldehyde reductant, with reactions even possible using a water solvent system. The mechanism of action is similar to the $LiAlH_4$, with a hydride from the polarised boron–hydrogen bonds, attacking the C=O bond, with stabilisation of the carbonyl oxygen by the Na^+ cation. Hydrolysis with acid and water is then performed, followed by extraction to isolate the alcohol product. The simplicity, bulk availability and cost efficiency of $NaBH_4$ has made it a widely used reductant in industry; however, its chemoselectivity is poor and, due to its size, enantioselectivity is lacking.[87] As an example of $NaBH_4$ chemoselectivity, the α,β-unsaturated ketone 5-methyl-2-cyclohexen-1-one was found to form a 49:51 mixture of the α,β-unsaturated alcohol and saturated ketone products after addition of 1 equivalent (Eq.) of $NaBH_4$.[88] More recently, it was found that the addition of an ionic liquid can be used to improve the chemoselectivity for the reduction of α,β-unsaturated ketones.[89] Ralphs and co-workers found that, after the addition of the ionic liquid, the reduction of cinnamaldehyde proceeded with 100%

selectivity towards the cinnamyl alcohol (α,β-unsaturated alcohol) product.[89] The use of $NaBH_4$ with additives such as chlorotrimethylsilane or bromine can lead to the introduction of enantioselectivity for its reduction of pro-chiral ketones; however these methods are limited by poor selectivity or the high cost of the additive.[90–97] A class of reductants pioneered by Hirao, Corey and their co-workers use BH_3THF with a chiral oxazaborolidine catalyst for the asymmetric reduction of pro-chiral ketones.[98–103] The reduction by a six-membered cyclic transition state has been shown to achieve high enantioselectivity. However, borane is a harmful and unstable gas[104] that, even when complexing with tetrahydrofuran (THF), requires inert low-temperature conditions. In 2014, Zhou *et al*. combined the relative safety of $NaBH_4$ with dimethyl sulphate and THF to produce the borane *in situ*, which is combined with a (*S*)-Me-CBS chiral oxazaborolidine catalyst to achieve the reduction of pro-chiral ketones with an e.e. of up to 99%.[105,106] To achieve the highest enantioselectivity, a temperature of lower than −10 °C was required.

A variety of other stoichiometric ketone reductants exist.[107–109] Along with those already described, they are all required in super-stoichiometric quantities, which leads to metal waste that has to be separated and disposed of during the reaction work-up. Thus, the process is not considered to be green. Furthermore, issues with economically achieving high selectivity in complex molecules persist.

1.1.4 Metal-catalysed asymmetric hydrogenation of ketones

The use of transition metal catalysts for the hydrogenation of ketones is widespread.[110] There are two pathways that have been extensively studied that both make use of precious-metal–ligand complexes. First, transition-metal-catalysed asymmetric hydrogenation (AH) reactions use molecular H_2 in a clean, cheap and highly atom-

efficient manner.[111] Alternatively, a transition-metal-catalysed asymmetric transfer hydrogenation ATH reaction abstracts two hydrogen atoms from a hydrogen donor (such as propan-2-ol) to perform a process classed as asymmetric transfer hydrogenation (ATH).[112] The benefits of ATH include avoiding the safety issues raised by using molecular H_2 at the high pressures (>50 atm) that are required for AH; however, it inherently requires a sacrificial substrate. The sacrificial substrates are often cheap and can sometimes be used as the reaction solvent; nonetheless, their use still raises some environmental concerns. The first asymmetric transfer hydrogenation of a ketone was described by Doering and Young in 1950 using an aluminium system based on the Meerwein–Pondorf–Verley reduction discovered in 1925.[113,114] Subsequently, metal–ligand hydrogenation complexes were developed that could be highly tuned to achieve asymmetric reductions on the basis of the sterics, chirality and electronics of the auxiliaries on the metal centre.

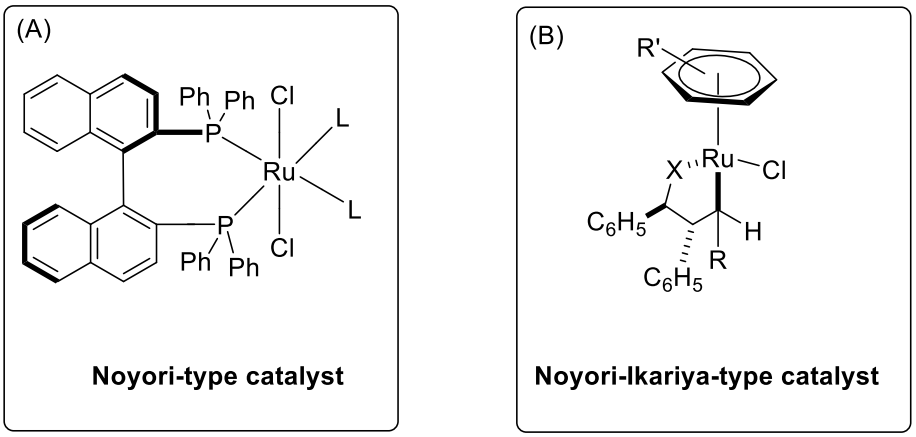


Figure 1-3: General structure of a Noyori-type pre-catalyst for asymmetric hydrogenation and a Noyori-Ikariya-type pre-catalyst for asymmetric transfer hydrogenation.

In 1995, work in AH and ATH reached the mainstream following research by Noyori and co-workers. For AH, a second-generation Ru-based catalyst, shown in Figure 1-3(A), that used 2,2′-bis(diphenylphosphino)-1,1′-binaphthyl (BINAP) or BINAP analogues was

shown to achieve asymmetric reduction of a large array of secondary ketones with >99.99% e.e. and turnover number (TON = moles of substrate per mole of catalyst) of up to 1 million.[115] This was achieved without the previous need for a secondary binding group on the ketone substrate. For this research, Noyori won a Nobel Prize in Chemistry.[116] Subsequently, the Ru-BINAP, BINAP analogues and other ligands have been well studied to improve the scope and performance of the system. As an example of such developments, in 2011, Ohkuma and co-workers exhibited a Ru-BINAP analogue complex ((*R*)-RUCY-XylBINAP) for the asymmetric reduction of acetophenone.[117] The catalyst achieved full conversion to (*S*)-1-phenylethanol at <50 atm H_2 pressure within 6 min, with >99% e.e. and a turnover frequency (TOF = TON per unit of time) reaching 35,000 min^{-1}. The most stable alternative transition metal that this type of system has been applied to is Ir and the most successful ligands tend to encapsulate at least a single N-H functionality. In 2011, Zhou *et al.* developed in a chiral iridium catalyst (Ir-SpiroPAP) encompassing a tridentate ligand with one N-H functionality.[118] It was shown to asymmetrically reduce acetophenone with a 91% yield and 98% *e.e.* to the (*S*)-alcohol product. It achieved a TON of 5×10^6 ; however, it required up 100 atm H_2 and a 15 day reaction time. In 2015, Zhang *et al.* developed an Ir(III)-f-Amphox hydrogenation catalyst that achieved >99% yield and 99.9% e.e. for the same transformation in 80 atm of H_2.[119] Although AH catalysts have been applied to a wide range of substrates, the reaction conditions required for success are a limiting factor.[120] The reactions often have to be carried out in isopropyl alcohol (IPA) or ethanol under basic conditions. By contrast, ATH reactions proceed with a variety of organic solvents and water, under a range of pH conditions and a choice of multiple hydride sources. In 1995, Noyori, Ikariya and co-workers introduced a family of bifunctional chiral (sulphonyl-diamine)RuCl(arene) complexes, shown in Figure 1-3(B), that demonstrated asymmetric reduction of ketones

through a six-membered transition state.[121–124] The 'outer-sphere' mechanism occurs without direct coordination of the ketone.[125] The stability of these complexes was greatly improved by Wills and co-workers when a diamine ligand was covalently linked to the arene ring, achieving a three-point attachment to the Ru metal.[126,127] The tethered Ru complexes were demonstrated for the reduction of acetylenic ketones with >99% e.e. and a high yield (up to 97%). The catalyst TON achieved was 200, a 100% increase in comparison to the non-tethered Noyori–Ikariya complexes. More recently, work has gone into developing Ru, Rh and Ir transfer-hydrogenation metal complexes that display a higher TON and TOF. In 2010, Baratta *et al.* implemented a Ru catalyst with phosphino-ferrocenyl ligands that achieved a TON of 20,000 in 10 min, for the asymmetric reduction of acetophenone to (*R*)-1-phenylethanol (92% e.e.).[128]

The homogeneous AH complexes have been reported for use on substrates of industrial relevance. The main impurity found by their use at a large scale is often the catalyst residue itself. The catalysts are also difficult to recycle and can often be very expensive (Noyori Ru catalyst ~£350 g^{-1}). Methods of immobilising these transition-metal catalysts have been developed; immobilisation eases the separation and recycling of the catalyst, in turn leading to less catalyst being required overall.[112] The typical immobilisation strategies have focused on both ion-pair interactions and covalent binding on to the support. Typical supports of choice are mesoporous silica, organic polymers, zeolites and carbon. Some brief examples of heterogeneous transition metal hydrogenations are discussed below.

Inorganic supports such as mesoporous silica have been widely studied for the immobilisation of Noyori–Ikariya type ATH catalysts. Liu *et al.* found that a three-dimensional flower-like silica had advantages over traditional silica for which the catalyst

displays loss of stereoselectivity and poor recyclability.[129] The chrysanthemum-like mesoporous silica acted as a covalent support for a chiral Ru catalyst, which displayed quantitative conversion of acetophenone with a 98% e.e. The immobilised catalyst could be recycled ten times without showing an effect on its TOF, although lower than the homogeneous counterpart. More recently a Noyori–Ikariya Rh catalyst was immobilised on a glass plate solid support; however, it suffered from low e.e. and conversion (90%), as well as a significant loss of activity when it was reused.[130]

Yang and co-workers have studied the use of polymer@silica composite supports for Noyori–Ikariya-style Rh catalysts.[131] The asymmetric reduction of acetophenone was achieved in an aqueous medium with 99% conversion in under 3 h. The immobilised catalyst displayed a greater TOF (585 h^{-1}) compared with its homogenous counterpart (340 h^{-1}); however, the enantioselectivity achieved (up to 94%) was lower and it decreased further for the conversion of more complex acetophenone analogues. The polymer@silica-immobilised Rh catalyst displayed activity over six uses, although the reaction time increased each time due to the degradation of the catalyst during the recycling process.

A lot of research has been conducted with polymer-based supports, which enable a more-simple purification step due to their water solubility. As an example, a Noyori–Ikariya-style Ru ATH catalyst was immobilised onto a poly(ethylene glycol) support through the amino nitrogen on the TsDPEN (*N*-tosylated 1,2-diphenyl-1,2-ethylenediamine) ligand.[132] Li *et al.*, found that the immobilised catalyst displayed excellent conversions (>99%) and reusability for the asymmetric reduction of a selection of acetophenone analogues. Unfortunately, the e.e. achieved on the alcohol products was ~90%. There has been much interest recently into the use of magnetic nanoparticles as a possible support

for chiral hydrogenation catalysts. Magnetic nanoparticles offer easy recovery of catalysts with an external magnetic field; however, their industrial application is hindered by magnetic aggregation and loss.[133,134]

Another family of catalysts for asymmetric ketone reduction are chiral modified Ni, Pt and Pd catalysts. The Ni, Pt and Pd catalysts are usually supported (for example, on C or TiO_2) to maximise their surface area and activity.[135] Supported Ni, Pt and Pd catalysts are already ubiquitous in industry for their ability to perform hydrogenations across a wide range of functional groups; however, to achieve high enantioselectivity, the use of a chiral auxiliary is often required in the reaction mixture or tethered to the Ni, Pt or Pd.[136] The most studied family of chiral modifiers for the Ni, Pt or Pd are derivatives of cinchona alkaloids, preferentially cinchonidine (CD).[137] The initial discovery by Orito and co-workers in the 1970's focused on the use of a CD and platinum-modified carbon for the enantioselective hydrogenation of α-ketoesters.[138] Indeed, the hydrogenation of functionalised ketones has been a major focus for the study of cinchona-modified metal catalysts and high enantioselectivity has been achieved.[139] It has proved much more difficult to achieve good enantioselectivity for the hydrogenation of unfunctionalised aliphatic ketones and aromatic ketones. With regard to the catalytic hydrogenation of α,β-unsaturated ketones, the 1,4-reduction is often favoured. In general, improved selectivity is required for this family of catalysts.

A large amount of work has gone into the immobilisation of transition metals for their use in AH reactions. Nonetheless, as of 2015, the homogeneous versions of these hydrogenation catalysts are still exclusively used in the pharmaceutical and fine-chemical sector.[140] Factors such as reproducibility, loss of activity on reuse, lower selectivity and lower catalytic activity overall for the heterogeneous catalysts compared with their

homogeneous counterparts have stalled their application. The industry has weighed up the separation of homogeneous catalysts against the extra steps that are required for heterogeneous catalysis and has to date decided against it for the majority of transformations.

Another drawback of the transition-metal catalysts described in this section is their expense, toxicity and abundance. Although a selection of Fe, Cu and Co catalysts are being developed in the hope of the replacing these metals, at present, the process is not considered to be green.[137–139]

1.2 Towards green hydrogenation chemistry

In recent times, there has been an overall effort to improve the sustainability of the chemical industry.[74] Chemical transformations inherently expend resources and can never be considered to be fully green; however, their impact on the environment can be decreased in an effort to make them greener. In 1998, Anastas and Warner laid out the key areas to consider when designing a chemical process in the 12 Principles of Green Chemistry (summarised in Table 1-1[144]).

Table 1-1: The 12 Principles of Green Chemistry summarised.

Principles of Green Chemistry		
1	**Prevention**	Aim to prevent waste - rather than finding ways to deal with it after creation
2	**Atom economy**	Maximise incorporation of starting materials into product
3	**Less hazardous chemical syntheses**	Substances generated should have minimised effect on human health and environment
4	**Designing safer chemicals**	Preserve efficacy and reduce toxicity
5	**Safer solvents**	Used wherever possible
6	**Design for energy efficiency**	The environmental impact of processes should be considered and minimised
7	**Renewable feedstocks**	Renewable materials are favoured over depleting materials
8	**Reduce derivatives**	Keep reaction steps to a minimum by avoiding derivatisation
9	**Catalysis**	Catalytic reagents > stoichiometric reagents
10	**Design for degradation**	Chemicals designed to leave little to no impact on the environment at the end of use
11	**Pollution prevention**	Real-time methods to monitor and control the production of hazardous chemicals
12	**Accident prevention**	Design chemical processes that decrease the potential for accidents

The most quantitative way to determine the sustainability of a chemical transformation is by a full life cycle assessment (LCA), in which large amounts of data are analysed across the entire process and the results can easily be compared.[145] Although LCA is an important tool used by the chemical industry to benchmark and optimise the environmental performance of their processes, it is highly resource and time intensive to perform. A more simple green metric is the atom economy, which is the ratio of the mass

of desired product against the mass of all the reaction products.[146] Although, atom economy is an important green metric, it has limitations by not taking into account, *inter alia*, overall yields, catalysts and solvents.[147] In 1992, Sheldon introduced the concept of an environmental factor (*E* factor) as a simpler alternative for the chemist's toolbox.[143,144] *E* factor is a ratio of the mass of reaction waste to the mass of desired product, according to:

$$E\ factor = \frac{\text{Total waste (g)}}{\text{Total product (g)}}$$

For an ideal process, the *E* factor would be 0. The metric does not include recycled catalysts or recycled solvents in the waste values and the convention does not include water either. A guideline for chemical reactions is that the *E* factor of the fine chemicals industry is >5–50, the pharmaceutical industry is >25 and the bulk chemicals industry is <1–5.[150] A limitation of the *E* factor is that it does not take into account the toxicity of reagents/products/catalysts or how efficiently the catalyst is utilised. Another metric of focus, with an impact on sustainability is the space–time yield (STY). The STY is a way of describing the productivity of a system by the amount of desired product formed with respect to the reactor volume and time, and is calculated according to:

$$\text{STY (g L}^{-1}\text{h}^{-1}) = \frac{\text{Desired product quantity}}{\text{Reactor volume} \times \text{Time}}$$

The STY enables the direct comparison of different reactor types and sizes, which is especially important when comparing batch and flow reactor systems. Although it is not inherently a green metric, the STY has many green implications. The time aspect has importance in sustainability because the length of time that a reactor is required to run in

an industrial environment to produce a certain amount of product has implications on the energy consumption, employees required and (toxic) emissions of the plant—all factors that can be considered for sustainability. Second, the reactor volume/size is of great importance. The ability to produce chemicals with a smaller space footprint enables the more efficient use of space and smaller production plants, leading to a lower impact on the environment with regard to building materials and reactor maintenance.

In Section 1.1, the credentials of existing hydrogenation methods were discussed, including their limitations. When these green principles are applied to the development of an improved hydrogenation strategy, an ideal system would have the following features:

- Be catalytic (ideally a cheap, non-toxic, renewable or biodegradable catalyst)
- Use a clean reducing equivalent (to decrease the *E* factor)
- Operate with a high STY at low catalyst loading
- Demonstrate very high selectivity (decreasing downstream separation requirements)
- Be applicable in a broad range of cleaner solvents (water, IPA, hexane, methanol)[151–153]
- Catalyst lifetime and ease of separation extended or improved by immobilisation
- Applicable to multiple reactor types and set-ups

The resulting system would result in easier separation, a smaller footprint and improved *E* factor, while being more economically viable. A system such as this would also present much better long-term stability in operating and materials cost due to the use of fewer rare materials, which is a bonus for the chemical industry.

1.3 Biocatalysis

The fine chemical sector has seen a recent shift towards biocatalysis for alkene (C=C) and ketone (C=O) reductions, which are extremely common reaction steps in the syntheses of complex chiral molecules.[154,155] Reductive biotransformations are known to have a number of advantages compared with transition-metal-catalysed approaches, most significantly, the near perfect enantioselectivity and chemoselectivity of reductive biotransformations that can be achieved under mild reaction conditions. Such advantages can lead to a decrease in downstream processing when compared to metal approaches for chemical reduction, which in turn can decrease manufacturing costs and the *E* factor.[156] Although biocatalysis is generally stated as the green approach, there are still factors that compromise its sustainability and require improvement. The use of aqueous solvents is generally viewed as a positive because water is a green solvent. However, after the reaction, the aqueous medium still requires difficult purification before it can be rereleased into the environment. Fortunately, biocatalysts often require low temperatures; nonetheless, the high heat capacity means that temperature control can necessitate large energy input. Furthermore, commonly used hydrophobic reagents will often be demonstrated at poor reagent concentrations (1–10 mM) or they require an organic co-solvent (such as dimethylsulfoxide (DMSO) or acetonitrile), which can often inhibit the enzyme and increase reaction waste.[145,157] Furthermore, enzyme production itself can be an energy- and resource-intensive process.

There are two widely used types of enzymes in biocatalysis. Whole cells—which contain the components for entire catalytic pathways, including redox enzymes—and in-built cofactor regeneration systems. Whole cells advantageously demonstrate high stability (for short time periods) and do not require any purification.[158,159] However, the reaction

conditions need to be balanced for cell growth and reagent catalysis, which can be difficult. This issue, in addition to the difficulty of transporting reagents and products through the cell membrane, can often lead to very low STYs and difficult product separation.[160,161] Recently, isolated enzymes have become much more frequently used for chemical transformations.[162,163] These overexpressed or purified enzymes result in products of higher purity compared with whole cells, while requiring simpler reaction conditions. However, they do introduce the need for a cofactor recycling system. Furthermore, isolating enzymes requires cloning, over-expression and expensive additional purification steps.

Biocatalysis has been shown to be an economically feasible process. In 2019, the global enzyme market size was estimated to be $9.9 billion, of which biotransformations make up at least 24% of the total revenue.[164] Furthermore, the market for enzymes is forecast to rise at a rate of 7.1% per year until 2027. There is a large variety in the cost of enzymes, and their cost contribution to a final product can differ depending on the application.[165] To fully consider an enzyme for a process, a balance of production cost and performance is required. The bulk chemical industry requires an enzyme turnover number (TN) of >5,000,000 $mol_{product}\ mol_{enzyme}^{-1}$, translating to an enzyme cost contribution of ~€0.05 $kg_{Product}^{-1}$. By contrast, for pharmaceutical production, the enzyme TN is expected to be >25,000, with an expected enzyme cost contribution of ~€10 $kg_{Product}^{-1}$.[166] The two industries are very different and, in the pharmaceuticals industry, the price of the drugs sold is based on many factors along with the cost of production. Furthermore, the molecules that are required in the pharmaceutical industry are much more complex and the enzymes can require extensive protein engineering to become feasible for a desired transformation. One such example was demonstrated by Codexis for an intermediate in

the synthesis of the highly prescribed anti-cholesterol generic drug Atorvastatin.[167] The process used a highly engineered ADH enzyme for the enantioselective ketone reduction of ethyl 4-chloro-3-oxobutanoate to (*S*)-ethyl-4-chloro-3-hydroxybutyrate. Synthesis was demonstrated with a 96% yield and a >99.5% e.e., affording a 2,500-fold improvement in STY when compared with the pre-engineered enzyme. Examples of protein engineering such as this are becoming increasingly common as the enzymes become more affordable. Nevertheless, the application of enzymes in industry is often hindered by poor long-term stability and the difficult recovery and recyclability of the enzyme.[168]

1.3.1 Enzyme immobilisation

Enzymes are increasingly being immobilised onto solid supports for use as biocatalysts in batch and flow reactions.[66–68] Immobilisation of the enzyme enables convenient handling of the enzyme and easier separation from the product mixture. More efficient separation enables easier reuse of the enzyme, therefore making their use more economically feasible. Moreover, immobilised enzymes often benefit from improved lifetime stability, under storage and operational use. These benefits often lead to improved productivities compared with free enzymes in solution—lowering the operating costs and increasing the green credentials. Enzymes can be entrapped into a polymer network, cross-linked to prepare carrierless macroparticles or bound to a solid support.

Entrapment involves the synthesis of a polymeric matrix (for example, polyvinylalcohol (PVA) or silica solgel) in the presence of the enzyme. For example, Gröger and coworkers used a Lentikat PVA hydrogel to entrap a hydroxynitrile lyase for the enantioselective hydrocyanation of benzaldehyde.[169] The reaction proceeded with >99% e.e. and no loss

of product yield after 20 cycles of use. No enzyme leaching was detected, which is often a problem with enzyme entrapment.[170]

Carrier-free strategies involve the cross-linking of enzymes to form insoluble gels that maintain the catalytic activity of the enzymes. The most convenient and cheap technique involves the precipitation of the enzymes out of aqueous media before being linked by a reagent (such as glutaraldehyde) to form cross-linked enzyme aggregates (CLEAs).[171] They can be prepared from crude enzyme preparations, exhibit high productivities and avoid potentially expensive carriers. Ferraboschi *et al.* demonstrated an alcalase-CLEA to catalyse the hydrolysis of a racemic unnatural amino acid to afford an (*S*)-acid product, which is an intermediate in the synthesis of the API Clopidogrel (anti-thrombotic).[172] A modest isolated yield (34%) and good enantioselectivity (98%) was achieved. Many CLEAs can now be purchased for commercial use.

A simple method of enzyme immobilisation is through direct adsorption onto the surface of a carrier. Binding can be by physical interactions, such as hydrophobic or Van der Waals, with no chemical step; however, this interaction can often be weak, leading to counterproductive enzyme leaching.[173] Recent advances in enzyme immobilisation have taken advantage of ionic- and covalent-binding techniques including HaloTag and histidine tagging onto an array of support materials, such as resins, agarose and microbeads.[69–72] However, many of these enzyme-immobilisation procedures involve costly supports, modification of the support and/or enzyme, lengthy immobilisation times and can cause a major decrease in catalytic activity when compared with the free enzyme in solution.

Different immobilisation methods will be discussed further for the use of immobilised enzymes for continuous flow in Section 1.9. However, to date, a 'one size fits all' solution has not been found for enzyme immobilisation. A single technique has not yet been demonstrated to work efficiently across a broad range of enzymes. Nevertheless, there is currently a great drive in this field of biocatalysis to continue improving on and developing new ideas, motivated by a desire for a greener, more efficient solution towards chemical synthesis.

1.4 Cofactor recycling

The majority of known enzymes that can be used for biocatalytic C=X bond reductions are dependent on the reduced cofactors NADH or NADPH (NAD(P)H), which are required for hydride transfer.[174] A family of redox NAD(P)H-dependent enzymes called oxidoreductases catalyse the transformation of a wide range of substrates, including ketones and amines.[175–177]

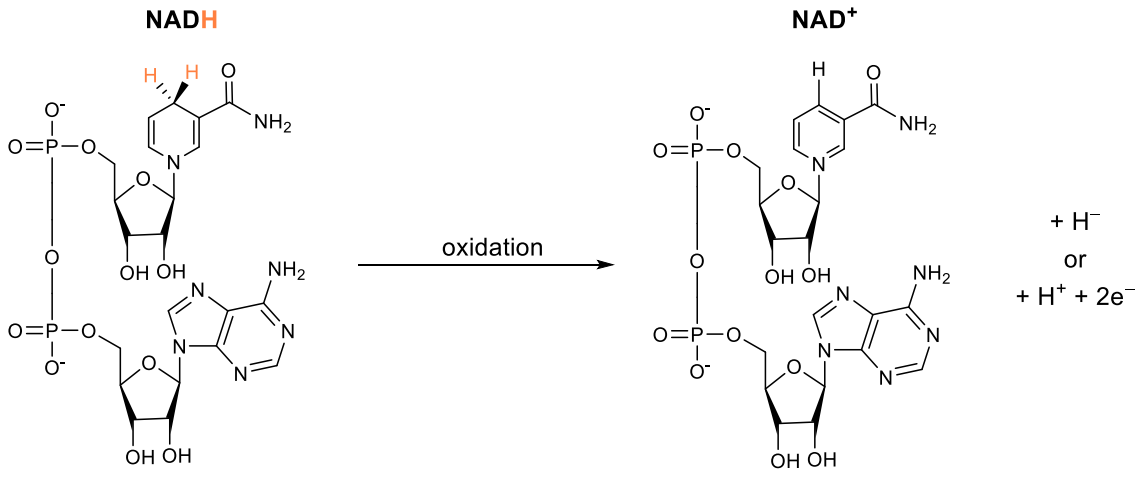


Figure 1-4: The structures of 1,4-NADH and NAD^+, highlighting the 1,4-NADH *si* or *re* hydride (orange) that is removed upon oxidation to NAD^+ depending on the enzyme.

They comprise approximately a quarter of the 8,149 enzymatic activities registered in the Braunschweig Enzyme Database (BRENDA) and of these, roughly 50% are NAD(P)H dependent. In biological cells, the enzymes have developed different specificities for NAD^+/NADH (Figure 1-4) or $NADP^+$/NADPH, acting as two essentially equivalent redox systems, differing only by the bearing of a phosphate group on the 2′-hydroxyl group of the adenine ring.[178] This enables two redox enzymes, each dependent on a differing form of cofactor, to act in tandem in opposite directions for key reaction steps.[179] With oxidoreductases in biocatalysis, the stoichiometric addition of a reduced cofactor to these reactions is not economically viable due to its high cost (Table 1-2); a cofactor recycling system is therefore essential.

Table 1-2: Cost to academia per mole of cofactor from a large cofactor supplier

Cofactor	Cost / £ mol^{-1*}
NAD^+	2,320
$NADP^+$	6,696
NADH	5,320
NADPH	51,511

*Prices acquired from Prozomix, 2019.

At present, enzymatic cofactor recycling systems are used at an industrial scale, the most commonly used of which is glucose dehydrogenase (GDH), formate dehydrogenase (FDH) and alcohol dehydrogenase (ADH), described in Figure 1-5.[157,180,181] They require the super-stoichiometric addition of a sacrificial carbon-based reductant such as glucose, isopropanol or formate, respectively, generating large quantities of carbon-based

waste.[182–186] The high waste generation is highlighted by the GDH–glucose system, whereby GDH removes just one atom of hydrogen from glucose (molecular weight = 180 g mol^{-1}) to a molecule of gluconolactone waste (molecular weight = 178 g mol^{-1}), which is typically burned. On the basis of the literature, it was calculated by Hollmann *et al.* that the two most widely used cofactor recycling systems—GDH–glucose and the ADH–isopropanol—can lead to waste generation of 196 g $mol_{product}^{-1}$ and 58 g $mol_{product}^{-1}$, respectively.[156] Work has been done to decrease the waste production and develop greener processes.[156] The wasteful nature of these reactions means that NADH-dependent biocatalysis is not as green as it is often considered. The complexity of these systems including waste and product separation is limiting the potential scale-up of NADH-dependent biocatalysis across the entire chemical sector, particularly for lower value chemicals.

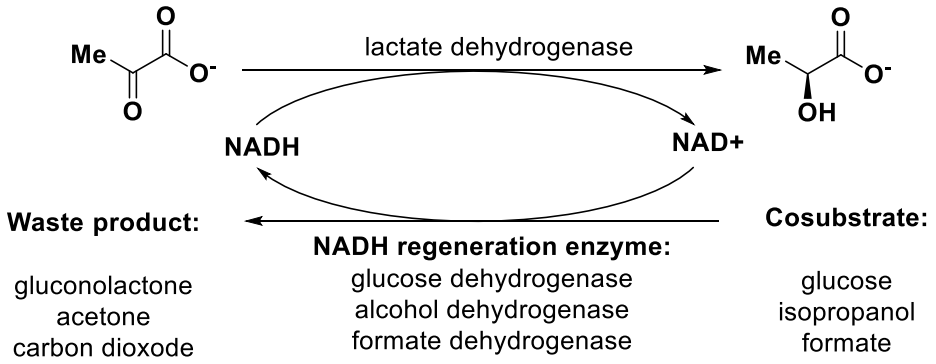


Figure 1-5: Commonly used enzymes for NADH regeneration; shown are the co-substrates required that form the waste product on reaction with the NADH regeneration enzyme. The scheme is illustrated here for the conversion of pyruvate to L-lactate by the NADH dependent enzyme, lactate dehydrogenase.

Although these systems generate waste products, they have been shown to regenerate cofactor very efficiently and enable industrial implementation of NADH-dependent biocatalysis, particularly in the fine-chemical and pharmaceutical sectors.[3-7] For example, Merck deployed the GDH recycling system for the asymmetric ketone reduction of 4,4-

dimethoxytetrahydro-2H-pyran-3-one, which required an NADH-dependent enzyme KRED-101 (Figure 1-6).[187]

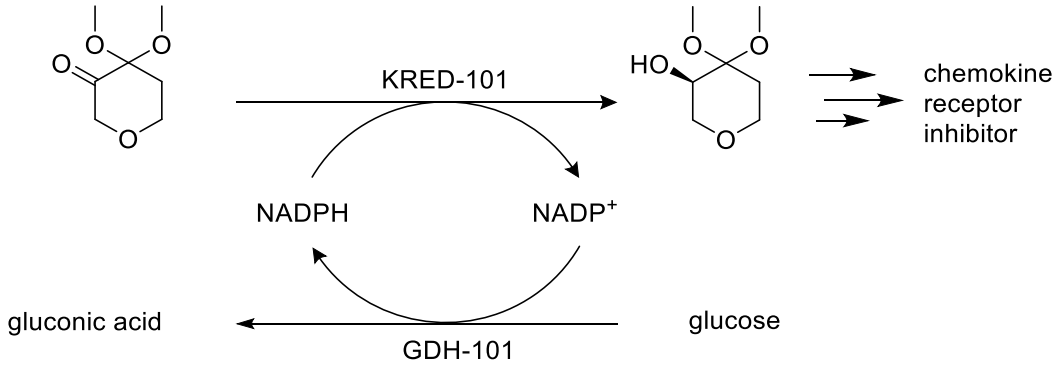


Figure 1-6: Biosynthesis of a chemokine receptor inhibitor precursor, performed with NADH recycling by use of GDH-glucose coupled with ketoreductase KRED-101 for highly enantioselective ketone reduction to generate (*R*)-4,4-dimethoxytetrahydro-2H-pyran-3-ol 2.

The (*R*)-α-hydroxyketal formed, which is an important chiral intermediate towards the preparation of a chemokine receptor inhibitor (human immunodeficiency virus (HIV) treatment), was formed in high yields and with a >99% e.e. This process far exceeded their previous attempts that achieved only 92% e.e. under modified Sharpless dihydroxylation conditions. The enzymatic route that was demonstrated on an 80 kg scale also avoided difficult and expensive separation of the toxic osmium by-product. However, the reaction was limited by the very poor performance of GDH above 25 °C because the optimum performance of the KRED-101 was achieved at 40 °C. The traditional enzyme-based cofactor regeneration systems are summarised below.

1.4.1 Alcohol Dehydrogenase

ADH is the most commonly deployed cofactor regeneration system in industry. It operates through a substrate-coupled approach, whereby the ADH catalyses the desired carbonyl reduction and the oxidation of a sacrificial substrate (often IPA, which is converted to acetone). However, the reaction in both directions is highly reversible and

therefore a large excess of sacrificial alcohol (>20-fold) is required.[188] The alcohol is often described as a co-solvent; however, it can cause enzyme inhibition when used with non-solvent tolerant enzymes.[163] The ADH often achieves very high activities because the cofactor is able to remain *in situ* of the active site. This method produces large quantities of carbon-based waste that requires additional removal steps and is not considered to be overly green.

1.4.2 Glucose Dehydrogenase

The GDH cofactor regeneration system oxidises glucose to gluconic acid, which undergoes immediate irreversible hydrolysis under aqueous reaction conditions. The activity of the GDH is very high (>300 U mg^{-1}, where U represents µmol min^{-1}) and the sacrificial substrate is cheap, which has made it favourable for use in industry.[189,190] However, the sacrificial substrate is required in excess and can cause acidification of the reaction solution and again leads to large quantities of carbon-based waste.

1.4.3 Formate Dehydrogenase

The FDH cofactor regeneration system oxidises formate (sodium formate or formic acid) to a waste product of CO_2. The advantage of this system is that the waste gas product is easily removed, providing a thermodynamic driving force towards cofactor regeneration. However, the CO_2 can also lead to acidification of the reaction solution and formate is required in much higher excess (>3 Eq.) than glucose (>1.1 Eq.) in the GDH system.[188,191–193] Compounding this, is the low specific activity of FDH (~0.2 U mg^{-1}) compared with the alternative cofactor recycling systems, thereby requiring the addition of greater amounts of cofactor recycling enzyme or longer reaction times. Nonetheless, since the first use of FDH in 1980 by Shaked and Whitesides for cofactor regeneration,

it has become a widely used system.[194] Recent developments in protein engineering have demonstrated variants of FDH with improved activity, stability and solvent tolerance.

1.4.4 Phosphite Dehydrogenase

Phosphite dehydrogenase (PDH) oxidises phosphites to a phosphate waste product. It is a relatively new system that is especially useful in phosphate buffer systems, which are commonly used in biocatalysis. Advantages of using PDH include the low expense of phosphites, the favourable equilibrium and the lack of additional separation steps from the buffer system.[195] However, the PDH system achieves a poor atom efficiency and there are few examples of its use for cofactor recycling.

1.5 H_2-driven cofactor recycling

There is a family of enzymes called soluble hydrogenases (SH), which contain both a hydrogenase and an $NAD(P)^+$ reductase module, that function by coupling the oxidation of H_2 to protons and electrons, to the reduction of $NAD(P)^+$ to NAD(P)H. Over the years, hydrogenases have been well studied as catalysts for H_2-driven NADH regeneration and Lauterbach *et al.* have reviewed these findings.[196] In 2011, Ratzka *et al.* successfully demonstrated the use of a SH from *Ralstonia eutropha* for NADH regeneration by coupling it with an ADH to perform the reduction of acetophenone to (*S*)-phenylethanol.[197,198] The SH achieved a TTN of 143,600 and was compared against a FDH-formate cofactor regeneration system which only achieved a FDH TTN of 1700. However, at 25 °C, the SH displayed a half-life at maximum activity of ~10 h, which decreased even further to 1 h at temperatures above 35 °C. Mertens *et* al. demonstrated the use of a thermophile SH (*Pyrococcus furiosis hydrongenase* I) for NADPH regeneration by coupling it with a thermophile ADH to perform the reduction of acetophenone to (*S*)-phenylethanol, which was achieved with high yield and >99.5% *e.e.*

and a SH TTN of 10,000.[199] However, the process was limited by the high O_2-sensitivity of the SH, giving it a limited wider applicability. There are currently no examples of SH being used for industrial cofactor regeneration, the uptake of SH has been limited, in general, by its stability and activity. The low solubility of H_2 in aqueous medium has further hampered the use of H_2-driven cofactor regeneration in industry.

Vincent and co-workers have developed and patented a novel approach to NADH recycling that uses H_2 as a clean reductant (Figure 1-7).[200–202] The HydRegen system requires two enzymes, a hydrogenase and a NAD^+ reductase, that are co-immobilised on electronically conductive carbon particle supports. The hydrogenase is a highly efficient catalyst for H_2 oxidation, releasing two protons and two electrons. The electrons can be transferred from the hydrogenase active site into the carbon particle by a chain of iron–sulphur clusters. The NAD^+ reductase is able to use these electrons, and a proton from solution, for the selective reduction of NAD^+ to NADH. The transfer of electrons from the hydrogenase to the NAD^+ reductase is facilitated by the carbon particle; thus, carbon is acting as both an enzyme support and an electronic linker. This can be extended to H_2-driven NADH-dependent biocatalysis using an NADH-dependent enzyme for C=X bond reductions. The overall reaction is then 100% atom efficient with both electrons and protons from H_2 being incorporated into the final product. Advantageously, this heterogeneous catalyst can be easily separated from the reaction solution and reused

.

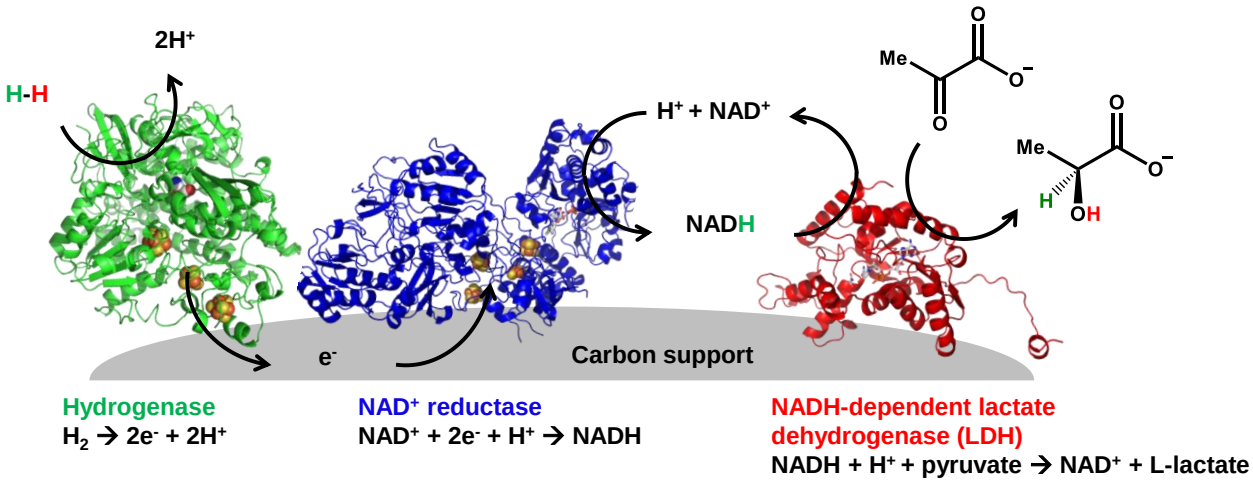


Figure 1-7: Schematic representation of the HydRegen system. A hydrogenase and NAD^+ reductase are co-immobilised on a carbon support for H_2-driven NADH recycling. This can be extended to biocatalytic hydrogenation by co-immobilising an NADH-dependent enzyme, shown here for pyruvate to L-lactate conversion by lactate dehydrogenase (LDH).

In 2012, the system was demonstrated with an initial rate of 2.2 ± 0.3 μmol min^{-1} per mg of NAD^+ reductase in the presence of H_2-saturated buffered solution containing 2 mM NAD^+.[200] Rabbit muscle lactate dehydrogenase (LDH) and pyruvate were then added to the solution and the conversion of pyruvate to lactate was monitored *in situ* using infrared spectroscopy. In 2015, Vincent and co-workers demonstrated the HydRegen system for >97% conversion to NADH after 30 min with an initial activity of 7.8 ± 0.5 μmol min^{-1} per mg NAD^+ reductase.[201] Furthermore, the parameters of the catalyst were studied and it was shown to give conversion to NADH between pH 6–8 and at H_2 pressures as low as 0.02 bar. The particles were recovered and reused, which was shown for four cycles, with an average activity of 77%. Co-immobilisation of an alcohol dehydrogenase with the cofactor recycling enzymes gave improved reaction kinetics, and showed conversion of 10 mM acetophenone to 1-(*S*)-phenylethanol with >98% conversion and >99% e.e. However, this was only demonstrated on a small scale after 21.5 h. Thus, further development would be required to increase the scale and productivity of the system towards a more industrially relevant process. Flow reactors offer a route to achieve this.

1.6 Flow chemistry

Flow chemistry is currently a topic of focus as a viable, sustainable manufacturing alternative to batch production.[203–206] A flow reactor is a device that enables the continuous performance of chemical reactions by the continuous pumping and combination of reaction mixtures through different types of reactor that can contain solid catalyst. The process meets the criteria of ten of the Twelve Principles of Green Chemistry[207], including prevention of waste, high atom economy and efficiency, reduction of derivatives (hazardous waste) and use of less hazardous syntheses. For example, the tight control of parameters such as temperature, pressure and reaction time means reactions can be designed to avoid forming unwanted by-products and synthetic steps involving protecting groups can be avoided.[206] In terms of speed and efficiency, continuous flow enables fast optimisation of reaction parameters and procedures, with features such as real time product analysis and feedback loops speeding up the intensification process. The efficiency of heat and mass transfer in flow tubes and columns is much better compared with in batch vessels, reducing energy usage, increasing conversions and decreasing run times. After scale-up, flow modules require less space and can be adapted more easily to new reactions. Overall, flow processes tend to lead to consistent product formation, which is a significant advantage in pharmaceutical manufacturing.[58]

Ley and co-workers have shown that continuous multi-step reactions are possible, with a number of flow natural product syntheses.[208] In 2006, Baxendale *et al.* demonstrated a continuous seven-step synthesis of oxomaritidine, with an overall yield of 40% and purity of 90%.[209] In 2012, Seeberger and coworkers used flow for the synthesis of the anti-malaria drug artemisinin from artemisinic acid, a previously discarded by-product from

the extraction of artemisinin from the sweet wormwood *Artemisia annua*.[210] However, this process generates multiple regioisomeric hydroperoxides in an intermediary step, only one of which can be used to synthesise the final product. In 2015, Amara *et al.* demonstrated a green continuous one-pot synthesis of artemisinin in liquid CO_2 with a dual-function heterogeneous catalyst in a fixed-bed photoreactor.[211] The porphyrin photosensitizer-Amberlyst heterogeneous catalyst elegantly achieved full conversion of dihydroartemisinic acid to artemisinin in a single pass, avoiding the generation of unusable by-products, fulfilling the first two Principles of Green Chemistry.

1.7 Biocatalysis in continuous flow

Biocatalysts have often been shown to work in continuous flow while in solution.[212] In 2014, Schmid *et al.* performed biocatalysed triphasic flow reaction using a tube-in-tube reactor (TiTR), the O_2-dependent HbpA-catalysed hydroxylation of 2-hydroxybiphenyl to 3-phenylcatechol with concurrent NADH regeneration by FDH-formate.[213] By taking advantage of the high mass transfer rates between the organic and aqueous layer that can be achieved in flow, after optimising the substrate concentration, flow velocity and phase ratio, a productivity of up to 17.7 ± 1.8 g L^{-1} h^{-1} could be achieved—this is much higher than the rate reported for the related batch process.[214] Performing biocatalysis in flow enables the collection of many more data points compared with in a batch reactor. Once a flow system has reached steady-state, each reactor volume (the system flow rate multiplied by the residence time) collected is a data point, whereas, in a batch reaction, it is common to take only an end-point. In flow, this leads to much greater information on the changing activity of the catalyst over time. However, the use of immobilised enzymes in continuous flow is more widely preferred. The downstream processes that are required to separate the enzymes from the product in solution are lengthy and costly;

immobilisation of the enzyme onto a solid support means that the fluid product medium can be easily separated by simple filtration or more ideally by loading the solid catalyst into a PBR and flowing the reaction solution through it. Another of the benefits of using immobilised enzymes in a continuous flow PBR over batch is that there is no catalyst regeneration or loss of catalyst after reuse because the catalyst can continue to be stored in the PBR, in contrast to in batch, which often required catalyst separation and regeneration. Moreover, the study of enzyme leaching from the support is very difficult in batch, which can lead to leached enzyme contributing to the conversion of the desired reaction. Whereas in continuous flow, the leached material is constantly pumped out of the reactor, the extent of leaching can be quantified and will have limited impact on the reaction conversion.

Another benefit of many continuous flow reactors is that they provide a high ratio of surface area to volume for the transfer of gaseous reagents into liquid reaction solution, which is beneficial for gas-dependent enzymes such as hydrogenases (H_2) or oxidases (O_2). This effect is particularly apparent in microreactors, which can achieve a surface-area-to-volume ratio of up to 18,000 $m^2\ m^{-3}$; however, a meso-sized PBR can achieve a surface-area-to-volume ratio of 1,700 $m^2\ m^{-3}$, which is comparable to cutting edge active agitation in batch (up to 2,000 $m^2\ m^{-3}$).

The safety of large-scale hydrogen use is traditionally a big concern with regard to large batch hydrogenation reactions, which require a very large amount of highly flammable H_2 in the system at a time to work efficiently. One key advantage that performing hydrogenations in continuous flow has over a batch system is that there is less H_2 in the system at one time due to the difference in reactor dimensions of batch production and continuous flow production. The increase in safety of a flow hydrogenation system is a

positive for its uptake in industry because their facilities could run at a lower risk level. Requiring a low but constant stream of H_2 would also open up the possibility of *in situ* H_2 generation, avoiding the risks of H_2 storage. Thus, many commercial flow hydrogenation systems have been developed.[215]

A significant challenge with biocatalysis in flow is immobilising enzymes onto a given support while maintaining a high activity when compared with the free enzyme in solution.[216] Enzyme deactivation on the support and enzyme leaching off the support are issues that must be studied and controlled. Another challenge with immobilised biocatalysis in continuous flow is that the enzymes often require the reaction to be performed in aqueous media; however, a lot of substrates and products of interest are sparingly soluble or insoluble in these media. As a result, this can lead to reactants coming out of solution and blocking parts of the reactor. Another drawback is the view that the implementation of continuous flow technology would require a considerable overhaul of the reaction infrastructure. Overall, the key to the uptake of flow biocatalysis and flow chemistry in general is to change this way of thinking by creating examples that demonstrate the benefits of the technology and overcome the existing challenges.

1.8 Continuous flow reaction design with immobilised biocatalysts

The core of each immobilised enzyme flow reactor set-up tends to be very simple, described in Figure 1-8(A). First, each reactor requires a pump: piston, syringe, peristaltic or gear pumps, which are used to drive reaction solutions and solvents through the reactor in a controlled manner. The type of pump required is chosen on the basis of the merits of the pump and the requirements of the reaction. Next, loops or mixing tubes are required. The internal diameter of the channels or tubes is chosen on the basis of the conditions of the reaction. Small-diameter tubing in microreactors (μm-scale) enables for strict

temperature control, but the mixing is limited by diffusion and the space can become easily blocked. By contrast, larger-diameter tubing in mesoreactors (>0.5 mm) has less-efficient temperature control but can handle high flow rates with low pressure drops (between different areas of tubing).

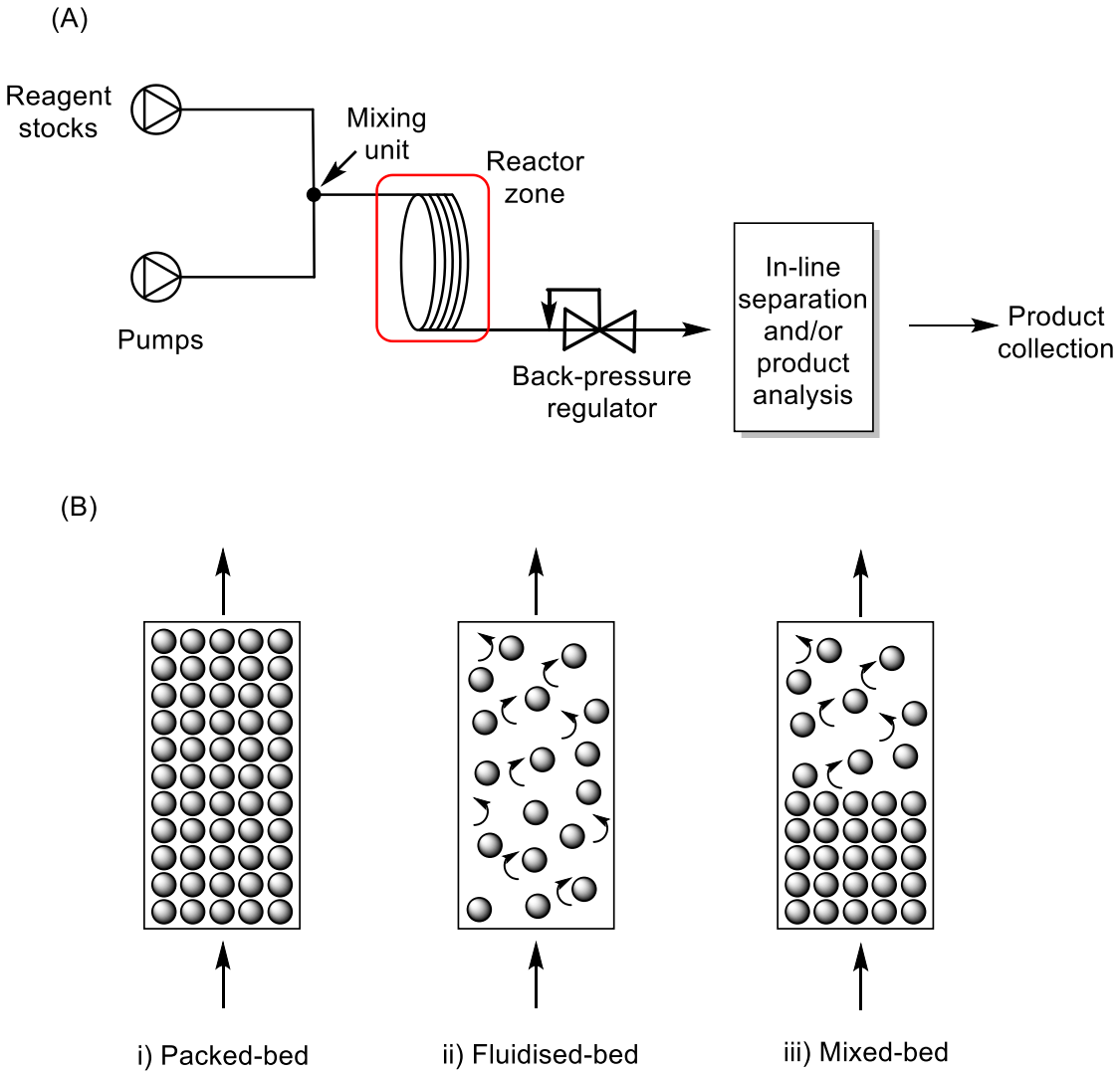


Figure 1-8: Flow reactor design. (A) Core set-up of a continuous flow reactor: (i) pumps (ii) mixing pieces (iii) reaction zone (iv) back-pressure regulators (v) in-line separation and analysis. (B) A PBR is typically loaded in three ways: (i) fully packed-bed (ii) fluidised-bed or (iii) mixed-bed reactor.

There are two typical ways that a solid catalyst such as an immobilised enzyme can be used in continuous flow. In a slurry reactor, the solid reagent and/or catalyst is mixed

with the liquid medium and continuously pumped through the tubing. The benefits of slurry include increased control over the contact time between the reagent and catalyst. More commonly used is a PBR, in which the catalyst is loaded into a column that has a frit on either end to contain the solid catalyst, while allowing liquid medium to flow through. Depending on the packing density of the solid-catalyst particles, the PBR can be referred to as packed-bed (i), fluidised-bed (ii) or mixed-bed reactor (iii), Figure 1-8(B).

Other common components of a flow set-up include mixers (for example, T-pieces or Y-pieces) and pressure regulators. The set-up can become more advanced by including additional in-line devices, such as separators and product purification devices. Analytical techniques such as ultraviolet–visible spectroscopy (UV–Vis), liquid chromatography coupled with mass spectrometry (LC–MS), gas chromatography coupled with MS (GC–MS) and bench-top nuclear magnetic resonance (NMR) may be connected in-line to provide real-time reaction monitoring.

The residence time (t_{Res}), is defined as the amount of time that one molecule of reagent takes to flow through the reactor. This can be determined using a tracer to analyse how long it takes to pass through the system or by calculating the void volume of the system. In a PBR system, it is common to refer to the total PBR volume (the volume of PBR when empty), the filled volume (the volume of the PBR filled with catalyst) and the void volume (the volume of empty space in a catalyst loaded PBR). The void volume and reactor flow rate are used to calculate the PBR t_{Res}. It is generally accepted that studies should aim to keep t_{Res} of a set-up below 1 h to maximise the benefits of continuous flow and achieve good system productivity.

As well as steady-state reaction conversion, there are a number of reaction metrics of focus for immobilised biocatalyst systems in continuous flow. Biocatalyst loading is the amount of biocatalyst (and solid support) that is added to the reactor. Specific biocatalyst activity is the enzyme activity before the process when measured free in solution. Biocatalyst activity is the enzyme activity measured at steady-state in continuous flow. The bioreactor productivity is stated as the STY and the biocatalyst productivity is the g of product formed per g of biocatalyst deployed in the continuous flow set-up. The stability of the bioreactor is also important and can be measured as biocatalyst activity or conversion over time. The *E* factor is used as a measure of the waste of the flow system.

1.9 Redox biocatalysis in flow with immobilised enzymes

There are many examples of the use immobilised enzyme catalysts in industry under batch conditions[217–219]; however there are fewer examples of the deployment of these catalysts in continuous flow. Nevertheless, in recent times, the number of examples using immobilised enzymes in continuous flow has expanded rapidly, and there are a number of very recent comprehensive reviews on this topic in the literature.[59,61,63,220–223] Despite this, the demonstration of redox biocatalysis in continuous flow set-ups remains limited. This is more complicated for redox biocatalysis in which an enzyme is required for both the chemical transformation and for cofactor recycling, which often demands a multi-enzyme immobilisation technique and support, as well as catalyst studies to determine the correct ratio of the enzymes to use for optimum activity. Different techniques and supports have been used to immobilise enzymes effectively for their use in continuous flow. Protein engineering techniques such as HaloTag[69] and histidine tagging for the immobilisation onto compatible supports have been shown. Different supports such as resins[70], agarose[71] and microbeads[72] have been shown to be effective as supports for

enzymes. These methods often lead to improved enzymatic stability and lifetime; however, many of these methods are specific for a certain enzyme or require specific modification to the enzyme, meaning that they are not applicable generally. As a result, a lot of specific research and development is required to implement a new immobilised enzyme, which can be costly in terms of time, economics and enzymatic activity when compared with the enzyme in free solution. In this section, the progress of redox biocatalysis with immobilised biocatalysts is discussed for each of the industry standard cofactor recycling systems. Then, the preliminary results with the H_2-driven cofactor recycling system in flow are introduced.

1.9.1 Immobilised GDH–glucose cofactor recycling system in continuous flow

The GDH–glucose cofactor recycling system is the most commonly deployed enzyme-coupled cofactor recycling system in the literature for immobilised biocatalysis in continuous flow.

In 2017, Dall'Oglio *et al.* immobilised GDH and a ketoreductase onto an aldehyde-activated agarose support for the reduction of a range of ketones in a PBR continuous flow set-up.[71] The immobilised enzymes displayed a 60% loss of total enzyme activity compared with the free enzymes in solution. Once more, the enzyme loading achieved was only 1.4 wt% of the supported-enzyme matrix, lowering the volumetric activity of the catalyst. Conversion of up to 60% for the reduction of a range of ketone substrates at t_{Res} of 7–180 min, with the system displaying a STY up to 0.0034 g L^{-1} h^{-1}. The system displayed steady-state conversion for 15 d and notably required 4 equivalents of glucose and up to 5 v/v% DMSO.

In 2019, Bitterwolf *et al*. displayed the reduction of broad range of ketones with a stereoselective Gre2p ketoreductase (*Saccharomyces cerevisiae*) and GDH self-assembled hydrogel loaded into a micro-PBR.[224,225] The hydrogel microreactor, tested at a flow rate of 5 μL min^{-1} (t_{Res} = 30 min), initially showed a loss of ketone reduction activity before reaching an activity plateau and achieving high substrate conversion at a STY of 13.3 g L^{-1} h^{-1} over 8 d. It was found that a sequence of up to 6 microreactors could be stacked in series to achieve good conversion at higher flow rates (up to 100 μL min^{-1}). The formation of the enzyme microgels is a lengthy process (~18 h) and requires protein modification.

In 2019, Adebar and Groger entrapped ADH into a polymer network using a superadsorber immobilisation technique for the reduction of a range of aryl-ketones in a continuous PBR.[226] The system, which pumped the GDH in solution, achieved peak conversion of acetophenone to (*R*)-phenylethanol at 63% before decreasing quickly to 24% over 6 h (t_{Res} = 1 h). The STY achieved of 7.5 g L^{-1} h^{-1} was relatively poor, along with limited enzyme stability in flow.

In 2020, Turner and co-workers demonstrated the use of his-tagged GDH and a reductive aminase (*Ajellomyces dermatitidis*) immobilised onto a EziG amber support for the enantioselective synthesis of a suite of secondary aryl-amines in a continuous PBR.[227] After computer modelling, the system was scaled up, achieving an isolated secondary amine yield of 56% over 132 h of flow, exhibiting a STY of 103 g L^{-1} h^{-1} in a t_{Res} of 1 min. However, the substrate loading was low (10 mM) considering the high loading of NAD^+ (10 mol%) and glucose (10 Eq). A follow-up experiment using 1 mol% loading of NAD^+ achieved a lower yield (44%) with a longer t_{Res}. The retention of enzyme activity after immobilisation was not stated in this work. In 2021, the system was extended to a

six-enzyme continuous cascade reaction for the synthesis of asymmetric secondary amines from an alcohol starting material. Overall, a t_{Res} between 49 and 64 min, up to 98% conversion was achieved at a STY of 8.4 g L^{-1} h^{-1}.

1.9.2 Immobilised FDH–formate cofactor recycling system in continuous flow

The FDH–formate cofactor recycling system has rarely been deployed as an enzyme-coupled cofactor recycling system for immobilised biocatalysis in continuous flow.

In 2014, Tomaszewski *et al*. reported the production of catechols using the enzymes FDH and 2-hydroxybiphenyl 3-monooxygenase in solution, with a high pressure flow TiTR.[228] The TiTR, consists of an outer tube and a gas-permeable membrane tube inside, which allows gas to pass in and out of the aqueous reaction medium; in this case, the 2-hydroxybiphenyl 3-monooxygenase was dependent on O_2. With a t_{Res} of 3– 23 min, up to 23% conversion was achieved at a peak STY of 17.7 g L^{-1} h^{-1}. As well as using the enzymes in solution, for optimum results, the system required high FDH loading and a large excess of formate, leading to high wastage.

In 2018, Velasco-Lozano *et al.* immobilised an amino acid dehydrogenase and FDH onto an agarose bead support for the synthesis of amino acids.[62] The system was shown to operate for 8 d with >50% conversion; however, the immobilised FDH retained only 13% activity when compared with the free enzyme in solution.

In 2021, Franklin *et al*. co-immobilised the his-tagged enzymes, amine dehydrogenase and FDH onto a Ni^{2+} resin for the flow production of a chiral amine in a PBR.[229] The supported biocatalysis displayed a half-life of 159 h and the system reached a STY of up to 18 g L^{-1} h^{-1}. However, the system achieved only up to 48% conversion of 20 mM substrate and required high NAD^+ loading (3 mol%) and enzyme loading. Once more,

the immobilisation process requires the use of tagged enzymes and is a lengthy process (>18 h). By contrast, the stability of the immobilised enzymes displayed in this process was an improvement on a similar system developed by Turner and co-workers in 2019, where the productivity of the system completely dropped off significantly after 6 h.[230] In this system, amine dehydrogenase and FDH were immobilised onto an EziG carrier resin for the flow production of a chiral amine in a PBR. During the 6 h of activity, the system achieved a STY of 24 g L^{-1} h^{-1} with 5 mol% NAD^+ loading and a large excess of formate (10 Eq.).

1.9.3 Immobilised ADH–IPA substrate-coupled cofactor recycling system in continuous flow

Earlier in this section, the enzyme ADH was shown to have been used in a number of immobilised enzyme-coupled cofactor regeneration systems in flow to reduce the ketone substrate. The enzyme has much less frequently been demonstrated in a substrate-coupled approach in continuous flow.

In 2015, Truppo and coworkers covalently bound ADH onto a polymer-based resin (EC-HFA) for the synthesis of a chiral alcohol precursor to the API, Aprepitant, in a continuous flow PBR.[231] Over a relatively long t_{Res} of 10 h, a 98% conversion was achieved under the optimised conditions of 10 v/v% IPA in water. Interestingly, the cofactor was bound alongside the enzyme during a 48 h immobilisation process, negating the need to deploy cofactor in the reaction solution. The system showed good stability—after being held for 7 d at 40 °C, the immobilised enzyme retained 94% of its initial activity.

In 2018, Döbber *et al*. demonstrated the immobilisation of ADH onto a HaloLink resin using the HaloTag immobilisation strategy for the continuous production of chiral

alcohols, epoxides and diols.[232,233] The immobilised ADH displayed 35% residual activity when compared to the free enzyme in solution and the immobilisation process required 90 mg of support per 1 mg of enzyme, making it somewhat inefficient. However, high conversions were achieved with a t_{Res} of 19 min. In contrast to the free enzyme in solution, the immobilised system showed good activity in IPA concentrations between 10 and 90 v/v%, demonstrating the stability of the immobilised enzyme. A 1 mol% loading of $NADP^+$ was used and, impressively, the reactions were analysed in real-time using in-line UV–Vis.

In 2020, Baumer *et al*. demonstrated the chiral reduction of acetophenone to (*R*)-phenylethanol by ADH immobilised by HaloTag in continuous flow.[234] A conversion of 92% was achieved using 50 mM substrate, 10% (v/v) 2-propanol and 4 mol% $NADP^+$ with flow rates up to 500 μL min^{-1}. Following on from this, an in-line organic/aqueous phase separator was placed into the reaction set-up and the aqueous medium containing the cofactor was recycled back into the reaction solution in a closed-loop manner (Figure 1-9). This set-up enabled a decrease in $NADP^+$ loading to 0.1 mol%. The closed-loop system was applied to a range of ketones, achieving a good STY (up to 117 g L^{-1} h^{-1}). In the longest experiment, the closed-loop system was shown to run over 32 h, without loss in biocatalyst activity, generating 1.36 g of product and achieving an impressive cofactor TTN of 12855 $mol_{product}$ $mol_{NADP+}{}^{-1}$.

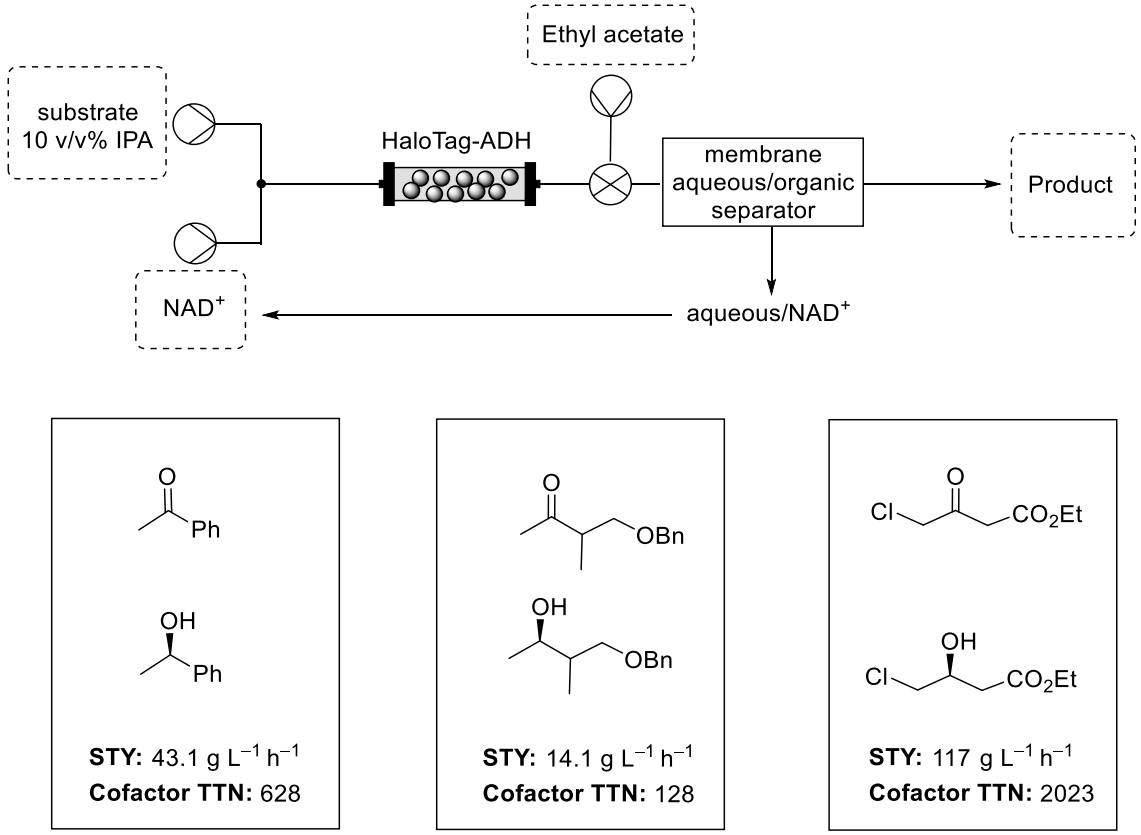


Figure 1-9: Overview of the closed-loop cofactor regeneration system developed by Baumer and coworkers for the biosynthesis of a number of chiral alcohols from ketones.[234] The set-up consists of a dual-liquid feed mixed by a *y*-piece. Channel 1 is used for the aqueous cofactor stream and channel 2 is used for the organic substrate and IPA stream. After passing over the PBR loaded with HaloTag immobilised ADH (HaloTag-ADH), the reaction solution is mixed with a third stream of ethyl acetate and pumped through a flow liquid-liquid extraction system. The aqueous/NAD^+ layer is recirculated back into the aqueous reaction solution vessel and the organic product layer is collected.

The outcomes when immobilised enzymes are deployed in flow with cofactor recycling have been shown to vary greatly. For many of the methods shown, the immobilisation technique was complex, time inefficient and requires modified enzyme and/or supports that can be costly. Furthermore, to achieve high conversions at a sensible t_{Res}, the deployment of these systems in flow can often be more wasteful than batch, requiring higher cofactor loadings, as well as a large excess of carbon-based sacrificial substrate.

1.10 H_2-driven cofactor recycling in flow

Catalytic hydrogenation reactions with metal catalysts are regularly carried out in flow reactors because of the increased performance due to the high interfacial area, enhancing the mass transfer rate in a gas–liquid system and for safety reasons concerning the use of H_2 under high pressures.[46,235] A number of commercial hydrogenation flow reactors are available, such as the H-Cube reactor (ThalesNano). The HydRegen system lends itself to implementation in a flow reactor, as all of the enzymes are immobilised on carbon and only H_2 gas is required as a reducing equivalent. This presents an opportunity to translate the HydRegen catalyst into existing flow hydrogenation technology. Two preliminary studies testing H_2-driven cofactor recycling in continuous flow have already been carried out using set-ups developed in house.

In 2017, Vincent and co-workers published a preliminary demonstration of the HydRegen system operating in semi-continuous flow with the enzymes immobilised on a carbon nanotube lined quartz column, using a H_2-saturated reaction mixture.[236] The flow system was applied to the reductive amination of pyruvate (12.5 mM) using L-alanine dehydrogenase (LAlaDH), which is known to act selectively to generate L-(*S*)-alanine using ammonium ions as the nitrogen source. Although some conversion (8%) was shown after a single pass, for higher conversion, the H_2-saturated reaction mixture was continuously cycled through the catalyst-loaded column (40%, 12 reaction solution passes, 24 h). The NAD^+ reductase enzyme displayed a peak TTN of 54,000 and the cofactor TTN achieved was poor (5 $mol_{product}\, mol_{NAD+}^{-1}$). A significant limitation of this work was the H_2 availability, demonstrating the need for an improved flow device such that high conversions can be achieved in a single pass.

More recently, Vincent and co-workers demonstrated soluble hydrogenase (SH; which contains both a hydrogenase and an NAD^+ reductase module) immobilised on a carbon nanotube lined quartz column, using a dual-feed continuous flow set-up in which the reaction solution and H_2 were pumped into the reactor separately and mixed. The flow system was applied to the generation of NADH and the reduction of a range of ketones by co-immobilising an additional NADH-dependent enzyme onto the carbon nanotube. Quantitative conversions were achieved in a single pass (t_{Res} <5 min); however, the biocatalyst system appeared to deactivate rapidly after 0.5–2 h reaction time. It was deemed that the system was limited by the stability of the immobilised SH, which displayed a peak TTN of 10,200, much lower than the NAD^+ reductase of the HydRegen system in the previous example.

In 2020, Lauterbach and co-workers immobilised SH and an NADH-dependent imine reductase onto an amberlite support in a PBR for the production of methylated N-heterocycles with H_2-driven cofactor recycling.[237] Interestingly, the H_2 required was generated by electrolysis in a reaction solution beaker and the H_2/reaction solution was recirculated through the PBR. In a scale-up experiment, over 16 h of recirculation the system was found to produce 69 mg of methylated N-heterocycle product in a 26% isolated yield, with a STY of 0.00014 g L^{-1} h^{-1}. The SH was found to achieve 10^5 TTN, however the SH immobilisation process was very inefficient with only 0.023 mg of SH immobilised per gram of support. The activity of the system was not monitored over time, so it was difficult to gauge the lifetime stability of the immobilised SH.

1.11 Aims and structure of this thesis

The aims of this project are twofold. To demonstrate the use of carbon particles as a simple and widely available biocatalyst support for the performance of continuous flow in a PBR. Next, to implement carbon-supported H_2-driven biocatalysis systems (such as HydRegen) into continuous hydrogenation reactor technology.

First, the translation of industry standard cofactor recycling systems (FDH–formate and ADH–IPA) onto the carbon particles and into flow was studied with an ultimate aim to demonstrate an alternative way to synthesise industrially relevant enantiomerically pure molecules. This also enabled the performance of the industry standard cofactor recycling systems to be benchmarked against subsequent results from the H_2-driven system.

Work on the H_2-driven cofactor recycling system in continuous flow aimed to overcome the previous limitations by studying the catalyst in greater detail and translating the technology into better-suited continuous reactor types, again to achieve the synthesis of industrially relevant enantiomerically pure molecules.

The Vincent Group has a proven track record in H_2-driven biocatalysis in batch mode; translation of this approach into flow hydrogenation reactors will establish a step-change for the implementation of biocatalysis and overcome barriers to adoption in industrial chemical synthesis.

The structure of this thesis is outlined below:

Chapter 3 discusses the application of carbon particles as a biocatalyst support for the enzymes FDH and LDH, for the continuous conversion of pyruvate to lactate in a continuous PBR with FDH–formate cofactor recycling. Optimisation studies were carried out for conversion, STY and *E* factor.

Chapter 4 seeks to extend the FDH–formate cofactor recycling flow system presented in Chapter 3 by co-immobilising a suite of different NADH-dependent enzymes onto the carbon particles alongside the FDH for the synthesis of industrially relevant molecules.

Chapters 5 and 6 discuss the application of carbon particles as a biocatalyst support for ADH enzymes, for continuous ketone reduction in a continuous PBR with substrate-coupled IPA-driven cofactor recycling. The systems were first studied in batch, comparing the performance of immobilised ADH against when free in solution, before being translated into flow. In Chapter 6, the continuous synthesis of a industrially relevant molecule is demonstrated and analysed in real-time using in-line benchtop flow NMR

Chapters 7 and 8 look to enable the effective translation the H_2-driven system into a commercially available flow reactor called the H-Cube. Initial studies focus on performing the conversion of NAD^+ to NADH, to help to determine the stability of the cofactor regeneration technique in continuous flow. Subsequently, the H_2-driven system is demonstrated for ketone reduction by the co-immobilisation of an NADH-dependent enzyme alongside the cofactor-recycling enzyme(s) onto a carbon particle support, exhibiting a viable approach to H_2-driven biocatalysis in a commercially available hydrogenation reactor.

2 General Methods and Theory

2.1 Flow Chemistry

2.1.1 Immobilised biocatalysts in packed-bed-reactors

The continuous flow reactions performed in this Thesis are all carried out with a reaction zone which consists of enzyme-modified carbon particles loaded into a PBR. For high productivity in a multi-phase (solid-liquid or solid-liquid-gas) continuous PBR, efficient mixing is required and there are broadly three different types of reactor bed. In a fully-packed-bed reactor, the entire column is loaded with solid material, meaning that solid particle movement is restricted.[46] The liquid pumped through this reactor is usually plug flow, so good mixing and high substrate/catalyst contact time can be achieved. A fluidised-bed reactor is characterised by the solid particles being free-flowing and suspended in the column by the liquid phase under turbulent flow. This allows for improved heat transfer; however, these beds are not fully understood and often a hybrid mixed bed is used instead. In a mixed-bed PBR, the solid at the bottom of the column has restricted movement, above this the solid is suspended and mixed in the flowing liquid phase.[222] Both fully packed beds and mixed beds can be easily implemented and are therefore most often used. In this Thesis the PBR set-up is mixed bed, unless stated otherwise.

With a PBR set-up for flow biocatalysis there are multiple ways to design the reaction column. Most simply, the free enzyme and substrate can be pumped through the PBR and separated by membrane filtration. Alternatively, an enzyme-modified support can be loaded into the PBR – this can be achieved by: enzyme-modified particles or beads, immobilising enzyme onto the surface of the column, immobilising enzymes onto monolith surfaces inside the column or by using a membrane immobilised enzyme. Each

have their benefits. In an immobilised biocatalyst PBR system, the rate of reaction can be largely impacted by mass transfer limitations, when compared to the activity of the free enzyme in solution.[45] There are two types of mass transfer in an immobilised biocatalyst PBR system. The external mass transfer entails the convection and fluid dynamics in the PBR as the substrate is transferred to the immobilisation matrix. The internal mass transfer is the diffusion of the substrate from the matrix to the biocatalyst active site. The degree of mass transfer limitation can be evaluated using an internal effectiveness factor, which is the ratio of observed immobilised biocatalyst reaction rate against the reaction rate without internal mass transfer limitation (free enzyme in solution).[223] This Thesis studies enzyme immobilisation onto carbon particles because enzyme-modified particles or beads are the type of support that achieve an improved internal effectiveness factor because these systems benefit from good mixing and the high total surface area of immobilised matrix.[221,222] A number of other factors have to be considered such as tortuosity and porosity in the immobilised matrix. In general, the activity of an immobilised biocatalyst PBR system can be improved by increasing the amount of immobilisation matrix in the system or by increasing the volume of the reactor.

2.1.2 Residence time and PBRs

The t_{Res} is the time it takes the reagent to go through the 'reaction zone' (reaction time). In this Thesis, it was calculated as follows:

$$t_{\mathrm{Res}} = \frac{Void\ reactor\ volume\ (mL)}{Flow\ rate\ (mL\ min^{-1})} \qquad [2\text{-}1]$$

Where the void reactor volume (total reactor volume minus the filled reactor volume) was calculated by the void fraction method,[238] where the void reactor volume is the total reactor volume minus the space occupied by the catalyst (filled reactor volume), calculated by the difference in column mass before and after priming the catalyst loaded PBR with water or aqueous buffer.

In this Thesis, three types of PBR were used: a glass Omnifit adjustable column (Kenesis, 6.6 mm i.d., variable bed length), a stainless-steel H-Cube CatCart (ThalesNano, 30 mm, length, reactor volume = 300 µL), in-house stainless-steel PBR (reactor volume = 700 µL). The PBR catalyst loading procedure for each type of PBR is described in the chapter in which it is used.

2.1.3 Additional flow equipment

Three different pumps are used throughout this Thesis. In Chapters 3 and 4 a syringe pump (Asia, Syrris) was used with a flow rate range of 1–250 µL min^{-1}. This pump had the benefit of very accurate and precise flow rate control; however, it could not pump gases or solids and could not pump at reactor pressure over 2 bar. In Chapters 4–7 a peristaltic pump (Vapourtec SF-10) was used with a flow rate range of 0.02–10 mL min^{-1}. The peristaltic pump could pump solid, liquid and gas, at reactor pressures of up to 10 bar and was used for its durability and versatility. In chapter 6 and 7 when using the H-Cube a piston HPLC pump (Knauer H-Cube) was used with a flow rate range of 0.1–3 mL min^{-1}, it could operate at reactor pressures >100 bar, making it suitable for the flow experiments which required elevated reactor pressures. Unless stated otherwise,

the components used in the experiments were PTFE tubing (0.5 mm ID) and ¼-28 PTFE flangeless fittings supplied by Kinesis. Samples were collected at the reactor outlet into microcentrifuge tubes (1.5 mL, Eppendorf) using a BioRad Model 2110 Fraction Collector.

2.2 Ultraviolet-visible spectroscopy

Ultraviolet-visible spectroscopy (UV-Vis) was used to determine NAD(P)H and $NAD(P)^+$ concentration in solution. This method of spectroscopy measures the absorbance of light in the UV-Vis region (200–800 nm). The absorption of energy in this wavelength region relates to the transition of electrons from an occupied (HOMO) to an unoccupied (LUMO) bonding orbital. The excitation energy required corresponds to the electronic transition, shown in order of decreasing energy:

$$\sigma \rightarrow \sigma* > n \rightarrow \sigma* > \pi \rightarrow \pi* > n \rightarrow \pi* \qquad [2\text{-}2]$$

UV-Vis is a valuable technique for studying molecules that contain conjugated systems and aromatic rings, where the transitions $\pi \rightarrow \pi^*$ and $n \rightarrow \pi^*$ are often in the UV-Vis region.

The structure of the cofactor NAD^+/1,4-NADH (NADH) contains an adenine and nicotinamide ring, which are connected by two phosphate groups. A $\pi \rightarrow \pi^*$ electron transition in the adenine ring of both NAD^+ and NADH causes an absorbance with a λ_{max} = 260 nm. The NADH can be distinguished from NAD^+ by the presence of absorbance at λ_{max} = 340 nm, caused by a $n \rightarrow \pi^*$ transition in the NADH which involves the non-bonding nitrogen electrons and the carboxyamide group (described in Figure 2-1).

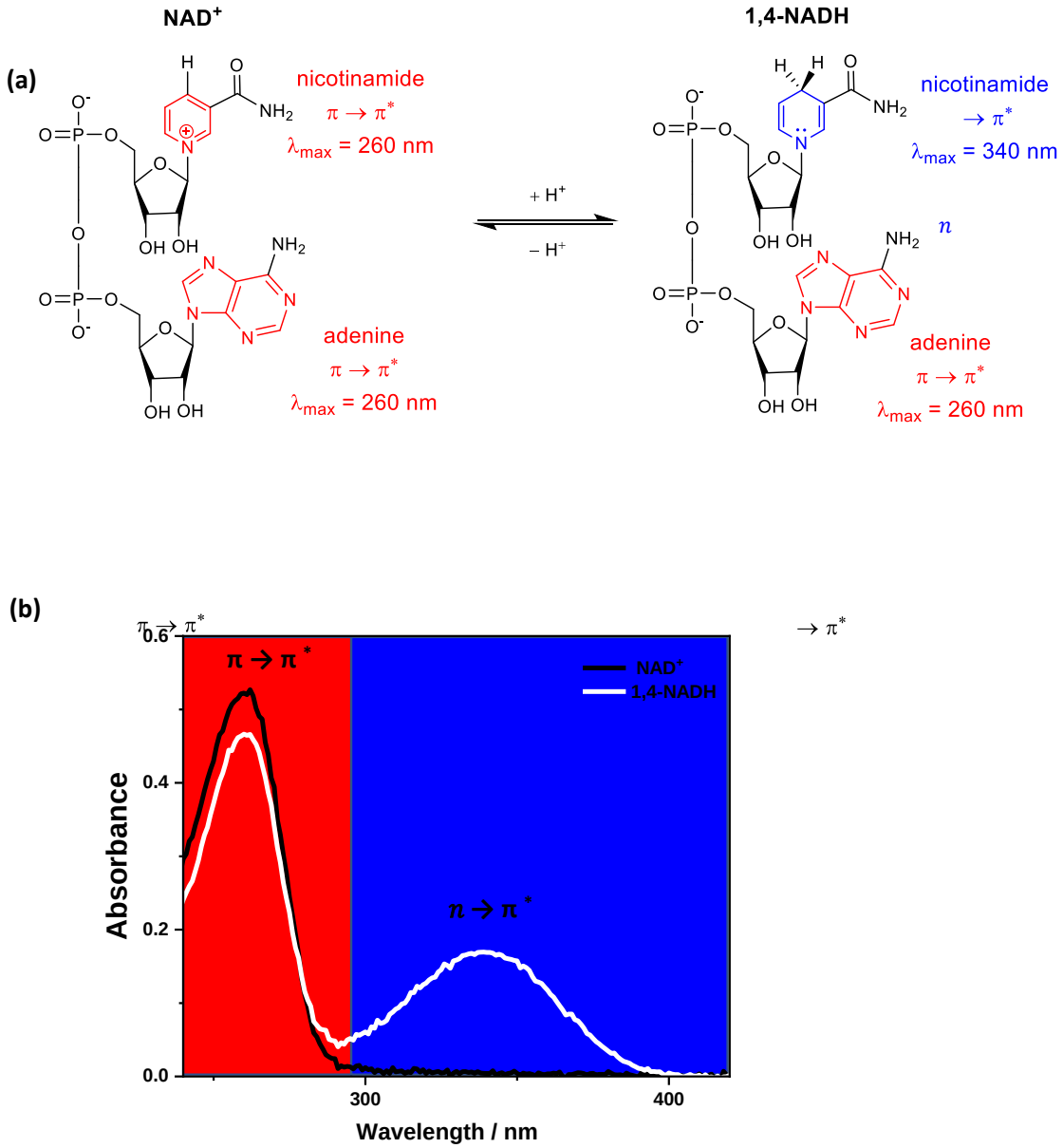


Figure 2-1: The UV-Vis activity of the cofactors NAD^+ and 1,4-NADH. (a) The adenine ring and the oxidised nicotinamide ring show absorbance at 260 nm due to a $\pi \rightarrow \pi^*$ transition (highlighted in red). With the addition of two electrons , the reduced nicotinamide ring shows absorbance at 340 nm due to a $n \rightarrow \pi^*$ transition (highlighted in blue). (b) Standard UV-Vis spectra of NAD^+ and NADH, determined in the laboratory.

In this work, UV-Vis was regularly used to determine the concentration of NADH or the concentration ratio of NAD^+ and NADH.

2.2.1 Determination of concentration using UV-Vis

The concentration of NAD^+ and NADH can be determined from UV-Vis using the Beer-Lambert law, shown below.

$$A = \varepsilon c l \qquad [2\text{-}3]$$

From this equation, the absorbance (A), extinction coefficient (ε) and path length (l) at a particular wavelength can be used to determine the concentration (c). The literature values for the extinction coefficient of NAD^+ at 260 nm and NADH at 260 nm and 340 nm are shown in Table 2-1.

Table 2-1: Literature molar extinction coefficient values for NAD^+ and NAD^+.[239]

Molecule	**λ_{max} / nm**	**ε / mM^{-1} cm^{-1}**
NADH (adenine ring)	260	14.1
NADH (nicotinamide ring)	340	6.22
NAD^+ (adenine and nicotinamide ring)	260	17.4

Interconversion between NAD^+ and NADH can also be studied with UV-Vis spectroscopy by comparing the ratio of the absorbance peaks at 340 nm and 260 nm (using previously described calibration curve of $[NAD^+]/[NADH]$ *vs* $A_{260\ nm} / A_{340\ nm}$).[201] This method was used when studying systems where the total cofactor concentration did not remain constant, for example when reaction samples were diluted or cofactor was adsorbed onto carbon nanoparticles. The NAD^+ and NADH concentration can also be determined, assuming that the initial concentration of cofactor has stayed constant.

In general, the buffers used in experiments throughout display absorbance below ~220 nm, therefore before experiments a baseline spectrum was measured using the buffer medium only (for example, Tris-HCl) and was automatically subtracted from the sample spectra. For the experiments which involve the enzyme immobilised on carbon, consistent light scattering was observed across the entire wavelength range, therefore a baseline correction was applied, using the absorbance at 500 nm (which is outside the range of cofactor absorption), before further data analysis.

The UV-Vis spectrometer used for all experiments is a Cary 60 (Agilent), with a holder (Agilent) for a UV-Vis cuvette (Hellma, 1 mL) with a defined path length of 1 cm. The maximum absorbance (A) that can be detected using this UV-Vis spectrometer is ± 4 A, including buffer contributions. For *ex situ* experiment samples with high cofactor concentrations, the samples would be diluted before being measured by UV-Vis, so that the absorbance at 260/340 would be within the detection limits.

To calculate enzyme specific activity, A graph of cofactor conversion (calculated using Beer-Lambert Law or ratio of cofactor technique) against time was plotted for each experiment. The gradient of the slope in the initial high activity region was used to calculate the specific activity of the free or immobilised enzyme (U mg_{enzyme}^{-1}, U = µmol min^{-1}). Unless stated otherwise, for *in situ* enzyme activity assays performed in the UV-Vis spectrometer, the reaction was monitored over 15 minutes with a cycle time of 0.5 minutes.

2.2.2 Protein concentration calibration curves

For enzyme immobilisation efficiency and enzyme leaching from carbon studies in this Thesis, a quick and accurate method of measuring the concentration of each enzyme in solution was required. Proteins are known to display absorbance at 280 nm due to the

presence of aromatic amino acids. Therefore, for each enzyme studied a protein concentration calibration curve was produced. Each enzyme was suspended in Tris-HCl buffer (50 mM, pH 8.0) to produce samples with a range of protein concentrations. The samples were analysed by UV-Vis using absorbance at 280 nm, to generate a plot of protein concentration *versus* A_{280nm} (see Appendix G). The protein concentration range studied for each calibration curve was within a useful range for the experiments detailed in this Thesis.

The protein concentration in unknown reaction samples was calculated using the gradient and intercept of the line of fit from the calibration curves, according to:

$$Abs_{280nm} = Intercept + (Gradient \times Protein\ concentration) \qquad [2\text{-}3]$$

$$Protein\ concentration = \frac{Abs_{280nm} - Intercept}{Gradient} \qquad [2\text{-}4]$$

2.3 Gas chromatography

Gas chromatography, GC is an analytical technique used to characterise the products formed in a reaction and to determine the reaction conversion from starting material to product. With a chiral GC column, the enantioselectivity of the desired product can also be determined.

The identification of compounds formed experimentally was elucidated by comparison with the retention times of pure commercial standards (see Appendix B).

In GC, a sample of reaction mixture or a compound standard is injected into an oven where it is vaporized and mixed with a carrier gas, which is subsequently passed through a stationary liquid phase column. The retention time of a compound, when using a chiral column with a chiral stationary phase is dependent on three factors: volatility, chirality, and stationary phase affinity.

The sample (200 µL) was removed from the reaction and placed in a microcentrifuge tube (Eppendorf) with ethyl acetate (400 µL, 2 mM undecane internal standard) and centrifuged (Eppendorf, MiniSpin Plus, 2 min, 10000 x *g*). A 100 µL aliquot of the organic layer was dried over anhydrous Na_2SO_4 and then placed into an inert glass vial for analysis.

For many of the starting materials and products analysed by GC, the 2 mM undecane internal standard was used to create compound concentration calibration curves from which the percentage reaction conversion could then be calculated (see Appendix C). For some compounds this was not possible and the ratio of peak area was used to determine the reaction conversion.

GC was performed on a ThermoScientific Trace 1300 equipped with a flame ionisation detector (FID), using the following conditions:

Column: CP-Chirasil-Dex CB 0.25 mm × 25 m, film thickness 0.25 µm

Inlet: Temperature: 200 °C, split flow: 60 mL/min , splitless time 0.8 min, purge flow 5 mL/min, injection volume: 0.1 µL.

Carrier gas: He (CP grade) constant pressure 170 kPa.

Oven program: Initial temp = 70 °C, hold for 5 mins, heat at 10 °C/min to 165 °C, heat at 50 °C/min to 200 °C, hold at 200 °C for 5 mins.

Detector: FID, temperature = 250 °C.

2.4 Nuclear magnetic resonance spectroscopy

Nuclear magnetic resonance spectroscopy, NMR, was used to determine the biocatalytic conversion of pyruvate to lactate throughout. A reaction sample (500 µL) was placed in a microcentrifuge tube and mixed with D_2O (100 µL) on a vortex mixer. The sample was then transferred into an NMR tube (Norell) and analysed by NMR. The instrument used was a Bruker AVIIIHD 400 nanobay, equipped with 5 mm z-gradient broad-band multinuclear probe, 60-position SampleExpress robotic sample changer and controlled with TOPSPIN 3 software. To suppress the dominant H_2O signal from the aqueous samples, a standard water suppression presaturation technique was deployed using the Bruker noesygppr1d sequence.

2.5 In-line benchtop flow NMR

In-line benchtop flow NMR was used to analyse the biocatalytic conversion of ketone to alcohol in real-time. The in-line benchtop was connected in series with the flow experiment after the PBR column. This was possible by using an NMR flow cell which could be placed through the benchtop NMR spectrometer. The instrument used was a Magritek Spinsolve 43 (43 MHz proton), equipped with hardware lock (does not require deuterated solvents), permanent and cryogen free magnet, stray field <2 G and controlled with Spinsolve software.

2.6 High performance liquid chromatography

High-performance liquid chromatography, HPLC was used to determine the conversion of substrate and product after biocatalytic chemical synthesis. This technique enables quantitative characterisation of each component in a mixture by comparison to known standards (see Appendix D). The component molecules are separated based on their affinity for a mobile and stationary phase. The reaction sample was placed in a microcentrifuge tube with acetonitrile (20 v/v%) and centrifuged (Eppendorf, MiniSpin Plus, 2 min, 14000 x *g*). A 100 µL aliquot was analysed placed in an inert glass vial and analysed by HPLC. The column used was a Chromolith Performance, 100-3 mm column (Merck). A Shimadzu Prominence HPLC equipped with a CBM-20 system controller, LC-20AD superior solvent delivery system, SIL-20A high-throughput autosampler, CTO-10AS column oven and SPD-20A UV-Vis absorbance detector was used running on LabSolutions software. The mobile phase was a mixture of 80 % water and 20 % acetonitrile running at 1 mL min^{-1}, the column was maintained at a temperature of 40 °C. The absorbance at 210 nm and 260 nm was recorded to enable detection of substrate and product.

2.7 Enzyme samples

2.7.1 NAD^+-reducing enzymes

There are two NAD^+ reducing enzymes used in this Thesis for the biocatalytic reduction of NAD^+. Both were prepared and purified in-house by Dr Miguel Ramirez from the Vincent group, according to a published protocol.[240] The first is soluble hydrogenase (SH), from *Ralstonia eutropha* (*R. eutropha*). The second is a construct of the SH, referred to in this Thesis as I64A, which has an inactive hydrogenase module because of a single amino acid substitution (I64A). Both enzymes were handled and used in aerobic conditions.

2.7.2 Hydrogenase enzymes

The hydrogenase enzyme used in this Thesis, *Escherichia coli* (*E. coli*) hydrogenase 1 (Hyd1) was prepared and purified in-house by Dr Miguel Ramirez from the Vincent group, according to established procedures. The enzyme was handled and used without strictly anaerobic conditions (no glovebox required).

2.7.3 Cofactor-dependent enzymes

The enzymes used in this work L-Lactate dehydrogenase (LDH, from rabbit muscle, Sigma Aldrich), formate dehydrogenase (FDH, Johnson Matthey), alcohol dehydrogenase 19, 21, 61, 101 and 105 (ADH-19, ADH-21, ADH-61, ADH-101, ADH-105, Johnson Matthey), KRED-101-NADH (Codexis), KRED (Codexis) are all commercially available and used without further purification. The alcohol dehydrogenase used in Chapter 6, referred to as ADH-1001 in this work, is manufactured in-house by Dr Reddy's Laboratories and is not commercially available. It was used without further purification.

2.7.4 Immobilising enzymes onto carbon particles

It has been found that the activity of enzymes immobilised onto carbon particles can vary greatly depending on the specific surface morphology, surface area, and the 'graphitic' nature of the carbon materials.[241] In this Thesis, multiple different types of carbon particle are studied. The Black Pearls 2000 (BP2000, Cabot Corporation) were prepared by firstly sonicating a 20 mg mL^{-1} suspension of the BP2000 in the desired reaction buffer for a minimum of 60 min. During this, the BP2000 suspension was agitated by vortex mixer every 30 min, until the BP2000 was evenly distributed throughout. The BP2000 was then ready to be used as a biocatalyst support. The Activated Charcoal (60–100 mesh, Sigma Aldrich), Aquasorb carbon particles (SpinChem, 20–50 mesh, mm scale), Norit A Supra (Sigma Aldrich), Norit C Extra (Sigma Aldrich), Norit SX Plus (Sigma Aldrich), Norit

CN 1 (Sigma Aldrich) and Acros organic activated charcoal (Sigma Aldrich) were used as supplied without any further preparation, unless stated otherwise. The enzyme immobilisation procedure for each type of carbon particle is described in the experimental section of the chapter in which it is used. The precise quantity of enzyme and carbon particles used for each experiment is detailed in the relevant results chapters.

2.8 Chemicals and buffers

2.8.1 Buffers

All of the biocatalytic redox experiments in this Thesis were performed in buffered solutions or ultrapure Milli-Q H_2O (resistivity 18.2 MΩ cm). A buffer acts to maintain the pH of a solution within a known range, as a consequence of a change in concentration of protons that occurs during redox reactions. Buffer systems tend to be effective in a pH range ± 1 of the pk_a. Two organic buffers are used in this Thesis (shown in Table 2-2), a large number of experiments are performed with Tris-HCl at pH 8 and some experiments are performed with potassium phosphate buffer solution at pH 6 or 7.

Table 2-2: Buffers used in this Thesis are shown with their pKa values (at 25 °C) and buffer ranges.

pH	Buffer	pK_a at 25 °C	Buffer Range / pH
8	Tris-HCl	8.1	7.0 – 9.0
6 – 7	Potassium phosphate	6.8 – 7.2	5.8 – 8

The Tris-HCl was prepared by dissolving an appropriate mass of Trizma (Sigma-Aldrich) in MilliQ H_2O to produce the required concentration (12.5–50 mM). The buffer solution

was subsequently titrated using conc. HCl to pH 8 using a Ag/AgCl pH electrode (Fisher) at the required experimental temperature.

The potassium phosphate buffer solution was prepared by dissolving an appropriate mass of K_2HPO_4 (Sigma-Aldrich) and KH_2PO_4 (Sigma-Aldrich) in MilliQ H_2O to produce the required concentration (50 mM) and pH.

2.8.2 Cofactors

The cofactors used in this thesis (NAD^+, NADH, $NADP^+$ and NADPH) were all purchased from Prozomix and made up freshly to 10 mM or 100 mM stocks in the appropriate reaction buffer when required. It is known that commercially available cofactors tend to contain impurities such as adenosine diphosphate, adenosine triphosphate or oxidised cofactor in the reduced cofactor etc. However, these impurities in the cofactors have been found by Vincent group to only affect the I64A or SH activity by <1% at the concentrations that they are used in this Thesis.

2.8.3 Other reagents

The starting materials and products for the experiments performed in this Thesis: pyruvate, lactate, acetophenone, phenylethanol, 2-chloro-1-(3,4-difluorophenyl)ethan-1-one, 1,2-difluorobenzene, aluminium chloride, chloroacetyl chloride, 1-(3,5-bis(trifluoromethyl)phenyl)ethan-1-one, ethyl 4-chloroacetoacetate, ethyl 4-chloro-3-hydroxybutanoate, 3-quinuclidinone, (*R*)-3-quinuclidinol and 1-(5-pyrimidinyl)ethenone were all purchased from Sigma-Aldrich and used directly as provided. Stock solutions of these substrates were made freshly when required in the appropriate buffer or solvent.

2.9 General Procedures

2.9.1 Biocataltyic ADH-IPA driven NADH generation in batch, for Chapters 5 and 6

For the biocatalytic ADH-IPA driven NADH experiments in homogeneous batch conditions: a specified amount of the appropriate ADH was added to a 1 mL solution of $NAD(P)^+$ (0.1 mM) and IPA (1–40 % v/v) in Tris-HCl (50 mM, pH 8.0) in a quartz cuvette (Hellma). The reaction was monitored for NADH generation using *in situ* UV-Vis.

For the biocatalytic ADH-IPA driven NADH experiments in heterogeneous batch conditions: to a microcentrifuge tube (1.5 mL) containing the appropriate amount of the specified ADH immobilised onto activated charcoal a 1 mL solution of $NAD(P)^+$ (5 mM) and IPA (1–40 % v/v) in Tris-HCl (50 mM, pH 8.0) was added. The reaction was agitated on a vortex mixer and placed on a shaker plate (Eppendorf, ThermoMixer C, 30 °C, 800 RPM) for the specified duration of the experiment. At regular time intervals a 20 µL reaction sample was removed, diluted fifty-fold in Tris-HCl (50 mM, pH 8.0) and monitored for NADH generation by UV-Vis.

2.9.2 Biocataltyic ADH-driven ketone reduction in batch for Chapters 5 and 6

For the 1 mL scale biocatalytic ketone reduction experiments in homogeneous batch conditions: the appropriate amount of the specified ADH in Tris-HCl (50 mM, pH 8.0) was added to a solution containing ketone substrate (10 mM), NAD(P)H (12 mM) and when specified DMSO (1 v/v%) in Tris-HCl (50 mM, pH 8.0) in a microcentrifuge tube (1.5 mL). The reaction was agitated on a vortex mixer and placed on a shaker plate (Eppendorf, ThermoMixer C, 30 °C, 800 RPM) for the specified duration of the experiment. Reaction samples were extracted and analysed by GC, following the procedure describe in Section 2.3.

For the 1 mL scale biocatalytic ketone reduction experiments in heterogeneous batch conditions: to a microcentrifuge tube (1.5 mL) containing the appropriate amount of the specified ADH immobilised onto activated charcoal, a 1 mL solution of ketone substrate (10 mM), NAD(P)H (12 mM) and when specified DMSO (1 v/v%) in Tris-HCl (50 mM, pH 8.0) was added. The reaction was agitated on a vortex mixer and placed on a shaker plate (Eppendorf, ThermoMixer C, 30 °C, 800 RPM) for the specified duration of the experiment. Reaction samples were extracted and analysed by GC, following the procedure described in Section 2.3.

2.9.3 Biocatalytic ketone reduction with ADH-IPA driven cofactor recycling in batch for Chapters 5 and 6

For the 1 mL scale full cycle biocatalytic ketone reduction with ADH-IPA cofactor recycling experiments in homogeneous batch conditions: the appropriate amount of the specified ADH in Tris-HCl (50 mM, pH 8.0) was added to a solution containing ketone substrate (50 mM), NAD(P)H (5 mM) and IPA (1–40 v/v%) in Tris-HCl (50 mM, pH 8.0) in a microcentrifuge tube (1.5 mL). The reaction was agitated on a vortex mixer and placed on a shaker plate (Eppendorf, ThermoMixer C, 30 °C, 800 RPM) for the specified duration of the experiment. Reaction samples were extracted and analysed by GC, following the procedure described in Section 2.3.

For the 1 mL scale full cycle biocatalytic ketone reduction with ADH-IPA cofactor recycling experiments in heterogeneous batch conditions: to a microcentrifuge tube (1.5 mL) containing the appropriate amount of the specified ADH immobilised onto activated charcoal (prepared as described in Section 4.2.8), a 1 mL solution of ketone substrate (50 mM), NAD(P)H (5 mM) and IPA (5–20 v/v%) in Tris-HCl (50 mM, pH 8.0) was added. The reaction was agitated on a vortex mixer and placed on a shaker plate (Eppendorf,

ThermoMixer C, 30 °C, 800 RPM) for the specified duration of the experiment. Reaction samples were extracted and analysed by GC, following the procedure described in Section 2.3.

2.9.4 Continuous flow ketone reduction reaction conditions for Chapters 5 and 6

Unless specified otherwise, all flow reactions in this Chapter were performed in an Omnifit adjustable PBR with a total bed volume of 500 μL. The ADH-modified activated charcoal particles were suspended in reaction buffer (200 μL) and then transferred into the PBR, followed by glass beads (1 mm diameter). Before sealing the PBR, cotton wool was added to the top of the column, to act as a frit. The reaction solution was pumped through the column using a peristaltic pump (Vapourtec SF-10) at a flow rate of 25 μL min^{-1}, to give a t_{Res} of 12 min. The reaction samples were collected into microcentrifuge tubes using a BioRad model 2110 fraction collector. The fractions were analysed by the stated technique, depending on the experiment.

2.9.5 General procedure for the specific activity of SH free in solution in batch for Chapters 7 and 8

To determine the specific activity of SH in solution for the conversion of NAD^+ to NADH, SH (0.1 μL, 0.0008–0.004 mg) were added to a UV-Vis cuvette containing a 1000 μL solution of NAD^+ (1 mM) in Tris-HCl buffer (50 mM, pH 8.0). The UV-Vis absorption (A_{340}) was measured at 1 min intervals, between intervals a regular stream of H_2 gas (5 mL min^{-1}) was supplied into the UV-Vis cuvette, the stream of H_2 provided sufficient mixing of the solution. The experiment was performed in aerobic conditions.

2.9.6 General procedure for the specific activity of SH immobilised onto carbon in batch for Chapters 7 and 8

To determine the specific activity of SH when immobilised onto activated charcoal, for the conversion of NAD^+ to NADH, SH (1 µL, 0.008–0.04 mg) was immobilised onto activated charcoal (1 mg) following the procedure outlined in Section 4.2.8. The enzyme-modified carbon particles were transferred with a solution of Tris-HCl buffer (990 µL, 50 mM, pH 8.0) to a UV-Vis cuvette. The study commenced on the addition of a solution 10 µL solution of NAD^+ (1 mM) and Tris-HCl buffer (50 mM, pH 8.0) to the UV-Vis cuvette. The UV-Vis absorption spectrum (200–800 nm) was measured at 30 s intervals, between intervals a regular stream of H_2 gas (5 mL min^{-1}) was supplied into the UV-Vis cuvette. The experiment was not performed under strictly anaerobic conditions.

2.9.7 General preparation of CatCart biocatalyst cartridges for H-Cube reactor experiments in Chapters 7 and 8

In this chapter an activated charcoal (Darco −100 mesh, Sigma Aldrich) carbon particle was used. The enzymes were removed from cold storage before use (−20 °C or −80 °C) and stored in a cold box. Solid enzymes were suspended in Tris-HCl buffer (50 mM, pH 8.0) to the required concentration. When using multiple enzymes, they were pre-mixed to the desired ratio. Biocatalytic cartridges were prepared by two different methods: (A) A CatCart cartridge (30 mm x 4 mm) was pre-packed with activated charcoal using a cartridge packer (ThalesNano). For enzyme immobilization, the required mixture of enzymes was manually syringed into the cartridge, which was then stored at 4 °C for 1 h. After 1 h, the column was installed in the H-Cube and was flushed with Tris-HCl buffer (50 mM, pH 8.0) to remove any un-adsorbed enzymes. (B) A CatCart cartridge was filled with activated charcoal and the required mixture of enzymes was then added into the cartridge. The cartridge was sealed using the cartridge packer, and the cartridge agitated on a vortex mixer and then stored at 4 °C for 1 h. After 1 h, the column

was installed in the H-Cube and was flushed with Tris-HCl buffer (50 mM, pH 8.0) to remove any un-adsorbed enzymes.

2.9.8 General procedure for H_2-powered biocatalytic cofactor reduction in the H-Cube flow reactor for Chapters 7 and 8

With a sealed CatCart biocatalyst cartridge installed in the H-Cube reactor, a liquid feed (Knauer H-Cube piston pump) containing NAD^+ (1–5 mM) in Tris-HCl (50 mM, pH 8.0) was pumped through the H-Cube with the H_2 that was (A) generated by the built-in electrolyser (gas feed flow rate was set to 7–12 mL min^{-1}); or (B) from a pure H_2 cylinder pumped in by a peristaltic pump (Vapourtec SF 10) at a gas feed flow rate 0.6–1.2 mL min^{-1} and mixing with H-Cube pump liquid solution at a Y-piece before entering the H-Cube reactor. The liquid feed flow rate was set to the stated flow rate to give the desired t_{Res} through the CatCart biocatalyst cartridge. Reactions were performed at the specified temperature and samples were collected using a fraction collector (BioRad 2110) at the specified time intervals. The biocatalytic generation of NADH was analysed by UV-Vis.

2.9.9 General procedure for H_2-powered biocatalytic ketone reduction in the H-Cube flow reactor for Chapters 7 and 8

Unless stated otherwise: with a sealed CatCart biocatalyst cartridge installed in the H-Cube reactor, a liquid feed (Knauer H-Cube piston pump) containing ketone (10–30 mM), NAD^+ (1 mM) in Tris-HCl (50 mM, pH 8.0) was pumped through the H-Cube with the H_2 that was (A) generated by the built-in electrolyser (gas feed flow rate was set to 7–12 mL min^{-1}); or (B) from a pure H_2 cylinder pumped in by a peristaltic pump (Vapourtec SF 10) at a gas feed flow rate 0.6–1.2 mL min^{-1} and mixing with H-Cube pump liquid solution at a Y-piece before entering the H-Cube reactor. The liquid feed flow rate was set to the specified flow rate to give the desired t_{Res} through the CatCart biocatalyst cartridge. Reactions were performed at the specified temperature and samples

were collected using a fraction collector (BioRad 2110) at the specified time intervals. The reactions were analysed using NMR or GC, as specified.

3 Immobilising FDH and LDH onto carbon for biocatalysis with cofactor recycling in continuous flow

The work presented in this Chapter was published in a special issue 'Flow Chemistry Enabling Efficient Synthesis': Poznansky et al., Org. Process. Res. Dev., 2020, 24, 10, 2281–2287.

Carbon has become the almost universal support for heterogeneous transition-metal nanoparticle catalysis in batch and flow.[140,242–244] By contrast, examples of carbon being used as a support for biocatalysis are limited. Carbon has been demonstrated as a practical enzyme support that can also facilitate electron transfer between enzymes, and the system has been proven in batch.[201,245] However, much less research has been carried out on the use of carbon as a biocatalytic support in flow, and this would present an opportunity to perform biocatalysis using industry standard flow equipment due to the similarity of enzyme-modified carbon with carbon-supported metal catalysts that are used in flow. This would enable benefits such as being able to directly compare biocatalysis with traditional transition-metal catalysis. Furthermore, this could also lead to easier and wider adoption of the technology if it were to prove successful.

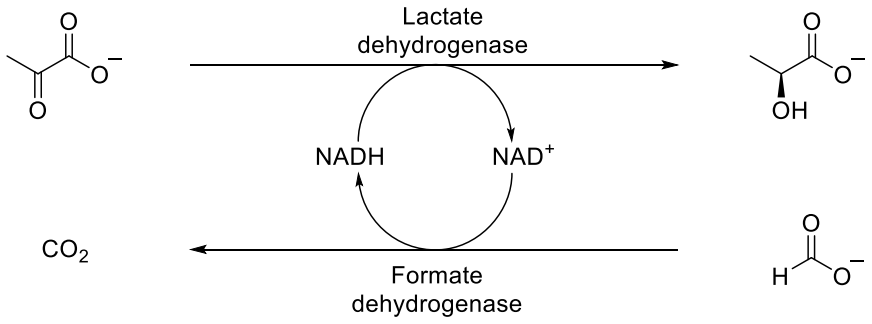
This chapter explores the use of carbon as a cheap and commercially available support for the one-step immobilisation of formate dehydrogenase (FDH) and lactate dehydrogenase (LDH) to demonstrate the biocatalytic reduction of pyruvate to lactate in a continuous packed-bed flow reactor with cofactor recycling driven by the FDH–formate system.

3.1.1 NADH-dependent biocatalytic pyruvate reduction

As guided by the Industrial partner, Dr Reddy's Laboratories, initial experiments focused on the conversion of pyruvate to lactate by the NADH-dependent enzyme lactate dehydrogenase (LDH), Scheme 3-1. This is due to the simplicity of the reaction, ease of analysis, low cost of pyruvate and generation of a chiral product. This makes it ideal for completing a large amount of optimisation studies. Furthermore, as a NADH-dependent process, it would serve as a model reaction for other NADH-dependent processes.

The LDH is NADH-dependent and therefore a cofactor recycling system is required. FDH regenerates NAD^+ to NADH by the conversion of formate to CO_2 (Scheme 3-1), which, compared to the commonly used GDH and glucose cofactor recycling system, generates less waste by mass. The rare examples of immobilised FDH in the literature have lengthy immobilisation processes and require a non-commercial enzyme support or further FDH engineering to aid immobilisation.[69–72] In this work, the immobilisation by simple adsorption onto carbon overcomes these issues.

Scheme 3-1. NADH-dependent biocatalytic conversion of pyruvate to lactate, using formate dehydrogenase for cofactor recycling.



3.1.2 Product analysis

Interconversion between NAD^+ and NADH was studied under UV-Vis spectroscopy by comparing the ratio of the absorbance peaks at 340 nm and 260 nm (using previously

described calibration curves).[201] The conversion of pyruvate to lactate was measured by ^{1}H NMR spectroscopy with an internal standard (see Appendix A).

3.2 Biocatalytic conversion of pyruvate to lactate in batch

3.2.1 General immobilisation procedure for FDH and LDH onto carbon particles

For the immobilisation of FDH and LDH, two different types of carbon particle were compared: BP2000 and Aquasorb.

Throughout this Chapter a general procedure for preparing the enzyme-modified carbon particles and implementing them into batch or continuous flow was followed. The BP2000 particles were prepared by sonicating a 20 mg mL^{-1} suspension in Tris-HCl buffer (50 mM, pH 8.0) for 90 min. Aquasorb were washed with Tris-HCl buffer (50 mM, pH 8.0). The enzymes were removed from cold storage (−20 °C or −80 °C) and stored in a cold box. Solid enzymes were suspended in Tris-HCl buffer (50 mM, pH 8.0) to the required concentration. When using multiple enzymes, they were pre-mixed to the desired ratio. The enzymes were exposed to the carbon particles and gently mixed in a 1.5 mL microcentrifuge tube. The enzymes were immobilised on to the carbon support by adsorption at 4 °C for 2 h (unless stated otherwise). Immobilisation times for each enzyme were determined by initial adsorption studies. The enzyme-modified particles were then centrifuged (Eppendorf, MiniSpin Plus, 2 min, 14000 x *g*) and the supernatant was removed. The BP2000 enzyme particles were then washed with Tris-HCl (50 mM, pH 8.0) and re-suspended in this buffer. The larger Aquasorb carbon enzyme particles were washed with Tris-HCl. The desired amount of enzyme-modified BP2000 or Aquasorb was then ready to be transferred into the batch vessel or flow PBR.

3.2.2 Conversion of pyruvate to lactate with FDH and LDH in solution or immobilised, under batch conditions

For the batch conversion of pyruvate to lactate by LDH with FDH–formate recycling in homogeneous conditions, LDH (0.025 mg) and FDH (0.4 mg) was added to microcentrifuge tube (1.5 mL) containing NAD^+ (1 mM), ketone (30 mM), sodium formate (100 mM) in Tris-HCl (50 mM, pH 8.0) with a total volume of 1 mL.

For the batch conversion of pyruvate to lactate by LDH with FDH–formate recycling in heterogeneous conditions, the appropriate amount of FDH and LDH immobilised onto carbon and added to microcentrifuge tube (1.5 mL) containing NAD^+ (1 mM), ketone (20 or 30 mM), sodium formate (100 mM) in Tris-HCl (50 mM, pH 8.0) with a total volume of 1 mL.

Each microcentrifuge tube was then agitated on a vortex mixer and placed on a shaker plate (25 °C, 1200 RPM) for 16 h. The reactions were monitored by NMR, according to the procedure described Section 2.4.

3.2.3 Determining the carbon type for enzyme immobilisation

Initial work sought to methodically determine whether FDH and LDH would display activity when co-immobilised on a carbon support and what type of carbon support would be best suited to the provide active immobilised enzymes suitable for application in flow. There are many different types of carbon particle available with different diameters, pore size and conductivity. The enzyme immobilisation yield (the percentage mass of added enzyme that is retained on solid support) is likely to be higher on carbon particles with a smaller diameter due to higher surface area. The carbon pore size and surface chemistry are also likely to have an important role in enzyme adsorption. In a packed-bed reactor (PBR), the carbon particle size will also have an effect on the mass transport and the

pressure of the system; in this case, a larger carbon might be more appropriate to avoid high column pressures. Table 3-1 shows a comparison of the conversions achieved when using LDH and FDH in solution and immobilised on different carbon types in batch. For the Aquasorb carbon, various loadings of enzyme were added to 100 mg of carbon support and, in the case of the BP2000 carbon, 0.5 mg of FDH and 0.01 mg of LDH were added to 0.2 mg of carbon support. Preliminary activity assays had shown that the FDH was around 100-fold less active than the LDH and therefore higher FDH loading, relative to LDH, was used in these experiments. A higher loading of Aquasorb (~mm diameter) than BP2000 (~nm–µm diameter) particles was used because of the approximate 10^3–10^6 difference in surface area.

Table 3-1: Systematic immobilisation of FDH and LDH onto carbon supports

Entry[a]	Carbon support	Mass of carbon / mg	Pyruvate / mM	FDH preparation	FDH / mg	LDH preparation	LDH / mg	Conversion[b] / %
1	N/A*	N/A	30	in solution	0.4	in solution	0.025	100
2	BP2000	0.2	30	immobilised	0.5	immobilised	0.01	84
3	Aquasorb	100	30	immobilised	0.4	in solution	0.025	12
4	Aquasorb	100	30	in solution	0.4	immobilised	0.025	94
5	Aquasorb	100	30	immobilised	0.4	immobilised	0.025	16
6	Aquasorb	100	30	immobilised	0.6	immobilised	0.025	25

[a]Reaction conditions: 1 mM NAD^+, 100 mM sodium formate, 50 mM Tris-HCl buffer, pH 8.0, room temperature, 1 mL reaction volume, 16 h, enzyme immobilisation time = 1 h; [b]Determined using ^{1}H NMR spectroscopy. *N/A = not applicable.

Entry 1 shows full conversion when both the LDH and FDH were used in solution in a 16 h reaction. The enzymes were immobilised onto BP2000 (Entry 6) and studied using

reaction conditions that were determined by our group in previous work with BP2000[201]; under these conditions 84% conversion was obtained. This result showed that high conversion could be achieved with the enzymes immobilised onto carbon using this system. Next, the Aquasorb particles were studied under reaction conditions that were designed for the difference in surface area between the BP2000 and Aquasorb. When FDH was immobilised onto Aquasorb and LDH was in solution (Entry 3) and when both enzymes were immobilised onto Aquasorb (Entry 5), the results showed a conversion of 12% and 16%, respectively. However, in Entry 3, when LDH was immobilised onto Aquasorb and FDH was in solution, 94% conversion was achieved. With both enzymes immobilised, an increase in FDH loading from 0.4 mg to 0.6 mg resulted in an increase in conversion from 16% to 25% (Entry 6). These results showed that FDH and LDH are active when immobilised onto carbon and suggest that FDH is the limiting enzyme. With FDH and LDH immobilised, the BP2000 carbon support showed greater activity compared with the Aquasorb particles. Owing to this increased activity, it was decided that the BP2000 would be used in further FDH and LDH studies, despite the smaller particle size. The performance of BP2000 as an enzyme support has been well characterised in batch, and using it for subsequent experiments would also enable the determination of whether the BP2000 is applicable to continuous flow.

3.2.4 Immobilisation studies for FDH and LDH on BP2000 carbon particles

Having shown that high levels of conversion could be achieved with LDH and FDH co-immobilised onto BP2000 carbon particles, further studies were then carried out to determine the immobilisation yield and the effect of immobilisation on the enzyme activities. The immobilisation yield was determined by comparing the mass of non-

immobilised enzyme, recovered in the supernatant, with the total mass of enzyme exposed to BP2000 (

Table 3-2). The mass of enzyme in the supernatant was determined by UV-Vis A_{280}, using the calibration curves described in Appendix G.

Table 3-2: Immobilisation yield of enzymes FDH and LDH onto BP2000

Enzyme	Mass of enzyme added / mg	Mass of carbon / mg	Immobilisation time / h	Supernatant A_{280}	Mass of enzyme in supernatant / mg	Immobilisation / %
LDH	0.1	2	2	0.077	1.6×10^{-5}	>99
FDH	1	2	2	0.33	0.18	82
FDH	1	2	16	0.04	0.04	97

The results show that >99% of LDH (0.1 mg) was immobilised onto BP2000 (2 mg) after 2 h, and an immobilisation yield of 82% was calculated for FDH (1 mg) onto BP2000 (2 mg) after 2 h, showing that the BP2000 readily adsorbs each of the enzymes tested, highlighting the simplicity and efficiency of the technique. When the enzyme was allowed to immobilise for 16 h, a 97% immobilisation yield was achieved. However, a 16 h immobilisation time was considered to be impractical for industrial application; therefore, for all future experiments with BP2000, an enzyme immobilisation time of 2 h was used. It was then important to deduce how much activity the enzymes retained, once immobilised.

3.2.5 Specific activity of LDH in solution and immobilised onto BP2000 in batch

Enzyme activity was measured using UV-Vis spectroscopy (A_{260} and A_{340}) to track the interconversion of cofactor between its oxidised and reduced state over time, following the procedures described in Section 2.2. A graph of conversion against time was plotted for each experiment. The gradient of the slope in the initial high activity region was used to calculate the specific activity of the free or immobilised enzyme (U mg_{enzyme}^{-1}, U = μmol min^{-1}). The calculations consider the immobilisation efficiencies determined in Section 3.2.4. First, the retention of LDH activity when immobilised on to BP2000 was studied. To determine the specific activity of LDH in solution for the ketone reduction of pyruvate to lactate (by monitoring the conversion of NADH to NAD^+), a 1 mL batch reaction was performed. The reaction was monitored using *in situ* UV-Vis (Figure 3-1).

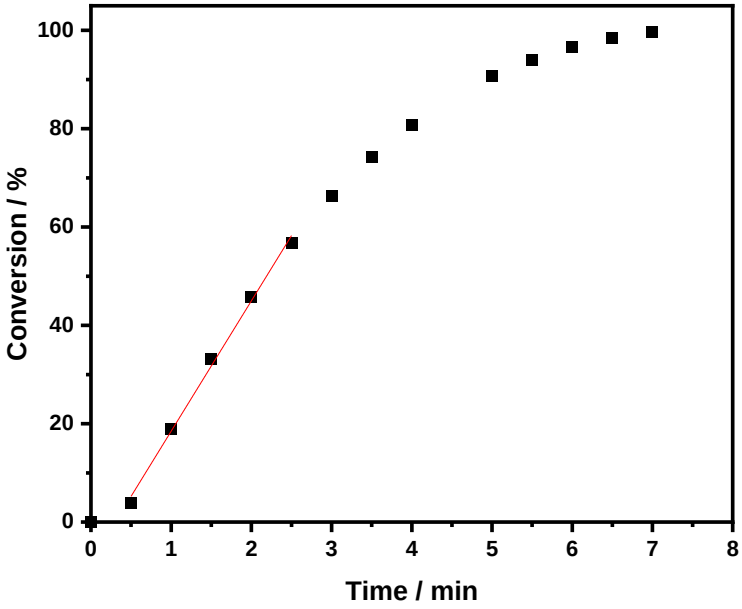


Figure 3-1: Batch enzyme activity measurement of free LDH in solution for the pyruvate driven oxidation of NADH. The conversion of NADH to NAD^+ over time was determined with *in situ* UV-Vis spectroscopy. Reaction conditions: LDH (0.025 mg), pyruvate (1 mM), NADH (0.1 mM), Tris-HCl (50 mM, pH 8.0).

From the results in Figure 3-1 the LDH in solution displayed a specific activity of 22.3 U mg^{-1}, calculated from the linear region of the graph up to 60% conversion. The enzyme activity can become limited by substrate availability and substrate inhibition above 60% conversion; thus, data in this region were not used to calculate specific activity.

Subsequently, an analogous activity assay was performed for LDH (0.0025 mg) immobilised onto BP2000 (0.2 mg) for the ketone reduction of pyruvate to lactate. The reaction was monitored using *in situ* UV-Vis (Figure 3-2). For the experiments involving the enzyme immobilised onto carbon, consistent light scattering from the particle suspension was observed across the entire wavelength range, giving a consistent baseline offset at all wavelengths. A baseline correction was therefore applied before further data analysis. In this experiment, tenfold lower LDH loading was used in comparison to the

activity assay with LDH in solution because, at higher enzyme on BP2000 loadings, the light scattering observed from the BP2000 was beyond the detection limit of the UV-Vis.

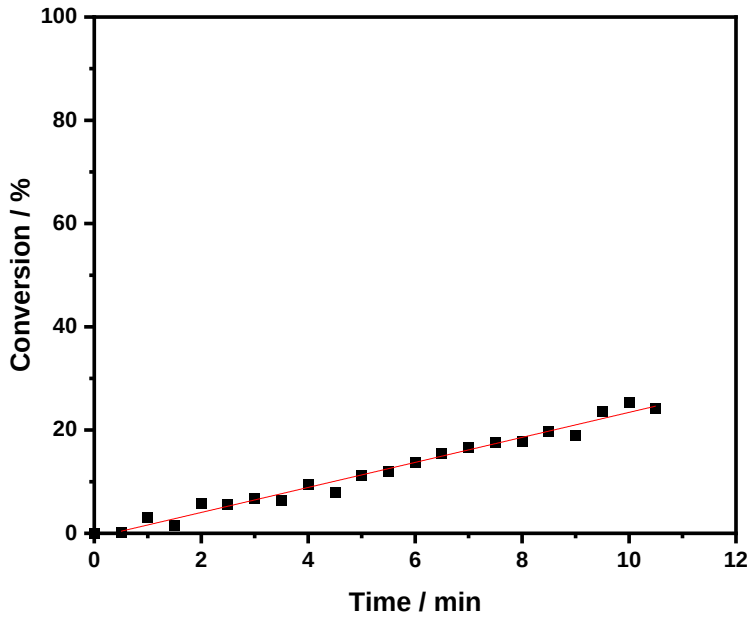


Figure 3-2: Batch enzyme activity measurement of LDH immobilised onto BP2000 for the catalysis of pyruvate-driven oxidation of NADH. The conversion of NADH to NAD^+ over time was determined using *in situ* UV-Vis spectroscopy. Reaction conditions: LDH (0.0025 mg), BP2000 (0.2 mg), pyruvate (1 mM), NADH (0.1 mM), Tris-HCl (50 mM, pH 8.0).

From the results in Figure 3-2 the LDH immobilised onto BP2000 (99% immobilisation yield) displayed a specific activity of 19 U mg^{-1}, corrected for incomplete enzyme immobilisation. The LDH retains 85% of activity when immobilised on BP2000 compared with the activity of LDH when free in solution, which is a good retention of activity.[246] The loss in activity after immobilisation might be due to the limitations of substrate mass transport to the heterogenous catalyst site, which tends to deposit at the bottom of the UV-Vis cuvette. Another limitation is that a small amount of cofactor is known to adsorb onto carbon particles, which would decrease cofactor availability under heterogeneous conditions, possibly decreasing the specific activity of the enzyme. When

comparing enzymes in solution against enzymes immobilised onto carbon, these challenges are probably always present to some degree.

3.2.6 The specific activity of FDH in solution and immobilised onto BP2000 in batch

Analogous experiments were next carried out with FDH to determine its activity in solution and its activity when immobilised onto BP2000. To determine the specific activity of FDH in solution for the conversion of formate to CO_2 (by monitoring the conversion of NAD^+ to NADH), a 1 mL batch reaction was performed. The reaction was monitored using *in situ* UV-Vis (Figure 3-3).

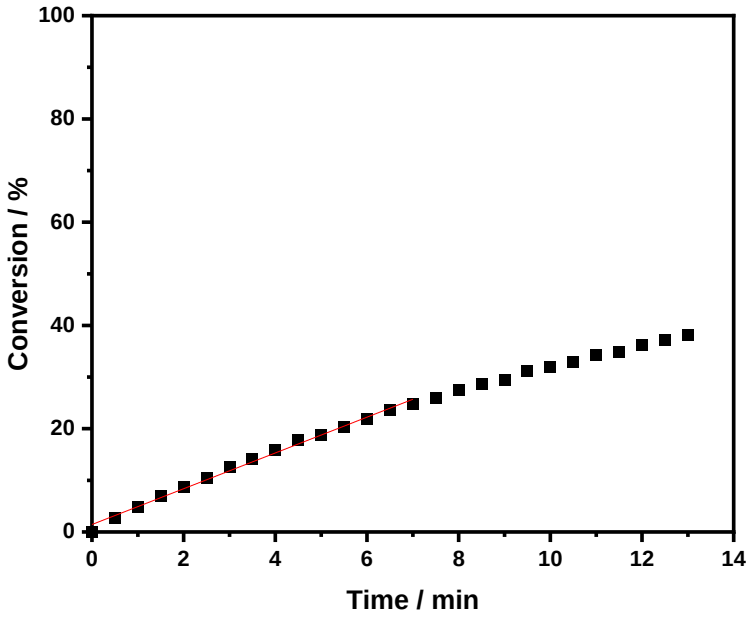


Figure 3-3: Batch enzyme activity measurement of free FDH in solution for the catalysis of NAD^+ to NADH. The conversion of NAD^+ to NADH over time was determined using *in situ* UV-Vis spectroscopy. Reaction conditions: FDH (0.05 mg), NAD^+ (0.1 mM), formate (1 mM), Tris-HCl (50 mM, pH 8.0).

The results in Figure 3-3 show that the FDH in solution displayed a specific activity of 0.20 U mg^{-1}.

Subsequently, to determine the specific activity of FDH (0.05 mg) when immobilised onto BP2000 (0.2 mg), an analogous 1 mL batch reaction was performed. The reaction was monitored using *in situ* UV-Vis (Figure 3-4).

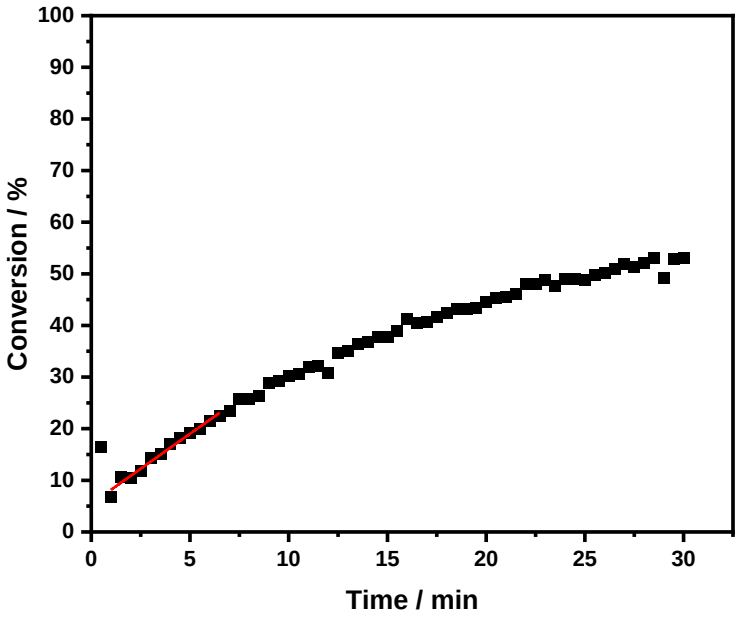


Figure 3-4: Batch enzyme activity measurement of FDH immobilised onto BP2000 for the catalysis of NAD^+ to NADH. The conversion of NAD^+ to NADH over time was determined using *in situ* UV-Vis spectroscopy. Reaction conditions: FDH (0.05 mg), BP2000 (0.02 mg), NAD^+ (0.1 mM), formate (1 mM), Tris-HCl (50 mM, pH 8.0).

From the results in Figure 3-2, the FDH immobilised onto BP2000 (82% immobilisation yield) displayed a specific activity of 0.02 U mg^{-1}, corrected for incomplete enzyme immobilisation. The FDH retains 10% of the activity when immobilised on BP2000 in comparison to its activity when free in solution. This is a lower specific activity compared with the immobilised LDH, and the results show that the FDH loading for future experiments would need to be much larger than the LDH loading, otherwise the FDH would limit the LDH.

3.3 Biocatalytic conversion of pyruvate to lactate in continuous flow

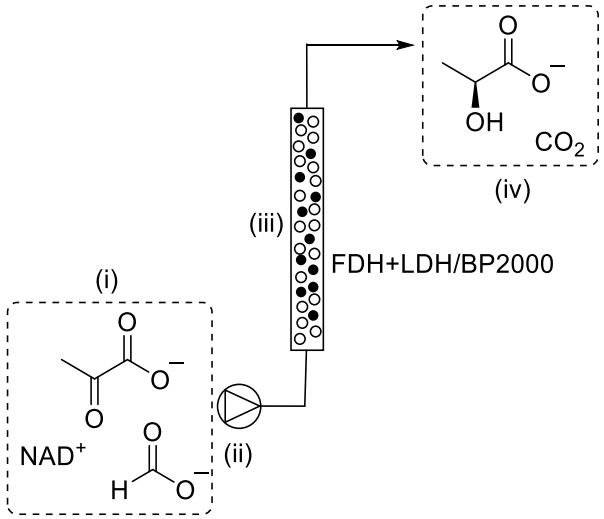
The BP2000 modified with FDH and LDH system was next transferred to a continuous reactor, guided by the immobilisation and activity results from Section 3.2, to determine its viability for solid-supported NADH-dependent biocatalysis in flow.

3.3.1 Continuous flow equipment set-up

The flow reactor was set up as shown in Scheme 1.2. The reaction solution was pumped from a reservoir (i) by a syringe pump (ii) through the PBR (iii), which contained LDH and FDH immobilised onto BP2000 mixed with glass beads. The enzyme-modified BP2000 was mixed with glass beads as a way to increase the total volume of solid support in the PBR. This enables a larger reactor column to be used, which is required to achieve the desired residence time (t_{Res}) (10–30 min) within the scope of flow rates of the available pumps. Mixing glass beads with the enzyme-modified BP2000 particles also helps to reduce pressure drop across the reactor bed. This is particularly important when using very fine catalyst particles, such as BP2000, which has a µm–nm-scale diameter, and even more so when moving towards a larger reaction scale. The product mixture was sampled with a fraction collector (iv), typically at time intervals of 1 to 4 times the magnitude of the t_{Res}.

The column bed length was adjusted to give an empty bed volume of 1.02 mL before being packed with the enzyme-modified BP2000 particles and glass beads. To transfer the enzyme-modified BP2000 particles from their preparative container to the column it was easiest to first suspend the enzyme-modified BP2000 particles in a liquid such as Tris-HCl buffer, and then pipette them into the column. The enzyme-modified BP2000 particles were mixed with glass beads in the PBR and the PBR was sealed for use.

Scheme 3-2: The set-up of the flow reactor for the continuous biocatalytic conversion of pyruvate to lactate. (i) Vessel containing the reactants (pyruvate, NAD^+, formate) in a solution of Tris-HCl or H_2O; (ii) syringe pump; (iii) LDH and FDH immobilised onto BP2000, mixed with glass beads in a PBR; (iv) the product-containing mixture is sampled using a fraction collector.



3.3.2 FDH and LDH leaching studies in continuous flow

Flow can provide an easier method to study the catalyst stability compared with batch. This is because, in a batch reaction, if an enzyme is detached from a particle of carbon, it is possible that it can re-immobilise onto another particle of carbon over the course of the reaction and it may also just react in solution. This can lead to an exaggerated idea of the success of the immobilised catalyst. In batch it would be difficult to get a measure of the scale of this process by taking time points or an end-point sample. In continuous flow, any enzyme that leaches off the carbon during the reaction will be pumped out of the column very quickly. Thus, the leached enzyme will not contribute towards the reaction progress and the amount of leached enzyme in each reactor volume can be quantified.

The enzyme leaching off the carbon in the continuous flow reactor was determined by pumping Tris-HCl buffer (50 mM, pH 8.0) through the PBR, which had been loaded with

a specific enzyme at a mass that is typical of a normal reaction. The outlet solution was then monitored using UV-Vis spectroscopy A_{280} to determine the concentration of any leached enzyme (using the calibration curves shown in Appendix G). The percentage of leaching was determined relative to the mass of enzyme that was added to the column initially to represent an accurate percentage of enzyme leached throughout the experiment.

Leaching experiments were first conducted with the LDH immobilised onto the BP2000, with particles prepared according to the standard procedure (outlined in Section 3.2.1).

Table 3-3 Protein leaching of LDH off the carbon

LDH added to BP2000 / mg[a]	LDH immobilised / mg	LDH leached over 6 h / mg	LDH leached over 6 h / %
0.1	0.099	0.0002	0.2

[a] 2 mg BP2000

The LDH leaching results in Table 3-3 show that the percentage of LDH immobilisation was determined to be 99% after a 2 h immobilisation period, which concurred with previous LDH immobilisation experiments (Section 3.2.4). The enzyme-modified BP2000 particles were loaded into the column (reactor volume, 1.02 mL) and Tris-HCl was pumped through the column at a flow rate of 30 μL min^{-1} (t_{Res} = 15 min). The enzyme mass in each reactor volume remained consistently below 0.003% of the total enzyme immobilised (measured by comparing the UV-Vis A_{280} in each reactor volume with the protein concentration calibration curve in Appendix G and, after 6 h of continuous flow, the total leaching was determined to be 0.2% of the total enzyme immobilised. These results demonstrate that, along with the LDH being highly efficient at immobilising onto the BP2000 particles, it is also robust with regard to its stability and lifetime once

immobilised, which is important because no chemical transformation or enzyme engineering was required for immobilisation.

Leaching experiments were next conducted with the FDH immobilised onto the BP2000, with particles prepared according to the standard procedure (outlined in Section 3.2.1).

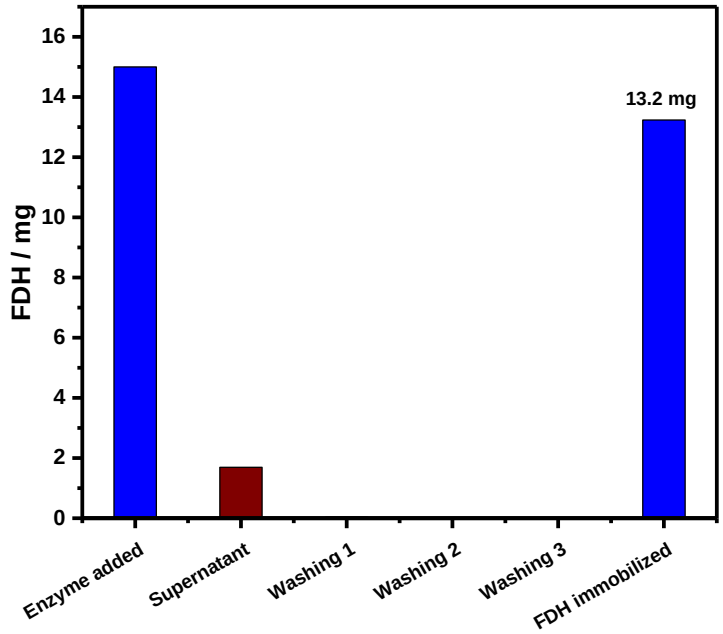


Figure 3-5: The total immobilisation of FDH (15 mg) onto BP2000 (15 mg) after a 2 h incubation period. The supernatant and three washings were analysed with UV-Vis A_{340}; the mass of non-immobilised FDH was calculated using the FDH concentration calibration curve shown in Appendix G.

The results in Figure 3-5 show that the percentage of FDH immobilisation onto BP2000 was 88%. This was determined by the presence of FDH in the supernatant and three subsequent washings of the FDH-immobilised BP2000 particles with Tris-HCl. Each washing consisted of the addition of Tris-HCl to the enzyme-modified carbon particles, followed by resuspension of the particles into solution on the vortex mixer and, finally, the washing solution was removed after centrifugation. The enzyme-modified BP2000 particles were loaded into the column (reactor volume, 1.02 mL) and Tris-HCl was

pumped through the column at a flow rate of 14 μL min^{-1} (t_{Res} = 30 min). Samples were collected every 0.5 h for the first 5.5 h and every 1 h thereafter for 22.5 h (Figure 3-6).

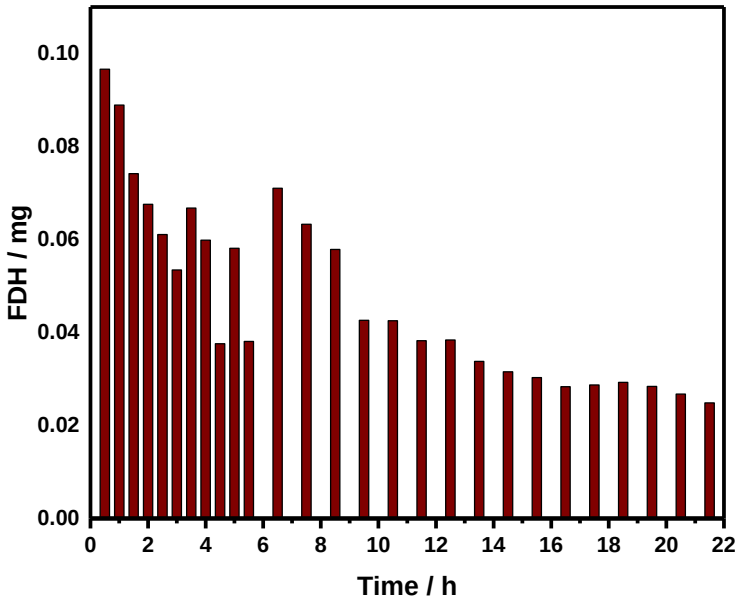


Figure 3-6: Leaching of FDH from the carbon was determined over time by flowing Tris-HCl over the immobilised FDH (13.2 mg) on BP2000 (15 mg) in a PBR. The collected fractions were measured by UV-Vis A_{280}, and the extent of FDH leaching was then calculated using the FDH concentration calibration curve shown in Appendix G.

The results in Figure 3-6 show that the enzyme loss for the first 7.5 h starts at 0.1 mg per sample, steadily decreasing to 0.06 mg per sample, equating to a 6.3% loss of the 13.2 mg FDH immobilised over this time period. The enzyme loss then steadily declines from 0.04 mg per sample to 0.02 mg per sample over the final 15 h, equating to a 2.6% loss of the 13.2 mg FDH immobilised. In total, the enzyme loss over the 22 h experimental run was 9.9% of the 13.2 mg FDH immobilised. Although this may be considered to be a modest total, it allowed for changes to be made to future experiments. For all future experiments, the PBR was flushed with Tris-HCl at a high flow rate for 10 min before the start of the experiment, to remove any enzyme, which appears to leaching off at quite

a high rate during the first 7 h of the leaching experiment, in order to obtain more consistent conversions during the flow reaction operation.

3.3.3 Conversion of pyruvate to lactate with FDH and LDH immobilised onto BP2000 in a continuous PBR

The specified PBR containing FDH and LDH immobilised onto BP2000 was prepared according to the procedures described in Section 3.2.1. The PBR was then connected to a liquid feed (Syrris, Asia syringe pump) and flushed with 3 reactor volumes of reaction buffer. The PBR was then disconnected and the pump was primed with reaction solution, before reconnecting the PBR. A reaction solution containing sodium pyruvate (10–50 mM), NAD^+ (0.1–1 mM), sodium formate (30–250 mM) in Tris-HCl buffer (12.5–50 mM, pH 8.0) or MilliQ water was pumped through the PBR at a flow rate of 17.2 µL min^{-1} (t_{Res} = 30 min), 34.4 µL min^{-1} (t_{Res} = 20 min) or 51.6 µL min^{-1} (t_{Res} = 30 min) through the biocatalytic cartridge. Samples were collected using a fraction collector (BioRad, 2110), and analysed by ^{1}H NMR spectroscopy, following the procedure described in Section 2.4.

3.3.4 Initial continuous flow reactions

The initial continuous flow experiments were performed in a fixed reactor volume metal column (void reactor volume = 700 µL). The preliminary experiments were performed to determine the effect on the pyruvate to lactate conversion in continuous flow through a PBR with FDH and LDH immobilised onto BP2000. A number of parameters were varied, and the effect on pyruvate to lactate conversion was monitored using NMR. The results are reported in Table 3-4.

Table 3-4: Comparison of initial flow experiments with FDH and LDH immobilised onto BP2000 in a PBR. Initially, the effect of changing the ratio of the two enzymes was analysed (Entry 1 and 2), and then the impact of changing the ratio of carbon to enzyme was assessed (Entry 3). The two final experiments measured the impact of varying the number of formate molar equivalents (Eq.) to the substrate (Entry 4) and the t_{Res} (Entry 5). Other conditions remained constant: pyruvate (10 mM), NAD^+ (10 mol%, molar percentage of NAD^+ with respect to the pyruvate loading), Tris-HCl buffer (50 mM) and LDH (0.1 mg). Each flow reaction was run over 4 h and the steady-state conversion is reported.

Entry	Mass of carbon / mg	Mass of FDH / mg	Formate / Eq.	t_{Res} / min	Conversion / %
1	4	3	10	30	64
2	4	5	10	30	86
3	8	5	10	30	67
4	4	5	5	30	85
5	4	5	5	15	44

When the FDH loading and ratio of FDH to LDH is increased between Entry 1 (3 mg, 30:1) and Entry 2 (5 mg, 50:1), the results show an increase in conversion from 64% to 86% respectively, confirming that FDH is the limiting part of the catalyst system even at large excess. However, increasing the BP2000 loading between Entry 2 (4 mg) and Entry 3 (8 mg), while keeping all other conditions the same, gave a decrease in conversion from 86% to 67% respectively. This is possibly because small amounts of cofactor are known to stick to BP2000; by increasing the amount of BP2000; more cofactor could have stuck to the BP2000, making the cofactor less available and lowering the rate of conversion. Overall, these results suggest that increasing the ratio of FDH to BP2000 was necessary for improved conversion. Decreasing the number of equivalents of formate between Entry 2 (10 Eq.) and Entry 4 (5 Eq.) showed no tangible change in conversion, implying that the FDH is substrate saturated even at lower formate concentrations. The response of the system to a decrease in t_{Res} between Entry 4 (30 min) and Entry 5 (15 min) was a decrease in conversion by almost half to 44%. This gave an indication that, under these

conditions, the system is consistent with a linear relationship, with regard to t_{Res} and conversion. These initial studies indicated that the FDH and LDH enzymes supported on BP2000 would be suitable for further study of NADH-dependent pyruvate reduction in flow

3.3.5 Seven-day continuous run

The lifetime of the preliminary system was studied to examine the operational stability over time. A reaction solution containing sodium pyruvate (10 mM), NAD^+ (10 mol%) and sodium formate (10 Eq.) in Tris-HCl buffer (50 mM, pH 8.0) was pumped through a PBR containing 0.6 mg LDH, 10 mg FDH immobilised on 12 mg BP2000 at a flow rate equivalent to a 30 min t_{Res}, for 330 reactor volumes (165 h). Figure 3-7 shows the conversion of pyruvate to lactate that was achieved in continuous flow with LDH and FDH immobilised onto carbon in a PBR.

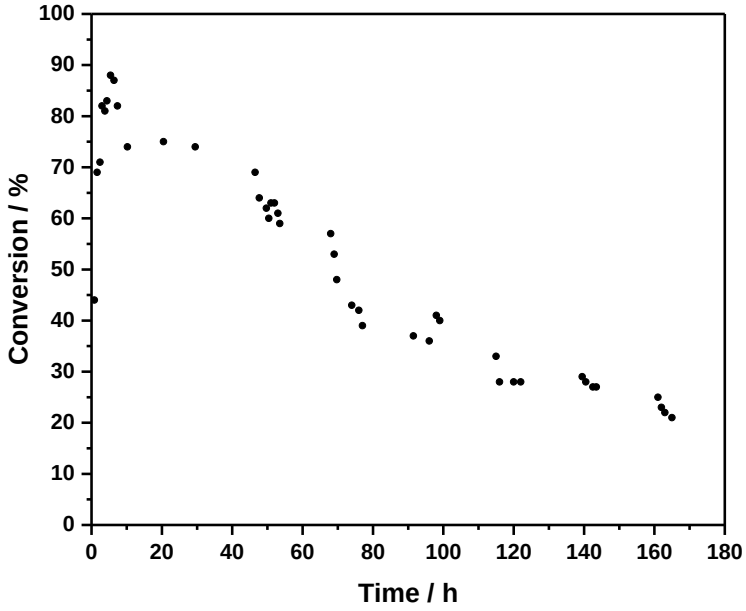


Figure 3-7: Conversion of pyruvate to lactate in continuous flow with LDH and FDH immobilised onto carbon in a PBR, with non-optimised conditions. The reaction was allowed to run over seven days to give insights into the system lifetime and stability. Reaction conditions: Pyruvate (10 mM), NAD^+ (1 mM), formate (100 mM), Tris-HCl (50 mM, pH 8), LDH (0.6 mg), FDH (10 mg), BP2000 (12 mg), 25 °C. Reactor volume = 0.7 mL, t_{Res} = 20 min.

The results in Figure 3-7 show that a steady state conversion of ~85% was maintained for the first 7.5 h. For a further 20 h, the system maintained a conversion of ~70%. The system then began to decline over the next 120 h, with periods of stability, before the experiment was ended at 21% conversion after 168 h (seven continuous days). Although the conversion metric was not high, the experiment yielded information on the lifetime of the immobilised enzymes in flow, as well as enzyme loading. Loading the catalyst into the PBR (reactor volume = 0.8 mL) was difficult and enzyme-modified carbon catalyst was lost in the process of transferring it to the column. Thus, further experiments were performed in an adjustable Omnifit column. This larger column enabled easier transferal of the enzyme-modified carbon catalyst, and offered the possibility of larger reactor volumes.

3.4 Optimisation of the immobilised FDH/LDH system in continuous flow

For the optimisation in the flow reactor, it was decided that the focus would be on the variables: NAD^+ mol%, equivalents of formate, t_{Res} and the solvent system, optimising one variable at a time while keeping the others constant. Throughout this section, the enzyme loading, BP2000 loading and pyruvate concentration were kept the same for each experiment. The loading used for all further experiments unless otherwise stated was 3 mg LDH, 30 mg FDH and 30 mg of BP2000. The increased mass of enzyme-modified carbon compared with in the previous experiments in Section 3.3 is due to the increased reactor volume of the PBR, which allowed for the increased loading of particles while maintaining reasonable residence times with flow rates that were achievable using the flow pumps that were available. The variable limits chosen were based on the goal of achieving a good conversion of 50 mM pyruvate to lactate (>80%), within a 30 min t_{Res} (for reasonable productivities), for the formate Eq. to be no more than 5 (to limit experimental waste) and the NAD^+ mol% loading to be no greater than 1 mol% (for viable cofactor turnover numbers). Keeping the t_{Res} below 30 min was chosen for reasonable experimental productivity values, which is a key metric for determining the scale-up viability of a continuous flow system.[205] The number of formate Eq. and the buffer concentration should be optimised to be as low as possible owing to the impact that they have on the *E* factor of the experiments.

The moderately long operational stability of the system offers the possibility of testing multiple sets of reactor conditions with a single packed column. The reaction conditions could be varied over time, allowing each set of conditions to reach steady state for at least 3 reactor volumes. When many sets of operating conditions were performed on the same

biocatalyst loading, at least one set of operating conditions was repeated to see if they gave consistent results, and ensure that catalyst stability was maintained. The effect of systematically changing one variable (t_{Res}, Tris-HCl concentration, NAD^+ mol%, or number of formate equivalents) was studied in single experimental runs. During the optimisation experiments, three sets of reactor conditions were repeated and the mean standard deviation in percentage conversion of pyruvate to lactate was found to be ±2.5%.

3.4.1 Variation in t_{Res}

The desired t_{Res} (10–30 min) was achieved by adjusting the flow rate (17.2–64.6 μL min^{-1}) through the PBR.

Figure 3-8 shows the effect on the pyruvate to lactate conversion in continuous flow through a PBR with FDH and LDH immobilised onto BP2000 by the variation in the t_{Res}. Using the conditions of pyruvate (50 mM), NAD^+ (1 mol%), formate (5 Eq.) and Tris-HCl buffer (50 mM, pH 8.0).

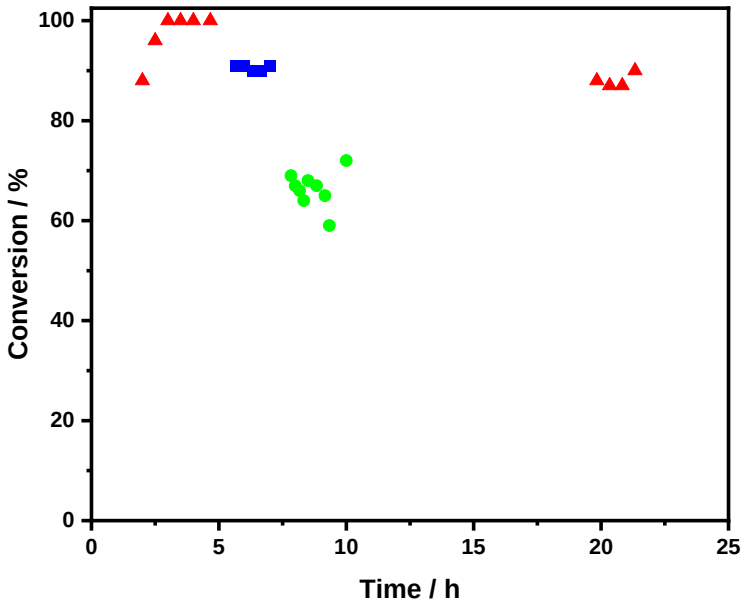


Figure 3-8: The effect of varying the t_{Res} on the conversion of pyruvate to lactate in the continuous PBR. t_{Res}: 10 min (green circles), 20 min (blue squares), 30 min (red triangles). Reaction conditions: pyruvate (50 mM), NAD^+ (1 mol%), formate (5 Eq.) and Tris-HCl buffer (50 mM).

The results in Figure 3-8 show that, after reaching steady state, the 30 min t_{Res} provided >99% conversion. The t_{Res} was then decreased to 20 min; under these conditions, the system reached a steady state conversion of 91%. The t_{Res} was further decreased to 10 min; under these conditions, the system reached a steady state conversion of 65%. The system was left running overnight and then the t_{Res} was returned to 30 min, achieving a steady-state conversion of 90%. This decrease in conversion from the initial results achieved at a 30 min t_{Res} could be due to leaching of the FDH from the BP2000, leading to a small decrease in the activity of the system. Overall, these results were consistent with the increased time of contact between the reactants and the catalyst at a longer t_{Res}, leading to a higher conversion. The system demonstrating >99% of pyruvate to lactate with a 30 min t_{Res} was a positive result. However, this degree of conversion does not indicate whether the system is operating at its optimum or whether it could achieve

conversion of a greater concentration of pyruvate. Thus, all further changes in reaction condition were still tested at a t_{Res} of 10 min and 20 min, in addition to at a t_{Res} of 30 min.

3.4.2 Variation of NAD$^+$ mol%

The NAD$^+$ mol% was varied to determine its effect on the conversion of pyruvate to lactate within the flow system. The PBR was assembled with FDH and LDH immobilised onto BP2000, and the NAD$^+$ mol% varied over time, using the reagents pyruvate (50 mM), formate (5 Eq.), Tris-HCl buffer (50 mM, pH 8.0) at t_{Res} of 10, 20 and 30 min. The results are shown in Figure 3-9. Each point is the average conversion achieved at the specified reaction condition once steady state has been reached, with a minimum of three fractions collected.

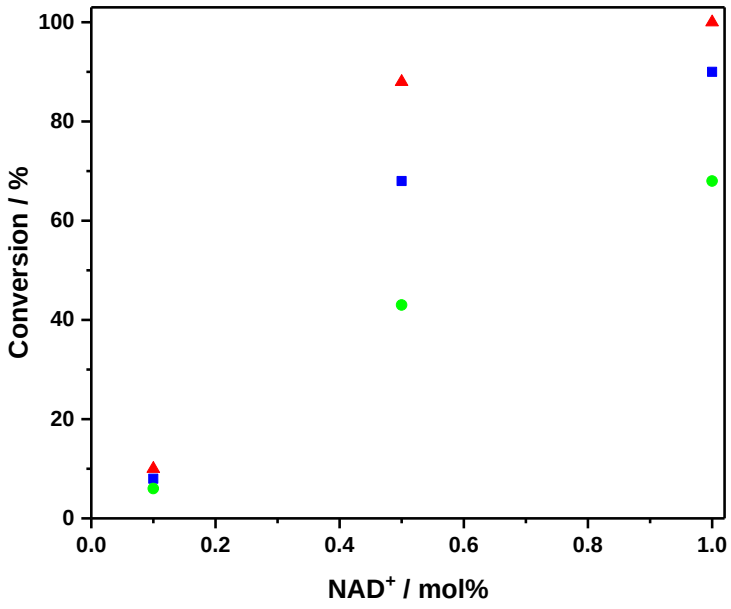


Figure 3-9: The effect of varying the NAD$^+$ mol% on the conversion of pyruvate to lactate in the continuous PBR, under the conditions of 50 mM pyruvate, 5 Eq. formate and 50 mM Tris-HCl buffer. t_{Res}: 10 min (green circles), 20 min (blue squares), 30 min (red triangles).

The results in Figure 3-9 show that the extent of conversion increases with NAD^+ concentration at all t_{Res} values. Very low conversion was achieved at low cofactor loading (0.1 mol%), suggesting that the process was cofactor limited under these conditions. At higher cofactor loadings, the system shows much higher conversions and a greater variation in conversion with t_{Res}; this suggests that the system becomes more t_{Res} dependent. Overall, the NAD^+ mol% should be >0.5 to achieve reasonable conversions.

3.4.3 Varying the number of equivalents of formate

Next, the number of formate equivalents was varied to determine its impact on reaction conversion. Figure 3-10 shows the effect on the conversion of pyruvate to lactate in continuous flow through a PBR with FDH and LDH immobilised onto BP2000 when varying the equivalents of formate using the reagents pyruvate (50 mM), NAD^+ (1 mol%), Tris-HCl buffer (50 mM, pH 8.0) at t_{Res} of 10 min, 20 min and 30 min.

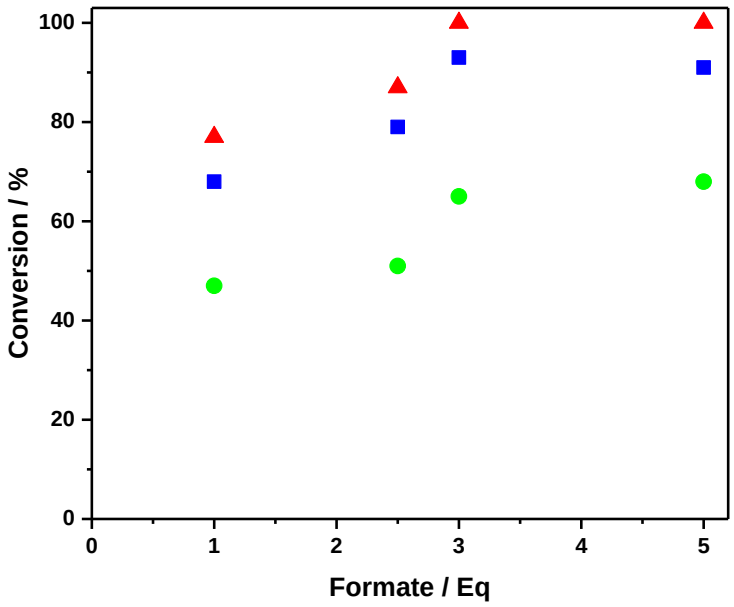


Figure 3-10: The effect of varying the number of formate equivalents on the pyruvate to lactate conversion in the continuous PBR, under the conditions of 50 mM pyruvate, 1 mol% NAD^+ and 50 mM Tris-HCl buffer. t_{Res}: 10 min (green circles), 20 min (blue squares), 30 min (red triangles).

The results show that the conversion achieved increases at all t_{Res} times as the number of formate equivalents are increased from 1 to 3. Furthermore, when varying the equivalents of formate, there is clear inflection point on conversion between 2.5 and 3 Eq. Increasing from 1 to 2.5 Eq. formate consistently showed a small effect on the conversion, whereas the jump from 2.5 to 3 Eq. formate showed a 13–26% increase in conversion across the residence times. Conversion appears to plateau between 3 and 5 Eq. formate; negligible differences in conversion were observed across all t_{Res}. This trend was observed for all t_{Res} values investigated and suggests that the reaction is formate limited up to 3 Eq.

3.4.4 Varying the concentration of Tris-HCl

Finally, the effect of the Tris-HCl buffer concentration on the reaction was studied. Figure 3-11 shows the effect on the conversion of pyruvate to lactate in continuous flow through a PBR with FDH and LDH immobilised onto BP2000 by the variation in Tris-HCl

concentration over time, under the following reaction conditions: pyruvate (50 mM), NAD^+ (1 mol%), formate (5 Eq.) at t_{Res} of 20 min.

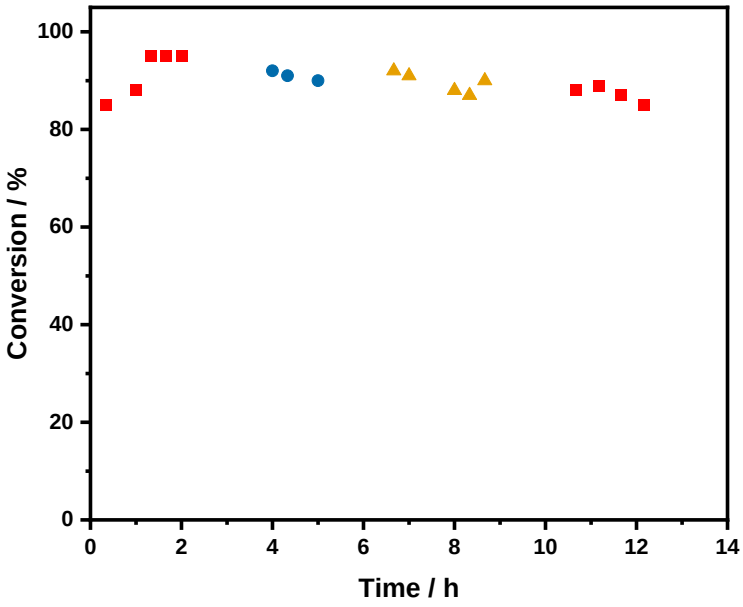


Figure 3-11: The effect of varying the Tris-HCl (pH 8.0) concentration on the conversion of pyruvate to lactate in the continuous PBR, under the following conditions: 50 mM pyruvate, 1 mol% NAD^+ and 5 Eq. formate. t_{Res} = 20 min. Tris HCl concentration: 50 mM (red squares), 12.5 mM (blue circles), 0 mM (MilliQ water) (yellow triangles).

The results in Figure 3-11 show that the steady-state conversions achieved at a Tris-HCl concentration of 50 mM, 12.5 mM and 0 mM (MilliQ water) were 95%, 92% and 90%, respectively. Lowering the Tris-HCl concentration did not appear to have a significant effect on the conversion. This was confirmed when the 50 mM Tris-HCl reaction conditions were repeated at the end of the experiment, achieving a steady-state conversion of 90%, indicating a slight drop in activity over the course of the experiment.

The studies showed that the operating conditions to achieve highest conversion for this system were a 20 min t_{Res}, 1 mol% NAD^+ and 5 Eq. formate. The concentration of Tris-

HCl buffer was shown to have little to no effect on the conversion, although the ability to run the reaction in MilliQ water may improve other aspects of the process, such as the cost efficiency and the *E* factor. Additional sustainability metrics of the system are discussed in the next section.

3.5 Additional process optimisation metrics

In Section 3.4, the reaction conditions were systematically changed to optimise the system for conversion. Although high conversion of pyruvate to lactate is a key target, other process metrics are also important. Running the reaction at many conditions meant that other important metrics for optimising a system, such as sustainability and productivity, could be considered using the same data. Changes in t_{Res}, formate Eq., NAD^+ mol% and buffer can have a large effect on these metrics. Thus, the optimum parameters for space–time yield (STY) and minimisation of waste (*E* factor) were also studied.

3.5.1 Analysis of system STY

The STY is a way of describing the productivity of a system by the amount of desired product formed with respect to the reactor volume and time.

The STY enables the direct comparison of different reactor types and sizes. Figure 3-12 is a compilation of the results from the optimisation experiments demonstrated in Section 3.4. The graph shows the STY against conversion for each set of reaction conditions studied.

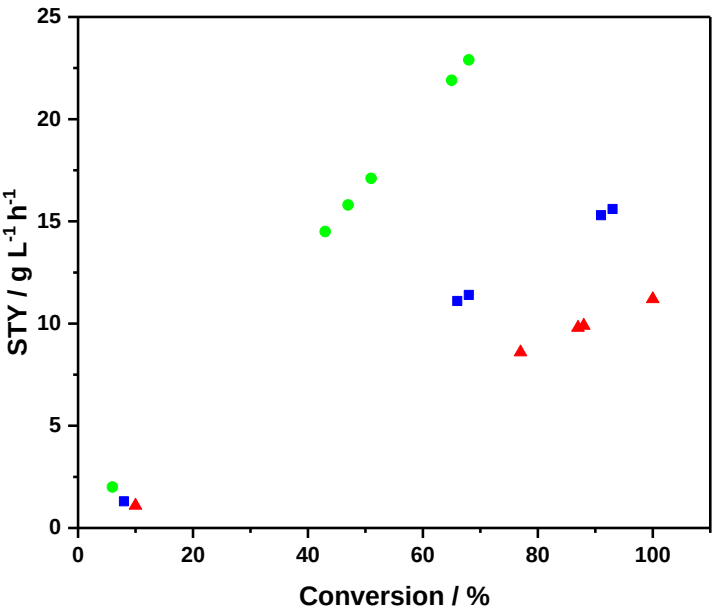


Figure 3-12: Compilation of the optimisation experiments carried out with the LDH and FDH immobilised onto BP2000 in the PBR for the conversion of pyruvate to lactate, with respect to the calculated STY *versus* conversion. t_{Res} ● = 10 min, ■ = 20 min, ▲ = 30 min.

The results in Figure 3-12 show that the highest STY achieved was 22.9 g L^{-1} h^{-1} with a 68% conversion under the conditions of 50 mM pyruvate, 1 mol% NAD, 5 Eq. formate, 50 mM Tris-HCl buffer and a 10 min t_{Res}. Although the conversion achieved was lower than that achieved under similar conditions but longer residence times, the higher flow rate means that more product is obtained in the same amount of time. The lowest STY demonstrated was 1.1 g L^{-1} h^{-1} with a 10% conversion under the conditions of 50 mM pyruvate, 0.1 mol% NAD^+, 5 Eq. formate, 50 mM Tris-HCl buffer and a 30 min t_{Res}. The STY for this process was most strongly affected by t_{Res}. The decrease in t_{Res} from 30 min to 10 min, more than doubled the STY from 11.2 $g_{lactate}$ L^{-1} h^{-1} to 22.9 $g_{lactate}$ L^{-1} h^{-1} when keeping all other reaction conditions consistent (50 mM pyruvate, 1 mol% NAD^+, 5 Eq. formate).

3.5.2 Analysis of system E-factor

The *E* factor, first proposed by Sheldon[247], is a ratio of the mass of reaction waste to the mass of desired product. Figure 3-13 is a compilation of the results from the optimisation experiments demonstrated in Section 3.4. The graph shows the *E* factor conversion, for each set of reaction conditions studied.

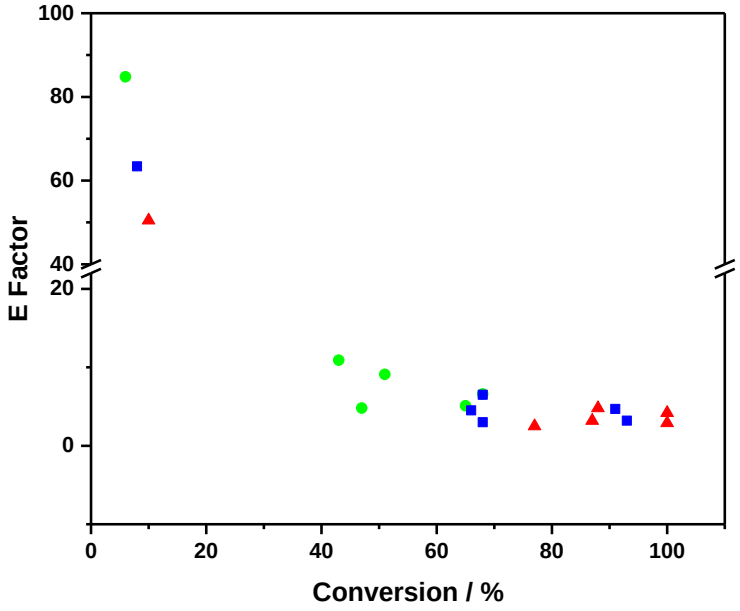


Figure 3-13: Compilation of the optimisation experiments carried out with the LDH and FDH immobilised onto BP2000 in the PBR for the conversion of pyruvate to lactate, with respect to the calculated *E* factor versus conversion. t_{Res}: 10 min (green circles), 20 min (blue squares), 30 min (red triangles).

The results show that the majority of the reactor conditions achieved an *E* factor of <10, which is very promising. The lowest *E* factor achieved was 2.5 with a 77% conversion under the conditions of 50 mM pyruvate, 1 mol% NAD, 1 Eq. formate, 50 mM Tris-HCl buffer and a 30 min t_{Res}. This is within the target for the bulk chemicals industry (*E* factor < 1–5).[247] However, lowering the formate to 1 Eq. does have a large detrimental effect on the conversion. Changing formate from 5 to 3 Eq. lowered the *E* factor from 4.2 to 2.9, while maintaining the high conversion. The highest *E* factor demonstrated was 85

with a 6% conversion under the conditions of 50 mM pyruvate, 0.1 mol% NAD, 5 Eq. formate, 50 mM Tris-HCl buffer and a 10 min t_{Res}. Similarly, the two other experimental conditions that displayed an *E* factor of >50 also displayed a conversion of <10%; from this, it was deduced that low conversion (unreacted pyruvate contributing to waste) was a key defining parameter for a high *E* factor. The other contributors to the *E* factor were the Tris-HCl concentration and the equivalents of formate. Analysis of the *E* factor achieved from the experiment in Section 3.4.4, which focused on changing the Tris-HCl concentration, shows that, under reaction conditions of 50 mM Tris-HCl, an *E* factor of 4.7 was achieved; by contrast, in MilliQ H_2O, the *E* factor was 3.5. This highlights a relatively significant sustainability benefit of performing the reaction in H_2O. Performing a reaction in H_2O can also have downstream processing benefits with regard to waste disposal.

3.5.3 Overall system analysis for multi-target optimisation

The data were then collated for multi-target optimisation. Figure 3-14 is a 3D plot showing all of the experiments carried out with the FDH and LDH on carbon-loaded PBR with regard to all three optimisation targets: STY (*x* axis), *E* Factor (*y* axis) and conversion (*z* axis).

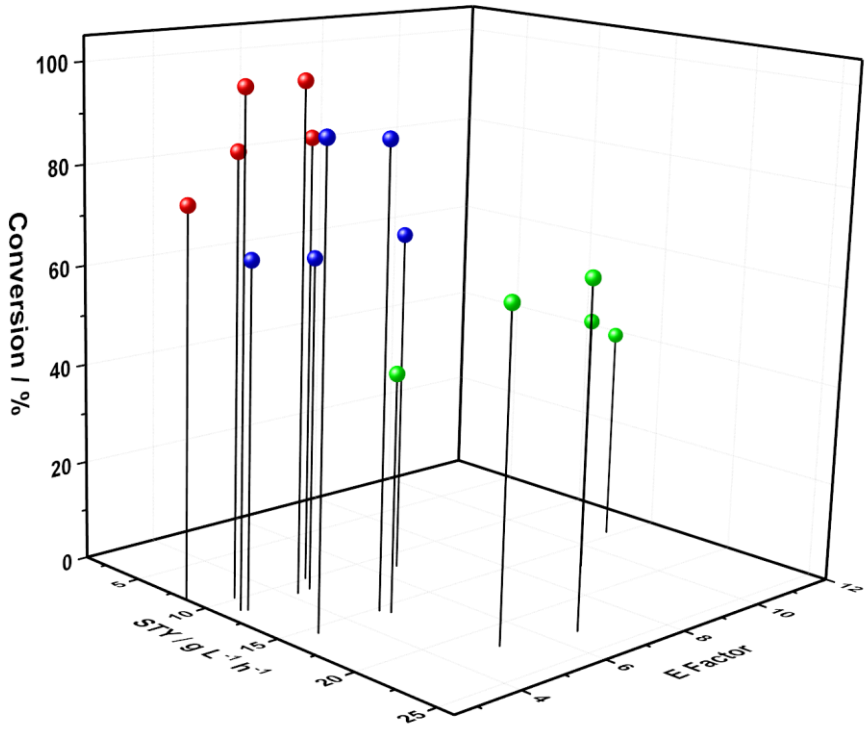


Figure 3-14: All of the experiments carried out with the FDH and LDH on carbon-loaded PBR with regard to the optimisation targets: STY (*x* axis), *E* Factor (*y* axis) and conversion (*z* axis). t_{Res}: 10 min (green circles), 20 min (blue circles), 30 min (red circles).

The results show that, to achieve the highest conversion values, the STY is far below its maximum due to the longer t_{Res} required to achieve the lowest *E* factors. This is also the case because lower conversion contributes greatly to high *E* factor values. On the other hand, when the system achieves the highest STY values, the conversion is often sacrificed because of the lower t_{Res} required.

From these studies, the operating conditions to achieve an optimum STY for this system were a 10 min t_{Res}, 1 mol% NAD^+ and 5 Eq. formate. The operating conditions to achieve an optimum *E* factor for this system were a 30 min t_{Res}, 1 mol% NAD^+ and 1 Eq. formate.

3.6 JMP modelling

In collaboration with the industrial partner for this project, the data points gathered from the optimisation experiments were used to generate reaction optimisation predictive models using the statistical analysis software JMP 14. For this, a number of reaction parameters are chosen as inputs (with desired response limits), then the results achieved in the wet laboratory for each set of the inputs are submitted and the computer modelling software can create plots that predict the results at any set of parameters within the ranges chosen.

The reaction parameters chosen for this JMP modelling experiment were the t_{Res}, NAD^+ mol% and the equivalents of formate, and the metrics for conversion, STY and *E* factor shown in Section 3.4 were inputted for all of the reactor conditions tested. Next, a set of desired response limits was chosen: >80% conversion, STY > 10 g L^{-1} h^{-1} and *E* factor < 4. The computer modelling software then generated a set of contour plots, shown in Figure 3-15, which predict the flow reactor operating conditions under which of these selected criteria are met (white areas of the contour plots). The non-white areas display the predicted responses for conversion (red), STY (green) and *E* factor (blue) under the reactor operating conditions under which the desired response limits are not fulfilled.

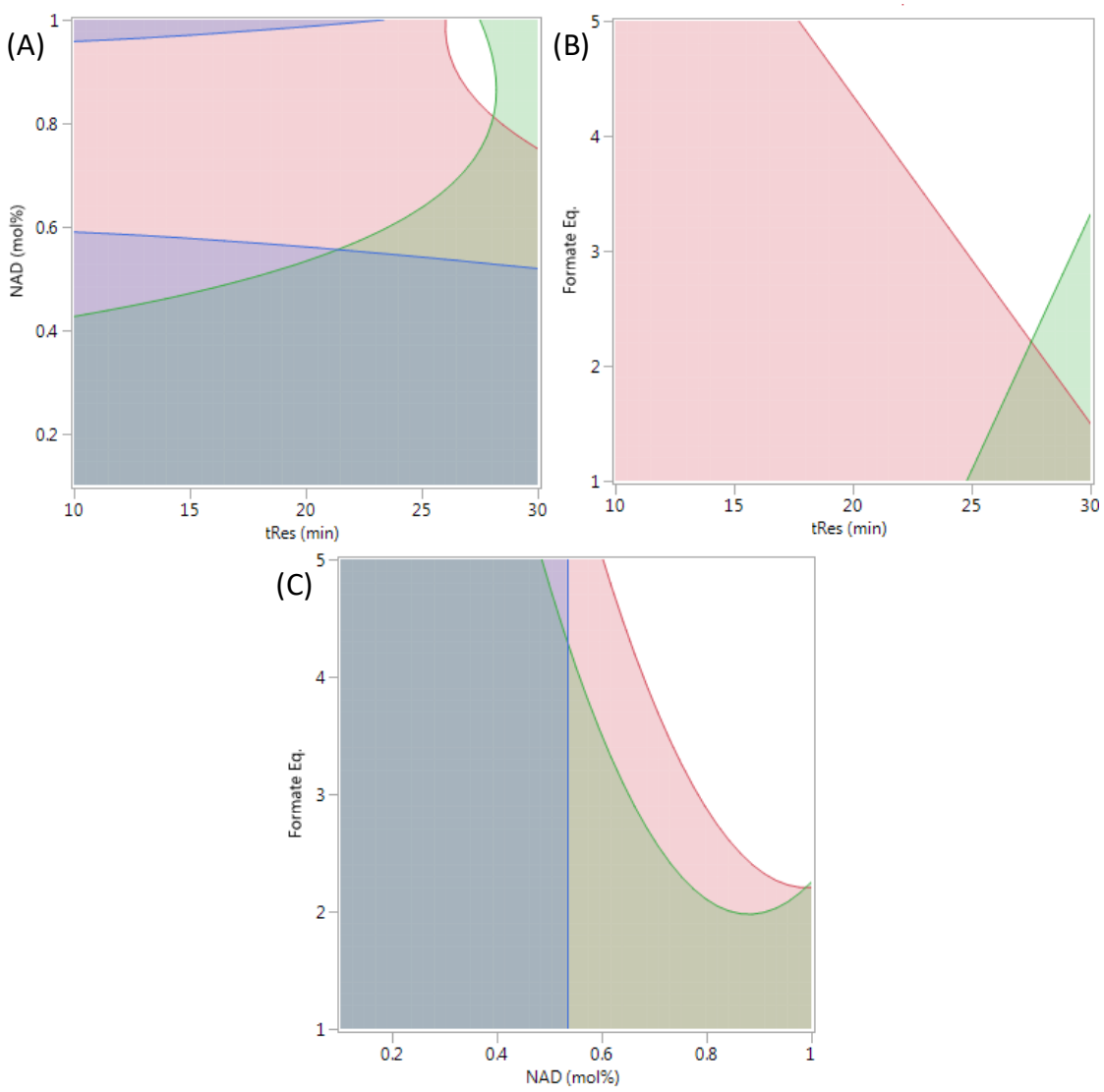


Figure 3-15: Contour profiles generated by the data analysis software JMP 14. The models show the merger of predicted responses for conversion (pink), STY (green) and *E* Factor (blue) for the conversion of pyruvate to lactate in continuous flow with LDH and FDH immobilised onto carbon in a PBR. The desired output limits were set to: conversion > 80%, STY > 10 and *E* factor < 4 The area within the coloured sections signifies the conditions under which the desired output will not be met. The area within the white coloured region signifies the conditions under which all of the desired system outputs will be met. (A) $\boldsymbol{t_{Res}}$ versus NAD , (B) $\boldsymbol{t_{Res}}$ versus formate, (C) NAD^+ mol% versus formate Eq.

The results in Figure 3-15(A) predict that, to meet the desired response criteria, the reactor should be operated at >~0.8 mol% NAD^+ and with a t_{Res} of between 26 and 28 min. The most restrictive metric contributing to this result is the conversion, which only has a small

portion at >~26 min t_{Res} and >~0.78 NAD^+ mol%, under which conditions the desired criterion of >80% conversion is predicted to be met.

The results in Figure 3-15(B) predict that, to meet the desired response criteria, the reactor should be operated at >2 Eq. formate and with a t_{Res} of between 18 and 30 min. The most restrictive metric contributing to this result is again the conversion, which displays a trend of requiring a longer t_{Res} as the number of formate equivalents decreases to meet the desired criteria of >80% conversion.

The results in Figure 3-15(C) predict that, to meet the desired response criteria, the reactor should be operated at around >2 Eq. formate and with >0.6 NAD^+ mol%. The most restrictive metric contributing to this result is again the conversion, which displays a trend of requiring greater NAD^+ mol% as the number of formate equivalents decreases to meet the criteria of >80% conversion. The STY also follows the same trend to meet the desired criteria of >10 g L^{-1} h^{-1}.

In general, to meet the desired criteria for STY, the models show a trend towards a shorter t_{Res} because more reactant and product is processed through the reactor in a shorter period of time.

By contrast, to meet the desired criteria for *E* factor, the models show a trend towards a longer t_{Res} due to the higher conversion, which inherently leads to less waste out of the reactor.

Interestingly, the conversion, STY and *E* factor would all improve at higher NAD^+ mol% and more equivalents of formate because the increased driving force leads to higher conversion (less starting material wastage) and reactor productivity. As mentioned in

Section 3.5.2, the modelling concurs that decreasing the excess of formate has a very positive effect on the *E* factor.

In summary, the contour plots suggest that the reaction parameters that are required for operation within the desired limits for all three metrics are t_{Res} = 25–30 min, 0.8–1 mol% NAD^+ and 2.5–5 Eq. formate. However, if the optimisation focus of the system was shifted away from high conversion to improving another response, such as the *E* factor, the desired operating criteria could be reassessed.

3.7 Operational viability

In this section, the lifetime and reusability of the system were tested. The deactivation or loss of activity of a catalyst with time is an ongoing challenge of catalytic processes conducted in industry. Owing to the industrial relevance of this project, it was of even greater importance to study this. The need to replace catalyst can lead to the temporary shutdown of a process, which can be costly to industry.[248] Traditional biocatalyst systems with enzymes in solution can be critiqued on the basis of the difficulty of separating the enzymes from the reaction mixture and subsequently reusing them.[249,250] Immobilised biocatalyst systems often show increased lifetime, as well as easier separation, allowing for increased reusability.[225,251–253]

3.7.1 The activity of FDH and LDH in continuous flow

The enzyme activity of FDH and LDH in continuous flow was calculated for the optimisation experiments in Section 3.4, so that they could be compared to the batch results in Section 3.2.5 and Section 3.2.6. The highest enzyme activity is recorded when the enzymes are operating as close to their optimum (or most strained) as possible; therefore, the overall conversion should be below 70% for this, such that the enzymes are

not limited by the supply of substrate. This was achieved for experiments with a t_{Res} of <10 min and therefore the highest flow rates. With the enzyme loading of FDH (30 mg) and LDH (3 mg) used throughout, the highest FDH activity achieved was 0.12 U mg^{-1}. This is six times higher than the recorded FDH activity when immobilised in batch (0.015 U mg^{-1}). This difference could be due to the increased substrate–catalyst contact time in flow caused by improved mixing and an increased catalyst-to-substrate ratio in the PBR. The FDH also retained 60% activity compared with FDH free in solution. This loss of activity could be caused by decreased access to the FDH active site when immobilised on the BP2000. To achieve high LDH activity, the LDH loading was decreased from 3 mg to 0.1 mg with the usual FDH loading (30 mg) to make LDH the limiting enzyme. A reaction solution containing sodium pyruvate (50 mM), NAD^+ (0.5 mM) and sodium formate (250 mM) in Tris-HCl buffer (50 mM, pH 8.0) was pumped through a PBR containing enzyme-modified BP2000 at a flow rate equivalent to a 10 min t_{Res} (52 µL min^{-1}), for 20 reactor volumes. In this reaction, a 21% steady-state conversion of pyruvate to lactate was achieved and the LDH specific activity was calculated as 10.7 U mg^{-1}, which is a 50% retention of activity compared with free LDH in solution. It is possible that this activity could be increased by decreasing the LDH loading even further.

3.7.2 Catalyst reusability in flow

To deduce the reusability of the system, a reaction solution containing sodium pyruvate (50 mM), NAD^+ (0.5 mM) and sodium formate (250 mM) in Tris-HCl buffer (50 mM, pH 8.0) was pumped through a PBR containing enzyme-modified BP2000 at a flow rate equivalent to a 30 min t_{Res} (16 µL min^{-1}), for 48 reactor volumes. Next, the PBR was flushed with Tris-HCl buffer (10 mL) and then stored at 4 °C overnight (16 h). The packed column was then used for a second run under the same reaction conditions. Figure 3-16 shows the conversion achieved over two reuses of a single PBR.

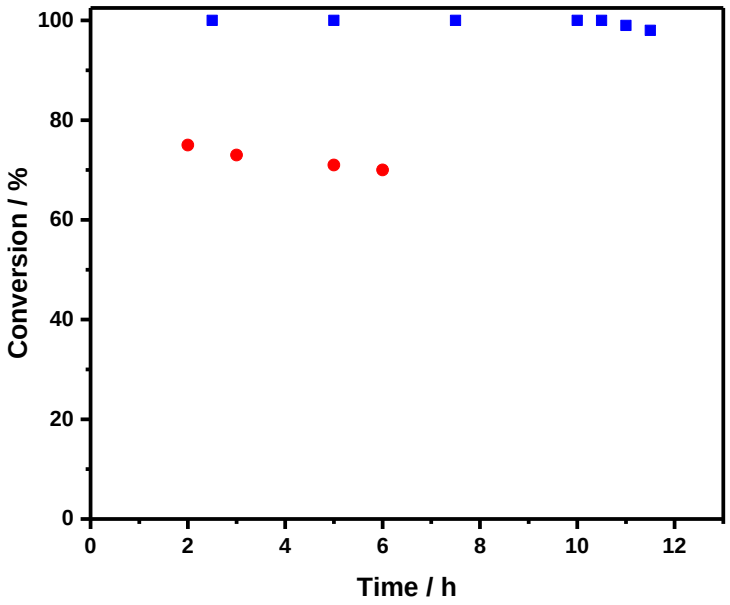


Figure 3-16: Conversion of pyruvate to lactate achieved across multiple uses of a PBR. The first (blue circles) and second (red circles) use are plotted. Reaction conditions: pyruvate (50 mM), formate (3 Eq.), NAD+ (1 mol%), Tris-HCl buffer (50 mM, pH 8.0), FDH (30 mg), LDH (3 mg), BP2000 (30 mg), 25 °C, t_{Res} = 30 min.

The results show that the first use of the PBR achieved full conversion for 10.5 h, on reuse, achieving 72% steady-state conversion. This demonstrates the potential for reusability and the stability of the catalyst column. To enhance reusability, the storage conditions, such as temperature and storage solvent, could be studied.

3.7.3 Longer-term operation

The stability of the system over time was studied using the optimal conditions for high conversion. Figure 3-17 shows the conversion of pyruvate to lactate achieved in continuous flow with LDH and FDH immobilised onto carbon in a PBR. A reaction solution containing sodium pyruvate (50 mM), NAD^+ (0.5 mM) and sodium formate (250 mM) in Tris-HCl buffer (50 mM, pH 8.0) was pumped through a PBR at a flow rate equivalent to a 30 min t_{Res} for 126 reactor volumes (63 h). For this experiment, the

enzymes were added to the carbon within the column and allowed to immobilise, therefore preventing loss of catalyst when transferring into the reactor column. This optimised the amount of catalyst in the column and improved the practicality of use, while making the experiments more reproducible. The column was flushed with a larger amount of Tris-HCl buffer at the start of this reaction to remove any non-immobilised enzyme.

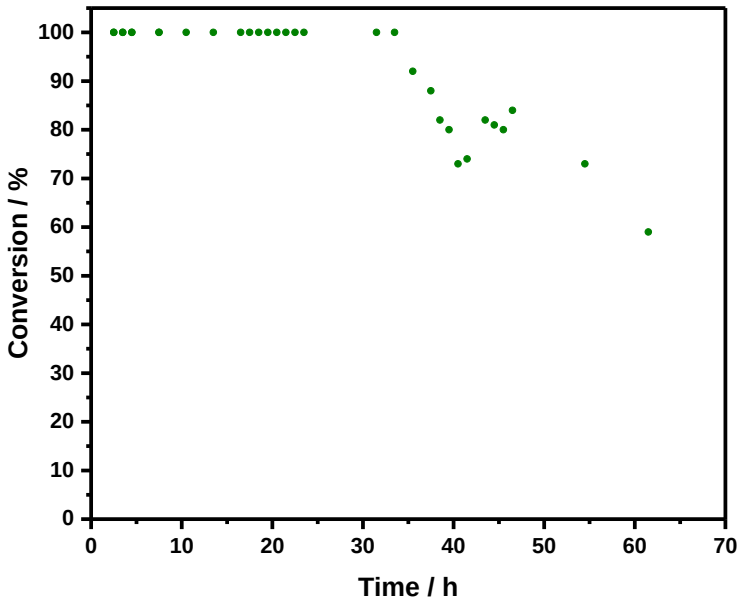


Figure 3-17: Long-term operation of the continuous PBR for the conversion of pyruvate to lactate. Reactor conditions: pyruvate (50 mM), formate (3 Eq.), NAD^+ (1 mol%), Tris-HCl buffer (50 mM, pH 8.0), FDH (30 mg), LDH (3 mg), BP2000 (30 mg), 25 °C, t_{Res} = 30 min.

The results show that full conversion was maintained for 33.5 h, demonstrating the viability of the biocatalyst over extended operating periods. During this period of operation, this reactor set-up demonstrated a STY, *E* factor and productivity of 11.1 $g_{lactate}\ L^{-1}\ h^{-1}$, 4.4 and 34.9 $\mu mol_{lactate}\ min^{-1}\ g_{support}{}^{-1}$, respectively. Long and consistent operational stability is very good for high productivities and is an important parameter to consider when analysing the applicability of a system to a scale-up in

production. In industry, long-term operation reduces the down-time in the plant, saving time and money. After 33.5 h, the conversion began to decrease, although the system maintained a high conversion (~82%) for a further 21 h. The point at which the system begins to decline allows for the conditions to be adjusted to maintain higher conversion. The extended operation increased the understanding of the system capabilities.

3.8 Summary

Quick and efficient immobilisation of FDH and LDH onto a simple carbon support for use in continuous flow has been developed. The technology was applied to the conversion of pyruvate to lactate with *in situ* NADH regeneration.

The system was optimised for conversion, STY and *E* factor. The operating conditions to achieve optimum conversion for this system are 30 min t_{Res}, 1 mol% NAD^+ and 3 Eq. formate. Optimum STY for this system can be achieved with 10 min t_{Res}, 1 mol% NAD^+ and 5 Eq. formate, and optimum *E* factor with 30 min t_{Res}, 1 mol% NAD^+ and 1 Eq. formate. The reaction conditions that are required for the system to run in the optimum window for the three parameters combined are 25–30 min t_{Res}, 0.8–1 mol% NAD^+ and 2.5–5 Eq. formate.

The BP2000 carbon has proven to be a feasible enzyme support with benefits such as quick and efficient immobilisation, involving a single-step adsorption procedure that compares favourably to other immobilisation methods, which can be lengthy, involve complex procedures and be costly. The enzyme-modified BP2000 catalyst has been shown to perform very well under flow conditions for long periods of time (>35 h) with high stability, high cofactor turnover numbers and high conversion.

Taken together, this Chapter has shown carbon as a viable support material for NADH-dependent biocatalysis in continuous flow with FDH–formate driven cofactor recycling. In subsequent chapters, this technology will be extended to additional enzymes and substrates in flow, as well as biocatalytic H_2-driven cofactor recycling.

4 Immobilising FDH and ketoreductase enzymes onto carbon for industrially relevant biocatalysis in continuous flow

4.1 Introduction

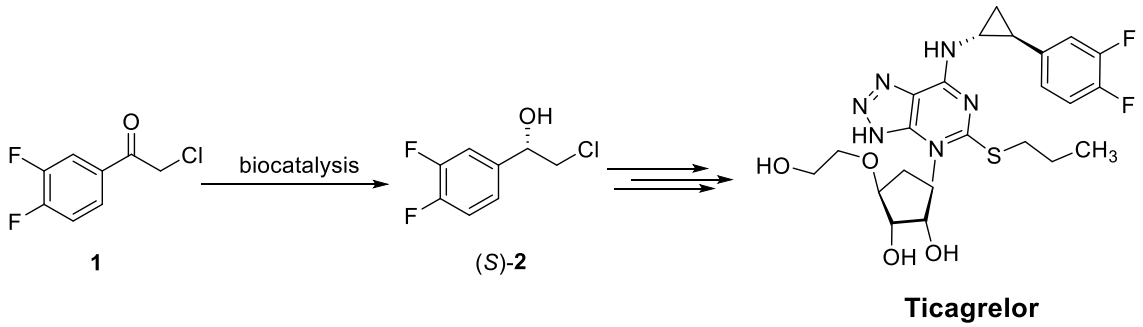
In the previous chapter, FDH and LDH immobilised onto BP2000 was shown to be a viable catalyst for the conversion of pyruvate to lactate in continuous flow with formate-driven cofactor recycling. The aim of this chapter was to apply the enzyme-modified BP2000 catalytic system to the biocatalytic synthesis of a range of API precursor molecules with formate-driven cofactor recycling. This was planned to be achieved by co-immobilising a suite of different NADH-dependent keto-reductases alongside the FDH onto the BP2000. The project was performed in collaboration with Dr Reddy's Laboratories, the industrial partner for this project, with some of the experiments taking place during an industrial placement at their research and development site in Cambridge, UK.

4.2 Biocatalytic synthesis of API precursor molecules with FDH recycling

4.2.1 Ticagrelor

The first biocatalytic transformation of interest was the synthesis of (*S*)-2-chloro-1-(3,4-difluorophenyl)ethan-1-ol ((*S*)-**2**) from 2-chloro-1-(3,4-difluorophenyl)ethan-1-one (**1**). The (*S*)-**2** is a precursor to the drug Ticagrelor, which is a blood thinning medication administered to people with acute coronary syndrome, aiming to prevent strokes and heart attacks.[254]

Scheme 4-1: Biocatalytic conversion of **1** to (*S*)-**2** in the synthesis of the API Ticagrelor.



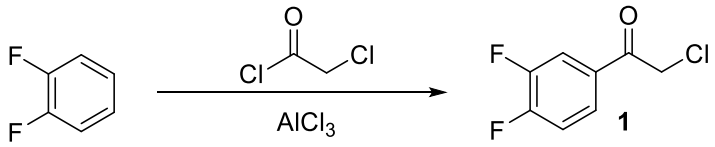
1 (*S*)-**2** **Ticagrelor**

Ticagrelor, which was discovered by Astra Zeneca and approved by the FDA for medical use in 2011, works as an antagonist on the P2Y receptor leading to inhibition of platelet aggregation.[255] Since 2019, the patent for Ticagrelor has begun to run out for its approved medical uses, meaning that any company can manufacture and sell it (assuming that the product meets the standards of the medical authorities). Thus, generic-drug companies such as Dr Reddy's, which specialises in the manufacture of 'off-patent' drugs, have a keen interest in the cheap and efficient manufacture of this drug and its precursors.

4.2.2 Synthesis of the starting material 2-chloro-1-(3,4-difluorophenyl)ethan-1-one

The synthesis of the starting material **1** (10.43 g) was achieved in an 84% yield by Friedel–Crafts acylation (Scheme 4-2), through the reaction of 1,2-difluorobenzene (9.00 g), aluminium chloride (9.43 g) and chloroacetyl chloride (6.23 mL).

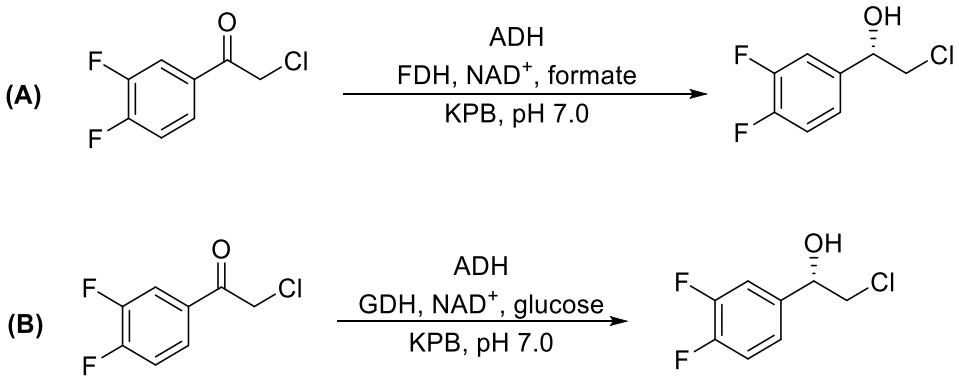
Scheme 4-2: Synthesis of **1** through Friedel–Crafts acylation (see Appendix E for experimental procedure).



4.2.3 Enzyme screening for ketone reduction of 2-chloro-1-(3,4-difluorophenyl)ethan-1-one, in solution

The aim of this section was to screen a number of viable enzyme candidates for the biocatalytic ketone reduction of **1** to (*S*)-**2**. The enzymes chosen (ADH-19, ADH-20, ADH-61, Johnson Matthey) with guidance from the industrial partner. The experiments aimed to test the biocatalytic systems in solution with FDH–formate cofactor recycling (Scheme 4-3(A)) and with GDH–glucose cofactor recycling (Scheme 4-3(B)). Guided by the industrial partner both systems were performed for comparison. The reactions were performed in a potassium phosphate buffer (KPB) because this is the standard initial testing buffer that is used for biocatalysis at the industrial partner.

Scheme 4-3: (A) Reduction of **1** to (*S*)-**2** by an NADH-dependent ADH with FDH-driven cofactor recycling, performed in solution. (B) Reduction of **1** to (*S*)-**2** by an NADH-dependent ADH with GDH-driven cofactor recycling, performed in solution.



The reactions were performed by adding a 1 mL solution of **1** (31 mM, 6 mg), NAD^+ (1 mM), formate (100 mM) and DMSO (3 v/v%) in KPB (50 mM, pH 7.0) to a 1.5 mL microcentrifuge tube containing FDH or GDH (2 mg, 33 wt%) and ADH-19, ADH-20 or ADH-21 (2 mg, 33 wt%) and then placing the resulting reaction mixture onto a microcentrifuge shaker for 17 h (30 °C, 1,200 RPM). The conversion of the reactions, shown in Table 4-1, was analysed by reverse-phase HPLC with a method already developed for this substrate by the industrial partner.

Table 4-1: Comparison of ADH-19, ADH-20 and ADH-61 for the batch conversion of **1** to (*S*)-**2** with FDH or GDH cofactor recycling. Performed with the enzymes in solution.

Entry	Enzyme	Cofactor recycling enzyme	Conversion / %
1	ADH-19	FDH	26
2	ADH-20	FDH	4
3	ADH-61	FDH	90
4	ADH-19	GDH	69
5	ADH-20	GDH	23
6	ADH-61	GDH	99

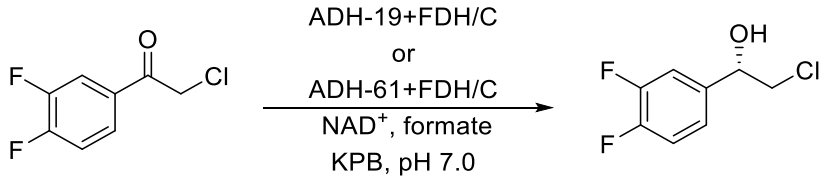
Reaction conditions: ketone (31 mM), NAD^+ (1 mM), formate (100 mM), DMSO (3 v/v%), KPB (50 mM, pH 8.0), ADH (2 mg), FDH (2 mg), 1 mL, 17 h, 30 °C, shaker speed: 1,200 RPM.

The results in Table 4-1 show that all three enzymes display some activity towards the conversion of **1** to (*S*)-**2** with both of the cofactor recycling systems. The ADH-61 displayed the best conversion with both the FDH–formate (Entry 3, 90%) and GDH–glucose (Entry 6, 99%) recycling systems. The ADH-19 achieved the next best levels of conversion; however, the reaction with the FDH–formate recycling system (Entry 1) achieved a far lower conversion (26%) than the reaction with the GDH–glucose recycling (Entry 4, 69%). It is probable that the low activity of the FDH limited this system. The ADH-20 achieved a relatively poor conversion with both recycling systems (Entry 2 and Entry 5). The next step was immobilisation of the ADH enzymes onto BP2000. It was decided to continue the study using only ADH-19 and ADH-61 because of the poor ketone reduction activity shown by ADH-20.

4.2.4 Biocatalytic ketone reduction of 2-chloro-1-(3,4-difluorophenyl)ethan-1-one, with enzymes immobilised onto BP2000

The aim of the next experiment was to determine whether ADH-19 or ADH-61 would display activity when immobilised onto BP2000. In this Chapter the enzymes were immobilised onto BP2000 by following the BP2000 procedure detailed in Section 3.2.1. The ADH-19 or ADH-61 and FDH were immobilised onto BP2000 and deployed in a batch experiment to determine whether the enzyme-modified particles would catalyse the conversion of **1** to (*S*)-**2** (Scheme 4-4).

Scheme 4-4: Reduction of **1** to (*S*)-**2** by an NADH-dependent ADH co-immobilised onto BP2000 with FDH for cofactor recycling.



The reactions were performed by adding a 1 mL solution of **1** (31 mM, 6 mg), NAD^+ (1 mM), formate (100 mM) and DMSO (3 v/v%) in KPB (50 mM, pH 7.0) to a 1.5 mL microcentrifuge tube containing FDH (2 mg, 33 wt%) and ADH-19 or ADH-21 (2 mg, 33 wt%) immobilised onto BP2000 (2 mg, 33 wt%) and then placing the resulting reaction mixture onto a microcentrifuge shaker for 17 h (30 °C, 1,200 RPM). The conversion of the reactions, shown in Table 4-2, was analysed using reverse-phase HPLC.

Table 4-2 Comparison of ADH-19 or ADH-61 and FDH immobilised onto BP2000 for the batch conversion of **1** to (*S*)-**2**.

Enzyme	Conversion / %
ADH-19	30
ADH-61	4

Reaction conditions: ketone (31 mM), NAD^+ (1 mM), formate (100 mM), DMSO (3 v/v%), KPB (50 mM, pH 8.0), ADH (2 mg) +FDH (2 mg) immobilised onto BP2000 (2 mg), 1 mL, 17 h, 30 °C, shaker speed: 1,200 RPM.

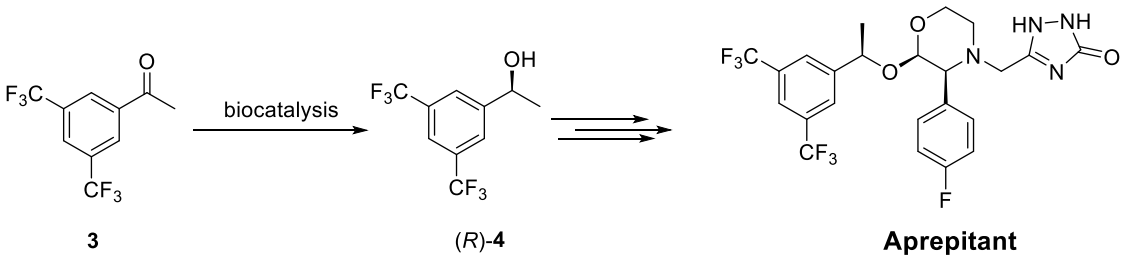
The results in Table 4-2 show that the immobilised ADH-19 achieved a greater conversion of **1** to (*S*)-**2** compared with the immobilised ADH-61. This was in contrast to the batch experiments with the enzymes in solution where the ADH-61 gave higher conversion than the ADH-19. However, the ADH-19 achieved a similar conversion when immobilised (30%) to when used in solution (26%), suggesting that the ADH-19 retains its activity when immobilised onto BP2000. Conversely, the results imply that the ADH-61 loses some catalytic activity when immobilised on BP2000.

In the next section, a biocataltyic transformation that was studied concurrently with the transformation in this section during the industrial placement is described. The aim was to implement the most promising candidate of the two transformations into continuous flow.

4.2.5 Aprepitant

The next biocatalytic transformation of interest was the synthesis of (*R*)-1-(3,5-bis(trifluoromethyl)phenyl)ethan-1-ol ((*R*)-**4)** from 1-(3,5-bis(trifluoromethyl)phenyl)ethan-1-one (**3**).

Scheme 4-5: Biocatalytic conversion of **3** to (*R*)-**4** in the synthesis of the API Aprepitant.



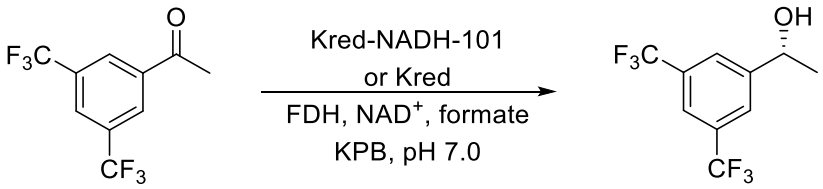
3 (*R*)-**4** **Aprepitant**

(*R*)-**4** is a precursor to the drug Aprepitant, which is used to prevent chemotherapy-induced nausea and vomiting.[256] Aprepitant, which was discovered by Merck & Co and approved by the FDA for medical use in 2003, works as an antagonist on the NK_1 receptor.[257]

4.2.6 Enzyme screening for ketone reduction of 1-(3,5-bis(trifluoromethyl)phenyl)ethan-1-one, in solution

In this section, two viable enzyme candidates are screened for the biocatalytic ketone reduction of **3** to (*R*)-**4**. The enzymes chosen (KRED-NADH-101 and KRED, Codexis) were recommended because they have been shown previously to catalyse this transformation.[258] The experiments looked to test the biocatalytic systems in solution with FDH–formate cofactor recycling (Scheme 4-6).

Scheme 4-6: Reduction of **3** to (*R*)-**4** by KRED-NADH-101 or KRED with FDH-driven cofactor recycling, performed in solution.



The reactions were performed by adding a 1 mL solution of **3** (30 mM, 8 mg), NAD^+ (1 mM), formate (100 mM) and DMSO (3 v/v%) in KPB (50 mM, pH 7.0) to a 1.5 mL microcentrifuge tube containing FDH or (2 mg, 25 wt%) and KRED-NADH-101 or KRED (2 mg, 25 wt%) and then placing the resulting reaction mixture onto a microcentrifuge shaker for 16 h (30 °C, 1,200 RPM). The conversion of the reactions, shown in Table 4-3, was analysed by GC.

Table 4-3: Comparison of KRED-NADH-101 and KRED for the batch conversion of **3** to (*R*)-**4** with FDH-driven cofactor recycling. Performed with the enzymes in solution.

Enzyme	Conversion / %
KRED-NADH-101	96
KRED	0

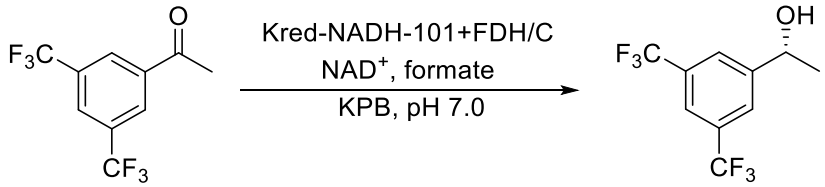
Reaction conditions: ketone (30 mM), NAD^+ (1 mM), formate (100 mM), DMSO (3 v/v%), KPB (50 mM, pH 8.0), KRED-NADH-101 or KRED (2 mg), FDH (2 mg), 1 mL, 16 h, 30 °C, shaker speed: 1,200 RPM.

The results in Table 4-3 show that the enzyme KRED-NADH-101 achieved a 96% conversion of **3** to (*R*)-**4** after 16 h. The KRED enzyme did not achieve any conversion, which concurs with the study by Dascier *et al.*, in which the KRED was found to display activity for this transformation only in the presence of NADPH.[258] Suggesting that the KRED enzyme is NADPH-dependent. Due to the promising result with KRED-NADH-101 and to the increased cost of $NADP^+$/NADPH, the KRED enzyme was not studied further. The next step was immobilisation of the KRED-NADH-101 onto BP2000.

4.2.7 Biocatalytic ketone reduction 1-(3,5-bis(trifluoromethyl)phenyl)ethan-1-one, with enzymes immobilised onto BP2000

The next experiment was designed to determine whether KRED-NADH-101 would display activity when immobilised onto BP2000. The KRED-NADH-101 and FDH were immobilised onto BP2000 and deployed in a batch experiment to discover whether the enzyme-modified particles would catalyse the conversion of **3** to (*R*)-**4** (Scheme 4-7).

Scheme 4-7: Reduction of **3** to (*R*)-**4** by an NADH-dependent KRED-NADH-101 co-immobilised onto BP2000 with FDH for cofactor recycling.



The reaction was performed by adding a 1 mL solution of **3** (30 mM, 8 mg), NAD^+ (1 mM), formate (100 mM) and DMSO (3 v/v%) in KPB (50 mM, pH 7.0) to a 1.5 mL microcentrifuge tube containing FDH (2 mg, 25 wt%) and KRED-NADH-101 (2 mg, 25 wt%) immobilised onto BP2000 (2 mg, 25 wt%) and then placing the resulting reaction mixture onto a microcentrifuge shaker for 16 h (30 °C, 1,200 RPM). The conversion of the reaction was analysed by GC.

Table 4-4: Conversion of **3** to (*R*)-**4** in batch with KRED-NADH-101 and FDH co-immobilised onto BP2000

Enzyme	Conversion / %
KRED-NADH-101	95

Reaction conditions: ketone (30 mM), NAD^+ (1 mM), formate (100 mM), DMSO (3 v/v%), KPB (50 mM, pH 8.0), KRED-NADH-101 (2 mg) + FDH (2 mg) immobilised onto BP2000 (2 mg), 1 mL, 16 h, 30 °C, shaker speed: 1,200 RPM.

The results in Table 4-4 show that the KRED-NADH-101 and FDH immobilised onto BP2000 achieved a 95% conversion of **3** to (*R*)-**4** after 16 h.

To determine the specific activity of the KRED-NADH-101 when it is immobilised onto the BP2000, four analogous batch experiments were performed and the reactions were quenched at a different period of time after $t = 0$. The reactions were performed by adding a 1 mL solution of **3** (30 mM, 8 mg), NAD^+ (1 mM), formate (100 mM) and DMSO (3 v/v%) in KPB (50 mM, pH 7.0) to a 1.5 mL microcentrifuge tube containing FDH (2 mg, 25 wt%) and KRED-NADH-101 (2 mg, 25 wt%) immobilised onto BP2000 (2 mg, 25 wt%) and then placing the resulting reaction mixture onto a microcentrifuge shaker for 16 h (30 °C, 1,200 RPM). The conversion of experiments 1 to 4 was analysed by GC after 20 min, 40 min, 60 min and 150 min, respectively and the results are displayed in Figure 4-1.

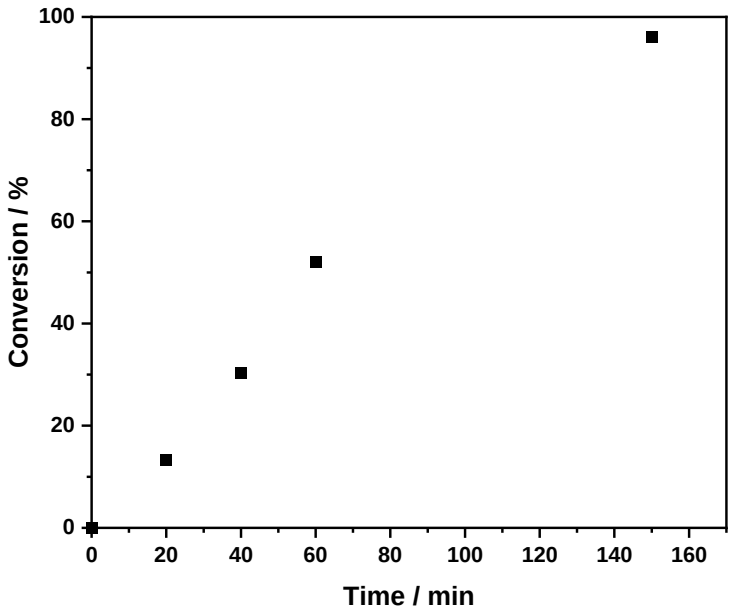


Figure 4-2: Conversion of **3** to (*R*)-**4** monitored over time in batch with KRED-NADH-101 and FDH co-immobilised onto BP2000. Reaction conditions: ketone (30 mM), NAD^+ (1 mM), formate (100 mM), DMSO (3 v/v%), KPB (50 mM, pH 8.0), KRED-NADH-101 (2 mg) + FDH (2 mg) immobilised onto BP2000 (2 mg), 1 mL, 2.5 h, 30 °C, shaker speed: 1,200 RPM.

The results in Figure 4-2 show that the KRED-NADH-101 and FDH immobilised onto BP2000 achieved a 95% conversion of **3** to (*R*)-**4** and the KRED-NADH-101 displayed an initial specific activity of 0.15 U mg^{-1}, which is a 15% retention of activity when compared to the specific activity of KRED-NADH-101 in solution for the transformation of **3** to (*R*)-**4**.[259] Although a modest retention of activity after immobilisation, the removal of the need for product and enzyme separation when performing the experiment with the enzymes in solution could be of benefit to the process in industry.

Next, an experiment was performed to compare the activity of the system with different reaction solution buffers. The reaction solution buffers tested were KPB (50 mM, pH 7.0), Tris-HCl (50 mM, pH 8.0) and unbuffered MilliQ H_2O. The reactions were performed by adding a 0.5 mL solution of **3** (30 mM, 4 mg), NAD^+ (1 mM), formate (100

mM) and DMSO (3 v/v%) in buffer (50 mM, pH 7.0) to a 1.5 mL microcentrifuge tube containing FDH (2 mg, 25 wt%) and KRED-NADH-101 (0.8 mg, 10 wt%) immobilised onto BP2000 (2 mg, 25 wt%) and then placing the resulting reaction mixture onto a microcentrifuge shaker for 3.75 h (30 °C, 1,200 RPM). The conversion from these experiments was analysed by GC.

Table 4-5: Conversion of **3** to (*R*)-**4** in batch with KRED-NADH-101 and FDH co-immobilised onto BP2000 in different buffer systems

Enzyme	Buffer	Conversion / %
KRED-NADH-101	Phosphate (50 mM, pH 7.0)	41
KRED-NADH-101	Tris-HCl (50 mM, pH 8.0)	34
KRED-NADH-101	MilliQ H_2O	21

Reaction conditions: ketone (30 mM), NAD^+ (1 mM), formate (100 mM), DMSO (3 v/v%), KRED-NADH-101 (0.8 mg) + FDH (2 mg) immobilised onto BP2000 (2 mg), 1 mL, 3.75 h, 30 °C, shaker speed: 1,200 RPM.

The results in Table 4-5 show that the KRED-NADH-101 and FDH immobilised onto BP2000 achieved conversion of **3** to (*R*)-**4** after 3.75 h, in every buffer system. The best conversion of 41% was achieved in the KPB. Therefore, the KPB remained the buffer system of choice for future experiments on this system.

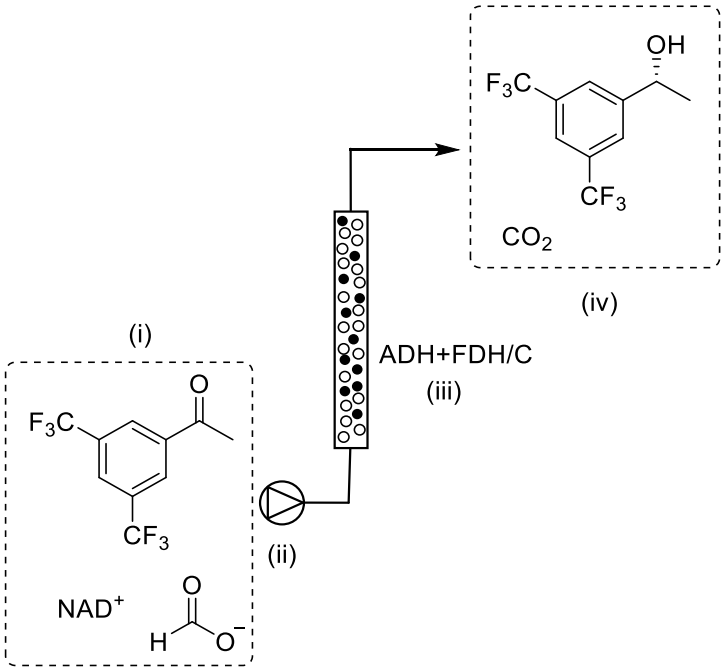
Overall, in this section, the Aprepitant precursor transformation has achieved greater conversion in batch with the enzymes immobilised onto BP2000 compared with the Ticagrelor precursor transformation in Section 4.2.4. It was therefore decided to proceed with the Aprepitant precursor transformation for translation into continuous flow.

4.2.8 Biocatalytic conversion of 1-(3,5-bis(trifluoromethyl) phenyl)ethan-1-one to (*R*)-1-(3,5-bis(trifluoromethyl) phenyl)ethan-1-ol in continuous flow

Having established activity of the BP2000 modified with FDH and KRED-NADH-101 in batch, the biocatalytic system was next translated to a continuous reactor. This was guided by the optimised conditions established in Chapter 3 for the FDH and LDH system, and the batch results from Section 4.2.7.

The flow reactor was set up as shown in Scheme 4-8. The reaction solution containing **3**, NAD^+, formate and DMSO (3 v/v%) in KPB was pumped from a reservoir (i) by a stainless-steel pump (VapourTec R2+) (ii) through the PBR (iii), which contained ADH-19 and FDH immobilised onto carbon mixed with glass beads. The product mixture was sampled with a fraction collector (iv). The flow experiments in this chapter were performed according to the general flow procedure specified in Section 3.3.3, unless specified otherwise.

Scheme 4-8: The set-up of the flow reactor for the continuous biocatalytic conversion of **3** to (*R*)-**4**. (i) Vessel containing the reactants (**3** , NAD^+, formate) in a solution of Tris-HCl or H_2O; (ii) syringe pump; (iii) ADH and FDH immobilised onto BP2000, mixed with glass beads in a PBR; (iv) product containing mixture is sampled with a fraction collector.



The first continuous flow experiment carried out using this set-up took place during an industrial placement. Here, the continuous flow manifold available (VapourTec R2) had a liquid flow rate range of 0.1–10 mL min^{-1}; by contrast, the syringe pump used in Chapter 3 had a flow rate range of 1–250 µL min^{-1}. This meant that the system had to be run at shorter t_{Res} than the typical experiments in Chapter 3, with the syringe pump (typical experimental flow rate = ~20 µL min^{-1}). However, the other experimental conditions chosen were analogous to the optimised conditions found for the pyruvate to lactate set-up in Chapter 3. The solubility of the substrate was poor in aqueous buffer; therefore, 3 v/v% DMSO was added to the reaction solution to help to improve the solubility. A reaction solution containing 1-(3,5-bis(trifluoromethyl)phenyl) ethan-1-one (50 mM), NAD^+ (0.5 mM), DMSO (3 v/v%) and sodium formate (250 mM) in KPB (50

mM, pH 7.0) was pumped through a PBR (Omnifit adjustable column, total volume = 1.02 mL) loaded with FDH (20 mg) and ADH-NADH-101 (8 mg) onto BP2000 (7 mg) at a flow rate of 0.1 mL min^{-1}, equivalent to a t_{Res} of 5 min.

Unfortunately, a considerable amount of leaching of the enzyme-modified BP2000 particles out of the PBR was observed at a liquid flow rate of 0.1 mL min^{-1}. This issue highlighted the challenges of working with the small diameter of the BP2000 particles (µm–nm scale), which made leaching of the BP2000 through the PBR frits (10 µm) increasingly likely at higher flow rates, where the pressure inside the PBR might be higher because of the relatively increased volumes of liquid exiting the PBR. To troubleshoot this, a suite of different carbon particles with larger diameters was tested for this reaction in batch. A successful candidate with an increased particle diameter could then be translated into the continuous flow reactor.

A series of batch reactions was performed using a suite of carbon types available in the laboratory at the industrial partner that all have >1 mm diameter. For the six larger types of carbon particle used in Table 4-6, a general procedure for preparing the enzyme-modified carbon particles was followed. The carbon particles were washed with phosphate buffer (50 mM, pH 7.0). The enzymes were removed from cold storage (−20 °C or −80 °C) and stored in a cold box. Solid enzymes were suspended in with phosphate buffer (50 mM, pH 7.0) to the required concentration. When using multiple enzymes, they were pre-mixed to the desired ratio. The enzymes were exposed to the carbon particles and gently mixed in a 1.5 mL microcentrifuge tube. The enzymes were immobilised on to the carbon support by adsorption at 4 °C for 2 h (unless stated otherwise). Immobilisation times for each enzyme were determined by initial adsorption studies. The enzyme-modified particles were then centrifuged (Eppendorf, MiniSpin

Plus, 2 min, 14000 x *g*) and the supernatant was removed. The enzyme-modified carbon particles were washed with phosphate buffer (50 mM, pH 7.0) and the desired amount was then ready to be transferred into the batch vessel or flow PBR.

The batch reactions were performed by adding a 0.5 mL solution of **3** (30 mM, 4 mg), NAD^+ (1 mM), formate (100 mM) and DMSO (3 v/v%) in KPB (50 mM, pH 7.0) to a 1.5 mL microcentrifuge tube containing FDH (2 mg, 25 wt%) and KRED-NADH-101 (0.8 mg, 10 wt%) immobilised onto the different types of carbon (2 mg, 25 wt%) and then placing the resulting reaction mixture onto a microcentrifuge shaker for 18 h (30 °C, 1,200 RPM). The conversion was analysed using GC.

Table 4-6: Conversion of **3** to (*R*)-**4** in batch with KRED-NADH-101 and FDH co-immobilised onto different types of carbon

Entry	Carbon	Conversion / %
1	BP2000	92
2	Norit A supra	N.D.[a]
3	Norit C Extra	N.D.
4	Norit SX Plus	N.D.
5	Norit CN 1	N.D.
6	Acros organic act. charcoal	N.D.
7	Darco activated charcoal (60-100 mesh)	90

[a]N.D. = none detected. Reaction conditions: ketone (30 mM), NAD^+ (1 mM), formate (100 mM), DMSO (3 v/v%), KPB (50 mM, pH 8.0), KRED-NADH-101 (0.8 mg) + FDH (2 mg) immobilised onto carbon (2 mg), 0.5 mL, 18 h, 30 °C, shaker speed: 1,200 RPM.

The results in Table 4-6 show that the FDH and KRED-NADH-101 immobilised onto the activated Darco (60–100 mesh) achieved a conversion of 90% **3** to (*R*)-**4** after 18 h (Entry 7). A performance that is comparable to the enzymes when immobilised onto BP2000, for which a 92% conversion was achieved (Entry 1). Next, the activated Darco was

transferred into continuous flow. For simplicity, the Darco-activated charcoal (60-100 mesh) will be referred to as 'activated charcoal' for the rest of this thesis.

A reaction analogous to the previous continuous flow experiment was performed with the FDH and KRED-NADH-101 immobilised onto activated charcoal. A reaction solution containing **3** (50 mM), NAD^+ (0.5 mM), DMSO (3 v/v%) and sodium formate (250 mM) in KPB (50 mM, pH 7.0) was pumped through a PBR (Omnifit adjustable column, total volume = 1.02 mL) loaded with FDH (20 mg) and ADH-NADH-101 (8 mg) immobilised onto activated charcoal (20 mg) at a flow rate of 0.1 mL min^{-1}, equivalent to a t_{Res} of 5 min. Each fraction was collected every 20 min and analysed by GC.

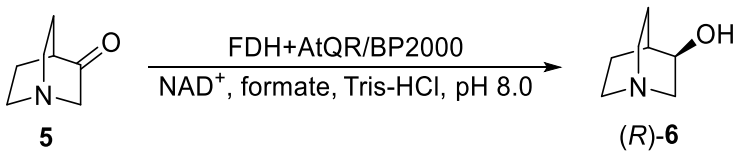
Promisingly, at a liquid flow rate of 0.1 mL min^{-1}, no leaching of the enzyme-modified activated charcoal out of the PBR was observed. However, after a 4 h reaction time, no conversion of **3** to (*R*)-**4** was detected in any of the collected reaction fractions. This was possibly because the starting material was sparingly soluble, despite 3 v/v% DMSO being used to improve this, meaning that the starting material was not being pumped into the PBR at all, although, it was hoped that the constant stirring of the reaction solution would overcome this. Alternatively, the starting material might have been adsorbing onto the activated charcoal through a π-stacking interaction or by interacting through the fluorine atoms. Unfortunately, availability of the enzyme KRED-NADH-101 stalled this project. Future work could explore this system further by focusing on discovering a more optimised solvent system or blocking the sites on the activated charcoal at which the

starting material could absorb with a cheap and readily available enzyme, such as bovine serum albumin.

4.3 Biocatalytic conversion of 3-quinuclidinone to (*R*)-3-quinuclidinol in with FDH–formate cofactor recycling in continuous flow

In the previous section, the target transformation could not be achieved in continuous flow. Importantly however, the activated charcoal was discovered to be a viable form of carbon support for the enzymes, which would enable the use of enzyme-modified carbon particles in a PBR at much higher flow rates without leaching. The work in this section seeks to apply the activated charcoal support in continuous flow for the transformation of 3-quinuclidinone (**5**) to (*R*)-3-quinuclidinol ((*R*)-**6**) by the quinuclidinone reductase (from *Agrobacterium tumefaciens*, *At*QR) with FDH–formate cofactor recycling.

Scheme 4-9: Biocatalytic reduction of **5** to (*R*)-**6** by an NADH-dependent *At*QR co-immobilised onto activated charcoal with FDH for cofactor recycling.



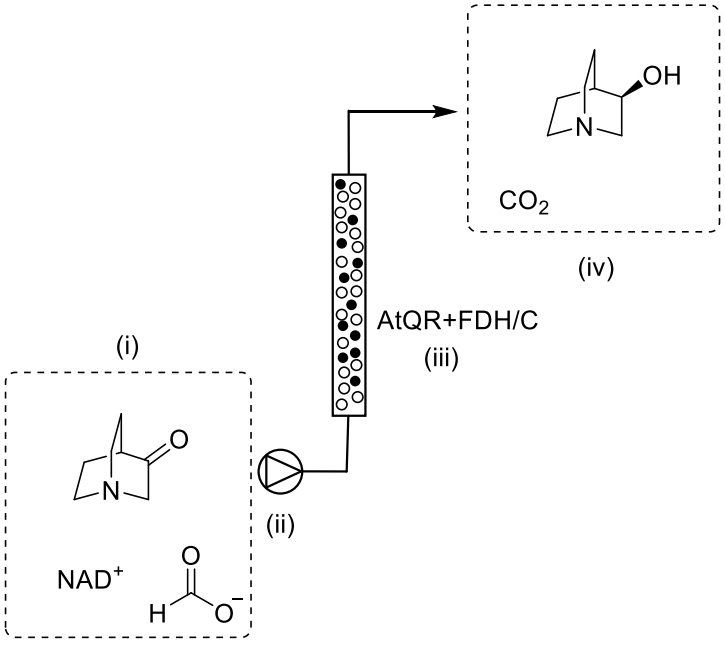
5 (*R*)-**6**

This transformation has been demonstrated by Vincent and co-workers with *At*QR and a soluble hydrogenase immobilised onto carbon nanotubes in continuous flow.[260] The (*R*)-**6** is an important precursor to a number of pharmaceutical molecules[261], including muscarine M1 and M3 agonists (possible treatment for Alzheimer disease and glaucoma, respectively), for which methods to synthesise the enantiomerically pure alcohol are required.

The flow reactor was set-up as shown in Scheme 4-10. The reaction solution containing 3-quinuclidinone, NAD^+ and formate in Tris-HCl buffer was pumped from a reservoir (i) by a peristaltic pump (VapourTec SF-10, flow rate range = 0.02–10 mL min^{-1}) (ii) through the PBR (iii), which contained *At*QR and FDH immobilised onto activated

charcoal mixed with glass beads. The product mixture was sampled with a fraction collector (iv).

Scheme 4-10: The set-up of the flow reactor for the continuous biocatalytic conversion of **5** to (*R*)-(**6**): (i) Vessel containing the reactants (3-quinuclidinone, NAD^+, formate) in a solution of Tris-HCl or H_2O; (ii) syringe pump; (iii) *At*QR and FDH immobilised onto BP2000, mixed with glass beads in a PBR. (iv) Product containing mixture is sampled with a fraction collector.



The first flow experiment for this transformation used a modest starting material concentration (10 mM) and NAD^+ concentration (1 mM) to establish whether the *At*QR would display activity when immobilised onto the activated charcoal in continuous flow. A reaction solution containing **5** (10 mM), NAD^+ (1 mM) and sodium formate (30 mM) in Tris-HCl buffer (50 mM, pH 8.0) was pumped through a PBR (Omnifit adjustable column, total volume = 1.02 mL) loaded with FDH (30 mg) and *At*QR (10.5 U) immobilised onto activated charcoal (30 mg) at a flow rate of 0.02 mL min^{-1}, the

equivalent to a t_{Res} of 30 min. The fractions were collected every 1 h and analysed using GC.

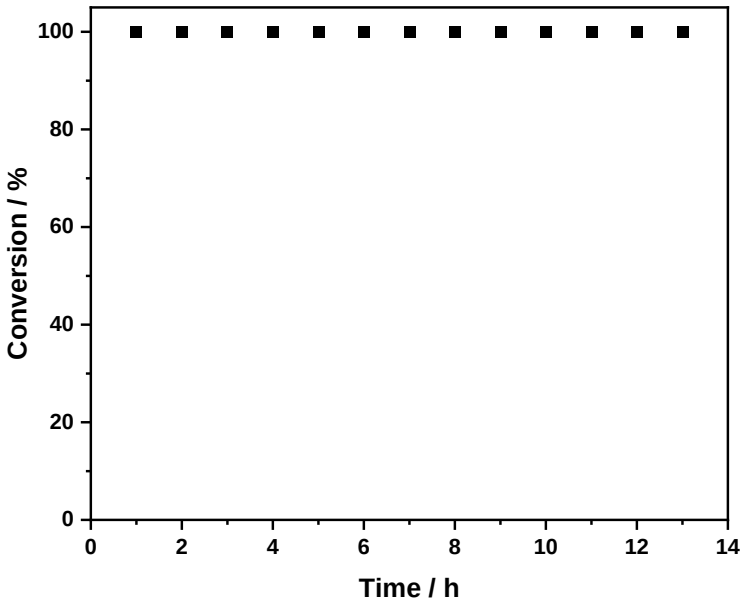


Figure 4-3: Operation of the continuous PBR for the conversion of **5** to (*R*)-**6** by FDH and *At*QR immobilised onto activated charcoal. Reactor conditions: **5** (10 mM), formate (3 Eq.), NAD^+ (10 mol%), Tris-HCl buffer (50 mM, pH 8.0), FDH (30 mg) + *At*QR (10.5 U) immobilised onto BP2000 (30 mg), 25 °C, t_{Res} = 30 min.

The results in Figure 4-3 show that the system achieved >99% of **5** to (*R*)-**6** continuously for 13 h. This provided a STY of 2.5 g L^{-1} h^{-1} and all of the reaction samples achieved an e.e. of >99.99%.

The next experiment tested the system under more strained conditions, achieved by increasing the substrate loading and decreasing the NAD^+ mol%, analogous to the reaction conditions used in Chapter 3 with the FDH–LDH system. A reaction solution containing **5** (50 mM), NAD^+ (0.5 mM), and sodium formate (150 mM) in Tris-HCl buffer (50 mM, pH 8.0) was pumped through a PBR (Omnifit adjustable column, total

volume = 1.06 mL) loaded with FDH (30 mg) and *At*QR (10.5) immobilised onto activated charcoal (30 mg) at a flow rate of 0.02 mL min^{-1}, equivalent to a t_{Res} of 30 min. The fractions were collected every 2 h and analysed by GC.

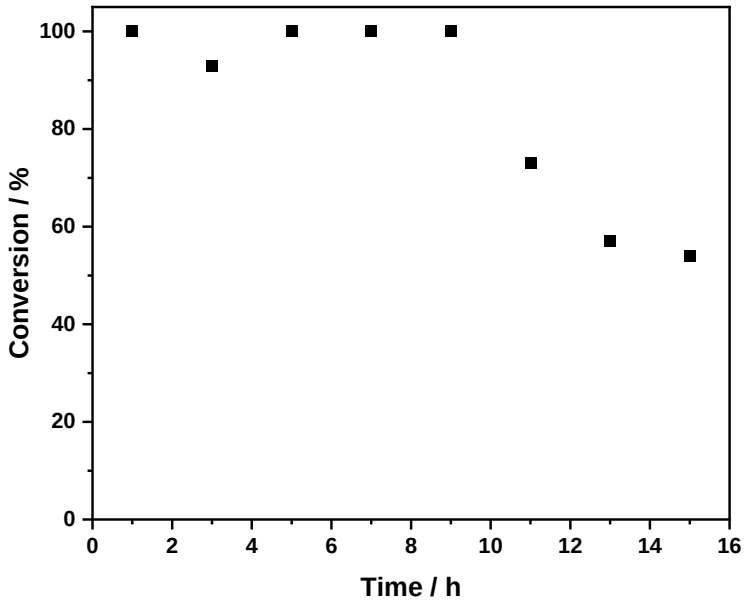


Figure 4-4: Operation of the continuous PBR for the conversion of **5** to (*R*)-**6** by FDH and *At*QR immobilised onto activated charcoal at higher starting material concentration. Reactor conditions: **5** (50 mM), formate (3 Eq.), NAD^+ (1 mol%), Tris-HCl buffer (50 mM, pH 8.0), FDH (30 mg) + *At*QR (10.5 U) immobilised onto BP2000 (30 mg), 25 °C, t_{Res} = 30 min.

The results in Figure 4-4 show that the system achieved a 93–100% steady-state conversion of **5** to (*R*)-**6** for the first 7 h of the experiment. The conversion steadily declined to 54% over the proceeding 8 h. All of the reaction samples achieved an e.e. of >99.99%. At its peak, the system provided a STY of 12.7 g L^{-1} h^{-1} and a very promising *E* factor of 1.6, within the desired range of the bulk chemicals industry. This process demonstrated the potential of the *At*QR and FDH immobilised onto activated charcoal for

the continuous production of chiral pharmaceutical compounds with FDH–formate cofactor recycling.

4.4 Summary

In this chapter, the synthesis of two API precursor molecules has been demonstrated with the ADH and FDH catalysts immobilised onto a carbon support in batch. Translation of the synthetic steps into continuous flow was not achieved; however, a viable carbon support alternative to BP2000 was found. The activated charcoal support, with a greater particle diameter than BP2000, demonstrated no leaching from the PBR at flow rates greater than 0.1 mL min^{-1} and the immobilised enzymes retained catalytic activity.

The new carbon support was further demonstrated when the enzymes *At*QR and FDH were immobilised onto the activated charcoal and used in a continuous flow PBR for the pharmaceutically relevant transformation of **5** to (*R*)-(**6**). The system displayed full conversion and an e.e. of >99.99% in a t_{Res} of 30 min, over 7 h of operation, at a STY of 12.7 g L^{-1} h^{-1} and an *E* factor of 1.6.

Overall, the Aprepitant and Ticagrelor precursor transformations still remain viable candidates for transformation into continuous flow. Once more, the *At*QR and FDH immobilised onto activated charcoal system demonstrated the potential of this set-up for the synthesis of pharmaceutical compounds.

5 Immobilising ADH onto carbon for ketone reduction and IPA-driven cofactor recycling in batch and continuous flow

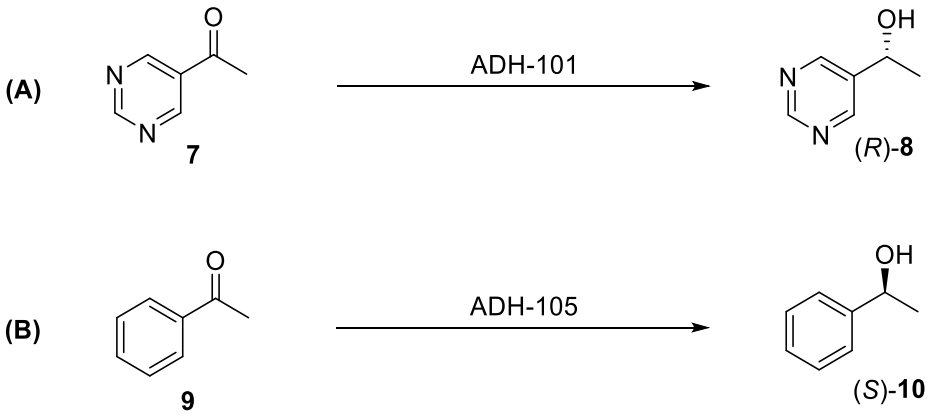
5.1 Introduction

This chapter explores the application of the enzyme-modified carbon support towards a coupled-substrate approach to cofactor recycling (ADH working to both reduce the ketone of interest and regenerate the cofactor with IPA) to perform biocatalytic ketone reduction reactions in continuous flow. As previously mentioned, ADHs are widely used in industry and the substrate-coupled cofactor approach is considered by some to be the 'gold standard'.[262] This is because of its advantages over the enzyme-coupled method, which includes the benefit of only requiring a single enzyme system and that the IPA doubles as a co-solvent, removing the requirement for an additional organic co-solvent that might affect enzyme activity, and the acetone by-product can be easily separated from the alcohol product of interest. Although, much research has been carried out on ADH substrate coupled systems for ketone reduction in homo- or heterogeneous batch conditions,[217–219,263–269] it has rarely been demonstrated heterogeneously in continuous flow, with the limited examples requiring long and complex enzyme immobilisation procedures and achieving variable results.[233,270]

In this chapter, the enzymes of focus that were capable of both a wide range of ketone reduction reactions and regenerating NADH with the sacrificial substrate IPA were ADH-101 and ADH-105, which are both manufactured and supplied by Johnson Matthey. In Vincent group, these two enzymes have been successfully shown to reduce a broad range of ketones in combination with the HydRegen cofactor regeneration system.[201,260] They

are also currently deployed homogeneously in batch reactions by the industrial partner for this project in a synthetic step with IPA cofactor recycling, towards the manufacture of an active pharmaceutical ingredient (API) and are regularly tested in their research laboratories for new routes towards target APIs. Therefore, the immobilisation of ADH-101 or ADH-105 on to carbon and use in continuous flow for ketone reductions with IPA cofactor regeneration would be of scientific interest. The model reactions of 1-(5-pyrimidinyl)ethenone (**7**) to (*R*)-1-(pyrimidin-5-yl)ethan-1-ol ((*R*)-**8**) catalysed by ADH-101, and acetophenone (**9**) to (*S*)-1-phenylethanol ((*S*)-**10**) catalysed by ADH-105 were chosen because the enzymes have been shown to accept their substrate and accurate analytical methods have already been developed in our group to study them.

Scheme 5-1: Biocatalytic transformations of interest in this chapter. (A) Conversion of **7** to (*R*)-**8** by ADH-101; (B) Conversion of **9** to (*S*)-**10** by ADH-105.



To better understand the IPA-driven cycle for both ADH-101 and ADH-105, the transformations were first implemented in batch and studied in two constituent parts (forward substrate reduction and cofactor reduction with IPA), before being combined for the full cycle and then translated into continuous flow. The studies in batch also allowed comparison of the enzymes in solution against the case in which they are immobilised on to carbon. The carbon used throughout the chapter is the activated

charcoal (~mm diameter) because of the ease of translating it into PBRs without leaching at high flow rates, and because of the previous demonstration in Chapter 4 that enzymes retain activity when immobilised onto it.

5.2 Immobilisation studies for ADH-101 and ADH-105 onto activated charcoal

The aim of this section was to determine whether the ADH-101, and ADH-105 would immobilise onto the activated charcoal and subsequently to devise a reliable protocol for their immobilisation. In Method A, ADH-101 (1 mg) suspended in Tris-HCl buffer (50 mM, pH 8.0) was added to activated charcoal (1-25 mg) in a microcentrifuge tube and placed on a microcentrifuge shaker plate (800 RPM, 25 °C), whereas in Method B the microcentrifuge tube containing the ADH-105 and activated charcoal was placed in the refrigerator (4 °C) and mixed on a vortex mixer every 20 min. The mixtures were centrifuged (Eppendorf, MiniSpin Plus, 5 min, 10,000 x g). The resulting immobilisation yield of each method was studied after 1 h and 2 h (Table 5-1) and determined by supernatant UV-Vis absorption (A_{280}), compared against protein concentration calibration curves in Appendix G. First, the immobilisation yield of ADH-101 onto activated charcoal was studied, the results are displayed in Table 5-1.

Table 5-1: Immobilisation yield of ADH-101 onto activated charcoal. Comparison of two different immobilisation strategies, where Method A is incubation of the particles on a shaker plate at 800 RPM and Method B is refrigeration of particles at 4 °C with periodic mixing. Standard deviations calculated for experiments that were performed in triplicate.

Mass of carbon / mg	Immobilisation efficiency / %			
	Method A		Method B	
	1 h	2 h	1 h	2 h
1	34 ±3.9	37 ±4.6	30	44
5	49 ±4.8	55 ±6.3	54	65
10	69	51	-	-
15	71	77 ±9.9	-	86 ±1.2
20	80	78	-	-
25	92 ±6.1	93 ±4.4	98	99

*Reaction conditions: ADH-101 (1 mg), Tris-HCl buffer (1 mL, 50 mM, pH 8.0)

The results in Table 5-1 show that there is a general trend with both methods for increased immobilisation yield with higher masses of activated charcoal. The extra hour for immobilisation appears to make a small difference at lower masses of activated charcoal for both methods, however at higher activated charcoal masses (20 mg and 25 mg) the difference is minimal. Overall, Method B appears to produce slightly higher immobilisation yields and the highest immobilisation yield achieved was 99% after 2 h, when Method B was deployed with 25 mg of activated charcoal.

Next, having determined that Method B resulted in slightly better immobilisation results than Method A, only Method B was tested to determine the immobilisation yield of ADH-105 onto the activated charcoal. The results are displayed in Table 5-2.

Table 5-2: Immobilisation yield of ADH-105 onto activated charcoal according to immobilisation Method B (refrigeration of particles at 4 °C with regular mixing). Standard deviations calculated for experiments that were performed in triplicate.

	Immobilisation Efficiency / %	
Mass of carbon / mg	**1 h**	**2 h**
1	56	58
5	83	83 ±4.3
15	90	90 ±0.7
25	97 ±0.6	97

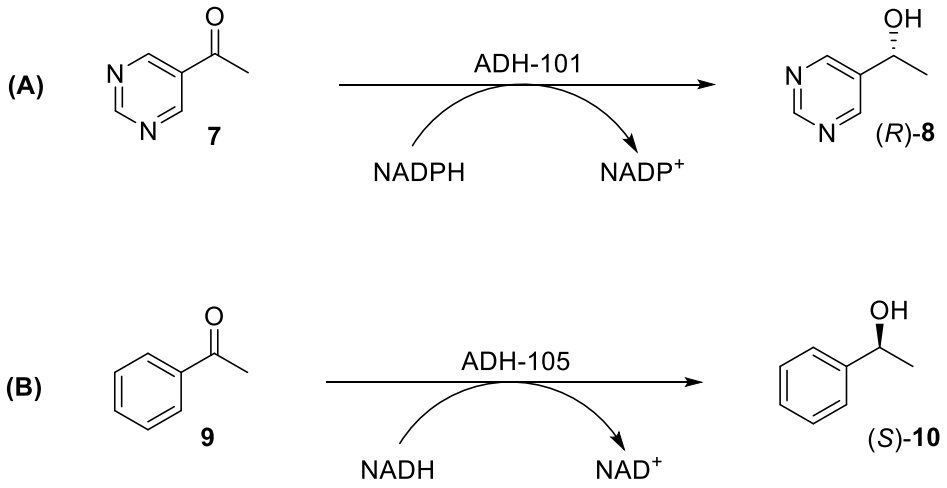
[a]T_1 = 1 h, [b] T_2 = 2 h, *Reaction conditions: ADH-105 (1 mg), Tris-HCl buffer (1 mL, 50 mM, pH 8.0)

The results in Table 5-2 show that the immobilisation yield of ADH-105 onto the activated charcoal increases as the mass of carbon increases. The highest immobilisation yield achieved was 97% after 1 h with 25 mg of activated charcoal. However, the immobilisation yield does not appear to increase proportionally with an increase in mass of carbon, therefore low masses of activated charcoal, still yield a good immobilisation yield, for example 83% for 5 mg. Once again, the difference between 1 h and 2 h immobilisation time appears to be minimal, therefore the enzyme immobilisation procedure for all subsequent experiments in this chapter was performed for 1 h.

5.3 ADH-101 and ADH-105 for the 'forward' ketone reduction reaction in batch

In this section the 'forward' ketone reduction for the transformation of **7** to (*R*)-**8** catalysed by ADH-101, and **9** to (*S*)-**10** catalysed by ADH-105 (shown in Scheme 5-2), were performed in batch mode with the enzyme in solution and with the enzyme immobilised onto activated charcoal to determine and compare the enzyme activity in both systems.

Scheme 5-2: (A) Ketone reduction of **7** catalysed by ADH-101 with super stoichiometric NADPH and (B) Ketone reduction of **9** catalysed by ADH-101 with super stoichiometric NADH



To determine the specific activity of ADH-101 in solution for the ketone reduction of **7** to (*R*)-**8** (Scheme 5-2(A)), a 1 mL batch reaction of **7**, NADPH and ADH-101 in Tris-HCl buffer was performed (Figure 5-1). The cofactors $NADP^+$/NADPH were used throughout to study this transformation because the ADH-101 has previously been shown to display greater activity in the presence of NADPH against NADH.[271] The course of the reaction was monitored by taking regular samples from the reaction solution for analysis by GC.

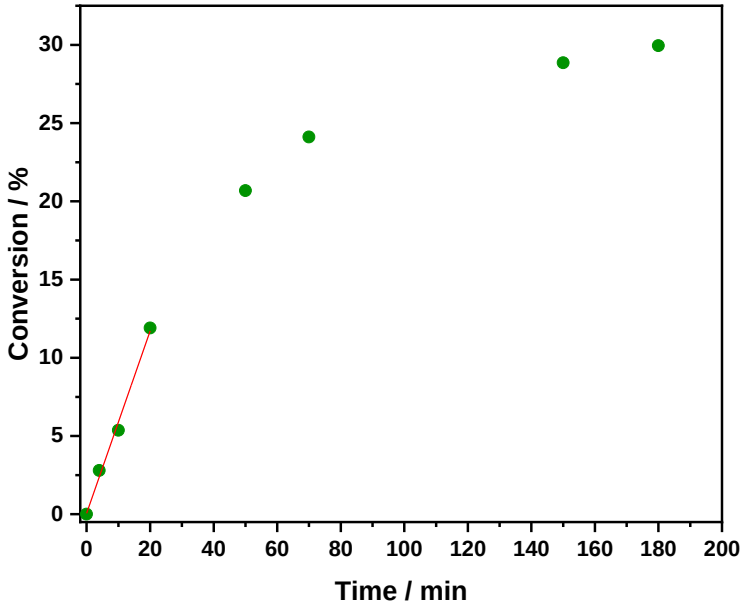


Figure 5-1: Batch enzyme activity measurement of ADH-101 in solution for the reduction of **7** with super stochiometric NADPH. The conversion of **7** to (*R*)-**8** was determined by extracting reaction solution samples for analysis by GC. Reaction conditions: ADH-101 (0.1 mg), **7** (10 mM), NADPH (12 mM), Tris-HCl (50 mM, pH 8.0), 1 mL, 25 °C, shaker plate 800 RPM.

From the results in Figure 5-1 it can be determined that the ADH-101 displayed a specific activity of 0.4 U mg^{-1}. The experiment confirmed that the ADH-101 does indeed display ketone reduction activity towards the substrate **7**.

An analogous experiment was performed to determine the specific activity of ADH-105 in solution for the ketone reduction of **9** to (*S*)-**10** (Scheme 5-2(B)), with NADH, shown in Figure 5-2.

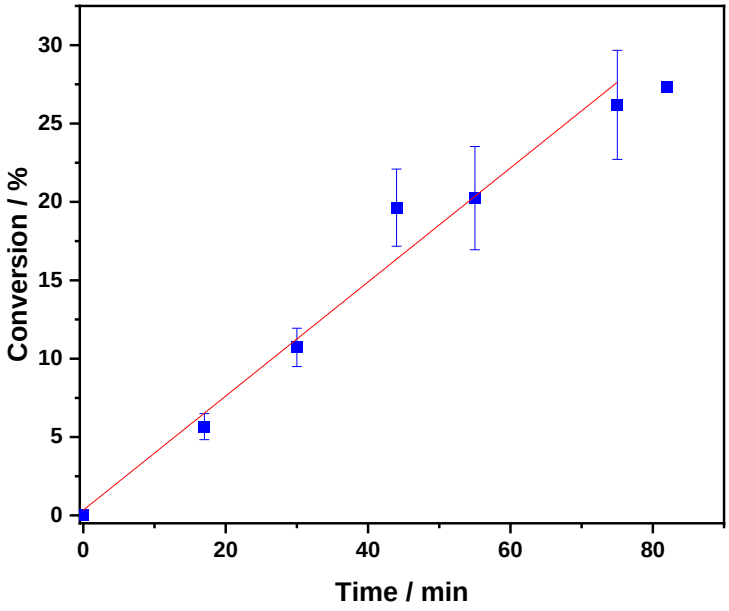


Figure 5-2: Batch enzyme activity measurement of ADH-105 in solution for the reduction of **9** with super stochiometric NADH. The conversion of **9** to (*S*)-**10** was determined by extracting reaction solution samples for analysis by GC. Reaction conditions: ADH-105 (0.1 mg), **9** (10 mM), NADH (12 mM), Tris-HCl (50 mM, pH 8.0), 1 mL, 25 °C, shaker plate 800 RPM. Error bars are shown for experiments performed in triplicate.

From the results in Figure 5-2 it can be determined that the ADH-105 displayed a specific activity of 0.4 U mg^{-1}. The experiment confirmed that the ADH-105 does display ketone reduction activity towards the **9** substrate, consistent with previous work.[201]

Subsequently, to determine the specific activity of ADH-101 when immobilised onto activated charcoal for the ketone reduction of **7** (Scheme 5-2(A)), a 1 mL batch reaction of **7** and NADPH in Tris-HCl buffer was prepared and added to a microcentrifuge tube containing ADH-101 immobilised onto activated charcoal. The reaction shown was monitored by taking regular samples from the reaction solution for analysis by GC.

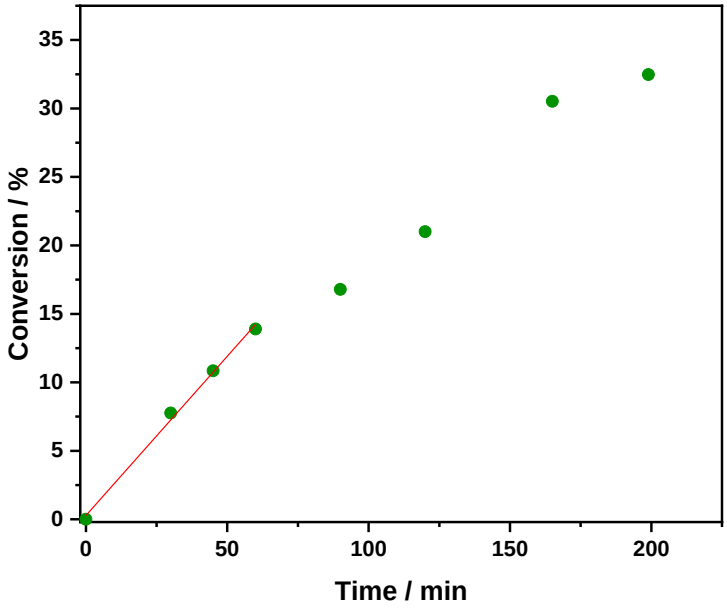


Figure 5-3: Batch enzyme activity measurement of ADH-101 immobilised on activated charcoal for the reduction of **7** with super stochiometric NADPH. The conversion of **7** to (*R*)-**8** was determined by extracting reaction solution samples for analysis by GC. Reaction conditions: ADH-101 (1 mg), activated charcoal (5 mg), **7** (10 mM), NADPH (12 mM), Tris-HCl (50 mM, pH 8.0), 1 mL, 25 °C, shaker plate 800 RPM.

From the results in Figure 5-3 it can be determined that the immobilised ADH-101 displayed a specific activity of 0.02 U mg^{-1} when immobilised onto the activated charcoal, compared with the ADH-101 free in solution was a 5% retention of activity. The specific activity value of ADH-101 immobilised onto activated charcoal is based on an 83% immobilisation efficiency. The immobilisation efficiency is factored into all further specific activity measurements of the enzymes immobilised onto activated charcoal.

An analogous 1 mL batch experiment was performed to determine the specific activity of ADH-105 when immobilised onto activated charcoal for the ketone reduction of **9** (Scheme 5-2(B)), with NADH, shown in Figure 5-4.

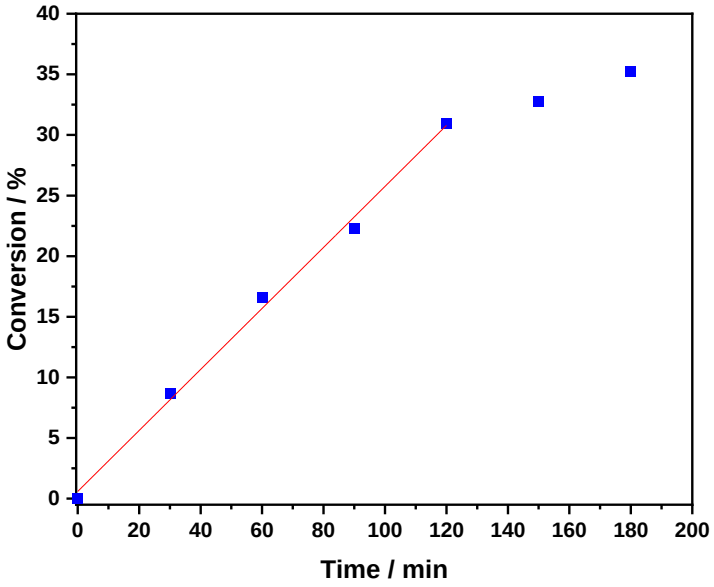


Figure 5-4: Batch enzyme activity measurement of ADH-105 immobilised on activated charcoal for the reduction of **9** with super stochiometric NADH. The conversion of **9** to (*S*)-**10** was determined by extracting reaction solution samples for analysis by GC. Reaction conditions: ADH-105 (1 mg), activated charcoal (5 mg) **9** (10 mM), NADH (12 mM), Tris-HCl (50 mM, pH 8.0), 1 mL, 25 °C, shaker plate 800 RPM.

From the results in Figure 5-4 it can be determined that **9** the immobilised ADH-105 displayed a specific activity of 0.04 U mg^{-1} when immobilised onto the activated charcoal, which represents 5% retention of activity compared with the ADH-105 free in solution for the same transformation.

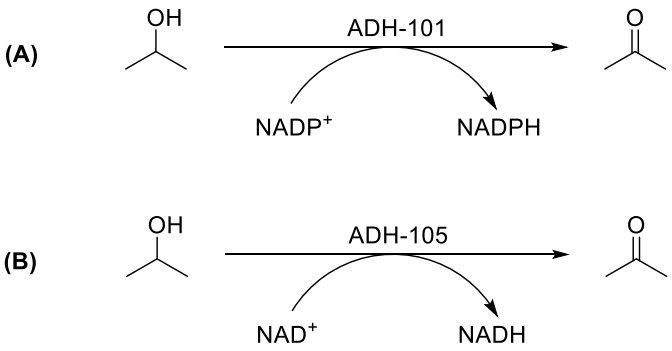
There are multiple ideas as to why the ADHs are retaining a low proportion of activity after immobilisation onto the activated charcoal. Previous research in the group has demonstrated that ADH-101 and ADH-105 show good activity when they were immobilised onto BP2000 (µm–nm scale diameter).[201] One factor is likely to be a mass transport effect, the enzyme active site less readily accessible by the substrate when immobilised onto the larger activated charcoal (~mm scale diameter) compared to the free enzyme in solution which is well mixed in with the substrate, and the enzyme-

modified BP2000 also mixes better in solution. In general, little is still known about the way in which the enzymes adsorb onto carbon, including the interaction between the enzyme and the carbon immobilisation site. Therefore, another explanation could be that the batch of these enzymes provided by Johnson Matthey for these experiments had an issue, such as being less active or containing an impurity. This is possible because experiments performed across the whole research group during this time period with the ADH-101 and ADH-105 batch used here, did not match previous experiments with other batches of the same enzymes. The ADH-101 and ADH-105 are crude enzymes, it is possible that a new chemical species or impurity could have been present in this enzyme batch impacted or impeded the enzyme immobilisation, such as blocking the enzyme active site. Alternatively, the enzyme interaction with the carbon immobilisation site could be in proximity to the enzyme active site, hampering its activity. Although not pursued in this Thesis, future experiments could be designed to study the enzyme immobilisation site on carbon, maybe using a technique such as super-resolution microscopy.

5.4 ADH-101 and ADH-105 for the 'backward' IPA-driven $NAD(P)^+$ reduction reaction in batch

In this section, the activity of ADH-101 and ADH-105 towards the 'backward' $NAD(P)^+$ reduction reaction that is driven by the NAD^+-dependent oxidation of the sacrificial reagent IPA to acetone (shown in Scheme 5-3), was studied for both enzymes in batch mode with the enzyme in solution and with the enzyme immobilised onto activated charcoal to determine and compare the enzyme activity in both systems.

Scheme 5-3: (A) $NADP^+$-dependent alcohol oxidation of IPA to acetone catalysed by ADH-101, regenerating NADPH and (B) NAD^+-dependent alcohol oxidation of IPA to acetone catalysed by ADH-105, regenerating NADH.



To determine the specific activity of ADH-101 in solution for the $NADP^+$-dependent oxidation of IPA (Scheme 5-3(A)), the conversion of $NADP^+$ to NADPH was monitored in a series of 1 mL batch reactions containing $NADP^+$ and ADH-101 in Tris-HCl buffer with a variety of IPA concentrations (1-40 v/v%). Multiple IPA concentrations were tested to determine the favoured conditions of the ADH-101 for best performance (Figure 5-5), considering that low concentrations of IPA could be rate limiting or that high concentrations could inhibit the enzyme. The course of the reaction was analysed by *in situ* UV-Vis spectroscopy.

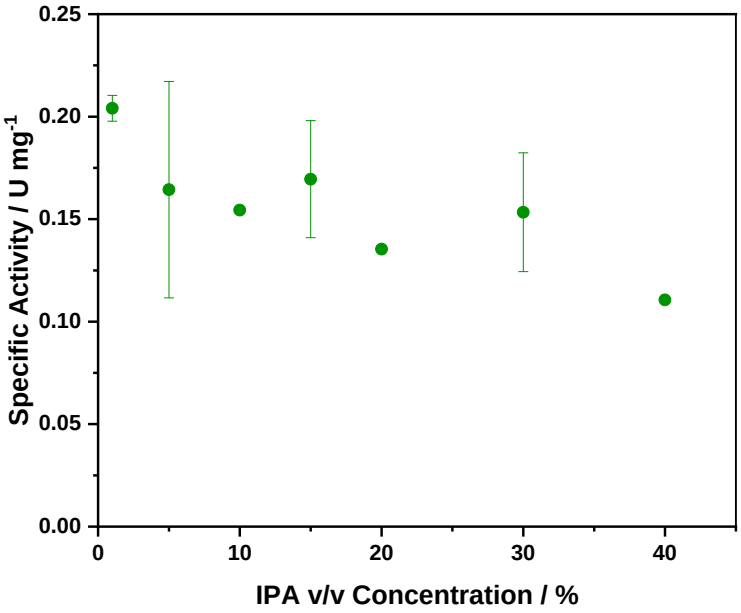


Figure 5-5: Comparison of batch enzyme activity measurements of ADH-101 in solution for the $NADP^+$ dependent reduction of IPA to acetone, at varied IPA v/v% concentrations. The conversion of $NADP^+$ to NADPH over time was determined with *in situ* UV-Vis spectroscopy for each individual experiment. Reaction conditions: ADH-101 (0.1 mg), $NADP^+$ (0.1 mM), Tris-HCl (50 mM, pH 8.0), IPA (1-40 v/v%), 1 mL, 25 °C, shaker plate 800 RPM. Error bars are shown for experiments performed in triplicate.

The results in Figure 5-5 show that the specific activity of ADH-101 for the $NADP^+$-dependent conversion of IPA to acetone (determined by monitoring the conversion of $NADP^+$ to NADPH), in general, appears to decrease as the IPA concentration is increased. The highest activity of 0.20 U mg^{-1} was achieved at an IPA concentration of 1 v/v% and the lowest activity of 0.11 U mg^{-1} was achieved at 40 v/v%. The results suggest that the ADH-101 is inhibited by IPA when used at higher concentrations.

An analogous series of batch experiments were performed to determine the specific activity of ADH-105 in solution for the NAD^+-dependent oxidation of IPA (Scheme 5-3(B)), with NAD^+, summarised in Figure 5-6.

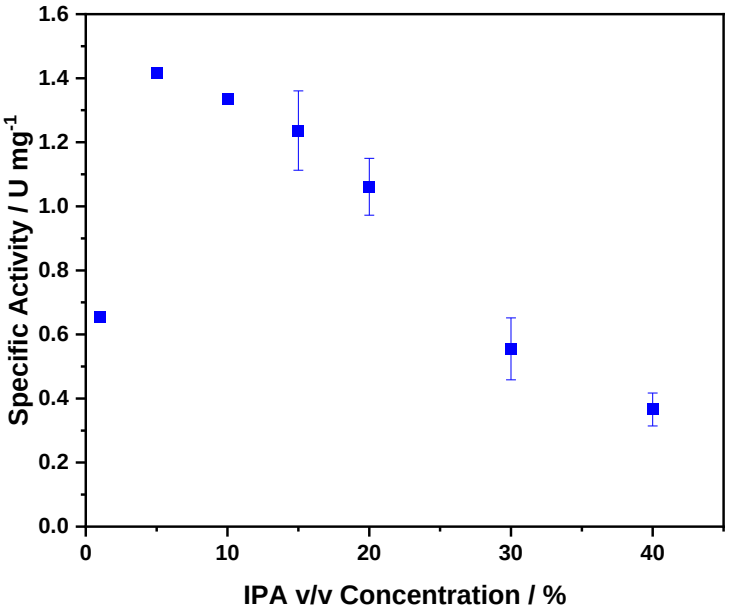


Figure 5-6: Comparison of batch enzyme activity measurements of ADH-105 in solution for the NAD^+ dependent reduction of IPA to acetone, at varied IPA v/v% concentrations. The conversion of NAD^+ to NADH over time was determined with *in situ* UV-Vis spectroscopy for each individual experiment. Reaction conditions: ADH-105 (0.1 mg), NAD^+ (0.1 mM), Tris-HCl (50 mM, pH 8.0), IPA (1-40 v/v%), 1 mL, 25 °C, shaker plate 800 RPM. Error bars are shown for experiments performed in triplicate.

The results in Figure 5-6 show that the specific activity of ADH-105 for the NAD^+-dependent conversion of IPA to acetone (determined by monitoring the conversion of NAD^+ to NADH), appears to decrease as the IPA concentration is increased. However, there is an increase in specific activity from 1 to 5 v/v% IPA, suggesting that the ADH-105 is substrate limited at an IPA concentration of 1 v/v%. The highest activity of 1.40 U mg^{-1} was achieved at an IPA concentration of 5 v/v% and the lowest activity of 0.30 U mg^{-1} was achieved at 40 v/v%. Indicating that the ADH-105 is inhibited by the IPA when used at higher concentrations.

Subsequently, to determine the specific activity of ADH-101 when immobilised onto the activated charcoal for the $NADP^+$-dependent oxidation of IPA (Scheme 5-3(A)), the IPA concentration that resulted in the best ADH-101 activity in solution (1 v/v%) was used. The experiment was performed in a 1 mL batch reaction containing $NADP^+$, and ADH-101 immobilised onto activated charcoal in Tris-HCl buffer (Figure 5-7).

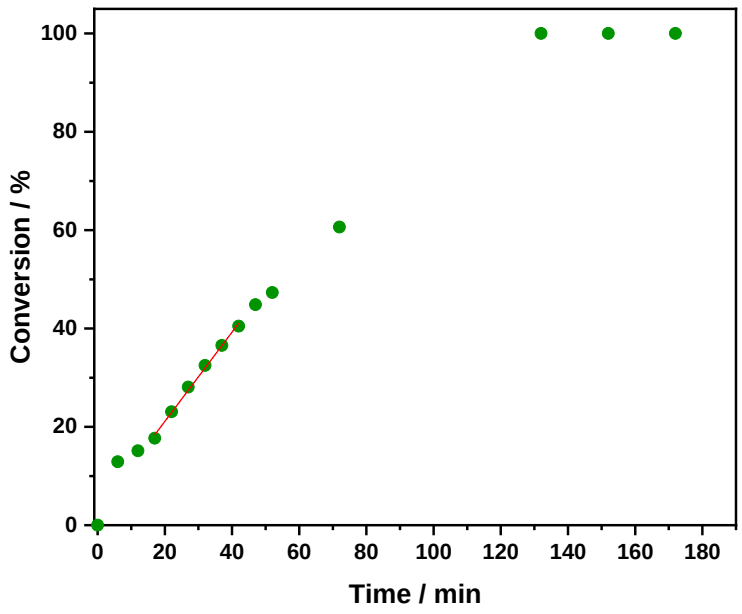


Figure 5-7: Batch enzyme activity measurement of ADH-101 immobilised on activated charcoal for the $NADP^+$ dependent reduction of IPA (1 v/v%) to acetone. The conversion of $NADP^+$ to NADPH over time was determined with *in situ* UV-Vis spectroscopy. Reaction conditions: ADH-101 (1 mg), activated charcoal (5 mg), $NADP^+$ (5 mM), Tris-HCl (50 mM, pH 8.0), IPA (1 v/v%), 1 mL, 25 °C, shaker plate 800RPM.

The results in Figure 5-7 show that after 135 min a 100% conversion of $NADP^+$ to NADPH was achieved. The ADH-101 immobilised onto activated charcoal displayed a specific activity of 0.06 U mg^{-1}, compared with the ADH-101 free in solution was a 28% retention of activity. This was expected after the retention of activity previously displayed by the ADH-101 immobilised onto activated charcoal towards the forward ketone

reduction. This retention of ADH-101 activity was higher than that of the forward ketone reduction, perhaps because mass transport is less of a problem when IPA is a solvent component in large excess.

An analogous batch reaction was performed to determine the specific activity of ADH-105 when immobilised onto the activated charcoal for the NAD^+-dependent oxidation of IPA (Scheme 5-3(A)), the enzyme-modified carbon particles were tested at two different IPA concentrations, including the IPA concentration that resulted in the best ADH-105 activity in solution (5 v/v%) and 20 v/v%, so that the heterogeneous results could be compared to the previous homogeneous data. The results are shown in Figure 5-8.

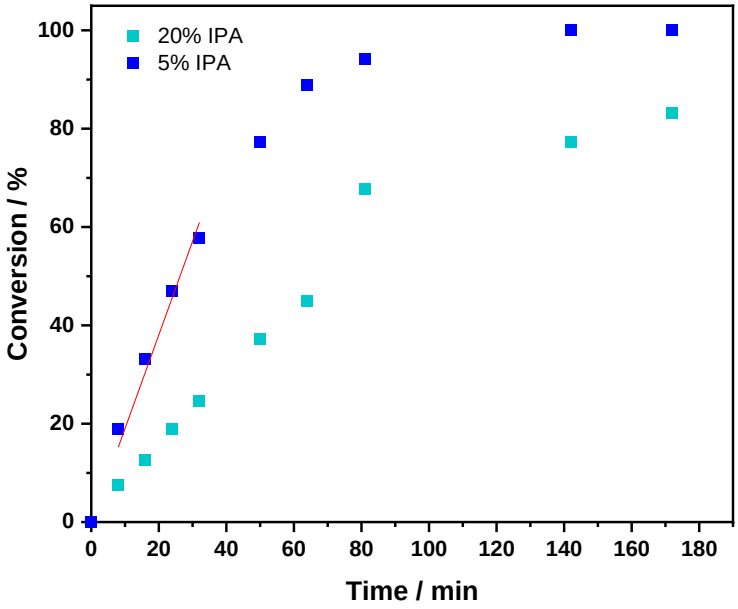


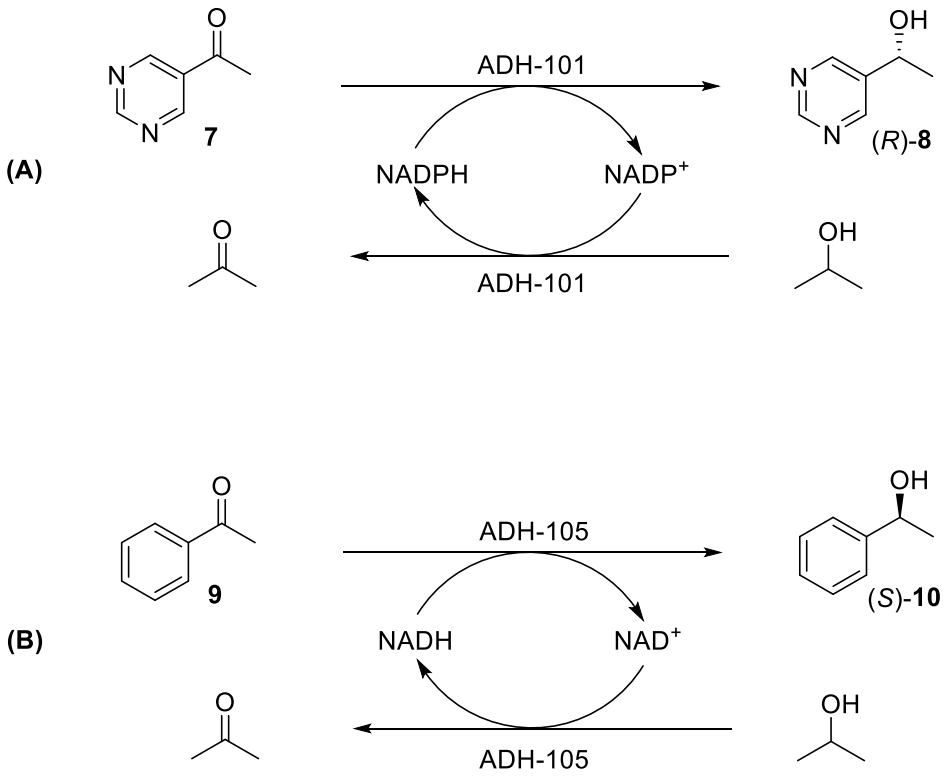
Figure 5-8: Batch enzyme activity measurements of ADH-105 immobilised on activated charcoal for the NAD^+ dependent reduction of IPA (5 v/v%, dark blue square) and IPA (20 v/v%, light blue square) to acetone. The conversion of NAD^+ to NADH over time was determined with *in situ* UV-Vis spectroscopy. Reaction conditions: ADH-105 (1 mg), activated charcoal (5 mg), NAD^+ (5 mM), Tris-HCl (50 mM, pH 8.0), IPA (5 and 20 v/v%), 1 mL, 25 °C, shaker plate 800 RPM.

The results in Figure 5-8 show that after 175 min a 100% conversion of NAD^+ to NADH was achieved at 5 v/v% IPA and an 82% conversion was at 20 v/v% IPA. The decrease in specific activity of the heterogeneous ADH-105 as the IPA concentration increases follows the same trend as the homogeneous ADH-105 for the same transformation. Overall, at 5 v/v% IPA, the ADH-105 immobilised onto activated charcoal displayed a specific activity of 0.1 U mg^{-1}, compared with the ADH-105 free in solution represents a 7% retention of activity.

5.5 Full cycle: ketone reduction and substrate coupled IPA-driven cofactor recycling with ADH-101 and ADH-105 in batch

After studying the 'forward' and 'backward' components of the reaction cycle for both ADH-101 and ADH-101, homo- and heterogeneously in the Section 5.3 and 5.4. The next step was to put the two components together and perform the full reaction cycle. In this section the full reaction cycle for the transformation of **7** to (*R*)-**8** catalysed by ADH-101 with substrate coupled IPA-driven cofactor recycling (shown in Scheme 5-4(A)), and the transformation of **9** to (*S*)-**10** catalysed by ADH-105 with substrate coupled IPA-driven cofactor recycling (shown in Scheme 5-4(B)), were performed in batch mode with the enzyme in solution and with the enzyme immobilised onto activated charcoal to determine and compare the enzyme activity in both systems.

Scheme 5-4: (A) NADPH-dependent biocatalytic conversion of **7** to (*R*)-**8**, employing ADH-101 for ketone reduction and cofactor recycling. (B) NADH-dependent biocatalytic conversion of **9** to (*S*)-**10**, employing ADH-105 for ketone reduction and cofactor recycling.



5.5.1 Full cycle: reduction of 1-(5-pyrimidinyl)ethenone with IPA-driven cofactor recycling by ADH-101 in batch

Firstly, to determine the specific activity of ADH-101 in solution for the full cycle ketone reduction of **7** to (*R*)-**8** with IPA-driven cofactor recycling (Scheme 5-4 (A)), initial experiments were performed with a variety of IPA concentrations. The IPA concentration that resulted in the best ADH-101 specific activity in solution could then be carried forward to the heterogenous reactions. A series of 1 mL batch reactions containing **7**, $NADP^+$, IPA and ADH-101 in Tris-HCl buffer were performed (Figure 5-9).

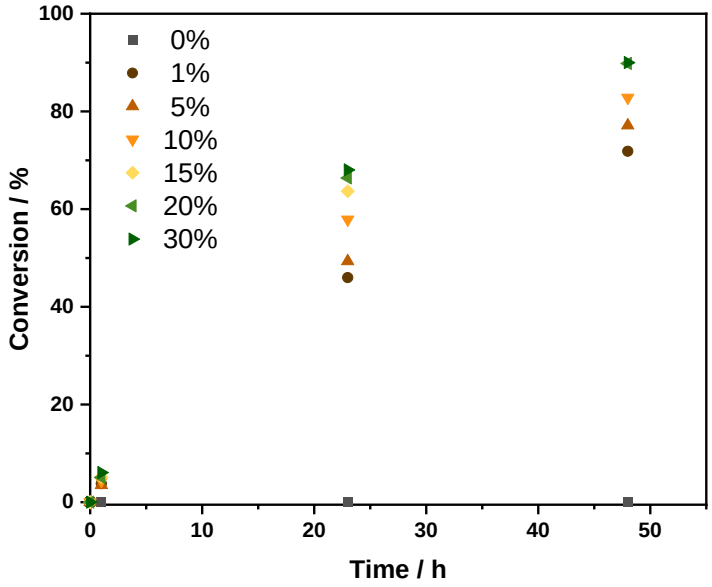


Figure 5-9: Batch biocatalytic conversion of **7** to (*R*)-**8** over time, employing ADH-101 in solution for ketone reduction and cofactor recycling at various IPA concentrations (0-30 v/v%). The conversion of **7** to (*R*)-**8** was determined by extracting reaction solution samples for analysis by GC. Reaction conditions: ADH-101 (0.1 mg), **7** (50 mM), $NADP^+$ (5 mM), Tris-HCl (50 mM, pH 8.0), IPA (0-30 v/v%), 1 mL, 25 °C, shaker plate 800 RPM.

The results in Figure 5-9 show that the full cycle system achieves higher conversion of **7** to (*R*)-**8** as the IPA concentration increases. This is in contrast to the results shown in Section 5.4, that showed the ADH-101 favoured lower IPA concentrations for the 'backward' cofactor regeneration step. This could be caused by improved substrate solubility at increased IPA concentrations shifting the equilibrium of the reaction more towards ketone reduction. The reactions at both 20 and 30 v/v% IPA resulted in a 90% conversion of **7** to (*R*)-**8** after 48 h, with the ADH-101 displaying a specific activity of 0.42 U mg^{-1} (calculated from 1 h time point). For the heterogenous reaction 20 v/v% IPA was chosen instead of 30 v/v%

Henceforth, to determine the specific activity of ADH-101 immobilised onto activated charcoal for the full cycle ketone reduction of **7** to (*R*)-**8** with IPA-driven cofactor recycling (Scheme 5-4 (A)), a 1 mL batch experiment containing **7**, $NADP^+$, IPA and ADH-101 immobilised onto activated charcoal in Tris-HCl buffer was performed (Figure 5-10).

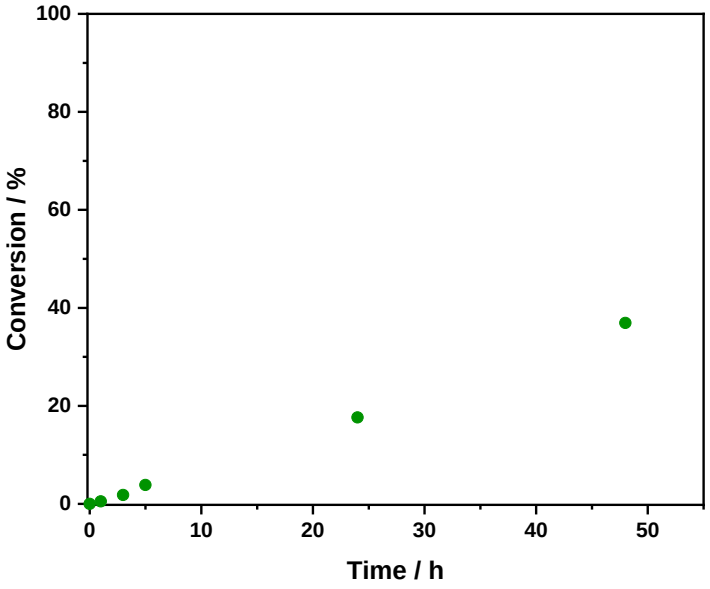


Figure 5-10: Batch biocatalytic conversion of **7** to (*R*)-**8** over time, employing ADH-101 immobilised on activated charcoal for ketone reduction and cofactor recycling at an IPA concentration of 1 v/v%. The conversion of **7** to (*R*)-**8** was determined by extracting reaction solution samples for analysis by GC. Reaction conditions: ADH-101 (1 mg), activated charcoal (5 mg), **7** (50 mM), $NADP^+$ (5 mM), Tris-HCl (50 mM, pH 8.0), IPA (1 v/v%), 1 mL, 25 °C, shaker plate 800 RPM.

The results in Figure 5-10 show that the heterogeneous full cycle system at 20% v/v% IPA achieved a 37% conversion of **7** to (*R*)-**8**, after 48 h. The ADH-101 immobilised onto activated charcoal displayed a specific activity of 0.01 U mg^{-1} (calculated from 1 h time point), this represents a 2% retention of activity compared with the ADH-101 free in

solution. This is similar to the retention of activity of ADH-101 after immobilisation displayed in the earlier sections (Section 5.3 and 5.4).

5.5.2 Full cycle: reduction of acetophenone with IPA-driven cofactor recycling by ADH-105 in batch

Having established the full cycle performance of ADH-101 homo- and heterogeneously. An analogous set of experiments to Figure 5-9 were designed to determine the activity of ADH-105 in solution for the full cycle ketone reduction of **9** to (*S*)-**10** with NAD^+ and IPA-driven cofactor recycling (Scheme 5-4 (B)). The results are shown in Figure 5-11.

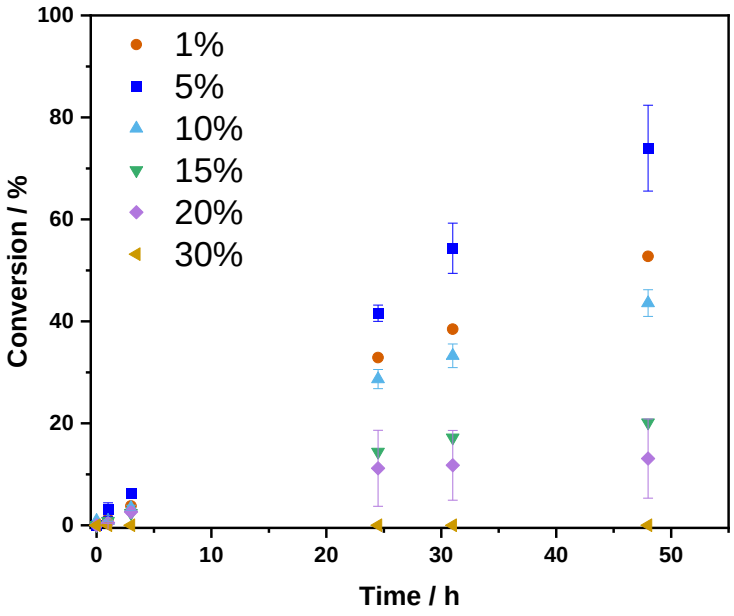


Figure 5-11: Batch biocatalytic conversion of **9** to (*S*)-**10** over time, employing ADH-105 in solution for ketone reduction and cofactor recycling at various IPA concentrations (1-30 v/v%). The conversion of **9** to (*S*)-**10** was determined by extracting reaction solution samples for analysis by GC. Reaction conditions: ADH-105 (0.1 mg), **9** (50 mM), NAD^+ (5 mM), Tris-HCl (50 mM, pH 8.0), IPA (1-30 v/v%), 1 mL, 25 °C, shaker plate 800 RPM.

The results in Figure 5-11 show that the full cycle system achieves higher conversion of **9** to (*S*)-**10** at lower IPA concentrations. However, the conversion achieved at 5 v/v% IPA

(73%) was higher than the conversion achieved at 1 v/v% (50%). This result correlates well with the trend observed in Section 5.4 for ADH-105 'backward' cofactor regeneration step. Interestingly, the trend is in contrast to the experiments with ADH-101. Possibly the ADH-105 is more greatly deactivated by higher concentrations of IPA than the ADH-101, as demonstrated by no conversion achieved by the ADH-105 (Figure 5-11, yellow arrow) at 40 v/v% IPA. The reactions at 5 v/v% IPA achieved a 73% conversion of **9** to (*S*)-**10** (calculated from 1 h time point), with the ADH-105 displaying a specific activity of 0.17 U mg^{-1}, over 48 h. Therefore, it was decided that 5 v/v% IPA would be the best condition to move forward with for the heterogenous reaction.

Subsequently, an experiment analogous to Figure 5-10 was performed to determine the specific activity of ADH-105 immobilised onto activated charcoal for the full cycle ketone reduction of **9** to (*S*)-**10** with NAD^+ and IPA-driven cofactor recycling (Scheme 5-4 (B)). Shown in Figure 5-12.

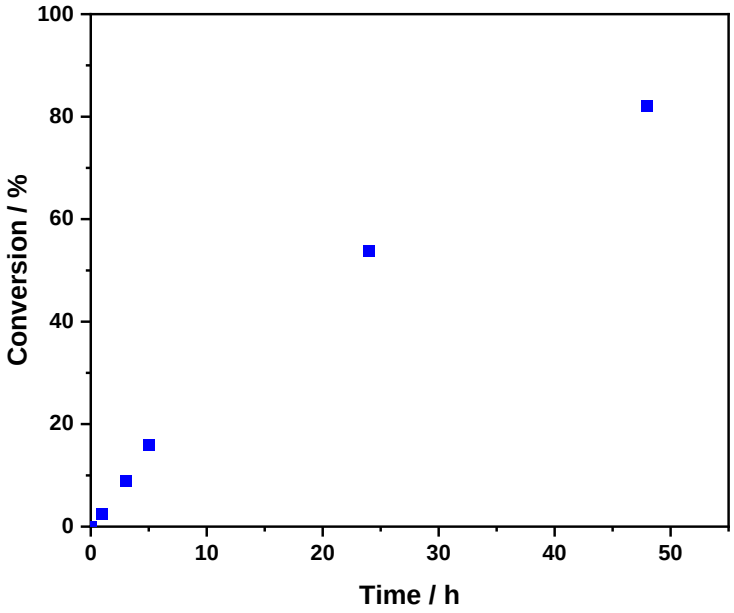


Figure 5-12: Batch biocatalytic conversion of **9** to (*S*)-**10** over time, employing ADH-105 immobilised on activated charcoal for ketone reduction and cofactor recycling at an IPA concentration of 5 v/v%. The conversion of **9** to (*S*)-**10** was determined by extracting reaction solution samples for analysis by GC. Reaction conditions: ADH-105 (1 mg), activated charcoal (5 mg), **9** (50 mM), NAD^+ (5 mM), Tris-HCl (50 mM, pH 8.0), IPA (5 v/v%), 1 mL, 25 °C, shaker plate 800 RPM.

The results in Figure 5-12 show that the heterogeneous full cycle system at 20% v/v% IPA achieved an 82% conversion of **9** to (*S*)-**10** (calculated from 1 h time point). The ADH-105 immobilised onto activated charcoal displayed a specific activity of 0.04 U mg^{-1} over 48 h, this represents a 22% retention of activity compared with the ADH-101 free in solution. This was expected and is similar to the retention of activity of ADH-105 after immobilisation displayed in the earlier sections (Section 5.3 and 5.4).

5.6 Translation from batch into continuous flow

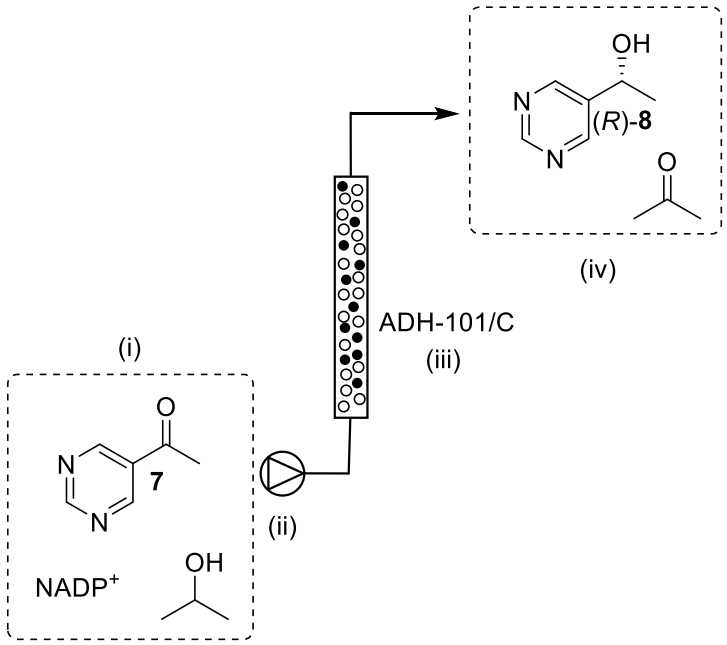
In this section the ADH-101 or ADH-105 immobilised onto activated charcoal was next transferred to a continuous reactor; guided by the batch immobilisation and activity results from the previous sections. Based on the activity of both the ADHs immobilised

on activated charcoal in batch, it was decided that the catalyst loading into the PBR would have to start relatively high (ADH (6.5 mg) and activated charcoal (30 mg)), compared with the batch reactions (ADH (1 mg) and activated charcoal (5 mg)). Also, a modest initial substrate loading of 10 mM was chosen (although still high enough to enable accurate reaction analysis). The t_{Res} studied was between 6-12 min, with the reactor volume set to ~300 µL throughout, 12 min was the longest t_{Res} possible with the peristaltic pump used that had a minimum flow rate of 25 µL min^{-1}. The minimum cofactor total turnover number deemed acceptable in continuous flow was chosen as 10, any lower would be too impactful on the *E* factor. The t_{Res} studied was between 6-12 min, with the reactor volume set to ~300 µL throughout, 12 min was the longest t_{Res} possible with the peristaltic pump used that had a minimum flow rate of 25 µL min^{-1}. Firstly, work focused on deploying the full reaction cycle for both the ADH-101 system and the ADH-105 system into flow with the enzymes immobilised onto activated charcoal and loaded into a PBR.

5.6.1 Full cycle: reduction of 1-(5-pyrimidinyl)ethenone with IPA-driven cofactor recycling by ADH-101 in continuous flow

To determine the viability of immobilised ADH-101 system in continuous flow for the reduction of **7** with IPA-driven cofactor recycling, the preliminary experiments focused on performing the full reaction cycle. The reactor was set-up as shown in Scheme 5-5. The reaction solution containing **7**, $NADP^+$ and IPA in Tris-HCl buffer was pumped from a reservoir (i) by a peristaltic pump (ii) through the packed PBR iii), which contained ADH-101 immobilised on activated charcoal and mixed with glass beads. The product mixture was sampled with a fraction collector (iv), typically at time intervals of 1 to 4 times the magnitude of the t_{Res}.

Scheme 5-5: Set-up of the flow reactor for the continuous biocatalytic conversion of **7** to (*R*)-**8**, employing ADH-101 immobilised on activated charcoal for ketone reduction and cofactor recycling: (i) Vessel containing the reactants (**7**, $NADP^+$, IPA) in a solution of Tris-HCl; (ii) syringe pump; (iii) ADH-101 immobilised on activated charcoal, mixed with glass beads in a PBR; (iv) Product containing mixture is sampled with a fraction collector and analysed by GC.



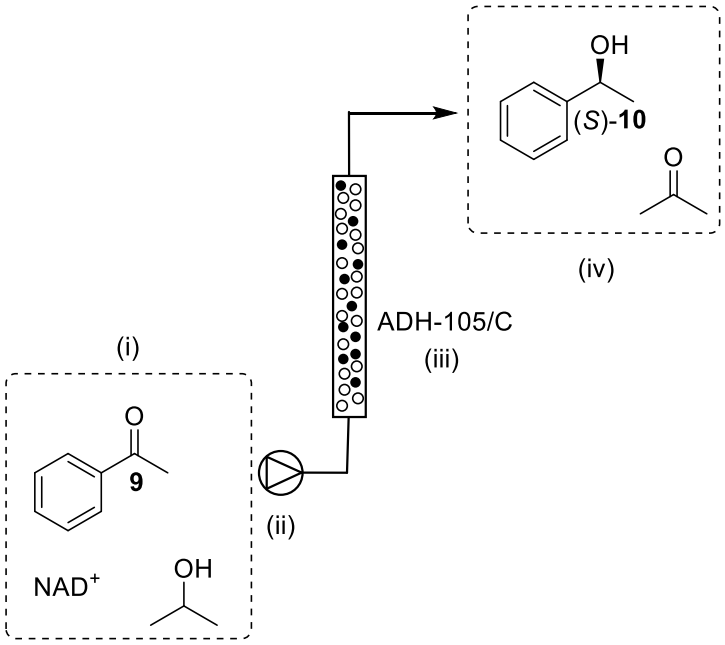
In the preliminary experiment an adjustable Omnifit column PBR was loaded with ADH-101 immobilised onto activated charcoal, according to the procedure in Section 5.2 was tested in the continuous reactor system for conversion of **7** to (*R*)-**8** with IPA-driven cofactor recycling. The reaction solution was pumped into the reactor at a flow rate of 25 µL min^{-1}, corresponding to a t_{Res} of 12 min. The fractions collected were analysed by GC. Samples were collected every 12 min over a period of 3 h, however, a steady-state conversion of <1% was observed throughout. Before troubleshooting experiments were performed the ADH-105 system was first tested.

5.6.2 Full cycle: reduction of acetophenone with IPA-driven cofactor recycling by ADH-105 in continuous flow

To determine the viability of immobilised ADH-105 system in continuous flow for the reduction of **9** with IPA-driven cofactor recycling, the reactor was set-up as shown in

Scheme 5-6. It was analogous to the reactor set-up in 5.5.1, differing only by the reaction solution vessel containing **9**, NAD^+ and IPA in Tris-HCl buffer.

Scheme 5-6: Set-up of the flow reactor for the continuous biocatalytic conversion of **9** to (*S*)-**10**, employing ADH-105 immobilised on activated charcoal for ketone reduction and cofactor recycling: (i) Vessel containing the reactants (**9**, NAD^+, IPA) in a solution of Tris-HCl; (ii) syringe pump; (iii) ADH-105 immobilised on activated charcoal, mixed with glass beads in a PBR; (iv) Product containing mixture is sampled with a fraction collector and analysed by GC.



A preliminary flow experiment analogous to Section 5.6.1 was performed with ADH-105 immobilised onto activated charcoal in the continuous reactor system for conversion of **9** to (*S*)-**10** with IPA-driven cofactor recycling. The reaction solution was pumped into the reactor at a flow rate of 25 or 50 µL min^{-1}, corresponding to a t_{Res} of 12 or 6 min respectively. The fractions collected were analysed by GC.

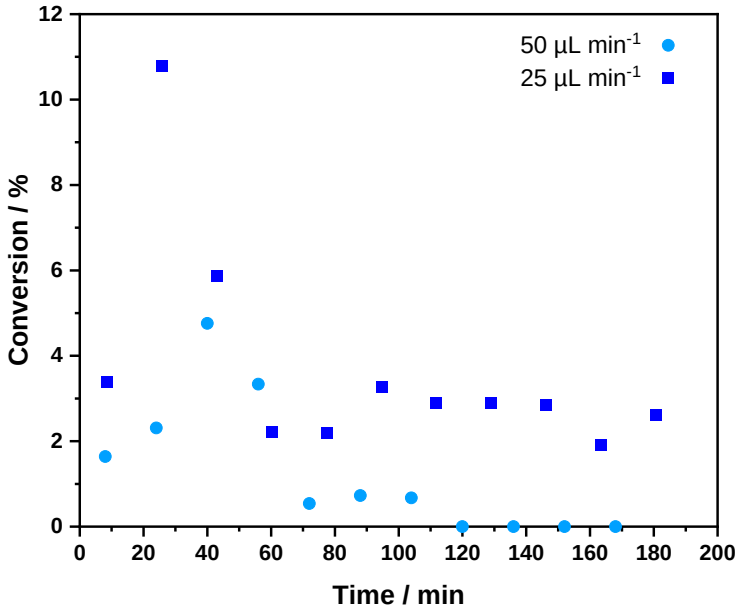


Figure 5-13: Conversion of **9** to (*S*)-**10** in continuous flow with ADH-105 immobilised on activated charcoal for ketone reduction and cofactor recycling, in a PBR. Studied at a reactor flow rate of 25 µL min^{-1} (dark blue square) and 50 µL min^{-1} (light blue square). The conversion of **9** to (*S*)-**10** was determined by collecting fractions for analysis by GC. Reaction conditions: ADH-105 (6.5 mg), activated charcoal (30 mg), **9** (10 mM), NAD^+ (1 mM), Tris-HCl (50 mM, pH 8.0), IPA (5 v/v%), flow rate = 25 or 50 µL min^{-1}, t_{Res} = 6 or 12 min, reactor volume = 300 µL.

The results in Figure 5-13 show that at a flow rate of 50 µL min^{-1} (t_{Res} = 6 min) the system reached a peak conversion of 4.8% after 36 min, before declining to 0% conversion over the subsequent 84 min. At a flow rate of 25 µL min^{-1} (12 min) the system reached a peak conversion of 11% before reaching a steady state conversion of 2-3% over the subsequent 3 h. The improved conversion at the lower flow rate is probably caused by the longer t_{Res} increasing the contact time between reagent and catalyst allowing the reaction to proceed further.

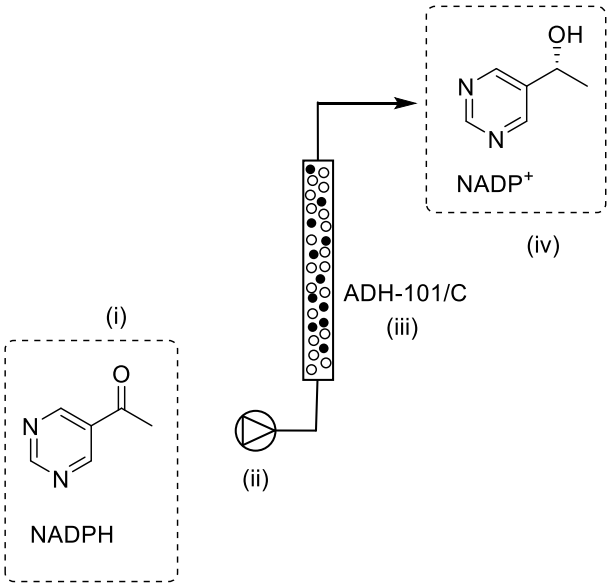
5.7 Troubleshooting poor continuous flow performance of ADH-101 and ADH-105 immobilised on activated charcoal

In this section a number of paths were followed in an attempt to troubleshoot the poor continuous flow performance demonstrated by both the ADH-101 and ADH-105. Firstly, the cycle was studied again by splitting it back into the 'forward' and 'backward' reaction, to give an insight on whether one of these components was contributing more to the poor performance than the other.

5.7.1 Forward ketone reduction catalysed by ADH-101 or ADH-105 in continuous flow

To study the 'forward' ketone reduction of **7** by the immobilised ADH-101 system in continuous flow, the reactor was set-up as shown in Scheme 5-7. It was analogous to the reactor set-up in 5.5.1, differing only by the reaction solution vessel containing **7** and NADPH in Tris-HCl buffer.

Scheme 5-7: Set-up of the flow reactor for the continuous biocatalytic conversion of **7** to (*R*)-**8**, employing ADH-101 immobilised on activated charcoal for ketone reduction with super stoichiometric NADPH: (i) Vessel containing the reactants (**7**, NADPH) in a solution of Tris-HCl; (ii) syringe pump; (iii) ADH-101 immobilised on activated charcoal, mixed with glass beads in a PBR; (iv) Product containing mixture is sampled with a fraction collector and analysed by GC.



An adjustable Omnifit column PBR was loaded with ADH-101 immobilised onto activated charcoal was tested in the continuous reactor system for conversion of **7** to (*R*)-**8**. The reaction solution was pumped into the reactor at a flow rate of 25 µL min^{-1}, corresponding to a t_{Res} of 12 min.

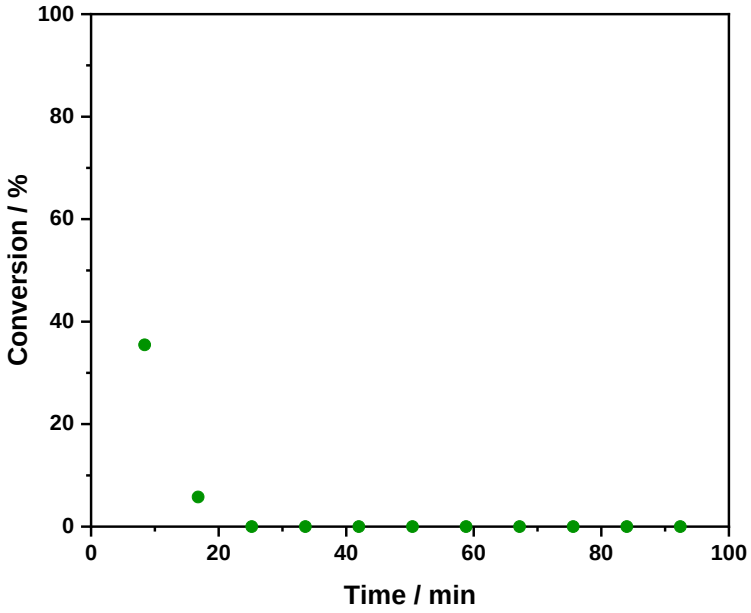
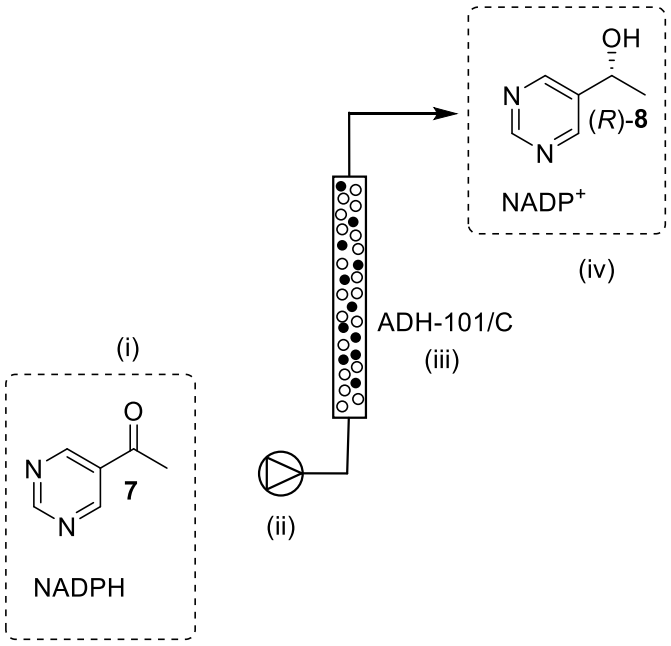


Figure 5-14: Conversion of **7** to (*R*)-**8** in continuous flow with ADH-101 immobilised on activated charcoal for ketone reduction with super stoichiometric NADPH, in a PBR. The conversion of **7** to (*R*)-**8** was determined by collecting reaction solution fractions for analysis by GC. Reaction conditions: ADH-101 (6.5 mg), activated charcoal (30 mg), **7** (10 mM), NADH (12 mM), Tris-HCl (50 mM, pH 8.0), flow rate = 25 µL min^{-1}, t_{Res} = 12 min, reactor volume = 300 µL.

The results in Figure 5-14 show that the system reached an initial peak conversion of 36% after 12 min, before declining rapidly to 0% conversion. This suggests that the ADH-101 is deactivating quickly, or possibly leaching off the activated charcoal at the beginning of the reaction.

To study the 'forward' ketone reduction of **9** by the immobilised ADH-105 system in continuous flow, the reactor was set-up as shown in Scheme 5-8. It was analogous to the reactor set-up described in Section 5.5.1, differing only by the reaction solution vessel containing **9** and NADH in Tris-HCl buffer.

Scheme 5-8: Set-up of the flow reactor for the continuous biocatalytic conversion of **9** to (*S*)-**10**, employing ADH-105 immobilised on activated charcoal for ketone reduction with super stoichiometric NADH: (i) Vessel containing the reactants (**9**, NADH) in a solution of Tris-HCl; (ii) syringe pump; (iii) ADH-101 immobilised on activated charcoal, mixed with glass beads in a PBR; (iv) Product containing mixture is sampled with a fraction collector and analysed by GC.



A flow experiment analogous to Figure 5-14 was performed with ADH-105 immobilised onto activated charcoal for conversion of **9** to (*S*)-**10** (Figure 5-15).

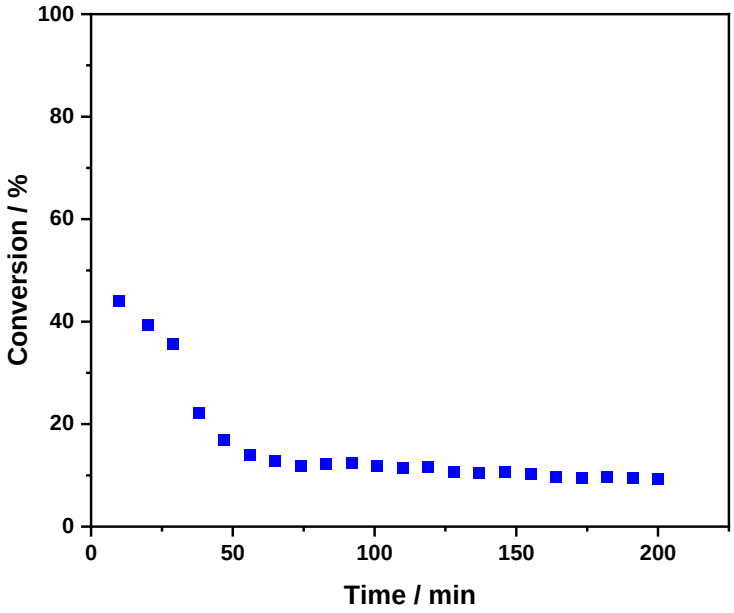


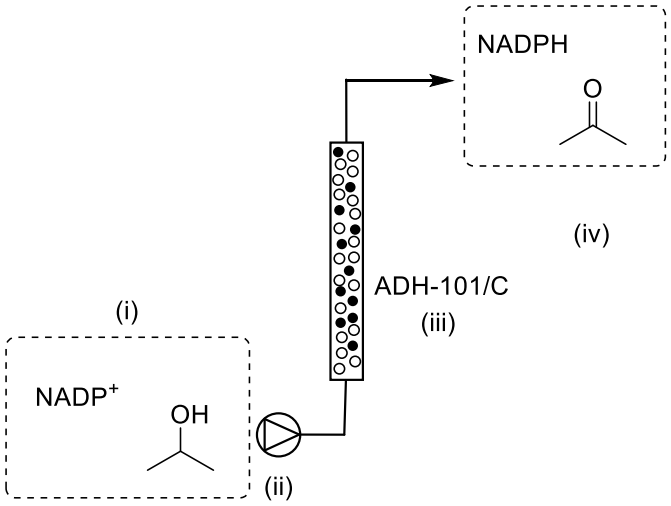
Figure 5-15: Conversion of **9** to (*S*)-**10** in continuous flow with ADH-105 immobilised on activated charcoal for ketone reduction with super stoichiometric NADH, in a PBR. The conversion of **9** to (*S*)-**10** was determined by collecting reaction solution fractions for analysis by GC. Reaction conditions: ADH-105 (6.5 mg), activated charcoal (30 mg), **9** (10 mM), NADH (12 mM), Tris-HCl (50 mM, pH 8.0), flow rate = 25 µL min^{-1}, t_{Res} = 12 min, reactor volume = 300 µL.

The results in Figure 5-15 show that the system reached an initial peak conversion of 44% after 12min, before declining to a steady-state conversion of ~ 10% conversion for the subsequent 150 min. Although the ADH-105 does not fully deactivate in the manner of ADH-101 in Section 5.7.1, the rapid drop-off in conversion at the beginning of the reaction still indicates an issue such as enzyme leaching off the activated charcoal is occurring. The 'backward' reaction was next studied in flow.

5.7.2 ADH-101 and ADH-105 for the backward IPA-driven NAD(P)$^+$ reduction reaction in continuous flow

To study the 'backward' NADP$^+$-dependent oxidation of IPA by the immobilised ADH-101 system in continuous flow, the reactor was set-up as shown in Scheme 5-9. It was analogous to the reactor set-up in 5.5.1, differing only by the reaction solution vessel containing NADP$^+$ and IPA in Tris-HCl buffer.

Scheme 5-9: Set-up of the flow reactor for the continuous biocatalytic conversion of NADP$^+$ to NADPH, employing ADH-101 immobilised on activated charcoal for the NADP$^+$-dependent conversion of IPA to acetone: (i) Vessel containing the reactants (NADP$^+$, IPA) in a solution of Tris-HCl; (ii) syringe pump; (iii) ADH-101 immobilised on activated charcoal, mixed with glass beads in a PBR; (iv) Product containing mixture is sampled with a fraction collector and analysed by GC.



An adjustable Omnifit column PBR was loaded with ADH-101 immobilised onto activated charcoal and tested in the continuous reactor system for conversion of NADP$^+$ to NADPH. The reaction solution was pumped into the reactor at a flow rate of 25 µL min^{-1}, corresponding to a t_{Res} of 12 min. The fractions collected were analysed by UV-Vis spectroscopy.

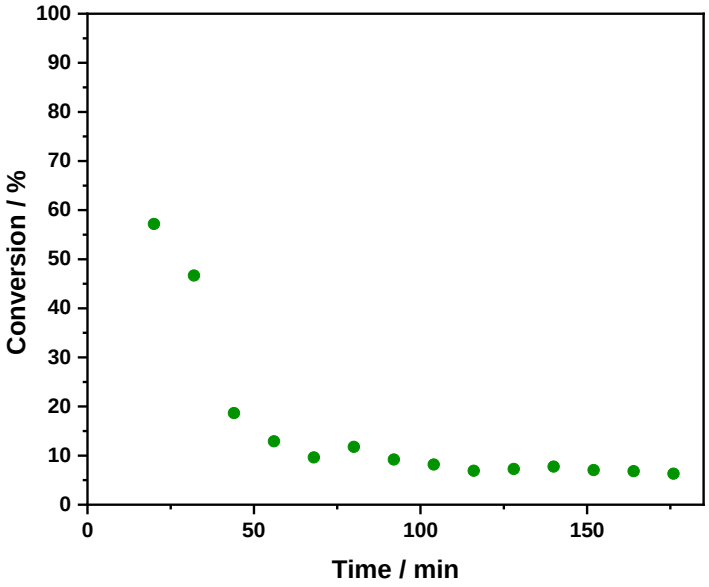
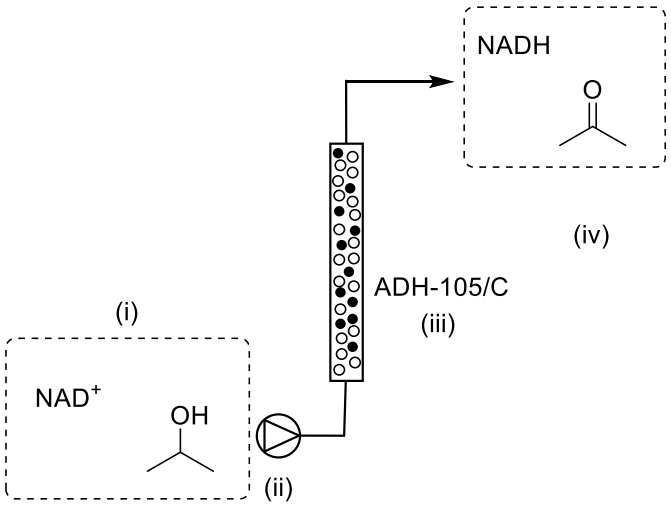


Figure 5-16: Conversion of $NADP^+$ to NADPH in continuous flow with ADH-101 immobilised on activated charcoal and IPA in solution, in a PBR. Monitored over time by UV-Vis spectroscopy. Reaction conditions: ADH-101 (6.5 mg), activated charcoal (30 mg), $NADP^+$ (1 mM), Tris-HCl (50 mM, pH 8.0), IPA (20 v/v%) flow rate = 25 µL min^{-1}, t_{Res} = 12 min, reactor volume = 300 µL.

The results in Figure 5-16 show that the system reached an initial peak conversion of 57% after 12 min, before declining to a steady-state conversion of ~10% conversion, which was maintained for 125 min. This again suggests that the ADH-101 is quickly deactivating or leaching when immobilised onto the activated charcoal at the beginning of the experiment and the system overall does not appear to be limited by a single component of the cycle. It was important to next determine whether the ADH-105 performs in a similar way.

To study the 'backward' NAD^+-dependent oxidation of IPA by the immobilised ADH-105 system in continuous flow, the reactor was set-up as shown in Scheme 5-10. It was analogous to the reactor set-up in 5.5.1, differing only by the reaction solution vessel containing NAD^+ and IPA in Tris-HCl buffer.

Scheme 5-10: Set-up of the flow reactor for the continuous biocatalytic conversion of NAD^+ to NADH, employing ADH-105 immobilised on activated charcoal for the $NADP^+$-dependent conversion of IPA to acetone: (i) Vessel containing the reactants (NAD^+, IPA) in a solution of Tris-HCl; (ii) syringe pump; (iii) ADH-105 immobilised on activated charcoal, mixed with glass beads in a PBR; (iv) Product containing mixture is sampled with a fraction collector and analysed by GC.



A flow experiment analogous to Figure 5-16 was performed with ADH-105 immobilised onto activated charcoal loaded in the continuous reactor system for conversion of NAD^+ to NADH. The results are shown in Figure 5-17.

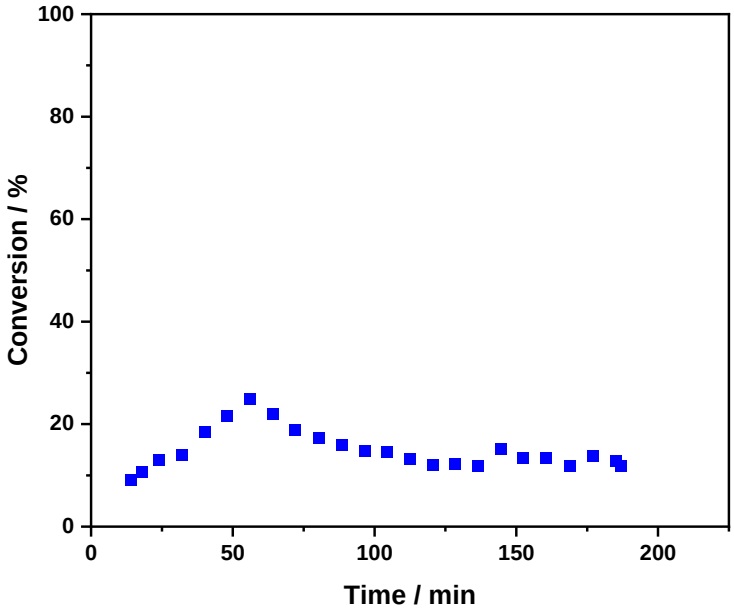


Figure 5-17: Conversion of NAD^+ to NADH in continuous flow with ADH-105 immobilised on activated charcoal and IPA in solution, in a PBR. Monitored over time by UV-Vis spectroscopy. Reaction conditions: ADH-105 (6.5 mg), activated charcoal (30 mg), NAD^+ (1 mM), Tris-HCl (50 mM, pH 8.0), IPA (5 v/v%) flow rate = 25 µL min^{-1}, t_{Res} = 12 min, reactor volume = 300 µL.

The results in Figure 5-17 show that the system reached an initial peak conversion of 24% after 56 min, before declining to a steady-state conversion of ~10% conversion for the remaining reaction time. The next experiments were designed to determine whether the poor enzyme performance was caused by enzyme leaching from the activated charcoal.

5.7.3 ADH-101 and ADH-105 leaching studies in continuous flow

To establish whether enzyme leaching from the activated charcoal was the cause of the rapid loss of performance displayed in continuous flow by both the ADH-101 and ADH-105, an enzyme leaching experiment for both ADH-101 and ADH-105 was carried out. An adjustable Omnifit column PBR was loaded with either ADH-101 (6.5 mg) or ADH-105 (6.5 mg) immobilised onto activated charcoal (30 mg). A reaction solution of IPA

(20 v/v% for ADH-101 and 5 v/v% for ADH-105) in Tris-HCl buffer (50 mM, pH 8.0) was pumped through the reactor at a flow rate of 25 µL min^{-1}, corresponding to a t_{Res} of 12 min. The fractions collected were analysed by UV-Vis A_{280} and the extent of leaching could be determined using the protein concentration calibration curves in Appendix G.

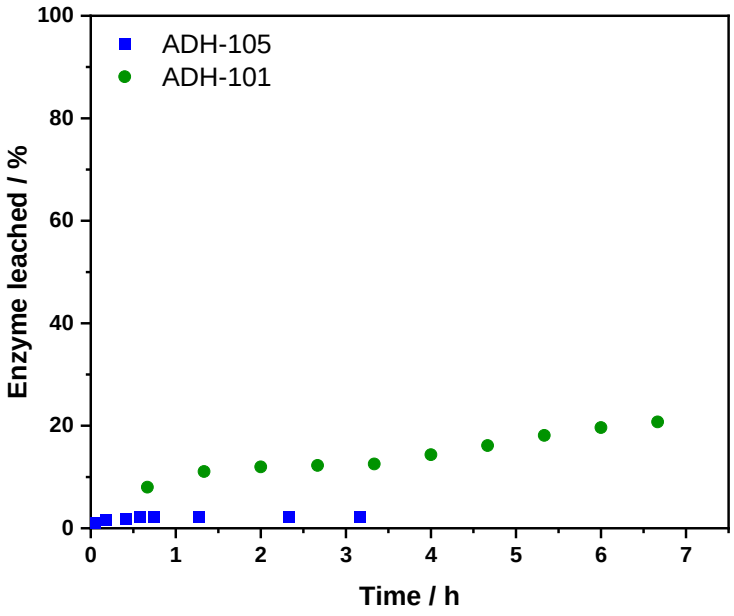


Figure 5-18: Cumulative leaching of enzyme from the activated charcoal. Determined over time by flowing Tris-HCl over the immobilised enzyme on activated charcoal in a PBR, the collected fractions were measured by UV-Vis A_{280}, the extent of enzyme leaching was then calculated using the protein concentration calibration curves in Appendix G. (A) ADH-105 immobilised on activated charcoal (blue squares). Reactions conditions: ADH-105 (6.5 mg), activated charcoal (30 mg), Tris-HCl (50 mM, pH 8.0, flow rate = 25 µL min^{-1}, $\boldsymbol{t_{Res}}$ = 12 min, reactor volume = 300 µL. (B) ADH-101 immobilised on activated charcoal (blue squares). Reactions conditions: ADH-105 (6.5 mg), activated charcoal (30 mg), Tris-HCl (50 mM, pH 8.0, flow rate = 25 µL min^{-1}, $\boldsymbol{t_{Res}}$ = 12 min, reactor volume = 300 µL.

The results in Figure 5-18 show that for ADH-101 system, 9% of the immobilised ADH-101 leached from the activated charcoal within 1 h and overall the system displayed a cumulative ADH-101 leaching of 21% over the 6.7 h period. The ADH-105 system displayed a cumulative 2.2% leaching of the immobilised ADH-105 from the activated

charcoal after 3 h. These results might explain the drop-in performance observed in the continuous flow experiments. Particularly, since the ADH-105 showed less leaching than ADH-101 and this correlates with the previous flow experiments in which the drop-in conversion of the ADH-105 system is often less severe than the ADH-101 system. Another factor to consider is that both the ADH-101 and ADH-105 are crude enzymes (non-purified) and they might contain impurities that could contribute to the observed deactivation of both systems. An impurity that often appears in crude enzymes is NAD(P)H oxidase. The next section seeks to determine whether NAD(P)H oxidase is an impurity present in the batches of ADH-101 and ADH-105 used here.

5.7.4 Exploring the presence of NAD(P)H oxidase in the crude ADH-101 and ADH-105 enzymes

The family of enzymes called NAD(P)H oxidases function with the presence of $O_{2(g)}$ by converting NAD(P)H to $NAD(P)^+$. There are several known NAD(P)H oxidases expressed by *E. coli* (ADH-101 and ADH-105 are expressed in *E. coli*) and they also absorb at 280 nm. The cofactors NAD(P)H are known to be relatively stable in aerobic, non-acidic conditions and the rate of NAD(P)H degradation (studied by monitoring absorbance at 340 nm) in Tris-HCl (17 mM, pH 7.0, 25 °C) has previously been found to be 0.044% min^{-1}, and is even slower at pH 8.0.[272] To test for the presence of NADPH oxidase in ADH-101, a 1 mL batch reaction was performed in a UV cuvette containing ADH-101 (0.1 mg) and NADPH (0.1 mM) in Tris-HCl buffer (50 mM, pH 8.0) in aerobic conditions. Conversion of NADPH to $NADP^+$ was monitored by using *in situ* UV-Vis spectroscopy.

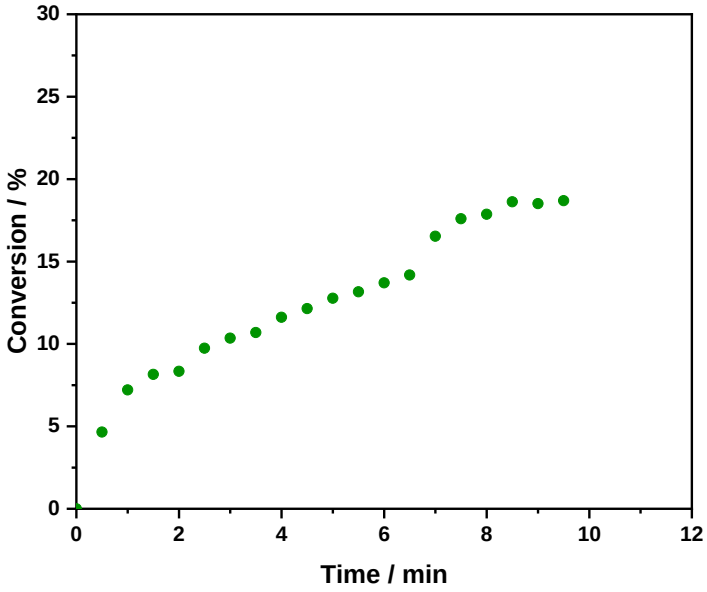


Figure 5-19: Conversion of NADPH to $NADP^+$ over time by suspected NADPH oxidase in the ADH-101 enzyme. Reaction performed with enzyme in homogenous solution and monitored by using *in situ* UV-Vis spectroscopy in aerobic conditions. Reaction conditions: NADPH (1 mM), ADH-101 (0.1 mg), Tris-HCl (50 mM, pH 8.0), 25 °C.

The results in Figure 5-19 show that the conversion of NADPH to $NADP^+$ in the presence of crude ADH-101 was 19% after 9.5 min. This result clearly indicates that a NADPH oxidase is present in the crude ADH-101.

To test for the presence of NADH oxidase in ADH-105, a 1 mL batch reaction was performed in a UV cuvette containing ADH-105 (0.1 mg) and NADH (0.1 mM) in Tris-HCl buffer (50 mM, pH 8.0) in aerobic conditions. Conversion of NADH to $NADP^+$ was monitored by using *in situ* UV-Vis spectroscopy.

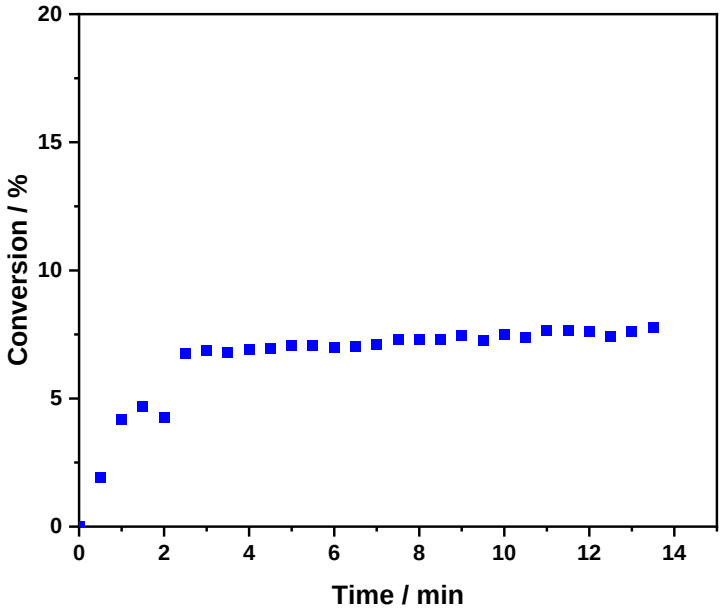


Figure 5-20: Conversion of NADH to NAD^+ over time by suspected NADH oxidase in the ADH-105 enzyme. Reaction performed with enzyme in homogenous solution and monitored by using *in situ* UV-Vis spectroscopy in aerobic conditions. Reaction conditions: NADH (1 mM), ADH-101 (0.1 mg), Tris-HCl (50 mM, pH 8.0), 25 °C.

The results in Figure 5-20 show that the conversion of NADH to NAD^+ in the presence of crude ADH-105 was 6.2% after 3 min but appears to plateau after this point. This result clearly indicates that a NADH oxidase is present in the crude ADH-105.

The presence of NAD(P)H oxidase in the crude ADH-101 or ADH-105 could have a number of effects. The NAD(P)H oxidase could out-compete the ADHs by consuming the NAD(P)H, thereby reducing the desired reaction conversion. This could be further extenuated if a build-up of $NAD(P)^+$ caused by the NAD(P)H oxidase led to the reverse reaction (desired alcohol to ketone starting material) to take place. Furthermore, the oxidation of NAD(P)H by NAD(P)H oxidase and $O_{2(g)}$ also generates H_2O_2 (or H_2O, depending on the enzyme type). A build-up of H_2O_2 around the ADH-101 and ADH-105 enzymes, could be denaturing the enzymes, causing a drop-off in enzyme activity. The

build-up H_2O_2 in the system could be neutralised by the addition of a catalase enzyme, which acts to disproportionate the H_2O_2 into H_2O and O_2. However, the use of an additional enzyme in solution would not be desirable for the translation of this system into flow because a major benefit of immobilised flow biocatalysis to industry is losing the requirement to separate the enzymes from the product solution.

It is probable that the negative effect of the NAD(P)H oxidase was enhanced in the continuous flow reactions over the batch reactions owing to the increased quantities of enzyme used. Also, the batch reactions were performed in sealed microcentrifuge tubes, leading to limited O_2-supply for the NAD(P)H oxidase. In contrast the reaction solution vessel for the flow reaction was left open to the air. Future flow experiments could overcome this by making the reaction solution vessel inert and sealed before the solution is pumped into the flow reactor. Although the presence of NAD(P)H oxidase is clear in batch, further future flow experiments could seek to perform analogous experiments to those in Figure 5-19 and Figure 5-20, to determine the impact of the NAD(P)H oxidase on the continuous flow systems.

5.8 Summary

In this chapter, a substrate-coupled IPA-driven cofactor system was studied homo- and heterogeneously (activated charcoal support) for the model reactions of **7** to (*R*)-**8** catalysed by ADH-101, and **9** to (*S*)-**10** catalysed by ADH-105 in batch and continuous flow. The homogeneous systems were shown to perform reasonably well in batch conditions for both ADH-101 and ADH-105. However, immobilisation of the enzymes onto an activated charcoal support appeared to detrimentally impact the performance of the enzymes. Heterogenous reactions with the full cycle system achieved a peak conversion of 37% and 82% after 48 h with immobilised ADH-101 and ADH-105,

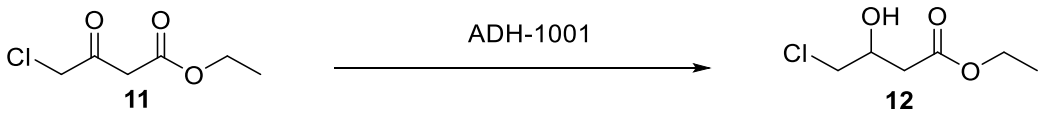
respectively. In continuous flow, the heterogeneous systems with both ADH-101 and ADH-105 achieved poor steady-state conversions over time. Troubleshooting experiments found that enzyme leaching and NAD(P)H oxidase activity could be major contributors to this problem. To conclude, the model ketone reduction reactions with IPA-driven cofactor recycling in continuous flow with the immobilised ADH-101 or ADH-105 system were found not to be feasible. By contrast, the study of the two systems was in-depth and it outlines a rigorous course of action for future studies of similar immobilised ADH systems. In the next chapter, focus shifts to another substrate coupled approach with a different ADH and target transformation, which is also of industrial interest.

6 Immobilising ADH-1001 onto carbon for synthesis of an API precursor with IPA-driven cofactor recycling in batch and continuous flow

6.1 Introduction

The aim of this chapter was to apply the approach and knowledge gained from the previous chapter onto a new ADH enzyme and transformation of industrial interest. The enzyme of interest, termed ADH-1001, is manufactured in-house by the industrial partner on this project and has been engineered to perform chiral ketone reduction on a wide-range of keto-esters including one precursor transformation for the production of an API precursor. This chapter focuses on the conversion of ethyl 4-chloroacetoacetate (**11**) to ethyl-4-chloro-3-hydroxybutanoate (**12,** Scheme 6-1), which is an analogue of the industrially relevant transformation with the ADH-1001 at production scale.

Scheme 6-1: Conversion of **11** to **12** by ADH-1001.



The ketone reduction of **11** is regularly used in industry as a model reaction when testing new strains of enzymes owing to the reagent and alcohol product being analogues of the precursors to a number of different APIs.[266] The transformation of ethyl 4-chloroacetoacetate to (*S*)-**12** is also used as a route towards the API atorvastatin.[167]

Before starting to research ADH-1001, it was tested alongside ADH-101 and ADH-105 for purity by performing SDS-PAGE. The enzyme separation showed that the ADH-1001

was deficient of low molecular weight impurities, seen in both ADH-101 and ADH-105, that are likely to include the NADH oxidase.

Currently, the industrial partner perform the transformation in batch with the enzyme in solution, highlighting clear scope that the successful implementation of the ADH-1001 immobilised onto activated charcoal into continuous flow could improve the efficiency and decrease the wastage of the process by removing the need to separate the enzyme from the product in solution.

6.1.1 Immobilisation of ADH-1001 onto activated charcoal

The aim of this section was to determine whether the ADH-1001 would immobilise onto the activated charcoal by following the ADH immobilisation protocol established in Section 5.2. To establish this, ADH-1001 (1 mg) was mixed with a variety of masses of activated charcoal (1-25 mg) in Tris-HCl buffer (50 mM, pH 8.0) and placed in the refrigerator (4 °C). The mixture was agitated on a vortex mixer every 20 min for 1 h before the immobilisation efficiency was determined by UV-Vis spectroscopy (Table 6-1).

Table 6-1: Immobilisation efficiency of ADH-1001 onto activated charcoal according to immobilisation protocol Method B (refrigeration of particles at 4 °C with regular mixing). Standard deviations calculated for experiments that were performed in triplicate.

Mass of carbon / mg	Immobilisation efficiency / %
1	96
5	98 ±0.4
10	94
15	98 ±1.7

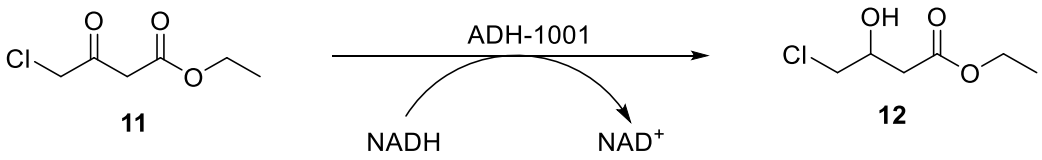
*Reaction conditions: ADH-1001 (1 mg), Tris-HCl buffer (1 mL, 50 mM, pH 8.0)

The results in Table 6-1 show that the immobilisation efficiency of ADH-1001 onto the activated charcoal is high through all the masses of activated charcoal tested. This result is positive for continuous flow experiments because a high ratio of enzyme to solid-support could lead to higher catalyst activity per volume of PBR. Theoretically, the effect this would have on the PBR flow system would be to achieve higher STYs. The next section seeks to establish whether the ADH-1001 retains activity when immobilised onto the activated charcoal.

6.2 ADH-1001 for the 'forward' ketone reduction of ethyl 4-chloroacetoacetate in batch

In this section the 'forward' ketone reduction for the transformation of **11** to **12** catalysed by ADH-1001 (shown in Scheme 6-2) was performed in batch mode with the enzyme in solution and with the enzyme immobilised onto activated charcoal to determine and compare the enzyme activity in both systems.

Scheme 6-2: Ketone reduction of **11** to **12** catalysed by ADH-1001 with super stoichiometric NADH.



To determine the specific activity of ADH-1001 in solution for the ketone reduction of **11** to **12** (Scheme 6-2), a 1 mL batch reaction of **11**, NADH and ADH-1001 in Tris-HCl buffer and DMSO (2 v/v%) was performed (Figure 6-8).

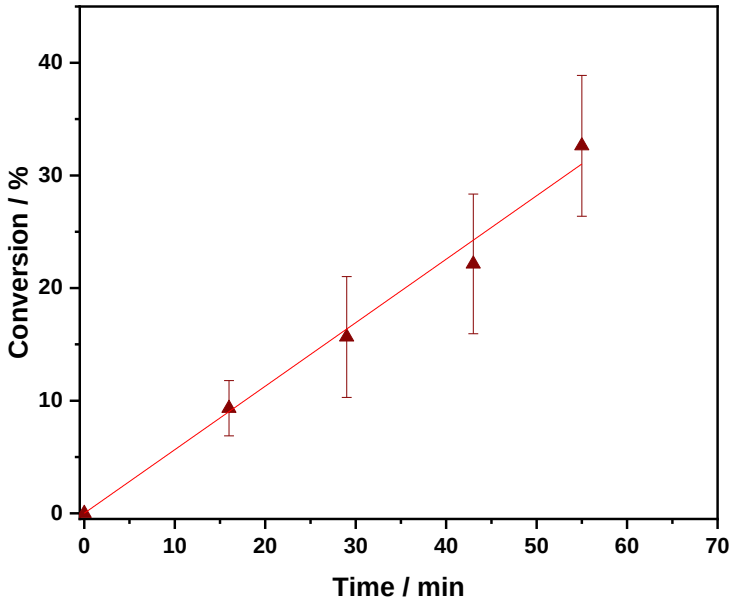


Figure 6-1: Batch enzyme activity measurement of ADH-1001 in solution for the reduction of **11** with super stochiometric NADH. The conversion of **11** to **12** was determined by extracting reaction solution samples for analysis by GC. Reaction conditions: ADH-1001 (0.005 mg), **11** (10 mM), NADH (12 mM), Tris-HCl (50 mM, pH 8.0), DMSO (2 v/v%), 1 mL, 25 °C, shaker plate 800 RPM. Error bars are shown for experiments performed in triplicate.

From the results in Figure 6-1 it can be determined that the ADH-1001 does display ketone reduction activity (11.3 U mg^{-1}) towards the **11** substrate.

Subsequently, to determine the specific activity of ADH-1001 when immobilised onto activated charcoal for the ketone reduction of **11** (Scheme 6-2), a 1 mL batch reaction of **11** and NADH in Tris-HCl buffer and DMSO was prepared and added to a microcentrifuge tube containing ADH-1001 immobilised onto activated charcoal.

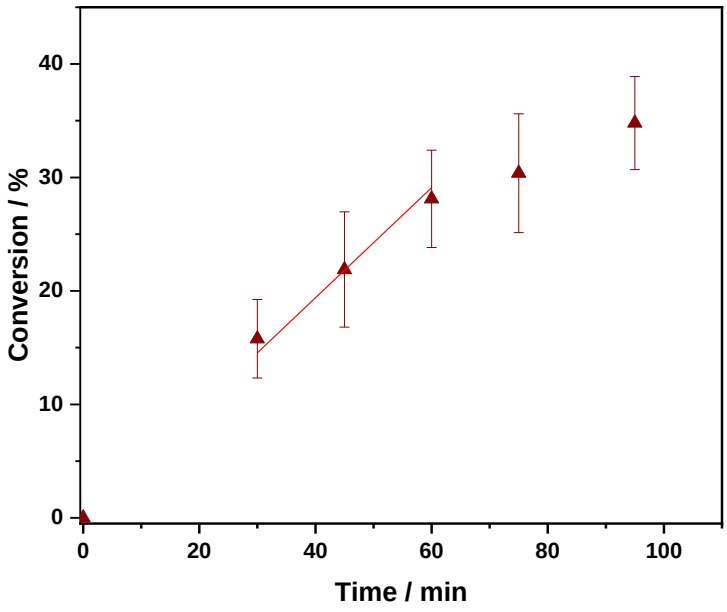


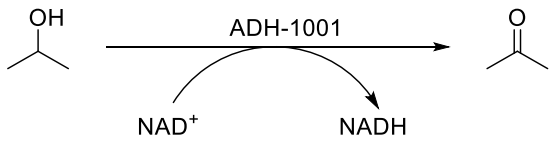
Figure 6-2: Batch enzyme activity measurement of ADH-1001 immobilised on activated charcoal for the reduction of **11** with super stochiometric NADH. The conversion of **11** to **12** was determined by extracting reaction solution samples for analysis by GC. Reaction conditions: ADH-1001 (0.1 mg), activated charcoal (5 mg) **11** (10 mM), NADH (12 mM), Tris-HCl (50 mM, pH 8.0), DMSO (2 v/v%), 1 mL, 25 °C, shaker plate 800 RPM. Error bars are shown for experiments performed in triplicate.

From the results in Figure 6-2 it can be determined that the immobilised ADH-1001 displayed a specific activity for ketone reduction of 1.0 U mg^{-1} when immobilised onto the activated charcoal, this represents 9% retention of activity compared with the ADH-1001 free in solution for the same transformation. However, the activity achieved was much higher than the analogous experiments performed with ADH-101 (0.02 U mg^{-1}) and ADH-105 (0.04 U mg^{-1}) in Section 5.3.

6.3 ADH-1001 for the 'backward' IPA-driven NAD^+ reduction reaction in batch

In this section, the activity of ADH-1001 towards the 'backward' NAD^+ reduction reaction, that is driven by the NAD^+-dependent oxidation of the sacrificial reagent IPA to acetone (shown in Scheme 6-3) was studied. Reactions were performed in batch mode with the enzyme in solution and with the enzyme immobilised onto activated charcoal to determine and compare the enzyme activity in both systems.

Scheme 6-3: NAD^+ dependent alcohol oxidation of IPA to acetone catalysed by ADH-1001, regenerating NADH.



To determine the specific activity of ADH-1001 in solution for the NAD^+-dependent oxidation of IPA (Scheme 6-3), the conversion of NAD^+ to NADH was monitored in a series of 1 mL batch reactions containing NAD^+ and ADH-1001 in Tris-HCl buffer at a variety of IPA concentrations (1-40 v/v%). Multiple IPA concentrations were tested to determine the favoured conditions of the ADH-1001. The course of the reaction was analysed by *in situ* UV-Vis spectroscopy and the specific activity for each IPA concentration is summarised in Figure 6-3.

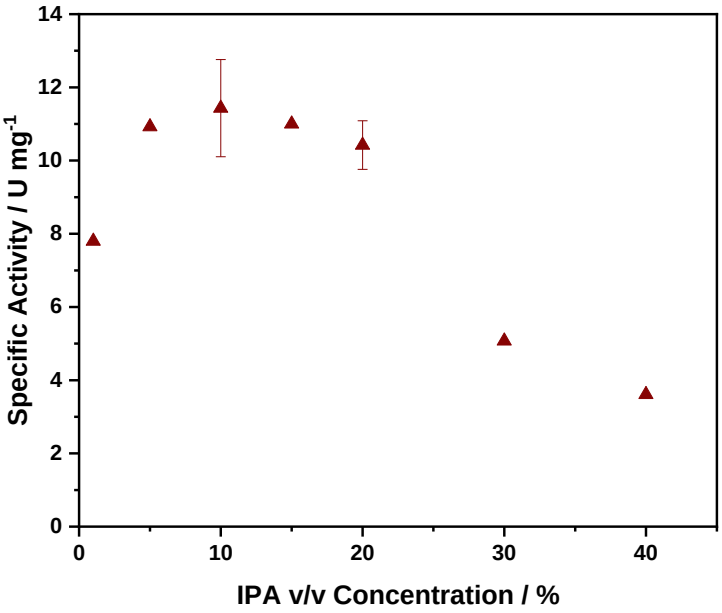


Figure 6-3: Comparison of batch enzyme activity measurements of ADH-1001 in solution for the NAD^+ dependent reduction of IPA to acetone, at varied IPA v/v% concentrations. The conversion of NAD^+ to NADH over time was determined with *in situ* UV-Vis spectroscopy for each individual experiment. Reaction conditions: ADH-1001 (0.005 mg), NAD^+ (0.1 mM), Tris-HCl (50 mM, pH 8.0), IPA (1-40 v/v%), 1 mL, 25 °C, shaker plate 800 RPM. Error bars are shown for experiments performed in triplicate.

The results in Figure 6-3 show that the specific activity of ADH-1001 for the NAD^+-dependent conversion of IPA to acetone (determined by monitoring the conversion of NAD^+ to NADH), is highest at IPA concentration between 5 to 20 v/v%. A favoured IPA concentration of 10 v/v% was carried forward to the analogous heterogenous reaction because it provided improved substrate solubility over 5 v/v% IPA and could possibly display improved enzyme lifetime against the higher IPA concentrations (15 and 20 v/v%). The highest activity of 11.4 U mg^{-1} was achieved at an IPA concentration of 10 v/v% and the lowest activity of 3.2 U mg^{-1} was achieved at 40 v/v%. Showing that the ADH-1001 is affected by high IPA concentrations.

The next experiment sought to determine the specific activity of ADH-1001 when immobilised onto the activated charcoal for the NAD^+-dependent oxidation of IPA (Scheme 6-3). The enzyme-modified carbon particles were tested at an IPA concentration of 10 v/v% in a 1 mL batch reaction containing NAD^+, IPA and ADH-1001 immobilised onto activated charcoal in Tris-HCl buffer (Figure 6-4).

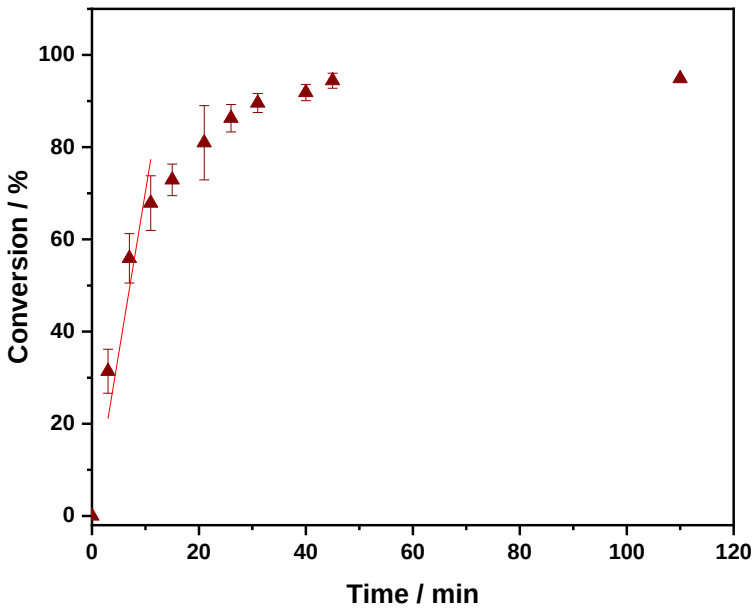


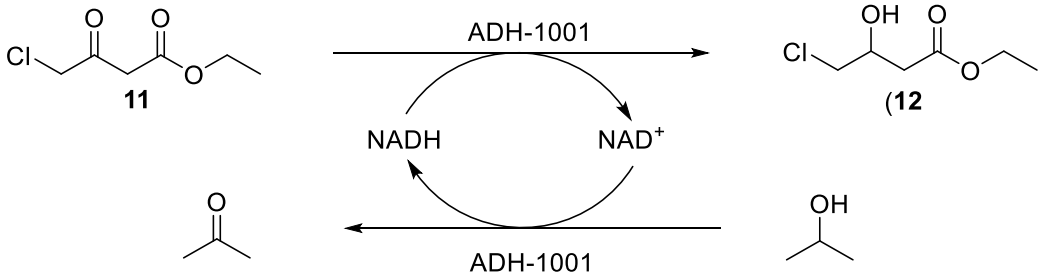
Figure 6-4: Batch enzyme activity measurements of ADH-1001 immobilised on activated charcoal for the NAD^+ dependent reduction of IPA to acetone. The conversion of NAD^+ to NADH over time was determined with *in situ* UV-Vis spectroscopy. Reaction conditions: ADH-1001 (0.1 mg), activated charcoal (5 mg), NAD^+ (5 mM), Tris-HCl (50 mM, pH 8.0), IPA (10 v/v%), 1 mL, 25 °C, shaker plate 800 RPM. Error bars are shown for experiments performed in triplicate.

From the results in Figure 6-4 it can be determined that the ADH-1001 immobilised onto activated charcoal displayed a specific activity of 10.5 U mg^{-1}, compared the ADH-1001 free in solution represents a 92.1% retention of activity. Promisingly, the activity achieved was much higher than the analogous experiments performed with ADH-101 (0.06 U mg^{-1}) and ADH-105 (0.1 U mg^{-1}) in Section 5.4.

6.4 Full cycle: ketone reduction of ethyl 4-chloroacetoacetate and substrate coupled IPA-driven cofactor recycling with ADH-1001 in batch

After studying the 'forward' and 'backward' components of the reaction cycle for the ADH-1001 homo- and heterogeneously, the aim of this section was to perform the full reaction cycle for the transformation of **11** to **12** catalysed by ADH-1001 with substrate coupled IPA-driven cofactor recycling (shown in Scheme 6-4), in batch mode. For comparison, reactions were performed with the ADH-1001 in solution and immobilised onto activated charcoal.

Scheme 6-4: NADH-dependent biocatalytic conversion of **11** to **12**, employing ADH-1001 for ketone reduction and IPA-driven cofactor recycling.



Firstly, experiments were designed to determine the activity of ADH-1001 in solution for the full cycle ketone reduction of **11** to **12** with IPA-driven cofactor recycling. A series of 1 mL batch experiments were performed at a variety of IPA concentrations (1-40 v/v%). The results are shown in Figure 6-5.

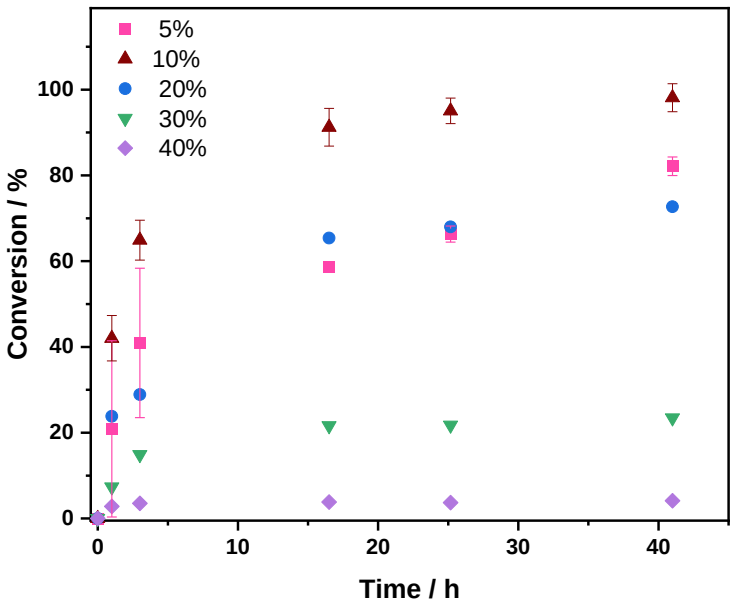


Figure 6-5: Batch biocatalytic conversion of 11 to **12** over time, employing ADH-1001 in solution for ketone reduction and cofactor recycling at various IPA concentrations (1-40 v/v%). The conversion of 11 to **12** was determined by extracting reaction solution samples for analysis by GC. Reaction conditions: ADH-1001 (0.01 mg), 11 (50 mM), NAD^+ (5 mM), Tris-HCl (50 mM, pH 8.0), IPA (1-40 v/v%), 1 mL, 25 °C, shaker plate 800 RPM. Error bars are shown for experiments performed in triplicate.

The results in Figure 6-5 show that after 41 h the full cycle system achieves the highest conversion (98%) of **11** to **12** at a 10 v/v% IPA concentration, corresponding to an ADH-1001 specific activity of 35 U mg^{-1} (calculated from 1 h time point). The next highest conversions after 41 h of 82% and 76% were achieved at IPA concentrations of 5 v/v% and 20 v/v% respectively; this correlates with results in Section 6.3 that showed 5-20 v/v% IPA was best for the cofactor recycling step.

Subsequently, to determine the specific activity of ADH-1001 immobilised onto activated charcoal for the full cycle ketone reduction of **11** to **12** with IPA-driven cofactor recycling. A series of 1 mL batch experiments containing **11**, NAD^+, and ADH-1001

immobilised onto activated charcoal in Tris-HCl buffer at a variety of IPA concentration (1-40 v/v%) were performed (Figure 6-6).

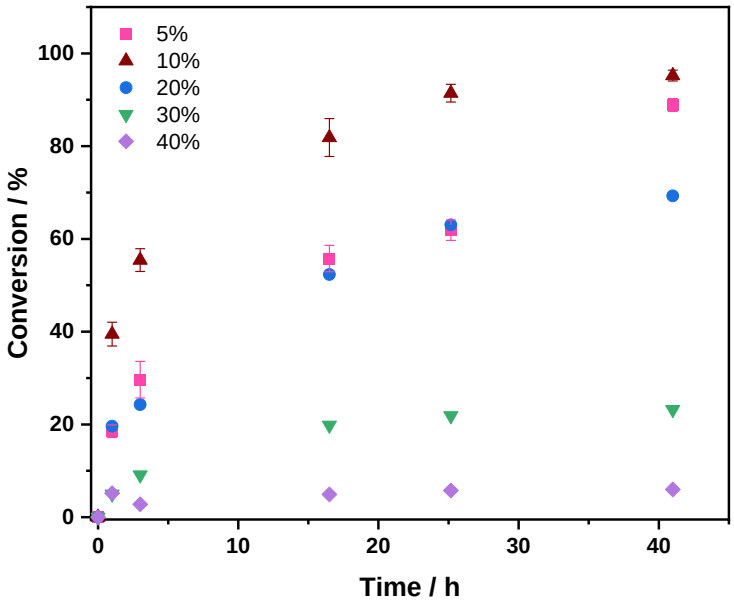


Figure 6-6: Batch biocatalytic conversion of **11** to **12** over time, employing ADH-1001 immobilised on activated charcoal for ketone reduction and cofactor recycling at various IPA concentrations (1-40 v/v%). The conversion of **11** to **12** was determined by extracting reaction solution samples for analysis by GC. Reaction conditions: ADH-1001 (0.01 mg), activated charcoal (5 mg), **11** (50 mM), NAD^+ (5 mM), Tris-HCl (50 mM, pH 8.0), IPA (1-40 v/v%), 1 mL, 25 °C, shaker plate 800 RPM.

The results in Figure 6-6 show that the heterogeneous full cycle system at 10% v/v% IPA resulted in the highest conversion of **11** to **12** (97%) after 41 h, correlating to a ADH-1001 specific activity of 3.3 U mg^{-1} (calculated from 1 h time point), this represents a 9.4% retention of activity compared with the ADH-1001 free in solution. This was expected and is similar to the retention in activity of ADH-1001 after immobilisation displayed in Section 6.3. Promisingly however, the activity achieved by the heterogeneous full cycle ADH-1001 was 100-fold higher than the specific activity

achieved by the ADHs when immobilised in Chapter 5. This system was deemed ready for translation into continuous flow.

6.5 Translation of ADH-1001 full cycle system from batch into continuous flow

The aim of this section was to translate the ADH-1001 immobilised onto activated charcoal from batch mode into a continuous reactor; by utilising the batch immobilisation and activity data obtained in the previous sections. To aid comparison with the ADH-101 and ADH-105 continuous flow systems in Chapter 5, the initial experiments with immobilised ADH-1001 used the same reactor conditions: ADH-1001 (6.5 mg) and activated charcoal (30 mg)), substrate loading (10 mM), NAD^+ (1 mM), t_{Res} = 12 min, reactor volume = ~300 µL (adjustable Omnifit column) with the same peristaltic pump at a flow rate of 25 µL min^{-1}. The initial experiment sought to determine the ADH-1001 leaching from the activated charcoal

6.5.1 ADH-1001 leaching study in continuous flow

To establish whether ADH-1001 leaches from the activated charcoal when used in a continuous flow set-up, an enzyme leaching experiment was carried out. An adjustable Omnifit column PBR was loaded with ADH-1001 immobilised onto activated charcoal. A reaction solution of IPA (10 v/v%, optimum in batch) in Tris-HCl buffer was pumped through the column at a flow rate of 25 µL min^{-1}, corresponding to a t_{Res} of 12 min. The fractions collected were analysed by UV-Vis A_{280} and the extent of leaching could be determined using the protein concentration calibration curves in Appendix G.

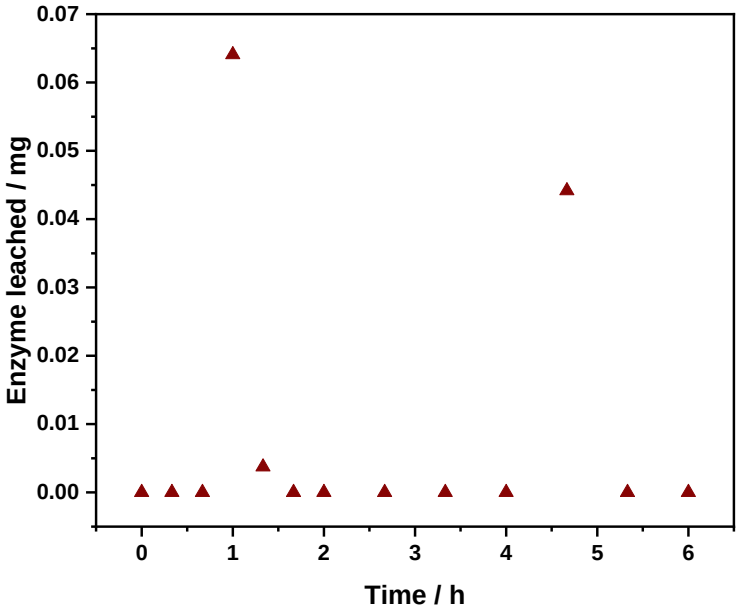


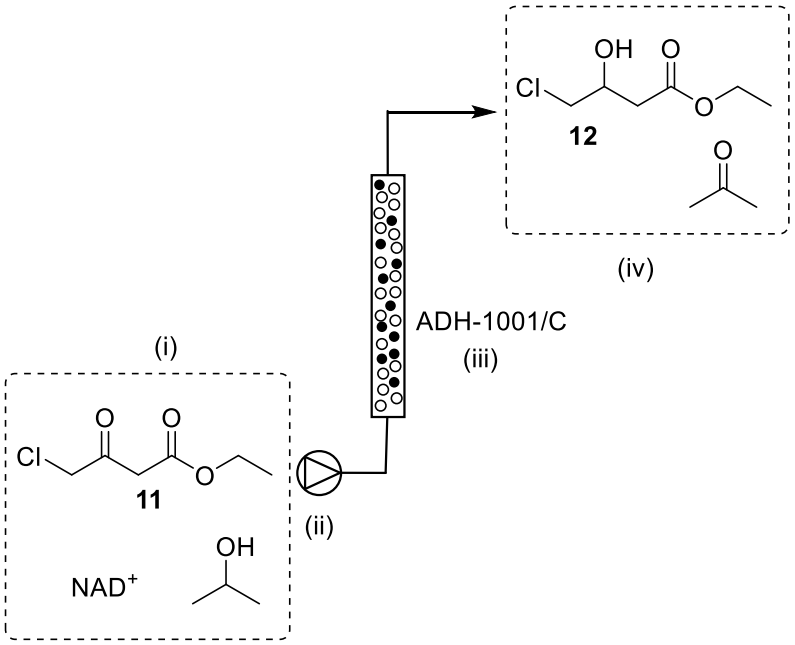
Figure 6-7: Leaching of ADH-1001 from the activated charcoal. Determined over time by flowing Tris-HCl over the immobilised enzyme on activated charcoal in a PBR, the collected fractions were measured by UV-Vis A_{280}, the extent of enzyme leaching was then calculated using the protein concentration calibration curves in Appendix G. Reactions conditions: ADH-1001 (6.5 mg), activated charcoal (30 mg), Tris-HCl (50 mM, pH 8.0, flow rate = 25 µL min^{-1}, t_{Res} = 12 min, reactor volume = 300 µL.

The results in Figure 6-7 show that over 6 h of continuous flow, two reaction samples were found to contain ADH-1001. After 1 h, 1.3 h and 4.6 h a sample was found to contain 0.065 mg, 0.005 mg and 0.045 mg of ADH-1001 respectively and no ADH-1001 was detected in other samples. This equates to a total enzyme leaching of ~2% (75% ADH-1001 immobilisation efficiency) over the reaction period. Although it was a modest amount of enzyme leaching for the time period, it was promising that the majority of reaction samples collected from the reaction contained no detectable ADH-1001. It was decided to move forward and test the full reaction cycle in continuous flow.

6.5.2 Full cycle: reduction of ethyl 4-chloroacetoacetate with IPA-driven cofactor recycling by ADH-1001 in continuous flow

The next set of experiments aimed to determine the viability of immobilised ADH-1001 system in continuous flow for the reduction of **11** with IPA-driven cofactor recycling. The reactor was set-up as shown in Scheme 6-5. The reaction solution containing **11**, NAD^+ and IPA in buffer was pumped from a reservoir (i) by a peristaltic pump (ii) through the packed adjustable Omnifit PBR iii), which contained ADH-1001 immobilised on activated charcoal and mixed with glass beads. The product mixture was sampled with a fraction collector (iv), typically at time intervals of 1 to 4 times the magnitude of the residence time (t_{Res}).

Scheme 6-5: Set-up of the flow reactor for the continuous biocatalytic conversion of **11** to **12**, employing ADH-1001 immobilised on activated charcoal for ketone reduction and cofactor recycling: (i) Vessel containing the reactants (**11**, NAD^+, IPA) in a solution of Tris-HCl; (ii) syringe pump; (iii) ADH-1001 immobilised on activated charcoal, mixed with glass beads in a PBR; (iv) Product containing mixture is sampled with a fraction collector and analysed by GC.



As previously mentioned, the first experiment performed with the ADH-1001 in continuous flow used analogous reaction conditions to the full cycle ADH flow reactions

in Chapter 5, to enable direct comparison. A PBR was loaded with ADH-1001 immobilised onto activated charcoal and was tested in the continuous reactor system for conversion of **11** (10 mM) to **12** with IPA-driven cofactor recycling. The reaction solution containing **11**, NAD^+ and IPA (10 v/v%) in Tris-HCl buffer was pumped into the reactor at a flow rate of 25 µL min^{-1}, corresponding to a t_{Res} of 12 min.

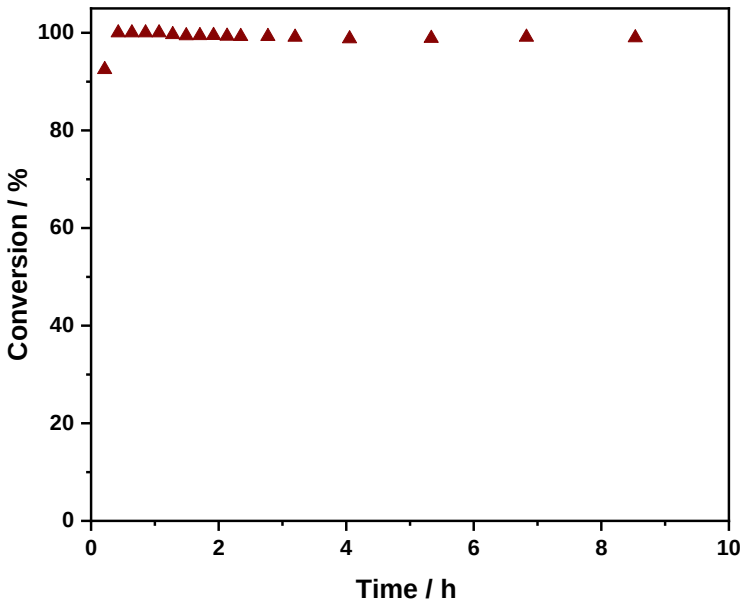


Figure 6-8: Conversion of **11** (10 mM) to **12** in continuous flow with ADH-1001 immobilised on activated charcoal for ketone reduction and cofactor recycling, in a PBR. The conversion of **11** to **12** was determined by collecting fractions for analysis by GC. Reaction conditions: ADH-1001 (6.5 mg), activated charcoal (30 mg), **11** (10 mM), NAD^+ (1 mM), Tris-HCl (50 mM, pH 8.0), IPA (10 v/v%), flow rate = 25 min^{-1}, $\boldsymbol{t_{Res}}$ = 12 min, reactor volume = 300 µL.

Promisingly, the results in Figure 6-8 show that the system displayed a 100% steady-state conversion of **11** to **12** over the course of the 6.8 h continuous flow reaction. This was, comparatively, a vast improvement on the continuous flow performance displayed by the immobilised ADH-101 and ADH-105 systems, in Chapter 5. As a preliminary experiment, the continuous system demonstrated a STY of 8 g L^{-1} h^{-1} and an *E* factor of

52. To improve upon both of these metrics the first strategy was to increase the reagent concentration. If the system could achieve high conversion at increased reagent concentration this would increase the amount of product formed (decreasing *E* factor) and improve reactor productivity. Furthermore, this would enable the performance of the immobilised ADH-1001 to be investigated further under more strenuous conditions, providing a greater understanding of its performance.

6.5.3 Increasing the substrate concentration to 50 mM

The immobilised ADH-1001 system was next investigated by increasing the **11** concentration from 10 to 50 mM. A PBR was loaded with ADH-1001 immobilised onto activated charcoal and was tested in the continuous reactor system for conversion of **11** to **12** with IPA-driven cofactor recycling (Figure 6-9).

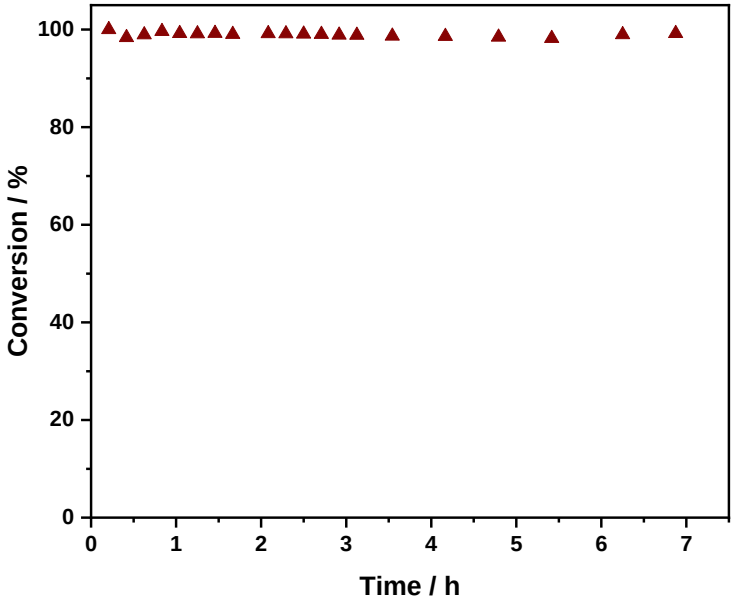


Figure 6-9: Conversion of **11** (50 mM) to **12** in continuous flow with ADH-1001 immobilised on activated charcoal for ketone reduction and cofactor recycling, in a PBR. The conversion of **11** to **12** was determined by collecting fractions for analysis by GC. Reaction conditions: ADH-1001 (6.5 mg), activated charcoal (30 mg), **11** (50 mM), NAD^+ (1 mM), Tris-HCl (50 mM, pH 8.0), IPA (10 v/v%), flow rate = 25 min^{-1}, t_{Res} = 12 min, reactor volume = 300 µL.

The results in Figure 6-9 show that at an increased substrate concentration the system again displayed a ~100% conversion of **11** to **12**, over the course of the 6.8 h continuous flow reaction. The continuous system achieved a STY of 40 g L^{-1} h^{-1} and an *E* factor of 10 throughout, representing a good improvement versus the system at 10 mM substrate concentration. It was clear that the immobilised ADH-1001 still had not been tested under strenuous conditions and it is difficult to gain more of an understanding of a continuous system at 100% conversion. Therefore, the system was once again tested at an increased substrate concentration.

6.5.4 Increasing the substrate concentration to 100 mM

The immobilised ADH-1001 system was next studied by increasing the **11** concentration from 50 to 100 mM. A PBR was loaded with ADH-1001 immobilised onto activated charcoal (30 mg) and tested in the continuous reactor system for the reduction of **11** (Figure 6-10).

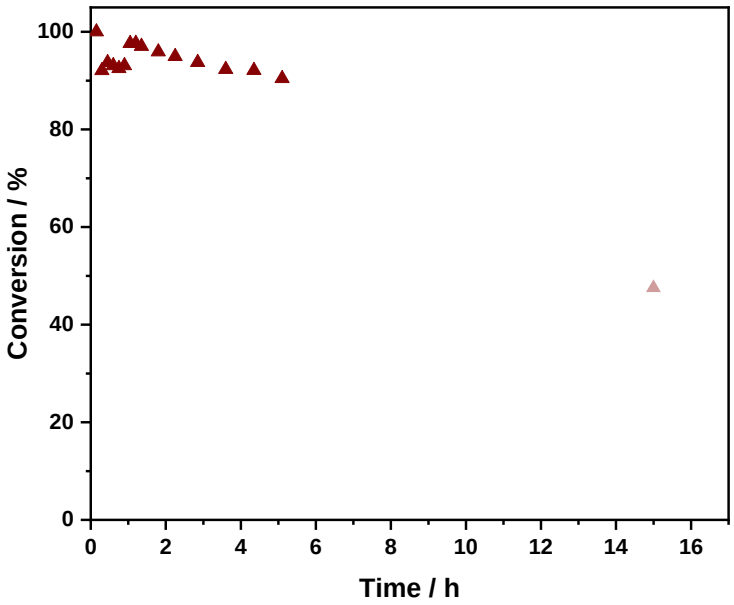


Figure 6-10: Conversion of **11** (100 mM) to **12** in continuous flow with ADH-1001 immobilised on activated charcoal for ketone reduction and cofactor recycling, in a PBR. The conversion of **11** to **12** was determined by collecting fractions for analysis by GC. Reaction conditions: ADH-1001 (6.5 mg), activated charcoal (30 mg), **11** (100 mM), NAD^+ (1 mM), Tris-HCl (50 mM, pH 8.0), IPA (10 v/v%), flow rate = 25 min^{-1}, t_{Res} = 12 min, reactor volume = 300 µL.

The results in Figure 6-10 show that at an increased substrate concentration of 100 mM, the continuous flow system resulted in an initial 100% conversion of **11** to **12**, before conversion decreased to 88% over the subsequent 5 h. The reaction was left to run overnight (further 10 h) and the eluted reaction solution (15 mL total) was collected into a sealed vessel. Overall, the reaction solution achieved a 48% conversion (represented by

faded data point at 15 h). The fraction collector could not be used overnight owing to the volatility of the starting material and product in open air. However, it is clear that the conversion continues to fall between 5 and 15 h. The continuous system achieved a peak cofactor TN of 100, a STY of 83 g L^{-1} h^{-1} and an *E* factor of 5. This brings the *E* factor within the expected range of the bulk chemicals industry (1 to 5). Another way of decreasing the *E* factor is to increase the molar ratio of substrate to NAD^+, thereby increasing the cofactor TN and using less NAD^+. This was also of industrial interest, not only because of the *E* factor but also the cost savings this could bring to the process. Currently, the model batch reaction system at the industrial partner for the conversion of **11** to **12** by ADH-1001 achieves a cofactor TN of 156. However, according to the industrial partner the % overall cost of cofactor for an in-house kilogram scale reaction such as this is ~8% (starting material = 90%, enzyme = 1%, other = 1%). Increasing the cofactor TN ≥ 1000 could have a substantial impact on the *E* factor and the manufacturing costs. Therefore, the next experiment investigated the impact of decreasing the NAD^+ concentration on the ADH-1001 continuous flow system.

6.5.5 Increasing the substrate to NAD^+ molar ratio to 1000:1 by decreasing NAD^+ to 0.1 mM

In this experiment the immobilised ADH-1001 continuous flow system was studied by decreasing the NAD^+ concentration from 1 to 0.1 mM whilst keeping the substrate concentration at 100 mM ([substrate]:[NAD^+] = 1000). A PBR was loaded with ADH-1001 immobilised onto activated charcoal and tested in the continuous reactor system for the reduction of **11** (Figure 6-11).

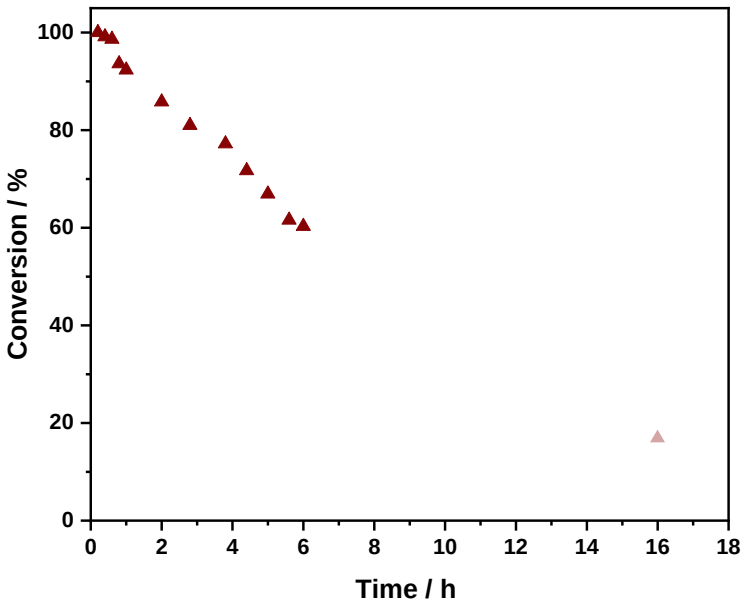


Figure 6-11: Conversion of **11** (100 mM) to **12** in continuous flow with ADH-1001 immobilised on activated charcoal for ketone reduction and cofactor recycling, in a PBR. The conversion of **11** to **12** was determined by collecting fractions for analysis by GC. Reaction conditions: ADH-1001 (6.5 mg), activated charcoal (30 mg), **11** (100 mM), NAD^+ (0.1 mM), Tris-HCl (50 mM, pH 8.0), IPA (10 v/v%), flow rate = 25 min^{-1}, t_{Res} = 12 min, reactor volume = 300 µL.

The results in Figure 6-11 show that at an increased substrate concentration of 100 mM, the continuous flow system achieved an initial 100% conversion of **11** to **12**, before decreasing to 58% after 6.5 h. The reaction was left to run overnight (further 9 h) and the eluted reaction solution (13.5 mL total) was collected into a sealed vessel. Overall, this reaction solution achieved 18% conversion (represented by faded data point at 15 h). It was promising that the system started off at such a high conversion, achieving a peak cofactor TN of 1000, a STY of 83 g L^{-1} h^{-1} and an *E* factor of 4.8. However, the proceeding decrease in conversion over time was of concern and the next set of experiments were designed to troubleshoot this.

6.6 Studying the continuous flow reaction with in-line benchtop flow NMR

At this point in the project, temporary access to a benchtop NMR spectrometer (Magritek Spinsolve 43 MHz) by the manufacturer was available. This was of interest because the benchtop NMR spectrometer does not require samples to be worked-up in deuterated solvents. Therefore, with the addition of a glass flow cell through the spectrometer, it could be connected in-line to a continuous flow set-up, to perform real time reaction monitoring. Early tests with the NMR spectrometer determined that it would only be useful quantitively for reagent/product concentrations >50 mM owing to its reasonably low field strength, which produced quite low-resolution spectra at concentrations <5-10 mM. Therefore, this project was an ideal candidate to test out the spectrometer because of reaction solution concentrations (up to 100 mM) that had been used so far. For quantitative analysis of the reaction - firstly, diagnostic NMR signals were determined for **11** and **12** (Figure 6-12) and subsequently concentration calibration curves were prepared for each (see Appendix F). The resolution of the NMR spectra acquired by the benchtop NMR spectrometer is relatively poor compared with a traditional high-field NMR spectrometer. The R^2 value of the calibration curves for the ketone and alcohol was 0.99, showing the sensitivity and value of the technique for quantitative reaction monitoring analysis.

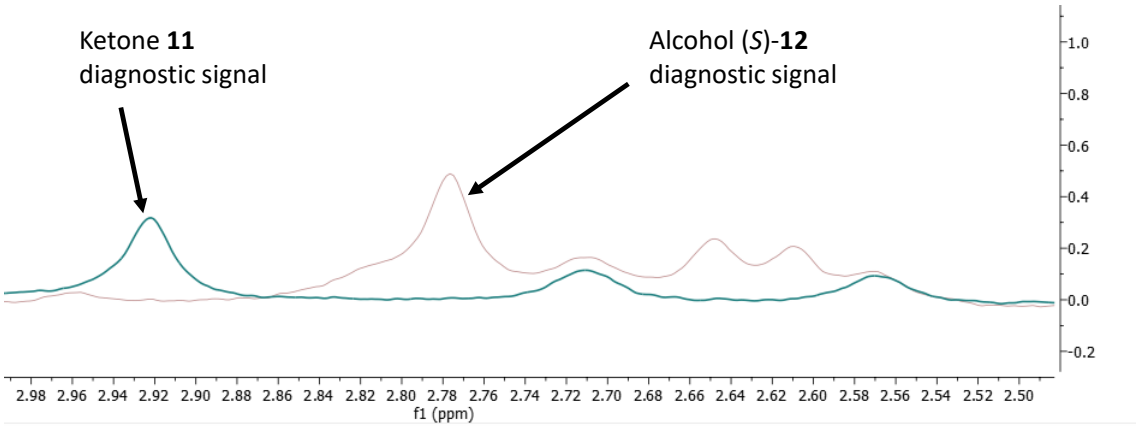
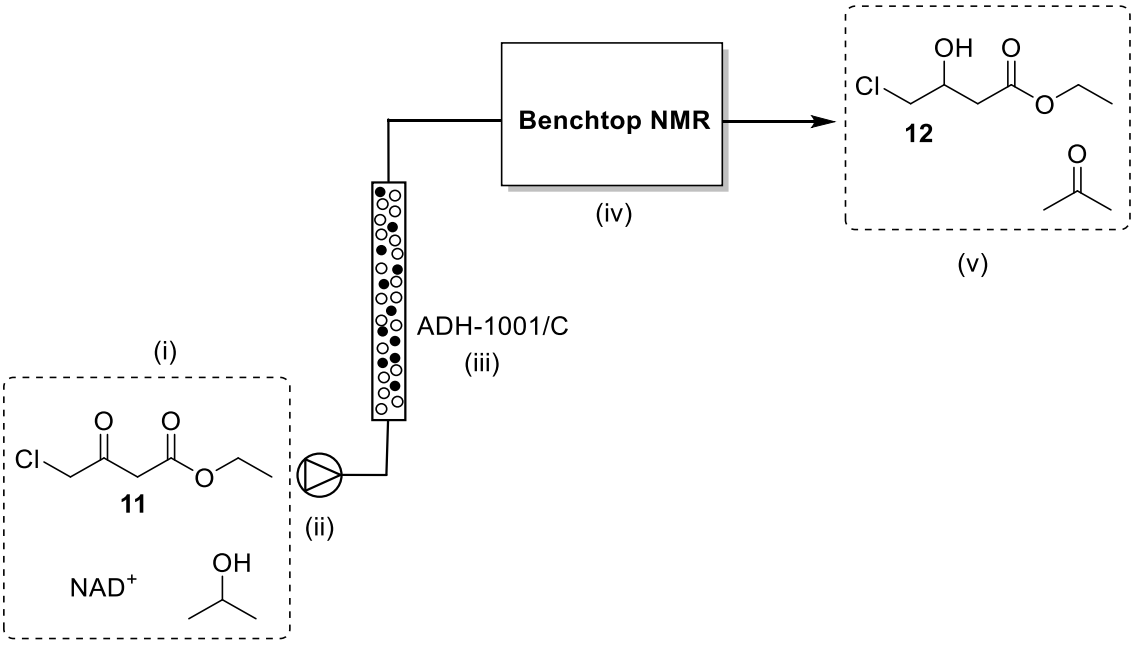


Figure 6-12: Diagnostic NMR signals for ketone **11** and alcohol **12** acquired by benchtop NMR spectroscopy.

With the addition of the in-line NMR spectrometer, the flow reactor was set-up as shown in Scheme 6-5. The reaction solution containing **11**, NAD^+ and IPA in buffer was pumped from a reservoir (i) by a peristaltic pump (ii) through the packed adjustable Omnifit PBR iii), which contained ADH-101 immobilised on activated charcoal and mixed with glass beads. The product mixture continued to be pumped through the benchtop flow NMR (iv), before being collected into a sealed vessel.

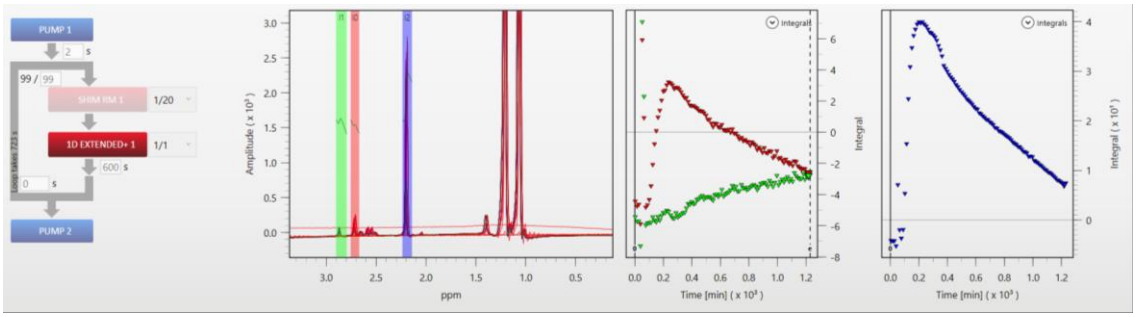
Scheme 6-6: Set-up of the flow reactor for the continuous biocatalytic conversion of **11** to **12**, employing ADH-1001 immobilised on activated charcoal for ketone reduction and cofactor recycling: (i) Vessel containing the reactants (**11**, NAD^+, IPA) in a solution of Tris-HCl; (ii) syringe pump; (iii) ADH-1001 immobilised on activated charcoal, mixed with glass beads in a PBR; (iv) Product containing mixture is pumped through the in-line benchtop NMR reaction monitoring machine; (v) Product containing mixture is collected in a vessel.



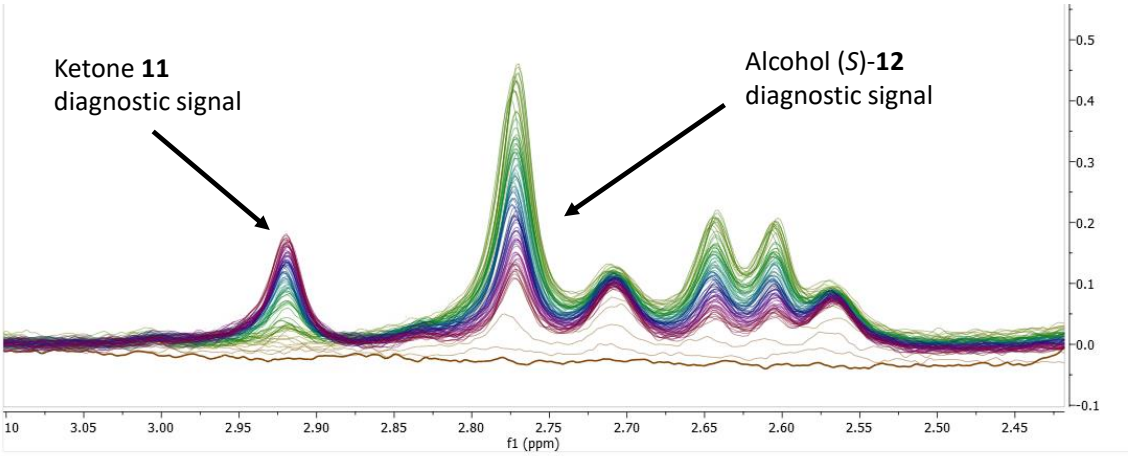
6.6.1 Comparing with GC analysis

The first experiment with the in-line flow NMR reaction monitoring aimed to investigate the reliability of the set-up compared to the standard GC analysis. Therefore, a repeat of the experimental conditions used in Figure 6-11 was performed, so that a comparison of the results could take place. A PBR was loaded with ADH-1001 immobilised onto activated charcoal and tested in the continuous reactor system for the reduction of **11** (Figure 6-13). The reaction solution containing **11**, NAD^+ and IPA (10 v/v%) in Tris-HCl buffer was pumped into the reactor at a flow rate of 25 µL min^{-1}, corresponding to a t_{Res} of 12 min. The reaction was monitored with in-line benchtop flow NMR.

(A)


PUMP 1
2 s
99 / 99
SHIM RM 1
1/20
1D EXTENDED+ 1
1/1
600 s
0 s
PUMP 2
Amplitude (x 10⁵)
ppm
Integrals
Integral
Time [min] (x 10³)
Integral (x 10⁷)

(B)


Ketone **11**
diagnostic signal
Alcohol (*S*)-**12**
diagnostic signal
f1 (ppm)

(C)

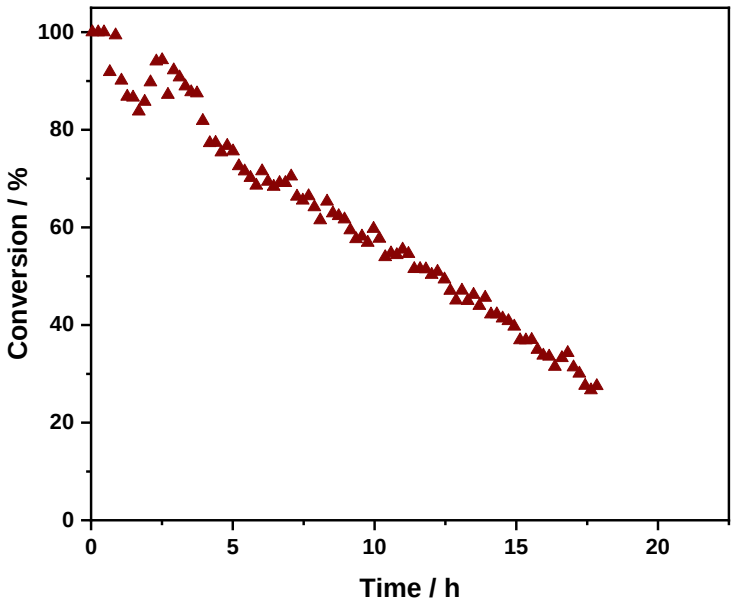


Figure 6-13: The conversion of **11** to **12** was determined by in-line flow NMR reaction monitoring (NMR scans every 600 s). (A) Real-time benchtop NMR analysis using the SpinSolve reaction monitoring software; (B) Overlay of the 97 NMR spectra obtained, highlighting the diagnostic signal region (C) Conversion of **11** (100 mM) to **12** in continuous flow with ADH-1001 immobilised on activated charcoal for ketone reduction and cofactor recycling, in a PBR. Reaction conditions: ADH-1001 (6.5 mg), activated charcoal (30 mg), **11** (100 mM), NAD^+ (0.1 mM), Tris-HCl (50 mM, pH 8.0), IPA (10 v/v%), flow rate = 25 min^{-1}, t_{Res} = 12 min, reactor volume = 300 µL.

Figure 6-13(A) shows the real-time benchtop NMR analysis that can be achieved using the Magritek SpinSolve software. The diagnostic NMR signals can be monitored in real-time, including the option to track the integral of the diagnostic signals. The green and red triangle data points show the integral of the diagnostic ketone **11** and alcohol **12** signal, respectively. It was also possible to monitor the acetone signal (2^{nd} graph, blue triangle data points) over time, which is a by-product of the IPA cofactor recycling system. Interestingly the acetone signal plot closely mirrors the alcohol **12** diagnostic signal plot, suggesting that future development of the system could monitor the acetone

signal instead of the reagent and product signals. This would be of benefit because the acetone signal is much more intense and might prove easier to monitor. Figure 6-13(B) shows the ketone and alcohol diagnostic signals overlaid, over the whole operational period. The concentration of starting material and product can be determined from the integral of these signals using the calibration curves in Appendix F. The results in Figure 6-13(C) show that the continuous flow system monitored by using quantitative in-line flow NMR achieved an initial 100% conversion of **11** to **12** for the initial 0.5 h, before conversion decreased to ~65% after 6.5 h. The data for the subsequent 11 h, show a gradual decline in conversion to 25% before the reaction was stopped. Encouragingly, the NMR system produced very similar conversion results over time to the GC analysis (Figure 6-11). Furthermore, vastly more data points were able to be collected, offering far greater insight into the system.

6.6.2 Variation of reaction buffer solution

Previous experiments on the ADH-1001 flow system at a substrate concentration of 100 mM showed a steady deactivation of catalyst over time. The aim of this section was to determine whether changing the buffer (and pH) of the system would have an impact on the activity lifetime of the immobilised ADH-1001 flow system. Firstly, the buffer was eliminated by switching from Tris-HCl (50 mM, pH 8.0) to unbuffered MilliQ H_2O. This is of interest because in Chapter 3, with the immobilised FDH/LDH system, the change from Tris-HCl to H_2O was shown to have little effect on the stability of the system. The other reaction conditions were kept the same as the experiment in Figure 6-13, to enable direct comparison. The results are shown in Figure 6-14.

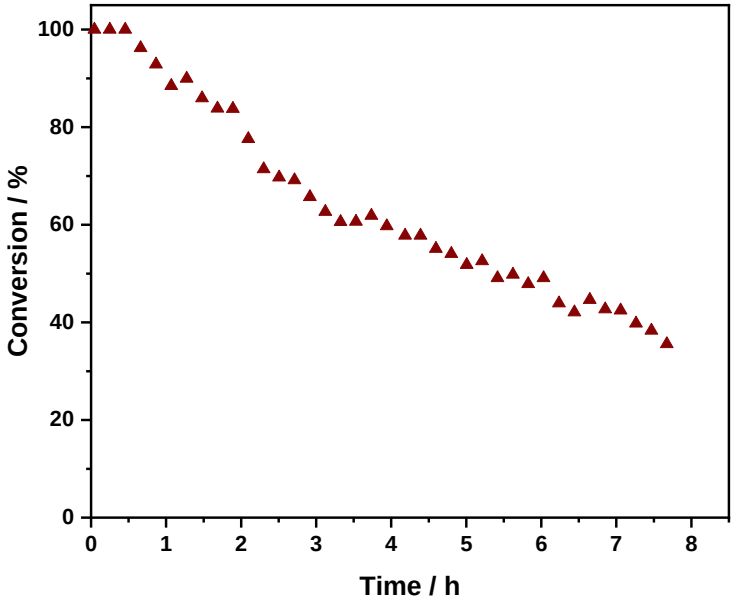


Figure 6-14: Conversion of **11** (100 mM) to **12** in continuous flow with ADH-1001 immobilised on activated charcoal for ketone reduction and cofactor recycling, in a PBR. Performed in MilliQ H_2O at pH 7.0. The conversion of **11** to **12** was determined by in-line flow NMR reaction monitoring (NMR scans every 600 s). Reaction conditions: ADH-1001 (6.5 mg), activated charcoal (30 mg), **11** (100 mM), NAD^+ (0.1 mM), H_2O, IPA (10 v/v%), flow rate = 25 min^{-1}, t_{Res} = 12 min, reactor volume = 300 µL.

The results in Figure 6-14 show that the continuous flow system achieved an initial 100% conversion of **11** to **12** for the initial 0.5 h, before conversion steadily decreased to 36% by 7.7 h. Although the system in MilliQ H_2O shows a similar performance to the Tris-HCl buffered system in the first hour, it does appear to drop-off more quickly than the Tris-HCl buffered system. However, performing the reaction in H_2O led to a decrease in the *E* factor compared to the Tris-HCl system (Figure 6-13) from 4.8 to 4.5.

Next, the ADH-1001 flow system was tested with a pH 6.0 potassium phosphate buffer (KPB, 50 mM). This was on the advice of the industrial partner for this project, who suggested this because their optimised batch system for this transformation with ADH-

1001 in solution uses this buffering system. An analogous flow experiment to Figure 6-13 was performed with the reaction solution in KPB, shown in Figure 6-15.

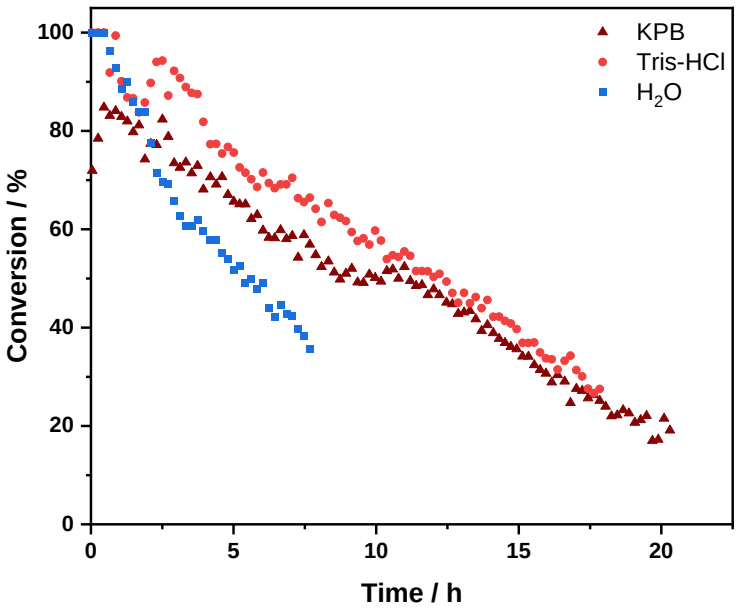


Figure 6-15: Conversion of **11** (100 mM) to **12** in continuous flow with ADH-1001 immobilised on activated charcoal for ketone reduction and cofactor recycling, in a PBR. Performed in KPB (50 mM, pH 6.0) overlaid with results from Figure 6-13 (Tris-HCl) and Figure 6-14 (unbuffered H_2O) for comparison. The conversion of **11** to **12** was determined by in-line flow NMR reaction monitoring (NMR scans every 600 s). Reaction conditions: ADH-1001 (6.5 mg), activated charcoal (30 mg), **11** (100 mM), NAD^+ (0.1 mM), KPB (50 mM, pH 6.0), IPA (10 v/v%), flow rate = 25 min^{-1}, t_{Res} = 12 min, reactor volume = 300 µL.

The results in Figure 6-15 show that the continuous flow system achieved an initial ~80% conversion of **11** to **12** for the initial 2.8 h of the reaction, before conversion steadily decreased to ~50% after 8 h. Interestingly, the system appears to maintain a steady-state conversion of ~50% for the subsequent 4 h, before conversion steadily decreases again. After 20 h the conversion recorded was 20%. The system in KPB at pH 6.0 does not reach the same initial conversion seen with the system in Tris-HCl (Figure 6-13) and H_2O

(Figure 6-14), however the subsequent decline in conversion was not as severe. Indicating that the interaction between the KPB and the immobilised ADH-1001 is complex.

6.6.3 Stabilising the ADH-1001 with zinc sulphate

During efforts to understand the drop-off in activity of the immobilised ADH-1001 over time in continuous flow, the industrial partner informed us that the ADH-1001 was a zinc-based alcohol dehydrogenase. It was hypothesised that the Zn^{2+} in the ADH-1001 could be dissociating from the enzyme over time, leading to deactivation of the enzyme. The industrial partner have in the past prepared the ADH-1001 with hydrated zinc sulphate ($ZnSO_4.7H_2O$) before adding the enzyme into the experiment, as a method of possibly improving the ADH-1001 activity. This would work by saturating the enzyme with Zn^{2+}, so that all the Zn^{2+} sites were occupied, possibly leading to the optimum activity of the ADH-1001. An experiment was performed to understand whether this preparation would impact the enzyme's performance when immobilised on to the activated charcoal in continuous flow. Firstly, a PBR was loaded with ADH-1001 immobilised onto activated charcoal, that had been prepared by initially incubating the ADH-1001 in a zinc sulphate (52 mM) and KPB (50 mM, pH 6.0) solution for 10 min before following the immobilisation procedure outlined in Section 5.2. The reaction solution containing **11**, NAD^+ and IPA (10 v/v%) in KPB was pumped into the reactor at a flow rate of 25 µL min^{-1} (Figure 6-16)

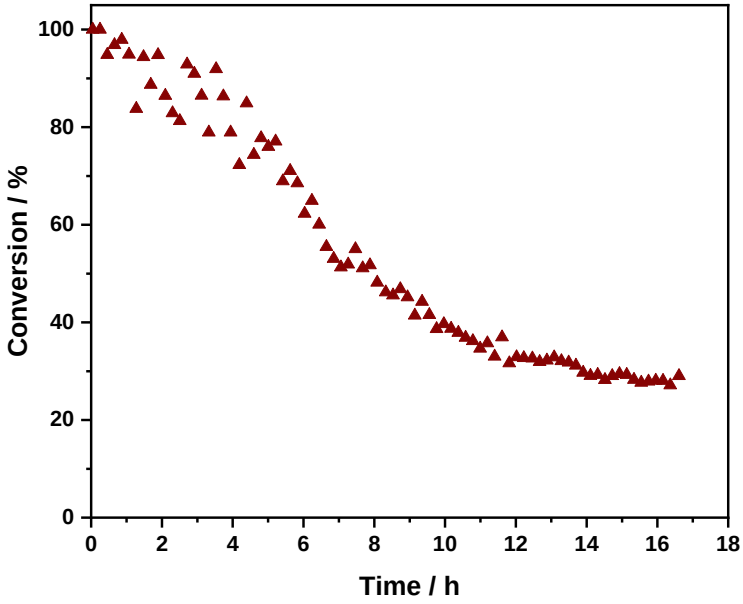


Figure 6-16: Conversion of **11** (100 mM) to **12** in continuous flow with ADH-1001 immobilised on activated charcoal for ketone reduction and cofactor recycling, in a PBR. The ADH-1001 was initially incubated in zinc sulphate solution before immobilisation on to activated charcoal. The conversion of **11** to **12** was determined by in-line flow NMR reaction monitoring (NMR scans every 600 s). Reaction conditions: ADH-1001 (6.5 mg), activated charcoal (30 mg), **11** (100 mM), NAD^+ (0.1 mM), KPB (50 mM, pH 6.0), IPA (10 v/v%), flow rate = 25 min^{-1}, t_{Res} = 12 min, reactor volume = 300 µL.

The results in Figure 6-16 show that the continuous flow system achieved an initial 100% conversion of **11** to **12** and then proceeded to maintain a conversion of between 75 to 100% for the first 6 h of the experiment. After this point the conversion continued to steadily decline before reaching a plateau at ~30% conversion for the final 6 h of the experiment. It is clear that the preparation of the immobilised enzyme with zinc sulphate had an improved effect on the activity of the system during the first 6 h, when compared against the near-identical experiment in Figure 6-15 (conversion after 6 h = ~60%). The activity of the system once again declined steadily over time, possibly supporting the hypothesis that Zn^{2+} in the ADH-1001 was dissociating from the enzyme over time, in

which case, it was hypothesised that addition of Zn^{2+} to the reaction solution in the PBR could overcome this.

An experiment was performed to test this. Firstly, a PBR was loaded with ADH-1001 immobilised onto activated charcoal, by following the normal procedure that does not use zinc sulphate, outlined in Section 5.2. The reaction solution containing **11**, NAD^+, zinc sulphate (1.7 mM) and IPA (10 v/v%) in KPB was pumped into the reactor at a flow rate of 25 µL min^{-1} (Figure 6-17).

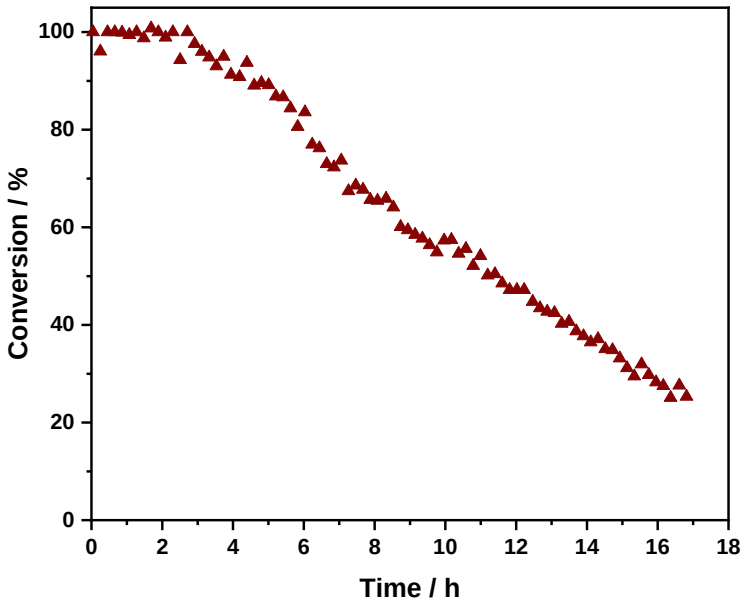


Figure 6-17: Conversion of **11** (100 mM) to **12** in continuous flow with ADH-1001 immobilised on activated charcoal for ketone reduction and cofactor recycling, in a PBR. Performed in KPB (50 mM, pH 6.0) with zinc sulphate (1.7 mM) dissolved in the reaction solution. The conversion of **11** to **12** was determined by in-line flow NMR reaction monitoring (NMR scans every 600 s). Reaction conditions: ADH-1001 (6.5 mg), activated charcoal (30 mg), **11** (100 mM), NAD^+ (0.1 mM), KPB (50 mM, pH 6.0), IPA (10 v/v%), $ZnSO_4.7H_2O$ (1.7 mM), flow rate = 25 min^{-1}, t_{Res} = 12 min, reactor volume = 300 µL.

The results in Figure 6-17 show that the continuous flow system achieved a 95 - 100% conversion of **11** to **12** over the first 3.3 h of the experiment and during the first 6.6 h of

the experiment the conversion was greater than 75% throughout. After this point the conversion continued to steadily decline before reaching a conversion of 25% after 16.8 h, at the time the experiment was stopped. Once again, it is clear that the use of zinc sulphate had a positive affect on the activity of the system when compared against the experiment without in Figure 6-15. The use of the zinc sulphate in the reaction solution also appears to give a slightly improved activity over the first ~6 h of the experiment compared with the previous experiment that used zinc sulphate in the preparation of the immobilised enzyme. Therefore, it was decided to use zinc sulphate in the reaction solution for all future experiments with the immobilised ADH-1001 flow system. Interestingly, the activity of the system once again declined steadily over time, indicating that the activity of the ADH-1001 might also be decreasing for another reason. It is possible that the enzyme begins to deactivate in other ways after a certain number of turnovers or that enzyme leaching occurs beyond the 6 h period that ADH-1001 leaching was studied in Figure 6-7. A time extended ADH-1001 continuous flow leaching experiment could be performed in the future to test this.

6.6.4 Increasing the catalyst loading in the PBR

The aim of the next experiment was to achieve full conversion of **11** to **12** for a longer period of time. It was hypothesised that one route towards this could be to increase the catalyst loading in the PBR, thus increasing the number of catalytic sites and compensating for any enzyme that may leach or become inactive. Firstly, a PBR was loaded with ADH-1001 (13 mg) immobilised onto activated charcoal (60 mg), which was double the catalyst loading of the previous experiments. The reaction solution containing **11**, NAD^+, zinc sulphate and IPA (10 v/v%) in KPB was pumped into the reactor at a flow rate of 25 µL min^{-1} (Figure 6-18).

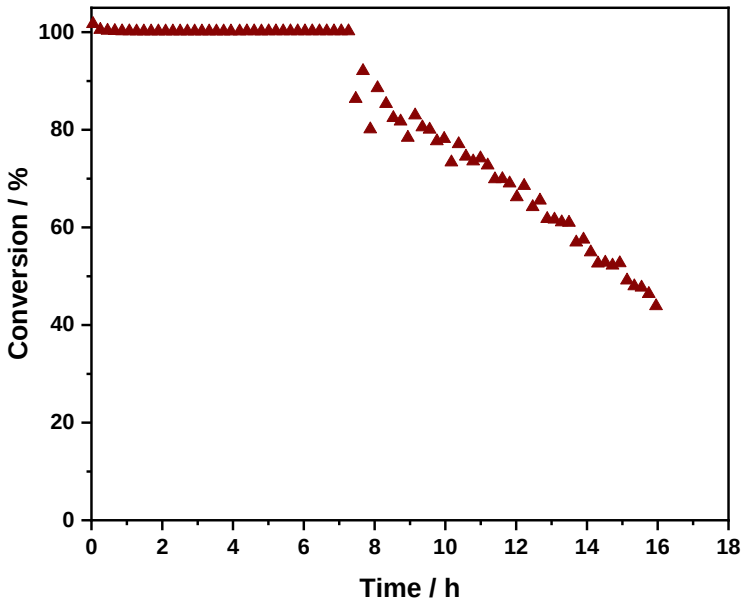


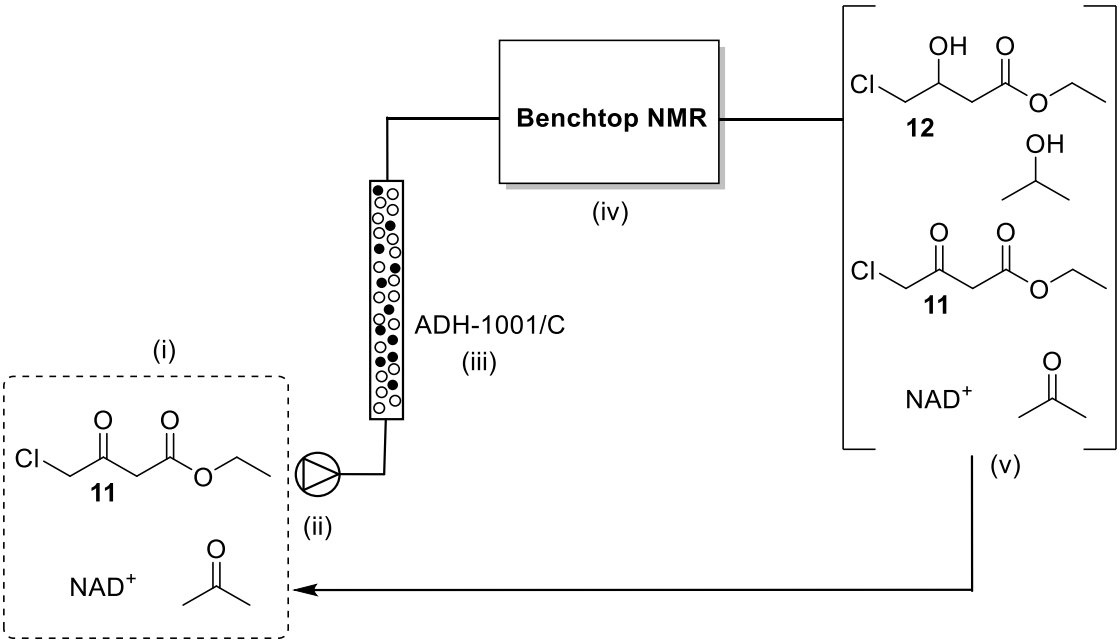
Figure 6-18: Conversion of **11** (100 mM) to **12** in continuous flow with ADH-1001 immobilised on activated charcoal for ketone reduction and cofactor recycling, in a PBR. To determine the effect of increased PBR size, the ADH-1001 on activated charcoal loading was doubled. The conversion of **11** to **12** was determined by in-line flow NMR reaction monitoring (NMR scans every 600 s). Reaction conditions: ADH-1001 (13 mg), activated charcoal (60 mg), **11** (100 mM), NAD^+ (0.1 mM), KPB (50 mM, pH 6.0), IPA (10 v/v%), flow rate = 25 min^{-1}, t_{Res} = 12 min, reactor volume = 300 µL.

The results in Figure 6-18 show that the continuous flow system achieved full conversion of **11** to **12** over the first 7.2 h, after this point the conversion steadily declined before reaching a conversion of 44% after 16 h, at the end of the experiment (total volume of reaction solution through the reactor = 24 mL). The system displayed >95% conversion for 2.2 times longer than the experiment in Figure 6-17, which had half the catalyst loading, suggesting a linear relationship between catalyst loading and the catalyst activity lifetime. Future experiments could increase the catalyst loading even more to achieve longer periods of full conversion from the flow system. This could be of industrial interest

because the ADH-1001 is currently a relatively cheap component of the reaction system (0.1% of total costs), by contrast, separation of non-reacted starting material can be very costly. Furthermore, costs might be decreased further by using this continuous set-up with the enzyme immobilised because it takes away the enzyme removal step.

A benefit of continuous flow, compared to batch mode, is the ease that the activity of the catalyst can be measured during the reaction. It is clear in Figure 6-17, although immobilised ADH-1001 was not achieving full conversion, that it was still active. It was hypothesised that the reaction solution could be recirculated through the PBR to achieve an improved overall conversion to product. This was the final experiment that the benchtop flow NMR was able to be used before it was returned to the company. The recirculation reaction set-up is shown in Scheme 6-7. The reaction solution containing **11**, NAD^+ and IPA in buffer was pumped from a reservoir (i) by a peristaltic pump (ii) through the adjustable Omnifit PBR iii), which contained ADH-1001 immobilised on activated charcoal and mixed with glass beads. The product mixture continued to be pumped through the benchtop flow NMR (iv), following this the product mixture was pumped back into the reaction solution reservoir for recirculation through the reactor (v).

Scheme 6-7: Set-up of the flow reactor for the continuous biocatalytic conversion of **11** to **12**, employing ADH-1001 immobilised on activated charcoal for ketone reduction and cofactor recycling: (i) Vessel containing the reactants (**11**, NAD^+, IPA) in a solution of Tris-HCl; (ii) syringe pump; (iii) ADH-1001 immobilised on activated charcoal, mixed with glass beads in a PBR; (iv) Product containing mixture is pumped through the in-line benchtop NMR reaction monitoring machine; (v) Product containing mixture is pumped back into reactant vessel for recirculation.



The experimental reaction conditions used were analogous to those in Figure 6-18. A PBR was loaded with ADH-1001 (13 mg) immobilised onto activated charcoal (60 mg). A 24 mL reaction solution (same as total volume through the reactor in Figure 6-18) containing **11**, NAD^+, zinc sulphate and IPA (10 v/v%) in KPB was prepared and recirculated through the reactor at a flow rate of 25 µL min^{-1} and the conversion of 4-chloroacetoacetate to **12** was monitored with in-line benchtop flow NMR. The time for one full pass of the reaction solution through the PBR was 16 h and t_{Res} per full pass was 12 min. Unfortunately, overnight when the reaction was left (between a reaction time of 20 to 30 h, the NMR and its computer monitoring system shut itself down (possibly due to a power cut) and the flow NMR data from this experiment was lost. However, after 32 h (2 full passes of reaction solution) the conversion of 4-chloroacetoacetate to **12** in the

reaction solution reservoir was found to be 100% after analysis by GC and the benchtop NMR. If the productivity of the system was to be measured by $g_{product}\ g_{enzyme}^{-1}$, this enzyme productivity of this experiment is 30.6 $g_{product}\ g_{ADH\text{-}1001}^{-1}$. This is almost a 50% increase in productivity to that achieved in Figure 6-19 (21.46 $g_{product}\ g_{ADH\text{-}1001}^{-1}$), which did not recirculate the reaction solution. However, the best enzyme productivity was achieved in Figure 6-20 (42.9 $g_{product}\ g_{ADH\text{-}1001}^{-1}$), which used a 50% lower ADH-1001 loading. These productivity values are competitive with the industrially relevant batch process for this transformation with ADH-1001 in solution, which achieves a productivity of 50 $g_{product}\ g_{ADH\text{-}1001}^{-1}$. Although the ADH-1001 productivity is lower than the industrially relevant batch process (enzymes in solution), the continuous process developed in this chapter has many possible benefits when they are directly compared. Firstly, the enzyme is immobilised and the product solution does not require the enzymes to be removed. The process has been shown to work well in a variety of buffers, including H_2O, which could be a route towards cost savings. Finally, the continuous flow element of the process offers constant in-line analysis from equipment such as the benchtop flow NMR, which has been demonstrated here and it would be much more difficult to achieve such a regular method of analysis in batch. The system developed here can certainly be optimised further.

6.7 Summary

This chapter has shown that an industrially used ADH can be quickly and efficiently immobilised on to a simple activated charcoal support for use in a continuous flow PBR reactor, for the model ketone reduction reaction of 4-chloroacetoacetate. The alcohol formed is used as a pre-cursor in the API synthesis of Atorvastatin but there are also many

industrially relevant analogues, including one used by the industrial partner who we collaborated with throughout this chapter.

The system was firstly optimised in batch before being translated into a continuous flow reactor. It was found that the system could achieve full conversion of 100 mM substrate to **12**, at a substrate:NAD^+ ratio of 1000:1 in two buffer systems and one unbuffered system. Addition of zinc sulphate to the reaction solution was found to improve the activity lifetime of the immobilised ADH-1001. It was found that increasing the catalyst loading enabled operation of the system at full conversion for over 7 h, this could be further improved at higher loadings. Also, recirculation of the reaction solution through the reactor was found to improve the overall performance of the reactor, achieving full conversion of a 24 mL reaction solution of 100 mM substrate in 32 h. The peak STY, enzyme productivity and *E* factor achieved by the system were 83 g L^{-1} h^{-1}, 42.9 $g_{product}$ $g_{ADH\text{-}1001}$ and 4.5 respectively. The peak STY and *E* factor compare favourably to similar reactions in the literature. Ma *et al.*, achieved an STY of 28 g L^{-1} h^{-1} and an *E* factor of 5.8 for the same ketone reduction of 4-chloroacetoacetate with an ADH and GDH in solution.[167] Döbber *et al.* achieved an STY of 1.58 g L^{-1} h^{-1} for the reduction of an aryl hydroxy ketone with an analogous system which immobilised an ADH onto a HaloTag fusion support to perform substrate coupled ketone reduction and IPA-driven cofactor regeneration.[233]

The continuous flow system was shown to be accurately analysed with a state-of-the-art in-line benchtop flow NMR system. This allowed the system to be monitored almost instantly and much more frequently than with other methods of analysis like GC, that requires the sample to be worked-up with additional chemicals and can require length analytical methods. Another benefit of the in-line flow NMR was that the product

solution could be collected straight into a sealed vessel without compromising on the analysis. An issue with using a fraction collector is that once collected the reaction samples remain open to the air, which is not ideal when using volatile reagents and products. Consequently, the samples have to be analysed immediately, making it difficult to collect fractions overnight.

In conclusion, this Chapter has again shown carbon as a viable support material for NADH-dependent biocatalysis in continuous flow. A substrate coupled IPA-driven ketone reduction/cofactor regeneration system was demonstrated by an ADH-1001 immobilised on activated charcoal for the conversion of **11** to **12**. Whilst the system still has plenty of scope for further optimisation, achieving the 'gold standard' of cofactor recycling with an ADH immobilised on a support in continuous flow has rarely been achieved in the literature.

7 H_2-driven NAD^+ reduction in the H-Cube flow reactor

7.1 Introduction

The work presented in this Chapter was published in a special issue 'Recent Developments in Process Intensification using Heterogeneous Catalysts in Continuous Flow': Poznansky et al., Front. Chem. Eng., 2021, 3, 35, DOI: 10.3389/fceng.2021.718257

and a ChemRxiv submission 'Accelerating Biocatalytic Hydrogenations using the H-Cube Flow Reactor', B. Poznansky et al, ChemRxiv, DOI: 10.26434/chemrxiv.12532301.v1.

The previous results chapters focused on implementing the well-established FDH–formate and ADH–IPA NADH regeneration systems in flow. The work studied the green metrics such as the *E* factor and focused on optimising them to make the system as environmentally sustainable as possible. Demonstrating *E* factors of <5, however, the sacrificial substrate formate was still required in excess. This could not be avoided to achieve high yields. The excess formate also has to be separated from the product mixture, making the system even less desirable at an industrial level. Requiring only H_2 as a sacrificial substrate and achieving 100% atom efficiency, the 'HydRegen' H_2-driven NADH regeneration system is well suited for translation into flow. This chapter will build on the previous use of carbon as a simple and efficient support for continuous flow, as the carbon will also act as an electron conductor in the multi-enzyme system.

The Vincent group has made preliminary progress into the translation of the H_2-driven NADH regeneration technology into flow. The work with carbon nanotubes as the support demonstrated that the technology is indeed viable, however, issues such as requiring recirculation of reaction material and poor stability of the immobilised SH, suggested that further, more thorough research into this space was indeed required.

Having described in previous chapters that the carbon particles are a reliable support in flow for biocatalysis with cofactor regeneration, the work in this chapter looks to build on this.

The form of carbon used in this chapter continues to be activated charcoal particles, it is hoped that the inherently larger surface area over the carbon nanotube columns might enable increased enzyme loadings and improved performance. The activated charcoal is also cheaper and more widely available than the carbon nanotube support, which had to be custom made, enabling a faster scale-up if required.

Multiple flow reactor set-ups will be compared in this chapter with an H-Cube reactor. The use of the H-Cube reactor for metal catalysed hydrogenation reactions has become widespread; in spite of this, the technology has never been demonstrated for H_2-driven biocatalysis. The H_2-driven biocatalytic NADH regeneration system developed in the Vincent group is an ideally suited candidate to exploit the H-Cube reactor. Translation into a standard flow reactor offers direct comparison to metal/C hydrogenation catalysts and rapid transfer of technology if it were to be successful. The research in this Chapter focuses on the H_2 driven conversion of NAD^+ to NADH, before the addition of NADH-dependent enzymes in Chapter 8.

7.2 Immobilisation studies for SH, I64A and Hyd1 onto activated charcoal

As determined in previous chapters, enzymes have been found to immobilise onto activated charcoal well, whilst displaying good retention of enzyme activity. The larger size of activated charcoal (mm) over BP2000 (μm) allows for flow experiments to be

conducted at higher flow rates, without the leaching of carbon particles through the frits and the build-up of high column pressure.

7.2.1 Immobilisation efficiency of for SH, I64A and Hyd1 onto activated charcoal

For the enzymes used in this chapter (SH, Hyd1 and I64A), initial studies were next carried out to determine the enzyme immobilisation efficiency and the effect of immobilisation on the enzyme activities. The immobilisation efficiency was determined by comparing the mass of non-immobilised enzyme, recovered in the supernatant, to the total mass of enzyme exposed to activated charcoal (Table 7-1). The mass of enzyme in the supernatant was determined by UV-Vis A_{280}, using the calibration curves described in Appendix G. The protein mass to activated charcoal ratio tested for each enzyme is complementary to their use in biocatalytic flow experiments described later.

Table 7-1: Immobilisation efficiency of enzymes SH, Hyd1 and I64A onto activated charcoal

Enzyme	Mass of enzyme added / mg	Mass of carbon / mg	Immobilisation time / h	Supernatant Abs280nm	Mass of enzyme in supernatant / mg	Immobilisation / %
SH	0.1	7	1	0	0	100
Hyd1	0.1	7	1	0	0	100
I64A	0.5	7	1	0	0	100

The results in Table 7-1 show that 100% of SH (0.1 mg) was immobilised onto activated charcoal after 1 h. A 100% immobilisation efficiency was calculated for Hyd1 (0.1 mg) onto activated charcoal (2 mg) and for I64A (0.5 mg), after 1 h immobilisation time. The activated charcoal has displayed rapid absorption of each of the enzymes tested, without the need for modification or a complex procedure, highlighting the simplicity and

efficacy of the technique. It was then important to deduce whether the enzymes retained their activity, once immobilised.

7.2.2 Batch specific activity of the enzymes in solution and immobilised onto activated charcoal

Throughout the majority of this project, the SH used for the experiments was produced in-house by Dr Ramirez Hernandez in regular batches. In this time the enzyme preparation protocol was in the process of optimisation, as well as expected variation batch-by-batch, leading to differential enzyme performance for each batch. To demonstrate this, the specific activity in solution and when immobilised onto activated charcoal of two batches of SH (batch-40 and batch-42) was measured and the batch specific activity was compared.

The specific activity of SH batch-40 in solution for the conversion of NAD^+ to NADH was determined by a UV-Vis solution assay for NADH formation. A mass of SH batch-40 (0.004 mg) were used. The A_{340} nm over time is shown in Figure 7-1, and activity was determined from the initial slope. Other SH batches were examined in the same way.

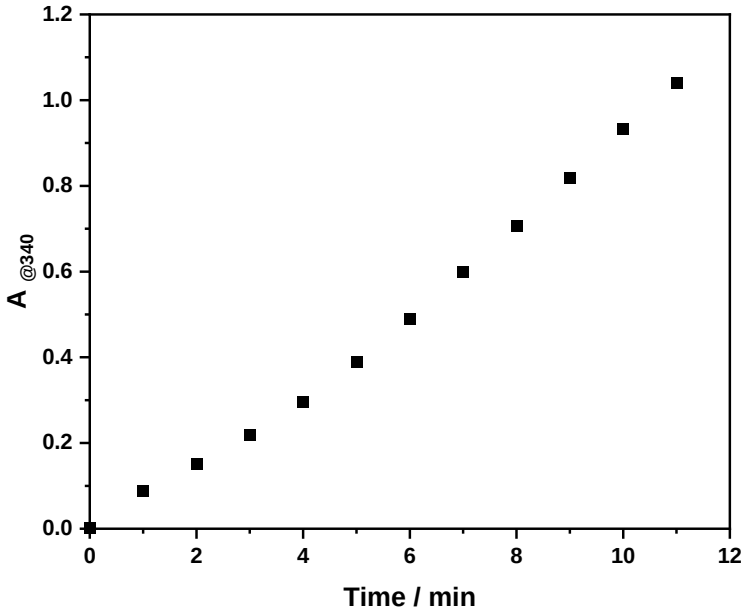


Figure 7-1: Batch enzyme activity measurement of free SH batch-40 in solution for the catalysis of NAD^+ to NADH, for which the calculated SH batch-40 activity is 4.1 U mg^{-1}. The conversion of NAD^+ to NADH over time was determined with *in situ* UV-Vis spectroscopy. Reaction conditions: SH batch-40 (0.004 mg), NAD^+ (1 mM), Tris-HCl (50 mM, pH 8.0), H_2 flow rate = 5 mL min^{-1}.

To determine the specific activity of SH batch-40 when immobilised onto activated charcoal, for the conversion of NAD^+ to NADH, 1 µL of SH batch-40 (0.04 mg) were immobilised onto activated charcoal (1 mg) according to the general procedure outlined in Section 5.2. The specific activity was measured by performing a heterogeneous UV-Vis assay for NADH formation. The A_{340} nm over time is shown in Figure 7-2. Other SH batches were examined in the same way.

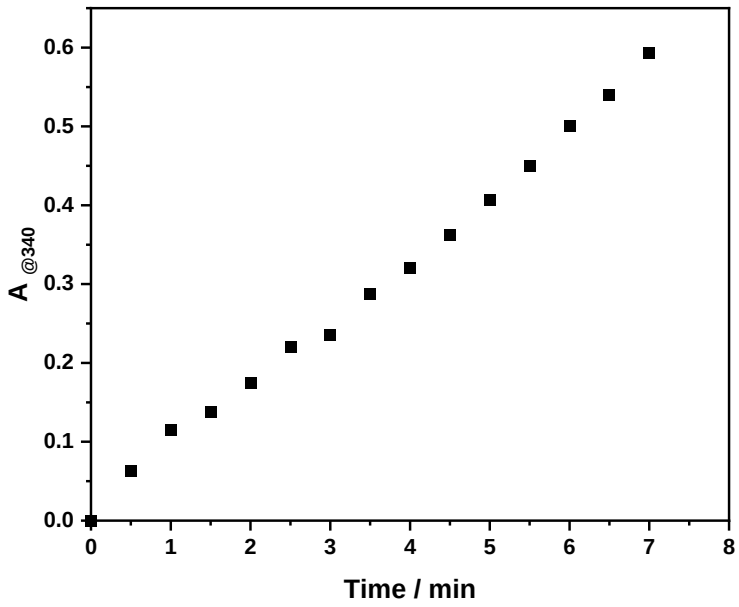


Figure 7-2: Batch enzyme activity measurement of SH batch-40 immobilised onto activated charcoal for the catalysis of NAD^+ to NADH, for which the calculated SH batch-40 activity is 0.34 U mg^{-1}. The conversion of NAD^+ to NADH over time was determined with in situ UV-Vis spectroscopy. Reaction conditions: SH batch-40 (0.04 mg), activated charcoal (1 mg), NAD^+ (1 mM), Tris-HCl (50 mM, pH 8.0), H2 flow rate = 5 mL min^{-1}.

The activity measurements are tabulated in Table 7-2, and show that SH batch-40 retains 8.2% of the activity when immobilised on activated charcoal (entry 3), compared with its activity free in solution (entry 1) and SH batch-42 retains 5.1% of the activity when immobilised on activated charcoal (entry 4), compared with its activity free in solution (entry 2). Although this is a low retention of activity, the work in Chapter 3 showed that enzymes can display an improved activity when immobilised on the carbon in flow over batch. Comparison of SH activity in solution (entries 1, 2, 5 and 6) suggests that there is a relatively large variation in batch-to-batch activity, therefore, future experiments in the same section aimed to use the same batch of enzyme to aid comparison.

Table 7-2: Specific activity of SH batches free in solution and immobilised on activated charcoal

Entry	Enzyme	Catalyst preparation	Enzyme mass / mg	Activated charcoal mass / mg	Activity / U mg_{enzyme}^{-1}
1	SH batch-40	Free enzyme	0.004	N/A	4.1
2	SH batch-42	Free enzyme	0.0008	N/A	35
3	SH batch-40	Immobilised on carbon	0.04	1	0.34
4	SH batch-42	Immobilised on carbon	0.008	1	1.8
5	SH batch-41	Free enzyme	0.0008	N/A	50
6	SH batch-56	Free enzyme	0.0035	N/A	6.5

Reaction conditions: 1 mM NAD^+, Tris-HCl buffer (50 mM, pH 8.0), $H_{2\,(g)}$ flow rate = 5 mL min^{-1}.

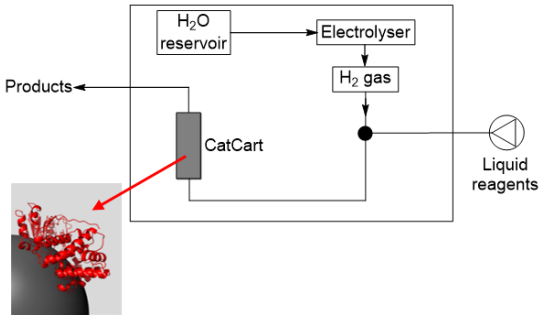
From this point forward in this chapter and the next chapter, by analogy with supported metal nanoparticle catalysts, the enzymes immobilised onto activated charcoal will be denoted as enzyme/C. For example, the SH immobilised onto activated charcoal will be referred to as 'SH/C'.

7.3 NAD^+ reduction with SH/C in the H-Cube reactor

7.3.1 H-Cube reactor flow set-up

The H-Cube flow reactor is a commercial flow reactor designed to generate $H_{2\,(g)}$ in-situ from water by an electrolyser at a range of system pressures. A liquid reagent is simultaneously pumped into the system and mixed with the $H_{2\,(g)}$ and then the mixture is pumped through a CatCart^{TM} cartridge, which is a purpose-built flow column that can be bought pre-packed with catalyst or self-packed with the desired catalyst using a separate machine. The H-Cube offers precise control of the pressure, temperature and flow rate with a computerised system and interface.

Scheme 7-1. Diagram of the H-Cube reactor, highlighting the in situ H_2 gas generation by the electrolyser. The liquid reagent is pumped into the system, mixed with the H_2 gas and pumped through the CatCart cartridge with precise control of the pressure, temperature and flow rate. The CatCart cartridges can be packed with enzyme-modified carbon.



Although there are no previous examples of biocatalysis being performed in an H-cube reactor, the flow reactor suits the needs of the HydRegen system well, and seemed to be a good starting point for the first deployment of the enzyme-modified particles in flow. The CatCart PBR system enabled good catalyst loading reproducibility; the strict pressure and temperature control enabled for the enzyme-modified particles to be tested under wide range of reaction conditions, with consistency. For example, reactions with the enzymes under high $H_{2\,(g)}$ pressure (>10 bar), which can prove to be difficult to conduct and reproduce safely when performed under batch conditions, can be safely achieved with the H-Cube reactor.

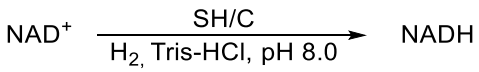
The H-Cube reactor set-up followed the general design shown in Scheme 7-1 . The CatCart PBR is loaded with the activated charcoal, onto which the enzyme solution is added. The CatCart PBR is sealed with the ThalesNano CatCart column packer. The reaction solution was pumped from a vessel by a piston pump into the H-cube reactor, in which it mixes with the $H_{2\,(g)}$ produced by the electrolyser and is pumped through the CatCart PBR. The product mixture was sampled with a fraction collector, typically at time intervals of 1 to 60 mins. It is not possible to collect the fractions at intervals of the

t_{Res} because in most cases the t_{Res} is between 1 to 20 s and the samples collected would not be large enough to analyse.

7.3.2 Initial SH/C H-Cube reactor results

The initial experiment with the H-Cube reactor was to determine whether the SH/C would demonstrate activity for the conversion of NAD^+ to NADH in the reactor, under the range of reaction conditions that the H-Cube offers (Scheme 7-2). The SH/C was chosen after the reported success of the SH immobilised onto the carbon nanotubes.[260] The experiment was performed with an H-Cube Pro reactor, which the manufacturers (ThalesNano) allowed us to test for two days, to determine the suitability of the H-Cube for biocatalysis.

Scheme 7-2: Biocatalytic conversion of NAD^+ to NADH, employing a SH/C catalyst, in the H-Cube reactor.



A CatCart cartridge (reactor volume = 300 µL) loaded with SH batch-41 (1.6 mg) immobilised onto activated charcoal (35 mg), according to the procedure in Section 2.9.7(A) was tested in the H-Cube reactor for conversion of 1 mM NAD^+ to NADH. The reaction solution containing NAD^+ in Tris-HCl buffer was pumped into the H-Cube reactor system at a range of flow rates of 0.3, 1 or 3 mL min^{-1}, where it was combined with the $H_{2\,(g)}$ from the built-in electrolyser (approx. 12 mL min^{-1}). As the gas flow rate was the major contribution to the total flow rate, this equated to t_{Res} through the reactor of 1, 0.9 or 0.8 s, respectively. The system pressure was tested at 2, 10 or 50 bar. The reaction samples were analysed by UV-Vis spectroscopy (A_{260} and A_{340}).

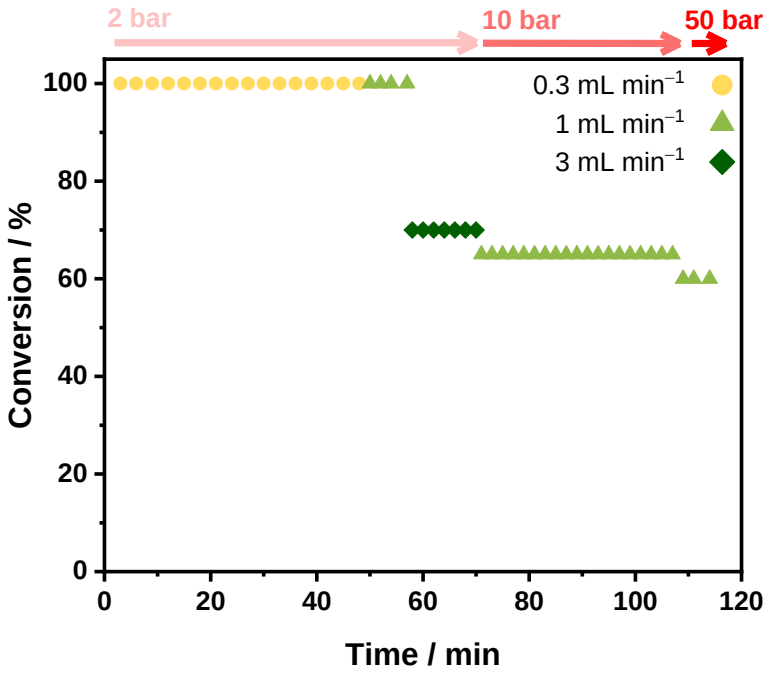


Figure 7-3. Continuous conversion of NAD^+ to NADH using SH/C in the H-Cube reactor under different liquid flow rates and pressures (top axis). Reaction conditions: NAD^+ (1 mM), Tris-HCl buffer (50 mM, pH 8.0), SH (batch-41, 1.6 mg), activated charcoal (40 mg), 25 °C, liquid flow rate = 0.3, 1 or 3 mL min^{-1}, H_2 flow rate ≈ 12 mL min^{-1}, t_{Res} = 0.8, 0.9 or 1.0 s, reactor volume = 0.2 mL.

The results in Figure 7-3 show that initially quantitative conversion to NADH was achieved at a liquid flow rate of 0.3 mL min^{-1} and 2 bar, demonstrating that the SH/C does show activity in the H-Cube reactor at a t_{Res} of 1 s. After 48 min, the liquid flow rate was increased to 1 mL min^{-1} (t_{Res} = 0.9 s) and the system continued to achieve quantitative conversion. At a liquid flow rate of 3 mL min^{-1}, the conversion dropped to 70%, demonstrating that the liquid flow rate had become a limiting factor on the conversion. At this liquid flow rate the highest enzyme turnover frequency (TOF) of 223 min^{-1} was achieved (70% conversion), likely owing to improved substrate availability pushing the catalyst harder. When the liquid flow rate was decreased back to 1 mL min^{-1} and the pressure was increased to 10 bar, a lower conversion of 65% was shown than at 2 bar for the same liquid flow rate, however further increasing the system

pressure to 50 bar had minimal further effect on the conversion (60%) compared to 10 bar. This demonstrated the stability of the biocatalytic cartridge at elevated pressure and, although the enzyme system does not require high pressure for operation, it shows the potential for use in multistep continuous processes in which higher pressures may be required for other reaction steps. Over the course of the reaction the TTN of the SH was 8400, which was comparable to the SH TTN achieved when immobilised onto carbon nanotubes (10,250). The highest specific activity achieved was 1.31 U mg^{-1}, this is a 2.6% retention of the activity recorded in free solution of the SH batch-41. Although, the activity could be considered low, this was just a preliminary experiment before optimisation. It was considered that an increased NAD^+ concentration and extended reaction time might lead to improved enzyme performance.

7.3.3 Increasing the cofactor throughput over the SH/C in the H-Cube reactor

After using the H-Cube Pro loaned to us for two days by the manufacturers (ThalesNano), an H-Cube Tutor was available to be borrowed from University of Oxford Chemistry Teaching Laboratories. Unfortunately the available system did not have the function to control the overall pressure of the system. Having established that the SH/C system performed well at converting a 1 mM NAD^+ solution to NADH, the concentration of NAD^+ and the experiment time was increased, to improve the understanding of the limits and stability of the system. A CatCart cartridge loaded with SH batch-42 (1.6 mg) immobilised onto activated charcoal (43 mg), according to the procedure in Section 2.9.7(A) was tested in the H-Cube reactor for conversion of 3 and 5 mM NAD^+. A liquid flow rate of 0.1 mL min^{-1} and a H_2 flow rate of 7 mL min^{-1} were used throughout, giving an overall t_{Res} of 1.7 s. The reaction samples were analysed by UV-Vis spectroscopy.

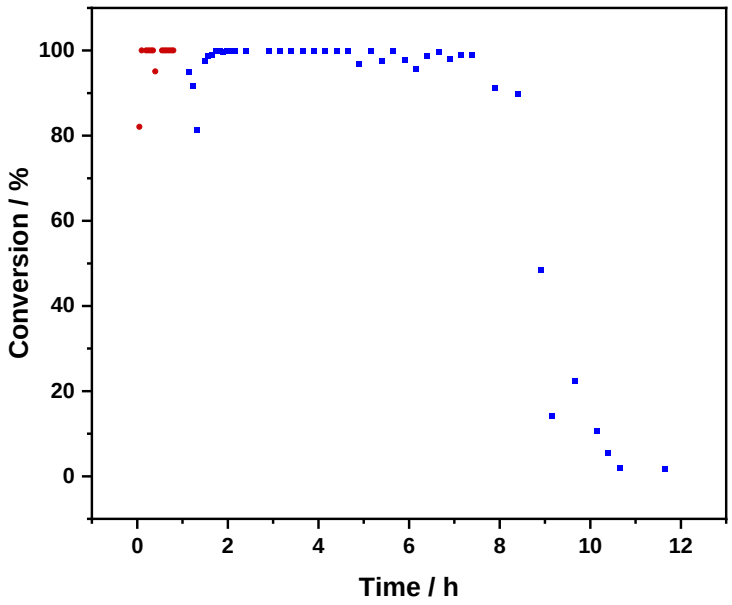


Figure 7-4. Conversion achieved of NAD^+ in continuous flow with SH/C in a 30 mm CatCart, at [NAD^+] of 3 mM (red) and 5 mM (blue). At 5 mM [NAD^+] the long-term stability of the immobilised SH was demonstrated. Under the reaction conditions of Tris-HCl (50 mM, pH 8.0), SH (1.6 mg), activated charcoal (40 mg), 25 °C. Reactor Volume = 0.3 mL , reaction solution flow rate = 0.1 mL min^{-1}, H_2 flow rate = ~7 mL min^{-1}, t_{Res} = 1.7 s. [NAD^+] ● = 3 mM, ■ = 5 mM .

The results in Figure 7-4 show full conversion of 3 mM NAD^+ to NADH was achieved for 1.1 h. The NAD^+ concentration was then increased to 5 mM, to see whether the catalyst could tolerate higher concentrations of NAD^+. A conversion of >98% was observed for a further 6.3 h (13300 reactor volumes), showing good stability. The conversion decreased over the subsequent 4 h, which could be caused by deterioration of the catalyst by enzyme leaching or enzyme deactivation. During the reaction the system was shown to operate with a space-time yield (STY) of 7.9 $kg_{NADH}\ L^{-1}\ h^{-1}$ and an *E* factor of 0.9. Overall, 173 mg of NADH was synthesised. Achieving a specific activity of 0.18 U mg^{-1} and near quantitative conversion for 7.4 h, suggests that even higher activity could be achieved by increasing the NAD^+ cofactor concentration further or lowering the

enzyme loading. Another approach to increase the activity might be to attempt to lower the H_2 flow rate (currently 7 mL min^{-1}), which is a large proportion of the overall flow rate. Lowering it, would increase the t_{Res}, without affecting the volume of reactant flowing through the cartridge, whilst leaving plenty of leeway to keep a high H_2 flow rate, which is a clear benefit of the system.

7.3.4 Varying the H_2 flow rate in the H-Cube to determine the effect on SH activity

After establishing that the SH/C system performed well at converting concentrations of up to 5 mM NAD^+ solution to NADH, to further improve the understanding of the limits of the system it was important to see how the SH/C performs at a conversion <60%, under strained conditions. It was decided to lower the enzyme and activated charcoal loading in the cartridge and continue to work at 5 mM NAD^+ concentration. Along with this, to monitor the effect on the SH activity of the H_2 flow rate, the H_2 produced by the H-Cube itself was switched off and instead pumped in separately from a H_2 cylinder. Here, the H_2 and reaction solution mix in a T-piece, before entering the H-Cube reactor, enabling precise control of the H_2 flow rate.

A CatCart cartridge was loaded with SH batch-56 (0.6 mg) immobilised onto activated charcoal (35 mg). From this point onwards in the Chapter, the CatCarts were packed and sealed according to the procedure (B) in Section 2.9.7, with the enzymes immobilised before sealing the cartridge. The loaded CatCart was tested in the H-Cube reactor for conversion of 5 mM NAD^+ to NADH. A liquid flow rate of 0.4 mL min^{-1} was applied throughout, whilst the H_2 flow rate was varied between 0.05 to 4 mL min^{-1}, giving a range of t_{Res} from 2.7 – 26.7 s. Data points were collected every 0.5 – 1 min and represent between 1.25 – 22 reactor volumes depending on the ratio of H_2 flow rate to liquid flow rate. At each new reaction condition at least 2 reactor volumes were allowed to flow

through for equilibration before the next sample was measured. The reaction samples were analysed by UV-Vis spectroscopy.

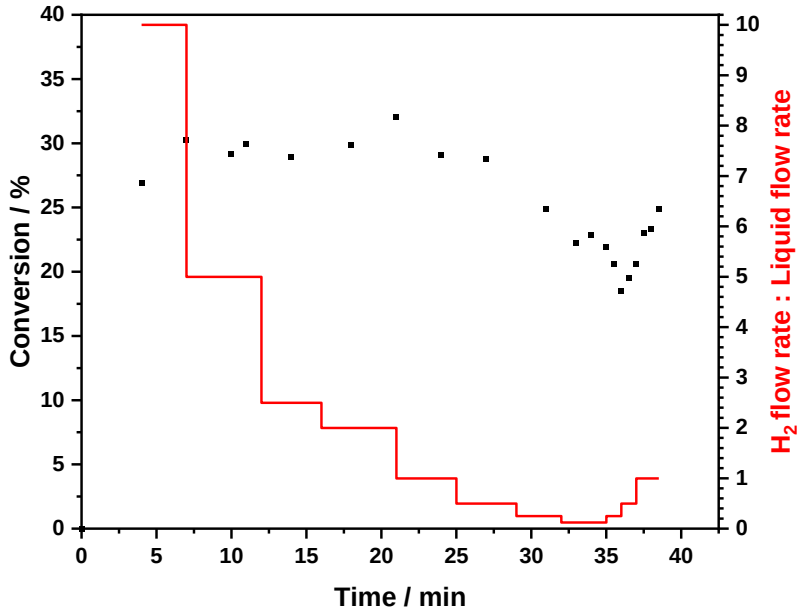


Figure 7-5. The effect of varying the ratio of H_2 flow rate to liquid flow rate (red line, right axis) on the conversion of NAD^+ to NADH (black squares, left axis) over time, using SH/C in the H-Cube reactor. Under the reaction conditions of NAD^+ (10 mM), Tris-HCl (50 mM, pH 8.0), SH (0.6 mg), activated charcoal (35 mg), 25 °C.

The results in Figure 7-5 show a steady state conversion of NAD^+ to NADH of ~30% was achieved between a starting H_2 flow rate to liquid flow rate ratio of 10 all the way down to a ratio of 1, displaying an average specific activity over the 25 min period of 2.0 U mg^{-1} (TOF = 250 min^{-1}). Below a H_2 flow rate to liquid flow rate ratio of 1, the conversion began to decrease, displaying a conversion of 18% at a 1/8 ratio of H_2 flow rate to liquid flow rate. This indicates that the H_2 is in excess up until it reached a 1:1 ratio with the liquid flow rate, before becoming the limiting factor for the experiment. To confirm this, a 1:1 ratio was reintroduced and the conversion began to return to the pre-H_2 limited conversion (26%). When the ratio of moles of H_2 to moles of NAD^+ in the

reaction system was considered, it correlates to a ratio of 2:1, as the turning point for when the reaction becomes H_2 limited. Any ratio of moles of H_2 to moles of NAD^+ below 2:1 appears to have an effect on the conversion, likely owing to lack of H_2 availability. This was useful for future reactions when deciding the H_2 flow rate. This experiment also highlighted that having a high H_2 flow rate (>2:1 mole of H_2 to moles of NAD^+) is not necessary for increased conversion but does not appear to affect the conversion as it increases. This means that the H-Cube reactor is still an ideal reactor for the system, especially the H-Cube Pro, for which the H_2 can be controlled to a certain degree.

7.3.5 Temperature stability of SH/C in the H-Cube

Having established the stability of the system with regard to the H_2 flow rate, the stability of the SH/C was tested. The H-Cube reactor offers precise control of the temperature in the PBR cartridge, with an in-built heating block. This makes it much easier to study the effect of reaction temperature than with standard PBR columns such as the Omnifit column used with the FDH recycling system. The temperature of the H-Cube reactor PBR cartridge can be varied throughout the reaction, making it possible to test multiple conditions with one biocatalytic cartridge. A CatCart cartridge was loaded with SH batch-56 (0.3 mg) immobilised onto activated charcoal (35 mg). The loaded CatCart was tested in the H-Cube reactor for conversion of 5 mM NAD^+. A liquid flow rate of 0.3 mL min^{-1} and a H_2 flow rate of 0.6 mL min^{-1} were used throughout, giving a t_{Res} of 13 s. These conditions were chosen so that the SH would be performing in highly strained condition (<60% conversion); therefore, the effect of temperature on the specific activity could be monitored very closely. The temperature was varied between 25 – 50 °C. Data points were collected every 2 min and 9 reactor volumes. The reaction samples were analysed by UV-Vis spectroscopy.

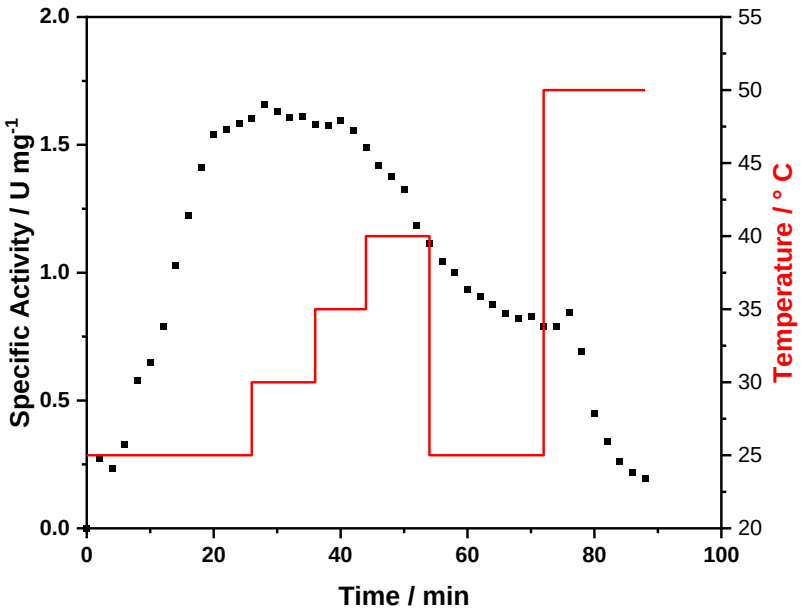


Figure 7-6. The effect of varying the temperature (red line, right axis) on the specific activity of SH (black squares, left axis) for the conversion of NAD^+ to NADH over time, using SH/C in the H-Cube reactor. Under the reaction conditions of NAD^+ (5 mM), Tris-HCl (50 mM, pH 8.0), SH (0.3 mg), activated charcoal (20 mg), 25 °C.

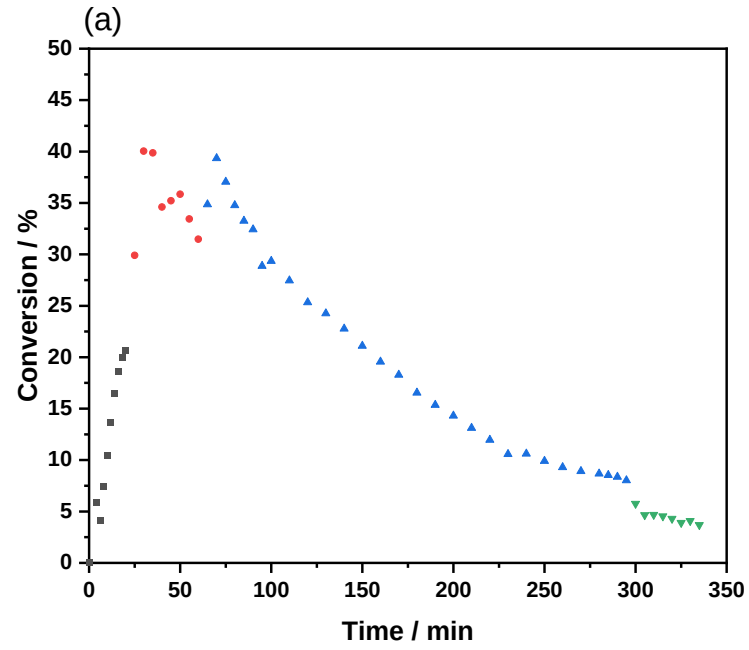
The results in Figure 7-6 show that the immobilised SH initially has an activity lag or build up period, which is possibly an activation period in which the SH is saturated by the H_2. Subsequently, the system reaches a steady state activity of ~1.6 U mg^{-1} (~32% conversion of 5 mM NAD^+ to NADH, TOF = 268 min^{-1}), under the starting temperature of 25 °C. The temperature was stepped up to 30 °C, whilst the SH maintained a steady state specific activity of 1.6 U mg^{-1}. On increase of the temperature to 35 °C, the SH specific activity began to decline to 1.5 U mg^{-1}. Once the temperature was stepped up to 40 °C, the specific activity of the immobilised SH is seen to clearly begin to decline, showing that the SH is unstable at this temperature and was deactivating/denaturing by some means. The temperature was decreased back to 25 °C; the system equilibrated and reached a steady state SH specific activity of 0.35 U mg^{-1} (TOF = 58 min^{-1}). To further

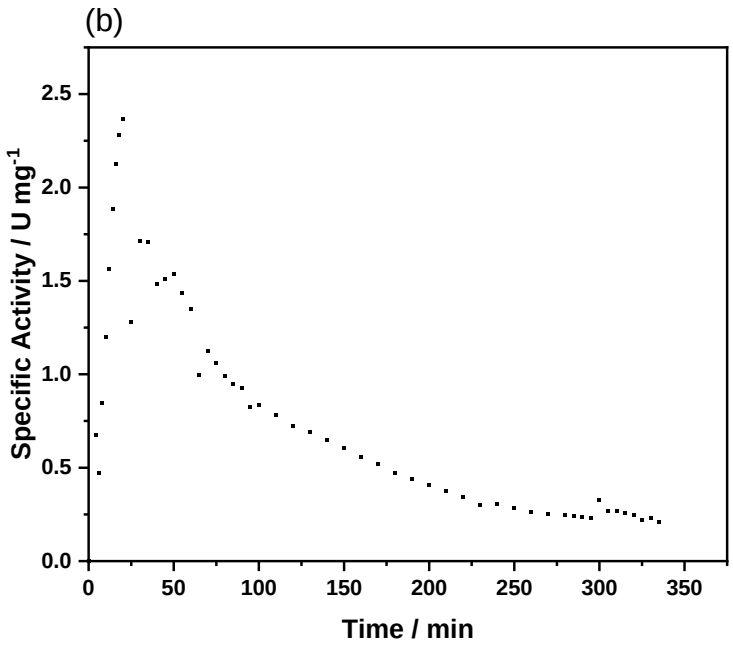
demonstrate the negative effect of temperature >35 °C on the SH specific activity the temperature was stepped up again to 50 °C. The SH specific activity in the system quickly reacted again, as it showed a rapid deactivation to 0.08 U mg^{-1}, before the reaction was ended. The ideal reactor temperature of the SH for specific activity was determined to be between 25–30 °C. Previously in batch experiments, the optimum temperature for activity of free SH in solution has been determined to be 33 °C,[273] which concurs with what has been determined in this experiment. However, this reaction was performed over a reasonably short time (88 min), with multiple reaction conditions tested: to ascertain the system's longer-term activity, a lifetime reaction was required.

7.3.6 Activity lifetime of SH/C in the H-Cube

After establishing the stability of the immobilised SH on activated charcoal with regard to the H_2 flow rate and temperature, it was apparent that the activity of the SH under strained conditions had not been tested beyond 90 min. This was a strategic decision, so that the enzyme could be monitored whilst it was at its peak activity and any activity fluctuations could be consigned to the reaction conditions imposed. To further understand the characteristics of the SH/C in the H-Cube reactor, a lifetime experiment was performed at strained conditions for the SH and the activity was monitored until the immobilised SH showed clear deterioration. A CatCart cartridge was loaded with SH batch-42 (0.18 mg) immobilised onto activated charcoal (20mg) and tested in the H-Cube reactor for conversion of 5 mM NAD^+. A range of liquid flow rates (0.1 – 0.4 mL min^{-1}) and a H_2 flow rates (0.3 – 1.2 mL min^{-1}) were used throughout the experiment, giving a t_{Res} of 7.5 – 30 s. The temperature was maintained at 25 °C, which has previously shown to be the optimum SH temperature for lifetime, in batch experiments. Data points were collected every 2 – 10 min and a total of 934 reactor volumes were collected.

The results in Figure 7-7(a) show that the conversion of NAD^+ to NADH peaked at 39.3% (t_{Res} = 30 s), after an initial activation period at a t_{Res} of 7.5 s. The conversion steadily declines over the proceeding 225 min at t_{Res} = 30 s, before the t_{Res} was decreased to 12 s and the conversion dropped below 5%. The t_{Res} was changed throughout the reaction, by decreasing the liquid flow rate, to reduce reagent waste at low conversions. The decrease in t_{Res} to 12 s was done to increase the number of data points collected, before the end of a shift in the laboratory. Along with the conversion of NAD^+ to NADH over time, Figure 7-7(b) shows that the specific activity of the SH/C maintains a peak performance of >1.3 U mg^{-1}, for the opening 60 min of the experiment, after the activation period. The highest specific activity of the SH (batch-42) immobilised onto the carbon achieved was 2.4 U mg^{-1}, this was the best specific activity achieved up to that point.


(a)
Conversion / %
Time / min
0
5
10
15
20
25
30
35
40
45
50
0
50
100
150
200
250
300
350


(b)
Specific Activity / U mg-1
Time / min
0.0
0.5
1.0
1.5
2.0
2.5
0
50
100
150
200
250
300
350

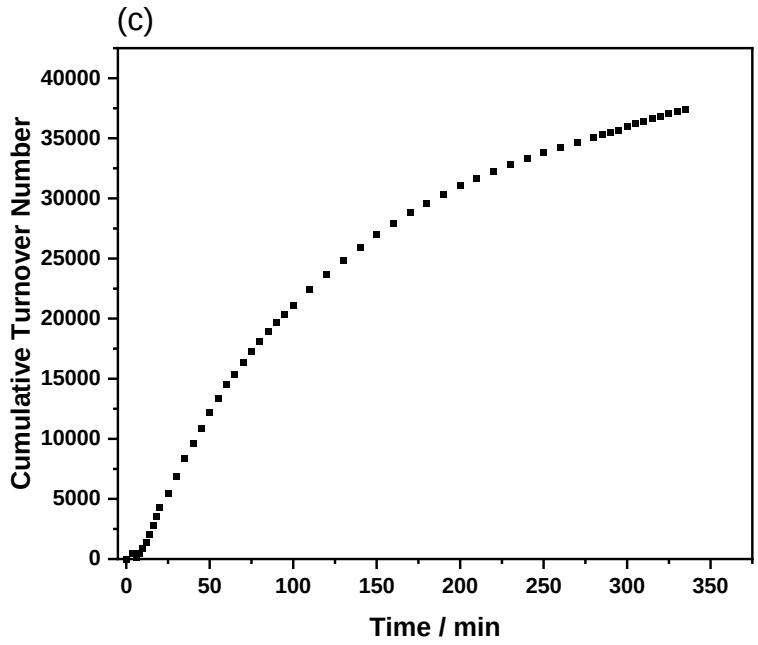


Figure 7-7. The activity lifetime of SH/C in the H-Cube flow reactor, for the conversion of NAD^+ to NADH at a range of liquid and H_2 flow rates. (a) Conversion of NAD^+ to NADH over time. t_{Res} ■ = 7.5 s (liquid flow rate = 0.4 mL min^{-1}, H_2 flow rate = 1.2 mL min^{-1}), ● = 20 s (liquid flow rate = 0.15 mL min^{-1}, H_2 flow rate = 0.45 mL min^{-1}), ▲ = 30 s (liquid flow rate = 0.1 mL min^{-1}, H_2 flow rate = 0.3 mL min^{-1}), ▼ = 12 s (liquid flow rate = 0.2 mL min^{-1}, H_2 flow rate = 0.8 mL min^{-1}). (b) Specific activity of the immobilised SH over time. (c) Cumulative turnover number of the immobilised SH over time. Under the reaction conditions of NAD^+ (5 mM), Tris-HCl (50 mM, pH 8.0), SH (0.18 mg), activated charcoal (20 mg), 25 °C.

In Figure 7-7(c) the cumulative turnover number of the immobilised SH is shown to reach 37,400 over the experiment, displaying a maximum TOF of 402 min^{-1}. Without an NADH dependent enzyme increasing the driving force of the reaction, this is a very respectable TOF, which compares favourably to the 18 min^{-1} achieved for the SH when immobilised on the carbon nanotubes.[260] In total 27 mg NADH was synthesised, corresponding to a reaction productivity of 158 g_{NADH} g_{SH}^{-1} and a peak STY of 0.24 kg L^{-1} h^{-1}.

Having established the activity of the SH/C over a period of ~350 min, at a range of liquid and H_2 flow rates. An experiment was performed at a fixed liquid flow rate of 0.05 mL min^{-1} and H_2 flow rate of 0.6 mL min^{-1} (t_{Res} = 18 s), over a longer period of time to establish a more complete lifetime activity of the immobilised SH under less strained conditions. Apart from the flow rates remaining constant, the experimental conditions were a repeat of those in Figure 7-7. A CatCart cartridge loaded with SH batch-42 (0.18 mg) immobilised onto activated charcoal (20mg) and tested in the H-Cube reactor for conversion of 5 mM NAD^+ to NADH. Data points were collected every 2.5 – 60 min over a total of 3,322 reactor volumes.

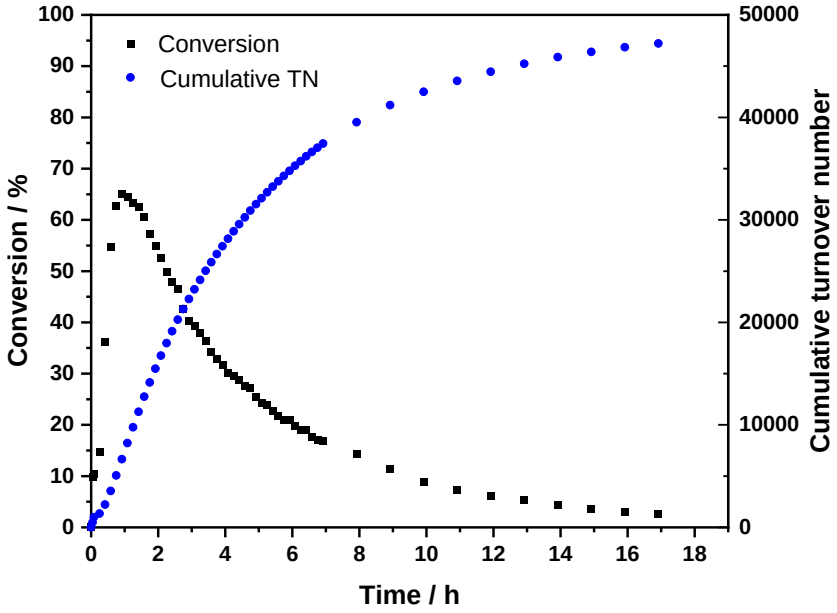


Figure 7-8: The extended activity lifetime of SH/C in the H-Cube flow reactor, for the conversion of NAD^+ to NADH at a fixed liquid and H_2 flow rates of 0.05 mL min^{-1} and 0.6 mL min^{-1}, respectively. The left y axis shows the conversion, and the right y axis shows the cumulative TTN of the SH. Under the reaction conditions of NAD^+ (5 mM), Tris-HCl (50 mM, pH 8.0), SH (0.18 mg), activated charcoal (20 mg), 25 °C, t_{Res} = 18 s.

The results in Figure 7-8 show that the conversion of NAD^+ to NADH peaked at 65% (t_{Res} = 18 s) after 0.9 h, showing that the less straining initial conditions allowed the system to achieve a higher conversion than in Figure 7-7. Characteristically, the conversion steadily declined over the proceeding 16 h to 2.6%. Overall, the SH TTN achieved was 47,200 and the specific activity of the SH immobilised peaked at 0.92 U mg^{-1} (TOF = 150 min^{-1}), before finishing at an activity of 0.27 U mg^{-1} (TOF = 50 min^{-1}). In total 34 mg NADH was synthesised, corresponding to a reaction productivity of 197 $g_{NADH}\ g_{SH}^{-1}$.

The experiments in Figure 7-7 and Figure 7-8 have demonstrated the best performance and lifetime of SH in flow so far. However, the constant decline in activity of SH over time highlights the instability of the SH that has been shown before. In the next section an enzyme leaching experiment is performed to establish whether the loss in activity is caused by enzyme leaching from the activated charcoal.

7.3.7 Leaching study of SH/C in the H-Cube

To determine the extent that SH leaching from the activated charcoal contributes to the loss of activity of the immobilised SH over time, a CatCart cartridge loaded with SH batch-56 (0.18 mg) immobilised onto activated charcoal (23 mg) was tested in the H-Cube reactor. A solution of Tris-HCl buffer (50 mM, pH 8.0) was pumped over the same cartridge at range of liquid flow rates (0.05 – 1 mL min^{-1}), to mimic different experimental conditions, in a t_{Res} range of 12 – 240 s. The temperature was maintained at 25 °C throughout. Data points were collected every 1 – 90 min. The mass of leached enzyme was calculated from the SH concentration calibration curve described in Appendix G using the UV-Vis A_{280}.

Table 7-3 Protein leaching of SH batch-56 off the activated charcoal

Entry	Time / min	Tris-HCl Volume over bed / mL	SH leaching / mg*
1[a]	100	1	0
2[b]	10	10	0
3[c]	960	4.8	0

[a] Flow rate = 0.1 mL min^{-1}; [b]flow rate = 1 mL min^{-1}; [c]flow rate = 0.05 mL min^{-1}; *SH detected by A_{280}. Reaction Conditions: SH (0.18 mg), activated charcoal (23 mg), Tris-HCl (50 mM, pH 8.0).

The results in Table 7-3, show that the cartridge of SH/C exhibited no detectable SH leaching, during all three entries, over a total time period of 1,070 min (~18 h). Of particular interest, was the detection of no leaching in entry 2, which demonstrates the tolerance of the SH to a high liquid flow rate, which would be important if the cartridge were to be used on a commercial scale.

To show that the SH had indeed remained immobilised onto the activated charcoal, the same CatCart cartridge loaded with SH batch-56 (0.18 mg) immobilised onto activated charcoal (23 mg) for the leaching experiment was tested in the H-Cube reactor for conversion of 5 mM NAD^+. A liquid flow of 0.3 and a H_2 flow rate of 1.2 mL min^{-1} were used throughout the experiment, giving a t_{Res} of 8 s. The temperature was maintained at 25 °C. Data points were collected every 3 min over a total of 360 reactor volumes.

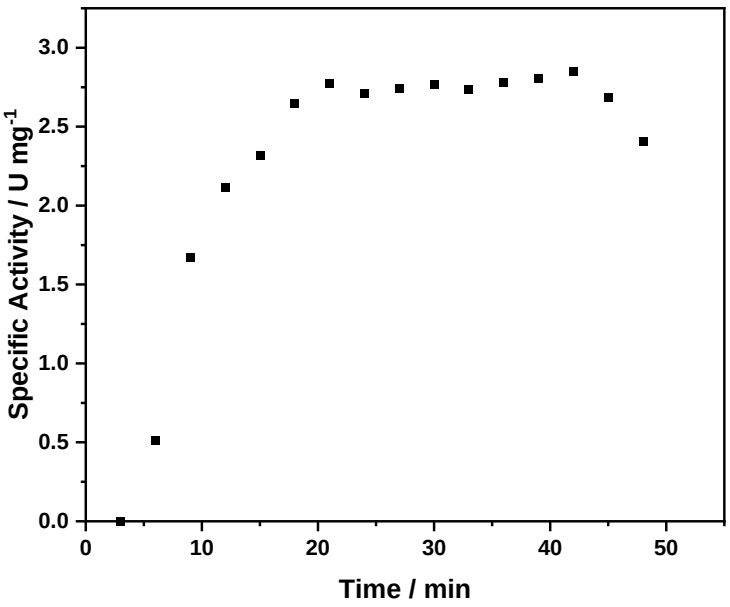


Figure 7-9: The specific activity of SH during the conversion of NAD^+ to NADH over time, using SH/C in the H-Cube reactor. Performed after a leaching experiment on the same loaded CatCart PBR, in which 15.8 mL of Tris-HCl had been pumped over it during an 18 h period. Reaction conditions: NAD^+ (5 mM), Tris-HCl (50 mM, pH 8.0), SH (0.18 mg), activated charcoal (23 mg), 25 °**C**.

The results in Figure 7-18 show that after a typical activation period, the specific activity of the immobilised SH was 2.7 U mg^{-1} (32% conversion of 5 mM NAD^+ to NADH). This demonstrates that the SH had remained fully immobilised during the leaching experiment. Furthermore, pumping 15.8 mL of Tris-HCl over the loaded CatCart over 18 h, had not impacted the activity at all, showing that the immobilised SH is stable at 25 °C, over long periods of time before use. Knowing that the SH does not leach from the activated charcoal, this experiment brings to the attention the general instability of the immobilised SH shown in Section 7.3.6, in which the system appears to deactivate quickly after reaching its peak operating activity. It was a good time to shift the focus towards translating the HydRegen system into the H-Cube reactor, which in batch has demonstrated much greater stability.[201]

7.4 NAD^+ reduction with HydRegen enzymes immobilised onto activated charcoal in the H-Cube reactor

In Section 7.3, it was established that the SH/C, illustrated in Figure 7-10(A), shows good activity for the conversion of NAD^+ to NADH over a ~100 min time frame. However, the immobilised SH fails to reach a steady state conversion and deactivates rapidly over time. It was hypothesised that deactivation of the hydrogenase module of the SH could be the cause of this instability. This was a good starting point for it to be combined with the HydRegen system. Previous Vincent group HydRegen batch mode studies, have focused on co-immobilising a separate NAD^+ reductase (termed I64A, an enzyme possessing the NAD^+ reductase activity of the SH without the hydrogenase activity) with a more robust hydrogenase enzyme (*E. coli* hydrogenase 1, 'Hyd1') onto carbon particles; as shown in Chapter 1, this system displayed greater stability and cofactor regeneration activity when compared with the SH. For the co-immobilised I64A and Hyd1 catalyst, the carbon acts as both an enzyme support and to electronically connect the two enzymes by conducting electrons generated through H_2-oxidation by the Hyd1 to the I64A, thus driving the I64A to regenerate NADH. It was hypothesised that co-immobilising the more robust Hyd1 with the SH could boost the activity and/or stability of the SH, in a similar way to the I64A and Hyd1 system, illustrated in Figure 7-10(B). In this section, the performance of SH and Hyd1 co-immobilised onto activated charcoal is explored.

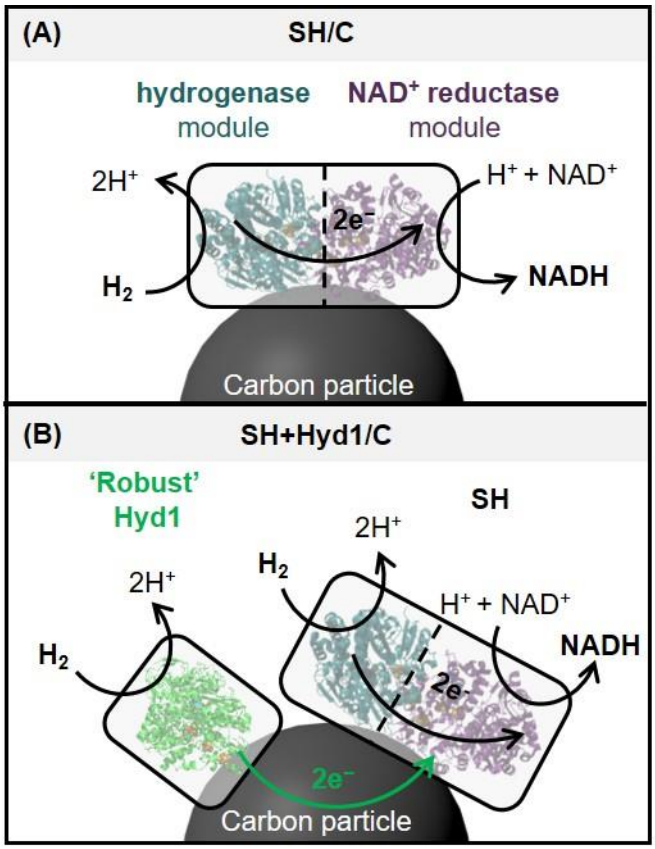
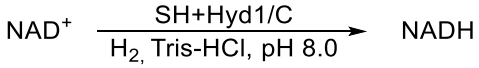


Figure 7-10: Illustration of the proposed boosting effect on NADH generation achieved by immobilising Hyd1 alongside SH onto activated charcoal. (A) The SH contains two modules: one for H_2 oxidation (hydrogenase, dark green) and one for NAD^+ reduction (NAD^+ reductase, purple), operating by electron transfer across the modules. Here, the SH is immobilised onto activated charcoal. (B) By co-immobilising Hyd1 (light green) additional H_2-derived electrons may be provided through the conductive activated charcoal to the NAD^+ reductase module, thereby supplementing the relatively unstable hydrogenase module of the SH.

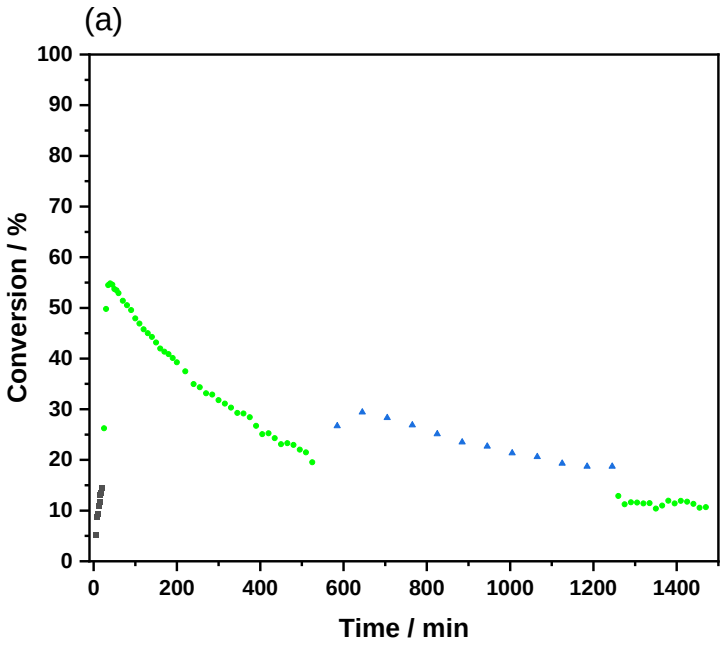
7.4.1 Activity lifetime of SH+Hyd1/C in the H-Cube

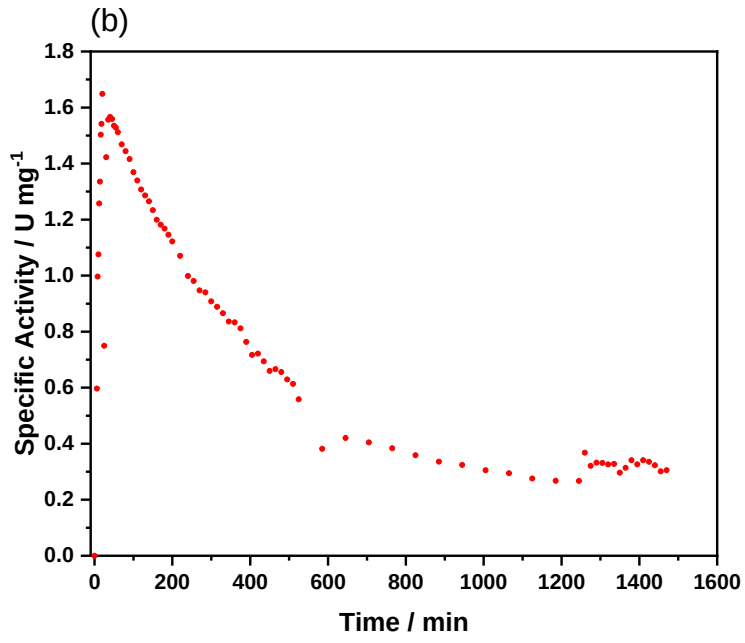
To determine whether the addition of the Hyd1 alongside the SH would have an effect on the NAD^+ reduction system (Scheme 7-3), a lifetime experiment was performed with near-identical conditions to the SH lifetime experiment performed in Section 7.3.6, in the H-Cube reactor.

Scheme 7-3: Biocatalytic conversion of NAD^+ to NADH, employing a SH+Hyd1/C catalyst, in the H-Cube reactor.



A CatCart cartridge was loaded with SH batch-56 (0.18 mg) and Hyd1 (0.15 mg) co-immobilised onto activated charcoal (20 mg) and tested in the H-Cube reactor for conversion of 5 mM NAD^+. A range of liquid flow rates (0.05 – 0.4 mL min^{-1}) and H_2 flow rates (0.6 – 1.2 mL min^{-1}) were used throughout the experiment, giving a t_{Res} of 7.5 – 18.4 s. The temperature was maintained at 30 °C for the duration. Data points were collected every 2 – 60 min over a total of 4,173 reactor volumes.


(a)
Conversion / %
Time / min
0
10
20
30
40
50
60
70
80
90
100
0
200
400
600
800
1000
1200
1400


(b)
Specific Activity / U mg-1
Time / min
0.0
0.2
0.4
0.6
0.8
1.0
1.2
1.4
1.6
1.8
0
200
400
600
800
1000
1200
1400
1600

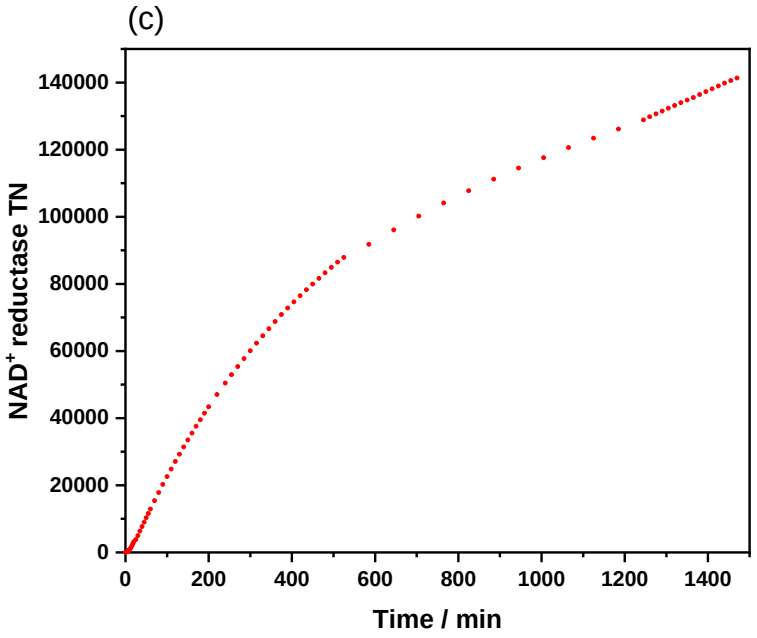


Figure 7-11. The lifetime of SH+Hyd1/C in the H-Cube flow reactor, for the conversion of NAD^+ to NADH. (a) Conversion of NAD^+ to NADH over time. (b) Specific activity of the NAD^+ reductase module in the SH over time. t_{Res} ■ = 7.5 s (liquid flow rate = 0.4 mL min^{-1}, H_2 flow rate = 1.2 mL min^{-1}), ● = 17 s (liquid flow rate = 0.1 mL min^{-1}, H_2 flow rate = 0.6 mL min^{-1}), ▲ = 18.5 s (liquid flow rate = 0.05 mL min^{-1}, H_2 flow rate = 0.6 mL min^{-1}). (c) Cumulative turnover of the NAD^+ reductase module in the SH over time. Under the reaction conditions of NAD^+ (5 mM), Tris-HCl (50 mM, pH 8.0), SH (0.18 mg), Hyd1 (0.15 mg), activated charcoal (20 mg), 30 °C.

The results in Figure 7-11(a) show that the conversion of 5 mM NAD^+ to NADH peaked at 56% (t_{Res} = 17 s), after the initial activation period at a t_{Res} of 7.5 s. From this point the conversion very steadily declines over the next 500 min to 20% (t_{Res} = 17 s). The reaction was left overnight, to decrease reagent waste, the H_2 flow rate kept at 0.6 mL min^{-1} but liquid flow rate was changed from 0.1 mL min^{-1} to 0.05 mL min^{-1} (t_{Res} = 18.5 s). At the lower liquid flow rate the conversion increased to 29%, demonstrating that the liquid flow rate might have a larger effect on the conversion than the overall t_{Res}. Overnight (660 min), the conversion continued to steadily decline. Owing to time restraints in the laboratory, to collect more data points, the liquid flow rate was increased again to

0.1 mL min^{-1}. The chart indicates that from 1260 min onwards, the system had reached a steady state conversion, with little to no decline in conversion during the subsequent 240 min. Along with the conversion of NAD^+ to NADH over time, Figure 7-11(b) shows that the specific activity of the NAD^+ reductase module of the SH/C maintains a peak performance of >1.3 U mg^{-1}, for the opening 130 min of the experiment, after the activation period. The highest specific activity of the SH (batch-56) immobilised onto the carbon recorded was 1.65 U mg^{-1}. The chart indicates that the specific activity has indeed reached a steady state activity of 0.3 U mg^{-1}, this highlights the improved stability of the system. In Figure 7-11(c) the cumulative turnover number of the NAD^+ reductase module of the SH is shown to reach 141,300 over the experiment, displaying a maximum TOF of 280 min^{-1}. A total 104 mg NADH was synthesised, corresponding to a reaction productivity of 324 g_{NADH} g_{enzyme}^{-1}. These metrics would have improved further if the experiment had been able to run for longer.

Having established the activity of the SH and Hyd1 co-immobilised onto activated charcoal over a period of ~1500 min (~25 h), at a range of liquid and H_2 flow rates. An experiment was performed at a fixed liquid flow rate of 0.05 mL min^{-1} and H_2 flow rate of 0.6 mL min^{-1} (t_{Res} = 18 s), over a longer period of time to establish a more complete lifetime activity of the co-immobilised SH and Hyd1 under consistent conditions. Apart from the flow rates remaining constant, the experimental conditions were a repeat of those in Figure 7-11. A CatCart cartridge was loaded with SH batch-56 (0.18 mg) and Hyd1 (0.15 mg) co-immobilised onto activated charcoal (20 mg) and tested in the H-Cube reactor for conversion of 5 mM NAD^+. The temperature was maintained at 30 °C for the duration. Data points were collected every 2 – 60 min over a total of 11,895 reactor volumes.

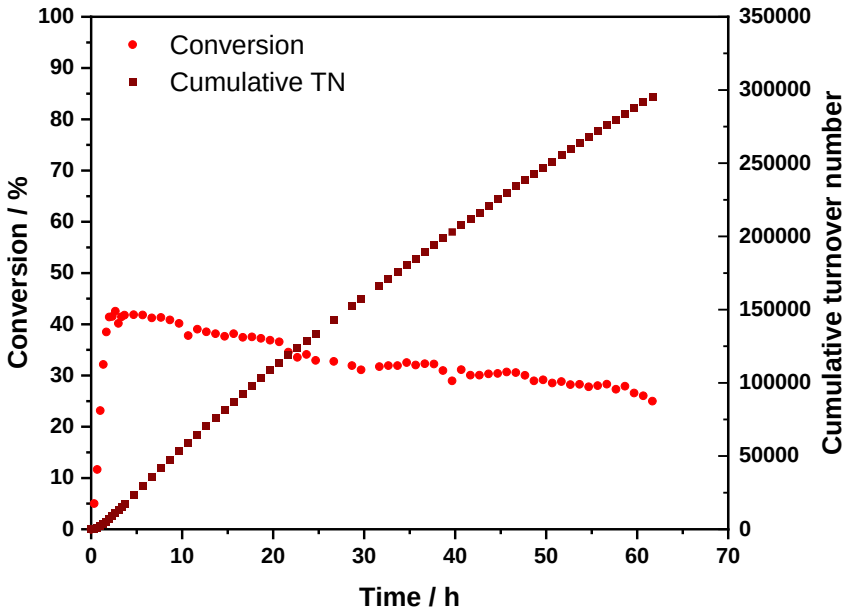


Figure 7-12: The extended activity lifetime of SH+Hyd1/C in the H-Cube flow reactor, for the conversion of NAD^+ to NADH at a fixed liquid and H_2 flow rates of 0.05 mL min^{-1} and 0.6 mL min^{-1}, respectively. The left y axis shows the conversion, and the right y axis shows the cumulative TTN of the SH (NAD^+ reductase module). Under the reaction conditions of NAD^+ (5 mM), Tris-HCl (50 mM, pH 8.0), SH (0.18 mg), Hyd1 (0.15 mg), activated charcoal (20 mg), 30 °C, t_{Res} = 18 s.

The results in Figure 7-12 show that the conversion of NAD^+ to NADH peaked at 43% (t_{Res} = 18 s) after 2.6 h. The conversion very steadily declined over the proceeding 70 h to 26%. Overall, the TTN of the SH NAD^+ reductase module achieved was 295,200 and the specific activity peaked at 0.62 U mg^{-1} (TOF = 110 min^{-1}), before finishing at an activity of 0.40 U mg^{-1} (TOF = 70 min^{-1}). In total 225 mg NADH was synthesised, corresponding to a reaction productivity of 674 g_{NADH} g_{SH}^{-1}.

Table 7-4: Comparison of lifetime experiments performed with the SH/C system against the SH+Hyd1/C system for conversion of NAD^+ to NADH

Figure	Enzyme(s)	Reactor Volumes	Peak specific activity[a] / U mg^{-1}	Final specific activity[a] / U mg^{-1}	SH productivity / g_{NADH} g_{SH}^{-1}	SH TTN[a]
Figure 7-7	SH	934	2.4	0.21	158	37,400
Figure 7-8	SH	3,322	0.92	0.27	197	47,200
Figure 7-11	SH & Hyd1	4,173	1.65	0.30	324	141,300
Figure 7-12	SH & Hyd1	11,895	0.62	0.40	674	295,200

[a]NAD^+ reductase module of the SH

In comparison to the lifetime experiment of SH/C performed in Section 7.3.6, the SH and Hyd1 on activated charcoal exhibited a higher TTN (SH = 47200, SH and Hyd1 = 295,200) and a much longer specific activity lifetime >0.4 U mg^{-1} (SH = 4.6 h, SH & Hyd1 = 60 h). The SH and Hyd1 on activated charcoal achieved a >3-fold improved SH productivity than the immobilised SH alone. This clearly indicates that the Hyd1 is supplementing the NAD^+ reductase module with electrons by conduction through the activated charcoal, thereby boosting the activity lifetime of the system. This means that the hydrogenase module of the SH is the cause of the instability displayed by the SH/C. The peak specific activities recorded and the activation period are similar in both systems, indicating that the NAD^+ reductase module of the SH is limiting the rate and the additional Hyd1 only begins to boost the system when the hydrogenase module of the SH begins to deactivate.

7.4.2 Temperature stability of SH+Hyd1/C in the H-Cube

Having established the lifetime stability boosting quality of the Hyd1 immobilised alongside the SH on the activated charcoal in the H-Cube reactor. Next, the SH+Hyd1/C were tested in the H-Cube reactor to determine whether the presence of Hyd1 (which has

been shown to display activity up to 60 °C),[274] improves the overall tolerance to higher temperatures of the system, where in Section 7.3.5, it was found that the SH/C rapidly deactivates at >35 °C. A CatCart cartridge was loaded with SH batch-56 (0.15 mg) and Hyd1 (0.15 mg) co-immobilised onto activated charcoal (20 mg). The loaded CatCart was tested in the H-Cube reactor for conversion of 5 mM NAD^+, whilst the temperature was increased periodically throughout. A liquid flow rate of 0.1 mL min^{-1} and a H_2 flow rate of 1.2 mL min^{-1} were used throughout, giving a t_{Res} of 9 s. These strained conditions (<60% conversion based on previous results) were used for the system; therefore, the effect of temperature on the specific activity could be monitored very closely. The temperature was varied between 30 – 80 °C. Data points were collected every 3 min over 1161 reactor volumes.

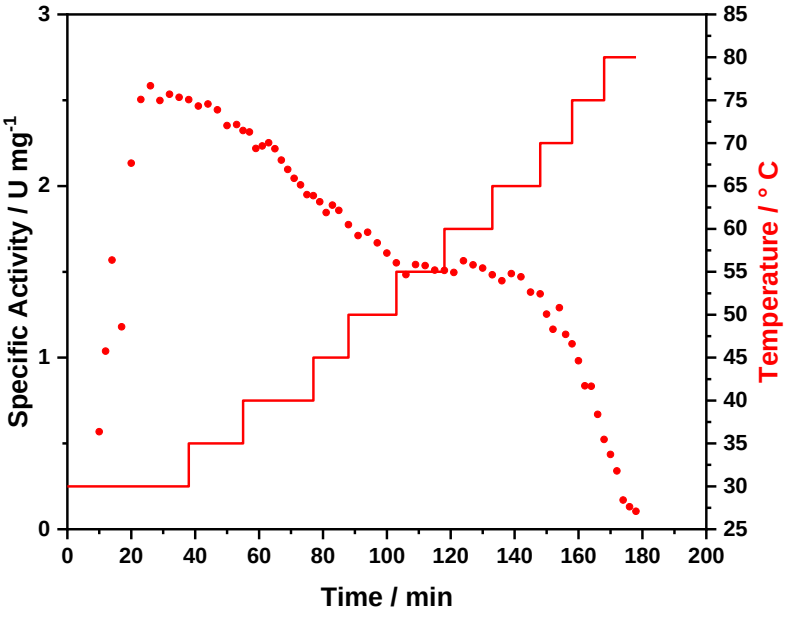


Figure 7-13. The effect of varying the temperature (red line, right axis) on the specific activity of the NAD^+ reductase module in the SH (black circles, left axis) for the conversion of NAD^+ to NADH over time, using SH+Hyd1/C in the H-Cube reactor. Under the reaction conditions of NAD^+ (5 mM), Tris-HCl (50 mM, pH 8.0), SH (0.15 mg), Hyd1 (0.15 mg), activated charcoal (20 mg).

The results in Figure 7-13 show that after the initial enzyme activation period, the SH+Hyd1/C display good activity as the temperature is increased by 5 °C increments from 30 to 60 °C, reaching a specific activity peak of 2.5 U mg^{-1} (TOF = 425 min^{-1}) and beginning to stabilise at 1.5 U mg^{-1} (TOF = 260 min^{-1}). The chart is similar to the specific activity displayed in the first 130 min of the lifetime experiment in Section 7.4.1. This indicates that the electrons produced by the Hyd1 are boosting the activity of the NAD^+ reductase module of the SH. It can be deduced that the hydrogenase module of the SH is unstable with respect to temperatures >35 °C; by contrast, the NAD^+ reductase module of the SH remains stable. The specific activity began to decline rapidly towards complete deactivation as the temperature was increased from 65 °C to 80 °C, although still displaying some activity over the 35 min period. It is difficult to deduce whether the deactivation of the Hyd1 or the NAD^+ reductase module triggers this decline. This experiment shows that the SH and Hyd1 combination on the activated charcoal display activity at a wide range of temperatures, over short periods of time at each temperature. To determine the lifetime of the system at the higher temperatures, longer experiments are required at fixed temperatures.

To establish the activity lifetime of the SH+Hyd1/C at 45 °C. A CatCart cartridge loaded with SH batch-56 (0.15 mg) and Hyd1 (0.15 mg) co-immobilised onto activated charcoal (20 mg). The loaded CatCart was tested in the H-Cube reactor for conversion of 5 mM NAD^+ to NADH, the temperature was maintained at 45 °C throughout. A liquid flow rate of 0.1 mL min^{-1} and a H_2 flow rate of 1.2 mL min^{-1} were used throughout, giving a t_{Res} of 9 s. Data points were collected every 2–60 min over 1,161 reactor volumes.

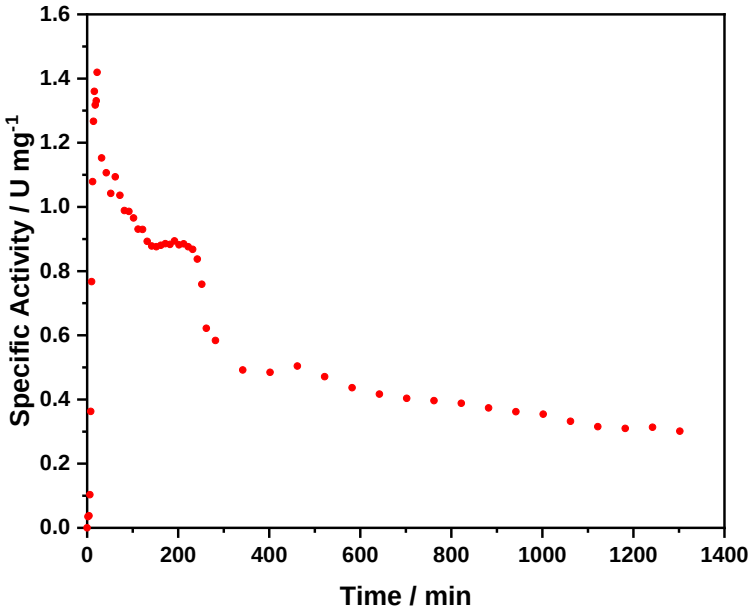


Figure 7-14. The effect of maintaining the temperature at 45 °C on the specific activity of the NAD^+ reductase module in the SH for the conversion of NAD^+ to NADH over time, using SH+Hyd1/C in the H-Cube reactor. Under the reaction conditions of NAD^+ (5 mM), Tris-HCl (50 mM, pH 8.0), SH (0.15 mg), Hyd1 (0.15 mg), activated charcoal (20 mg), 45 °C.

The results in Figure 7-14 show that the initial peak specific activity achieved after the activation period was 1.42 U mg^{-1} (40% conversion of NAD^+ to NADH), with a liquid flow rate of 0.1 mL min^{-1} and H_2 flow rate of 1.2 mL min^{-1}. Compared with the initial activity of the SH and Hyd1 at a temperature of 30 °C in Section 7.4.1 of 1.65 U mg^{-1}; that used the same batch of SH; the specific activity is 15% lower. This could be an effect of the increased temperature. Between 200 and 250 min into the experiment the specific activity shows a rapid drop of activity from a 0.88 – 0.5 U mg^{-1}, which could be an effect of the deactivation of the unstable hydrogenase module in the SH. Subsequently the specific activity of the system remains relatively stable between 0.3 – 0.5 U mg^{-1}, over the remaining 1,050 min (17.5 h) reaction time, mimicking the activity of the SH and Hyd1 at a temperature of 30 °C in Section 7.4.1. In total, a TTN of 110,100 for the NAD^+

reductase module in the SH was achieved and the biocatalytic system seemingly could have continued for longer, but limited laboratory time prevented further measurements.

To establish the activity lifetime of the SH+Hyd1/C at 55 °C. A CatCart cartridge loaded with SH batch-56 (0.15 mg) and Hyd1 (0.15 mg) co-immobilised onto activated charcoal (20 mg). The loaded CatCart was tested in the H-Cube reactor for conversion of 5 mM NAD^+, the temperature was maintained at 55 °C throughout. A liquid flow rate of 0.1 mL min^{-1} and a H_2 flow rate of 1.2 mL min^{-1} were used throughout, giving a t_{Res} of 9 s. Data points were collected every 2 - 6 min over 1,161 reactor volumes.

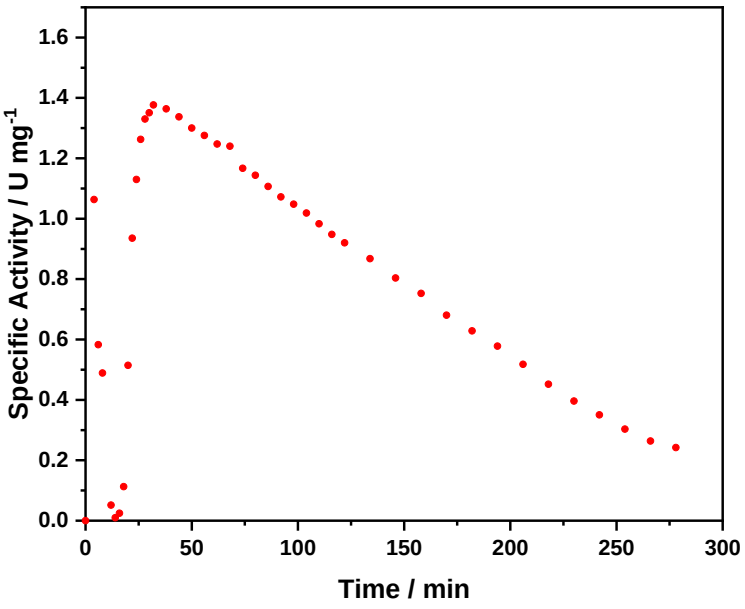


Figure 7-15. The effect of maintaining the temperature at 55 °C on the specific activity of the NAD^+ reductase module in the SH for the conversion of NAD^+ to NADH over time, using SH+Hyd1/C in the H-Cube reactor. Under the reaction conditions of NAD^+ (5 mM), Tris-HCl (50 mM, pH 8.0), SH (0.15 mg), Hyd1 (0.15 mg), activated charcoal (20 mg), 55 °C.

The results in Figure 7-15 show that there is an initial peak specific activity achieved of 1.08 U mg^{-1} (30% conversion of NAD^+ to NADH), in the fraction collected after 4 min,

under a liquid flow rate of 0.3 mL min^{-1} and H_2 flow rate of 1.2 mL min^{-1}. Over the subsequent three fractions, collected every 2 min, the activity of the system drops to zero. At 18 min, the system reactivated, displaying a peak specific activity of 1.37 U mg^{-1} (38.5% conversion of NAD^+ to NADH), before declining over the following 246 min period to 0.24 U mg^{-1}. The deactivation and reactivation of the system is likely because of the Hyd1 activation period. The Hyd1 requires exposure to H_2 for activation before it begins to oxidise the H_2, this had not been done before the reaction for ease of use because previous experiments had shown that it appeared to activate well in-experimental-*situ*. However, the chart indicates that the SH was initially activated before the hydrogenase module of the SH very rapidly deactivated. Leaving a lag period before the Hyd1 was activated and the NAD^+ was converted to NADH again.

The tolerance of the SH and Hyd1 co-immobilised on the activated charcoal displayed in Figure 7-14 and Figure 7-15 to elevated temperatures is useful for when the system is combined with a NADH reducing enzyme and its substrate. It opens up the possibility of increasing the temperature to increase the solubility of a substrate or if using a thermophilic enzyme. Alternatively, if the system were to be coupled with another reaction system, for a cascade synthesis, it allows for broader scope of the reaction conditions.

7.4.3 Stability of SH+Hyd1/C in alternative buffer systems

Potassium phosphate buffer solution (KPB) is a common buffer used for biological experiments in academia and industry. To test the suitability of the buffer using the SH+Hyd1/C, a CatCart cartridge loaded with SH batch-56 (0.15 mg) and Hyd1 (0.15 mg) co-immobilised onto activated charcoal (20 mg) was tested in the H-Cube reactor for conversion of 5 mM NAD^+, in KPB (50 mM, pH 8.0). A range of liquid flow rates

(0.05 – 0.1 mL min^{-1}) and H_2 flow rates (0.6 mL min^{-1}) were used throughout the experiment, giving a t_{Res} of 17 – 18.5 s. The temperature was maintained at 30 °C for the duration.

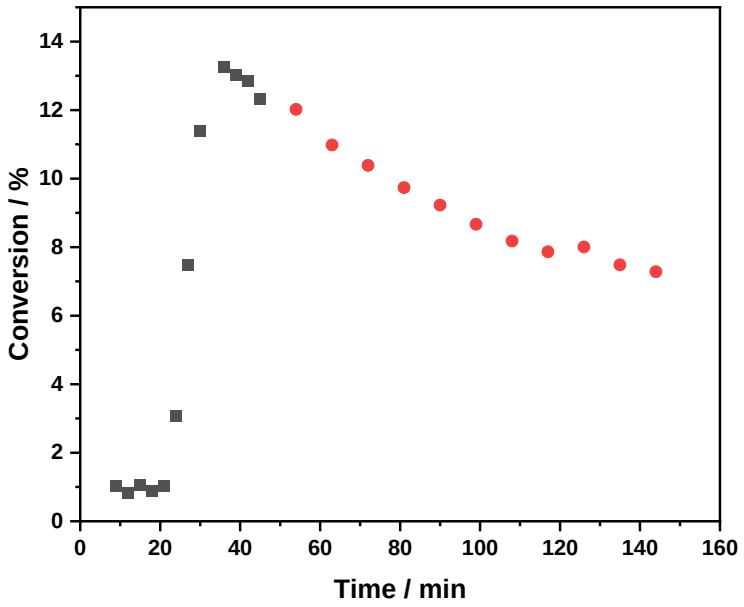


Figure 7-16: The conversion of NAD^+ to NADH over time, using SH+Hyd1/C in the H-Cube reactor. Under the reaction conditions of NAD^+ (5 mM), KPB (50 mM, pH 8.0), SH batch-56 (0.15 mg), Hyd1 (0.15 mg), activated charcoal (35 mg), 30 °C. t_{Res} ■ = 17 s (liquid flow rate = 0.1 mL min^{-1}, H_2 flow rate = 0.6 mL min^{-1}), ● = 18.5 s (liquid flow rate = 0.05 mL min^{-1}, H_2 flow rate = 0.6 mL min^{-1}).

The results in Figure 7-16 show that there was a 20 min lag period before the SH+Hyd1/C began converting the NAD^+ to NADH. This is possibly because the phosphate in the buffer solution inhibits the hydrogenase module in the SH and the initial conversion is seen once the Hyd1 has been activated. The system achieved a 13% conversion of the 5 mM NAD^+ to NADH at its most active, with a specific activity of 0.38 U mg^{-1}. This is significantly lower than the specific activity demonstrated in Tris-HCl buffer previously in this chapter, this overall lack of activity could be caused by the phosphate inhibiting

the enzymes on the carbon. This experiment has shown that PBS is not a suitable buffer system using the cofactor regeneration system moving forward.

7.4.4 Establishing SH and Hyd1 activity when co-immobilised onto alternative carbon types in the H-Cube

The activated charcoal had proven to immobilise the enzymes efficiently and show durability over long reaction periods. Its particle diameter (mm) was sufficient to remain in the CatCart during the flow reactions without leaching. However, the carbon had been found to clump, leading to a build-up of pressure in the reaction system across a longer reaction time. This was acceptable in the H-Cube reactor which can work up to 100 bar, but for translation into other reactor types, would be more problematic. A larger carbon particle, would reduce pressure build-up in a PBR system owing to the extra space around the larger carbon particles, enabling an easier route through the reactor. Here, the SH batch-56 (0.35 mg) and Hyd1 (0.17 mg) were co-immobilised onto a Darco activated carbon (80 mg, >mm diameter), in a CatCart cartridge and were tested in the H-Cube reactor for conversion of 5 mM NAD^+. A liquid flow rate of 0.1 mL min^{-1} and a H_2 flow rate of 1 mL min^{-1} were used throughout the experiment, giving a t_{Res} of 11 s. The temperature was maintained at 30 °C for the duration.

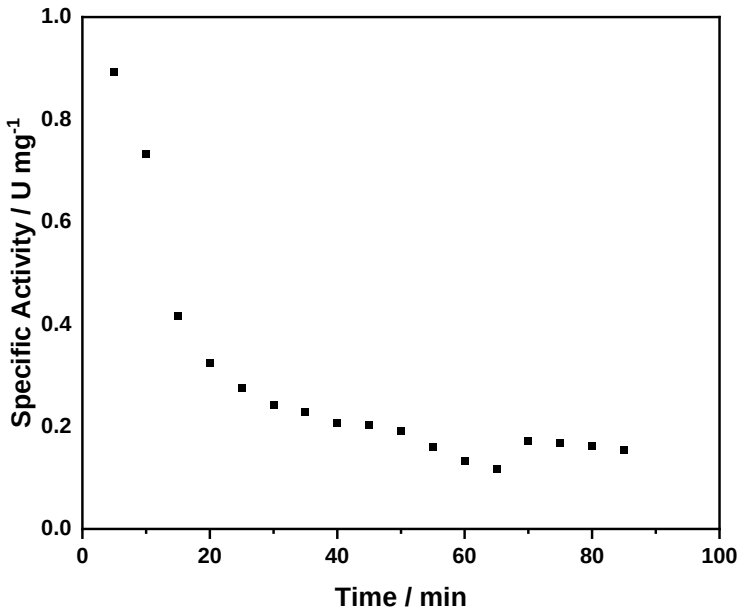
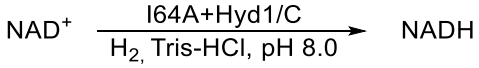


Figure 7-17: The specific activity of SH during the conversion of NAD^+ to NADH over time, using SH and Hyd1 co-immobilised on Darco activated carbon in the H-Cube reactor. Reaction conditions: NAD^+ (5 mM), Tris-HCl (50 mM, pH 8.0), SH (0.35 mg), Hyd1 (0.17 mg), Darco activated carbon (80 mg), 30 °C.

The results in Figure 7-17 show that in the first fraction collected the NAD^+ reductase module of the SH displayed a specific activity of 0.89 U mg^{-1} (62.5% conversion of NAD^+ to NADH). Before its specific activity dropped and steadily declined from 0.27 to 0.15 U mg^{-1} over 330 reactor volumes. The pressure of the system remained <0.5 bar throughout the reaction, showing the benefit of the larger carbon size. The activity of the system exhibited was lower than with the activated charcoal, however, this was a preliminary experiment. The enzyme loading and Darco activated carbon loading would require further optimisation before the two systems could be directly compared. This experiment displays the versatility of the HydRegen system, enabling easy and quick translation onto an alternative carbon support.

7.4.5 Preliminary test of I64A+Hyd1/C in the H-Cube

An alternative formulation of the HydRegen particle system is a combination of I64A (NAD^+ reductase) and Hyd1. The I64A is variant of the SH, with no hydrogenase activity i.e. it can only reduce NAD^+ when supplied with electrons from another source . A preliminary experiment was performed in which I64A (1 mg) and Hyd1 (0.35mg) were co-immobilised onto activated charcoal, in a CatCart cartridge and were tested in the H-Cube reactor for conversion of 5 mM NAD^+.



A liquid flow rate range of $0.02 - 0.1$ mL min^{-1} and a H_2 flow rate range of 0.2 - 1 mL min^{-1} were used in the experiment, giving a t_{Res} range of $12 - 54$ s. The temperature was maintained at 30 °C for the duration.

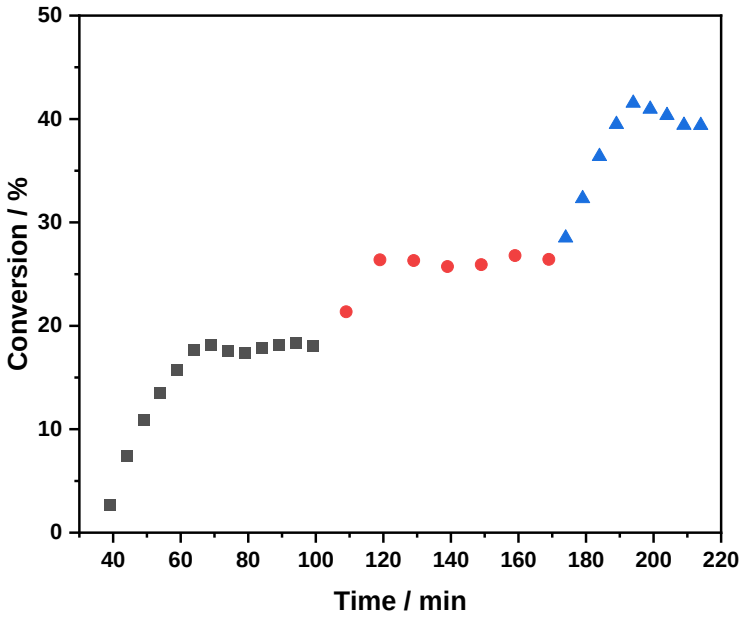


Figure 7-18: The effect of varying the t_{Res} for the conversion of NAD^+ to NADH over time, using I64A+Hyd1/C in the H-Cube reactor. Under the reaction conditions of NAD^+ (5 mM), Tris-HCl (50 mM, pH 8.0), I64A (100 µL), Hyd1 (0.35 mg) activated charcoal (20 mg), 25 °C. t_{Res} ■ = 12 s (liquid flow rate = 0.4 mL min^{-1}, H_2 flow rate = 1.2 mL min^{-1}), ● = 22 s (liquid flow rate = 0.1 mL min^{-1}, H_2 flow rate = 0.4 mL min^{-1}), ▲ = 54 s (liquid flow rate = 0.02 mL min^{-1}, H_2 flow rate = 0.2 mL min^{-1}).

The results in Figure 7-18 show that after a reaction time of 38 min under the initial liquid flow rate of 0.1 mL min^{-1} and H_2 flow rate of 1 mL min^{-1} (black square, t_{Res} = 12 s) the I64A+Hyd1/C began to activate. The system reached a steady-state conversion of 18% (0.15 U mg^{-1}), displaying good stability over a 40 min period (reaction time 59 to 99 min). The system responded linearly to the increase of the t_{Res} to 22 s (red circle, liquid flow rate = 0.05 mL min^{-1}, H_2 flow rate = 0.5 mL min^{-1}) and to 54 s (blue triangle, liquid flow rate = 0.02 mL min^{-1}, H_2 flow rate = 0.2 mL min^{-1}), reaching a steady state conversion of 26% (0.10 U mg^{-1}) and 40% (0.05 U mg^{-1}) respectively. A promising preliminary experiment with the I64A+Hyd1/C system which requires further optimisation.

7.5 Summary

In this chapter, the H-Cube reactor (designed for metal catalysed hydrogenations) has been demonstrated as a viable reactor for H_2-driven heterogeneous biocatalysis. In the H-Cube reactor, the SH/C was shown to achieve good conversions of NAD^+ to NADH at pressures up to 50 bar and flow rates up to 3 mL min^{-1}. The robustness of the biocatalytic system at a reasonably high pressure presents the possibility to perform reaction types such as chemo-bio cascades in the H-Cube reactor. Continuing studies with the H-Cube reactor, the performance of immobilised SH against co-immobilised SH and Hyd1 for cofactor reduction was compared. It was shown that the SH+Hyd1/C system exhibits improved SH productivity, TTN, activity lifetime and resilience at higher temperatures than the immobilised SH alone. This indicates that the Hyd1 is supplementing the NAD^+ reductase module with electrons by conduction through the activated charcoal (behaving in an analogous manner to the HydRegen system with I64A and Hyd1), thus boosting the activity lifetime of the system. At the end of the chapter, a preliminary experiment using the HydRegen system with co-immobilised I64A and Hyd1 onto activated charcoal was demonstrated in the H-Cube reactor, achieving modest results, that were still an improvement on the Vincent group's previous research with the system in continuous flow. In the next chapter, the systems developed here are expanded towards heterogeneous biocatalytic ketone reduction reactions with H_2-driven cofactor recycling in the H-Cube reactor, by the additional immobilisation of a NADH-dependent keto-reductase enzyme.

8 Biocatalytic ketone reductions with H_2-driven cofactor recycling in the H-Cube reactor

8.1 Introduction

The work presented in this Chapter was published in a special issue 'Recent Developments in Process Intensification using Heterogeneous Catalysts in Continuous Flow': Poznansky et al., Front. Chem. Eng., 2021, 3, 35, DOI: 10.3389/fceng.2021.718257

and a ChemRxiv submission 'Accelerating Biocatalytic Hydrogenations using the H-Cube Flow Reactor', B. Poznansky et al, ChemRxiv, DOI: 10.26434/chemrxiv.12532301.v1.

In the previous chapter, a number of biocatalytic systems were developed using heterogeneous H_2-driven cofactor reduction in the H-Cube reactor. It was shown that SH+Hyd1/C outperformed SH/C, in a number of key metrics. These results indicated that the Hyd1 was boosting the activity lifetime of the system, by supplementing the NAD^+ reductase module of the SH with electrons through the activated charcoal. The aim of this chapter was to co-immobilise a NADH-dependent keto-reductase onto the activated charcoal alongside the cofactor reduction enzyme systems to perform biocatalytic ketone reduction reactions with H_2-driven cofactor recycling continuously in the H-Cube reactor. From this it could be distinguished whether the Hyd1 boosting effect is carried forward to cofactor recycling experiments and the cofactor reduction systems could be applied towards the biocatalytic synthesis of more varied products. It was also hypothesised that the presence of a NADH-dependent would further boost the activity of the cofactor reduction enzyme systems by rapidly consuming the NADH and pushing the equilibrium towards the conversion of NAD^+ to NADH.

First of all, the co-immobilisation of lactate dehydrogenase (LDH) onto activated charcoal was studied in the H-Cube reactor, to perform the conversion of pyruvate to lactate with H_2-driven cofactor recycling. This is because in Chapter 3, it was found that LDH showed good activity after immobilisation onto carbon. Furthermore, continuation of the pyruvate to lactate model system would enable direct comparison between the FDH and H_2-driven cofactor recycling systems on carbon. Another aim of studying this transformation was to create a model biocatalytic ketone reduction system that could be applied to any pair of keto-reductase and ketone, in the H-Cube reactor. Next, studies shift to the co-immobilisation of alcohol dehydrogenase 1001 (ADH-1001) for the conversion of ethyl 4-chloroacetoacetate (**11**) to ethyl (S)-4-chloro-3-hydroxybutanoate (**12)**, so that the results can be directly compared to those in Chapter 6.

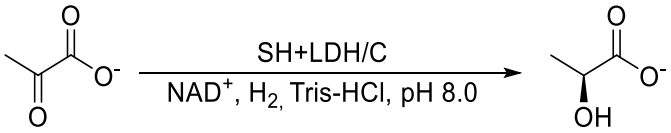
8.2 Biocatalytic conversion of pyruvate to lactate in the H-Cube reactor

The first cofactor-dependent transformation that was targeted in the H-Cube reactor was the conversion of pyruvate to lactate. These results can be directly compared to the FDH and LDH modified carbon catalyst extensively studied in Chapter 3.

8.2.1 Implementation of SH+LDH/C in the H-Cube reactor

To first establish whether a system of SH and LDH co-immobilised onto the activated charcoal (SH+LDH/C) would display activity for the conversion of pyruvate to lactate (Scheme 8-1) a preliminary flow experiment was performed under moderate reaction conditions, in the H-Cube Tutor (H_2 provided by electrolyser at ~7 mL min^{-1}).

Scheme 8-1: NADH-dependent biocatalytic conversion of pyruvate to lactate, employing a SH+LDH/C catalyst, in the H-Cube reactor.



A CatCart cartridge was loaded with SH (1.6 mg) and LDH (3 mg) co-immobilised onto activated charcoal (43 mg). A single liquid feed containing sodium pyruvate (10 mM) and NAD^+ (1 mM) in Tris-HCl buffer (50 mM, pH 8.0) was pumped through the H-Cube reactor. The H_2 flow rate was 7 mL min^{-1} and the liquid flow rate was varied between 0.1, 0.5 or 1 mL min^{-1}, equating to t_{Res} of 1.7 s, 1.6 s or 1.5 s. The temperature was maintained at 25 °C for the duration. During the NAD^+ reduction experiment in Chapter 6, a small amount of NAD^+ in the reaction solution had been found to stick to the activated charcoal at the start of the reactions. For all experiments involving an NADH dependent co-immobilised enzyme, a NAD^+ solution was pumped over the activated charcoal (~1 mg NAD^+ per 3 mg activated charcoal) at the beginning of the reaction, before the reaction solution. To enable immediate system activity upon contact with the substrate.

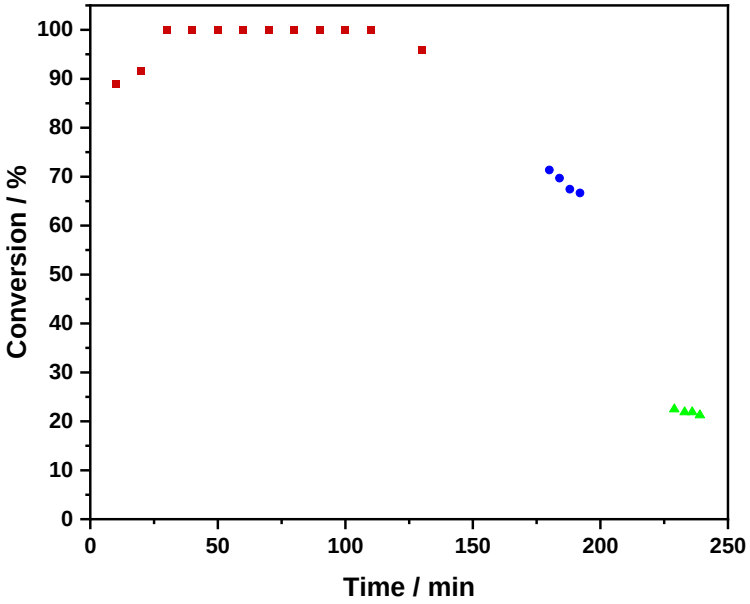


Figure 8-1. Conversion achieved of pyruvate to lactate in continuous flow with SH+LDH/C in a 30 mm CatCart, performed at reaction solution flow rates of 0.1 mL min^{-1} (red), 0.5 mL min^{-1} (blue), 0.1 mL min^{-1} (green). Under the reaction conditions of sodium pyruvate (10 mM), NAD^+ (1 mM), Tris-HCl (50 mM, pH 8), LDH (3 mg), SH (1.6 mg), activated charcoal (40 mg), 25 °C. Reactor Volume = 0.3 mL, H_2 flow rate = ~7 mL min^{-1}.

The results in Figure 8-1 show that a liquid flow rate of 0.1 mL min^{-1} (red squares) resulted in a pyruvate to lactate conversion of >96% over a period of 100 mins. Increasing the flow rate leads to a decrease in conversion, showing that substrate supply is not limiting the reaction. The highest STY of 2.5 $kg_{lactate}$ L^{-1} h^{-1} was achieved at a liquid flow rate of 0.1 mL min^{-1}, this result is two orders of magnitude greater than the STYs achieved with the immobilised FDH regeneration system in Chapter 3. The highest SH specific activity displayed in this experiment was 2.21 U mg^{-1} at a liquid flow rate of 0.5 mL min^{-1} (blue squares) and overall the SH TTN was 43,000. These preliminary results show that the SH+LDH/C system does display activity towards the H_2-driven conversion of pyruvate to lactate. In this experiment, the SH demonstrated similar TTN and specific activity to when it was immobilised for conversion of NAD^+ to NADH. Further

experiments would be required to determine whether the LDH enzyme provides a driving force to these metrics, by its immediate consumption of the NADH synthesised by the SH during the reaction.

8.2.2 Specific activity of SH+LDH/C for the conversion of pyruvate to lactate in the H-Cube

Having shown that the SH+LDH/C system displayed activity for the conversion of pyruvate to lactate in Section 8.2.1, next the focus shifted to determine the peak SH specific activity that could be achieved. To push the SH to its limits, the pyruvate concentration was increased and the SH loading onto the carbon was decreased from the experiment in Section 8.2.1. To add further strain on the SH, the reaction was performed at a higher flow rate of 0.5 mL min^{-1} and the LDH was added in an activity excess, so that it was not limiting the experiment. Overall, a CatCart cartridge was loaded with SH (0.8 mg) and LDH (3 mg) co-immobilised onto activated charcoal (30 mg). A single liquid feed containing sodium pyruvate (20 mM) and NAD^+ (1 mM) in Tris-HCl buffer (50 mM, pH 8.0) was pumped through the H-Cube reactor. The H_2 flow rate was 7 mL min^{-1} and the liquid flow rate was set to 0.5 mL min^{-1}, equating to t_{Res} of 1.6 s. The temperature was maintained at 25 °C for the duration. Fractions were collected every 3 min (113 reactor volumes), however, some fractions were collated before analysis by NMR.

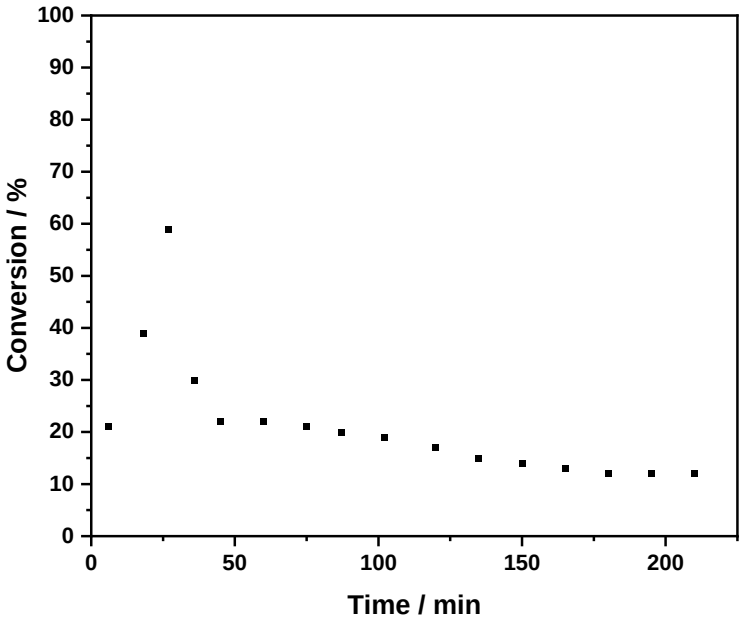


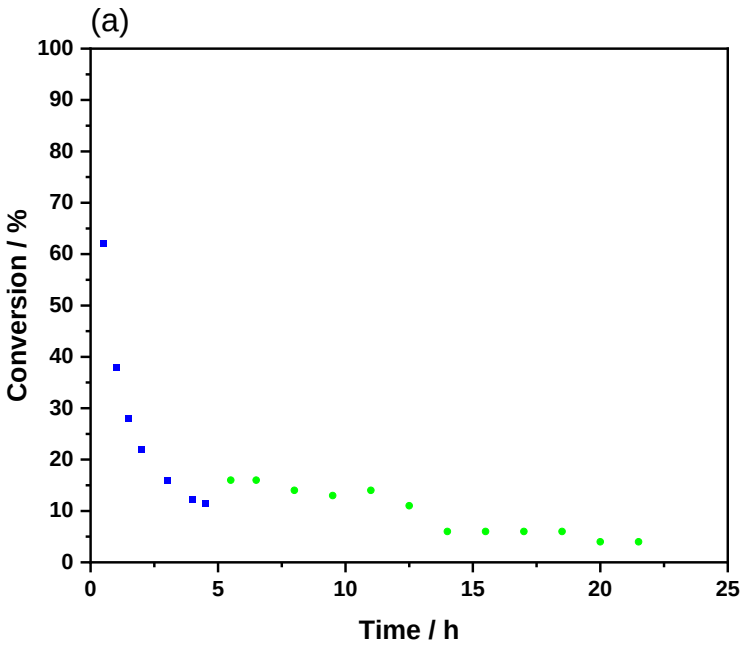
Figure 8-2: Conversion achieved of pyruvate to lactate in continuous flow with SH+LDH/C in a 30 mm CatCart, performed at reaction solution flow rate of 0.5 mL min^{-1}. Under the reaction conditions of sodium pyruvate (20 mM), NAD^+ (1 mM), Tris-HCl (50 mM, pH 8), LDH (3 mg), SH (0.8 mg), activated charcoal (30 mg), 25 °C. Reactor Volume = 0.3 mL, H_2 flow rate = ~7 mL min^{-1}, t_{Res} = 1.7 s, liquid flow rate 0.5 mL min^{-1}.

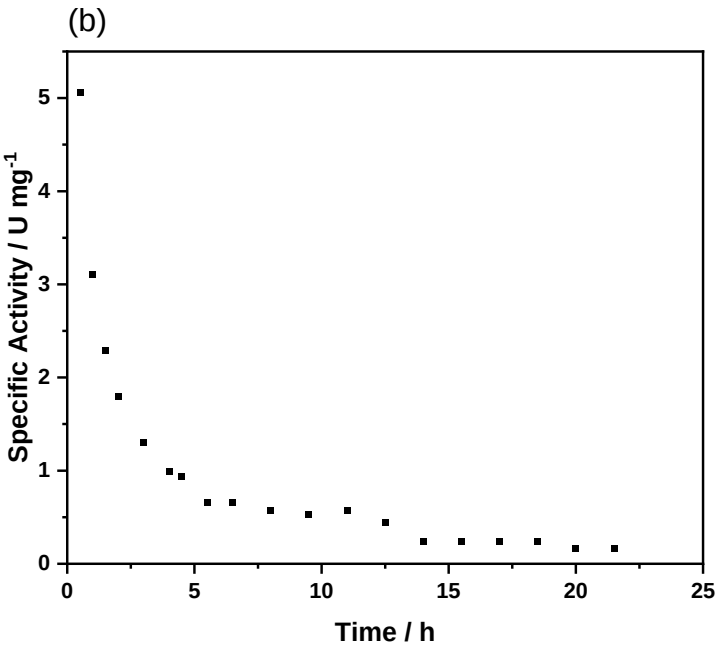
The results in Figure 8-2 show that a 59% peak conversion of pyruvate to lactate was achieved after 24 min. The conversion then dropped to 22% after 45 min, before slowly falling to 12% over the following 165 min of the reaction. At the peak conversion, the SH achieved a specific activity of 8.4 U mg^{-1}. This compares favourably to the performance of the SH demonstrated in the previous chapter for the conversion of NAD^+ to NADH (peak specific activity achieved of 2.6 U mg^{-1}). This indicates that the co-immobilised LDH does act as a driving force for SH activity, by consuming the NADH in the system. This means that the SH is not limited by NAD^+ availability or inhibited by the NADH, forcing it to perform at its limits. Over 210 min, a TTN of 98,000 for the cofactor recycling system with a peak TOF of 1420 min^{-1} (85,200 h^{-1}), this is at the top

end of typical rates achieved for the metal-catalysed transfer hydrogenation of ketones ($10^2 – 10^5$ h^{-1}).[112]

8.2.3 Activity lifetime of SH+LDH/C for the conversion of pyruvate to lactate in the H-Cube

After establishing the peak activity of the system under highly strained reaction conditions over short periods of time, focus shifted to the lifetime of the SH and LDH modified activated charcoal. A lifetime experiment was performed at strained conditions for the SH and the reaction was analysed until the system showed a clear depreciation of activity. Once again, the LDH was added in excess, so that its potential activity was beyond SH, enabling the cofactor regeneration system to be the focus of the studies. The SH loading for the experiment was decreased to the same amount as for the SH lifetime experiment for NAD^+ to NADH conversion in Section 7.3.6. The H_2 was supplied by a pump from a cylinder for this experiment, to enable stricter control of the reaction conditions and direct comparison to Section 7.3.6. A CatCart cartridge was loaded with SH batch-56 (0.25 mg) and LDH (3 mg) co-immobilised onto activated charcoal (30 mg). A single liquid feed containing sodium pyruvate (20 mM) and NAD^+ (1 mM) in Tris-HCl buffer (50 mM, pH 8.0) was pumped through the H-Cube reactor. The H_2 flow rate was varied from 0.6 – 1.2 mL min^{-1} and the liquid flow rate was varied from 0.05 – 0.1 mL min^{-1}, equating to a t_{Res} range of 9 – 18 s. The temperature was maintained at 30 °C for the duration. Fractions were collected every 30 – 60 min.


(a)
Conversion / %
Time / h
0
10
20
30
40
50
60
70
80
90
100
0
5
10
15
20
25


(b)
Specific Activity / U mg-1
Time / h
0
1
2
3
4
5
0
5
10
15
20
25

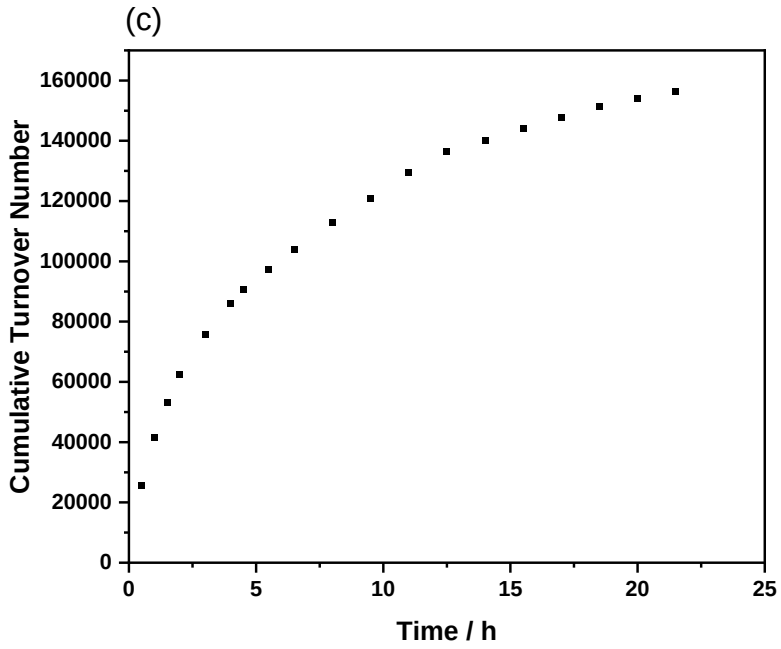


Figure 8-3. Extended run of SH+LDH/C in the H-Cube flow reactor to monitor the deactivation of the catalytic system under strain, for the conversion of pyruvate to lactate. (a) Conversion of pyruvate to lactate over time. t_{Res} ■ = 9 s (liquid flow rate = 0.1 mL min^{-1}, H_2 flow rate = 1.2 mL min^{-1}), ● = 18 s (liquid flow rate = 0.05 mL min^{-1}, H_2 flow rate = 0.6 mL min^{-1}). (b) Specific activity of the immobilised SH over time. (c) Cumulative turnover number of the immobilised SH over time. Under the reaction conditions of sodium pyruvate (20 mM) NAD^+ (1 mM), Tris-HCl (50 mM, pH 8.0), SH (0.25 mg), LDH (3 mg), activated charcoal (30 mg), 30 °C.

The results in Figure 8-3(a) show that the conversion of pyruvate to lactate peaked at 62%, with a liquid flow rate of 0.1 mL min^{-1} and H_2 flow rate of 1.2 mL min^{-1} (t_{Res} = 9 s, blue squares). The conversion steadily declines over the subsequent 4.5 h, under these conditions, to 11.5%. Owing to the relatively low conversion at that point, the liquid flow rate and H_2 flow rate were adjusted to 0.05 mL min^{-1} and 0.6 mL min^{-1} respectively (t_{Res} = 18 s, green circles) to decrease the reaction waste. The longer t_{Res}, the conversion increased to 16.5% and over the following 16 h it decreased to 4%. At this point the reaction was stopped due to availability of laboratory time. Alongside the conversion of pyruvate to lactate of the flow system over time, Figure 8-3(b) shows that the specific

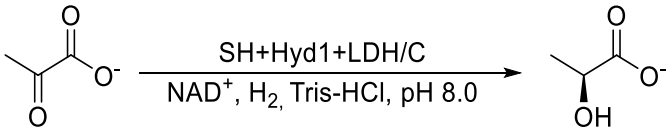
activity of the SH/C maintains a peak performance of >1.3 U mg^{-1}, for the opening 3 h of the experiment, a period three times longer than when the SH was immobilised alone on the activated charcoal in Section 7.3.6. The highest specific activity of the SH (batch-56) immobilised onto the carbon achieved was 5.1 U mg^{-1} after 30 min. In Figure 8-3(c) the cumulative turnover number of the immobilised SH is shown to reach 156,500 over the whole experiment, displaying a maximum TOF of 860 min^{-1} and an average TOF of 121 min^{-1} over the 21.5 h experiment. With the LDH, an NADH dependent enzyme increasing the driving force of the reaction, the metrics exceed the TTN (10,260) and peak TOF (77 min^{-1}) achieved for the SH when immobilised alongside NADH-dependent enzymes on the carbon nanotubes in flow.[260] In total 25 mg NADH was synthesised, corresponding to a reaction productivity of 102 $g_{lactate}\ g_{SH}^{-1}$ and a peak STY of 0.56 kg $L^{-1}\ h^{-1}$.

When compared directly to the results in Section 7.3.6, the SH+LDH/C has displayed a greater TTN, TOF, STY and productivity, over a much-extended period of time. It was next important to see whether the addition of Hyd1 to activated charcoal would show a similar boost as seen in Section 7.4.1

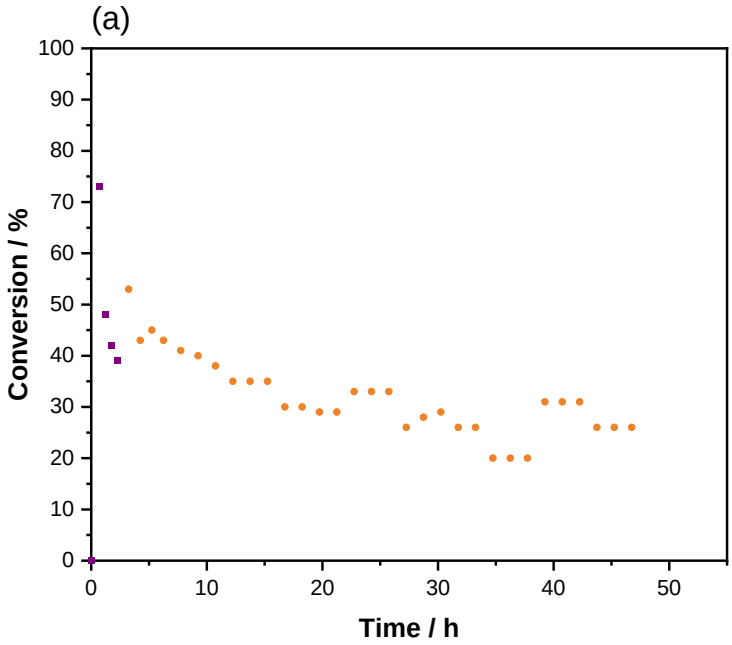
8.2.4 Activity lifetime of SH+Hyd1+LDH/C for the conversion of pyruvate to lactate in the H-Cube

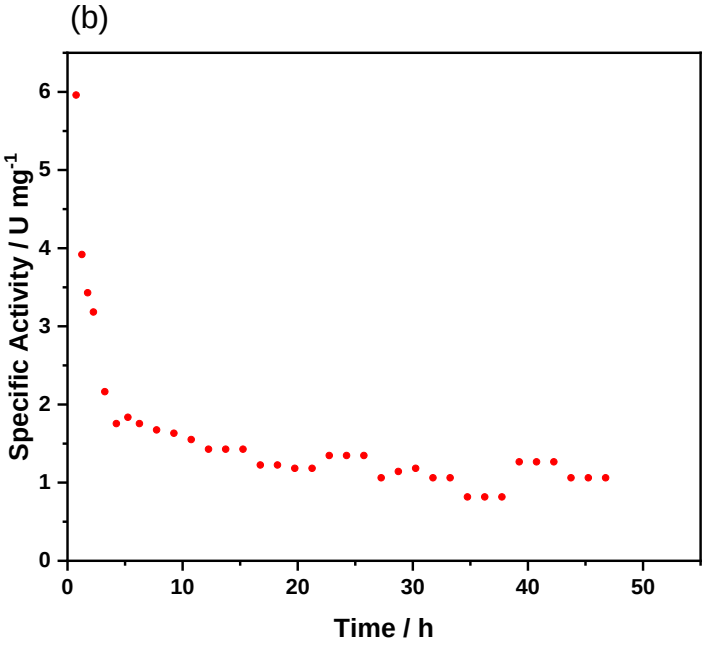
It was shown in the previous chapter that the addition of Hyd1 to the activated charcoal with the SH, boosted the activity lifetime of the SH by four-fold, for the conversion of NAD^+ to NADH. To establish whether the addition of the Hyd1 alongside the SH and LDH (SH+Hyd1+LDH/C) would have an effect on the system, for conversion of pyruvate to lactate (Scheme 8-2). A lifetime experiment was performed with near-identical conditions to the SH and LDH lifetime experiment performed in 8.2.3, in the H-Cube.

Scheme 8-2: NADH-dependent biocatalytic conversion of pyruvate to lactate, employing a SH+Hyd1+LDH/C catalyst, in the H-Cube reactor.



The H_2 was again supplied by a pump from a cylinder for this experiment, to enable stricter control of the reaction conditions and direct comparison to previous system lifetime experiments. A CatCart cartridge was loaded with SH batch-56 (0.25 mg), Hyd1 (0.18 mg) and LDH (3 mg) co-immobilised onto activated charcoal (30 mg). A single liquid feed containing sodium pyruvate (20 mM) and NAD^+ (1 mM) in Tris-HCl buffer was pumped through the H-Cube reactor. The H_2 flow rate was varied from 0.6 – 1.2 mL min^{-1} and the liquid flow rate was varied from 0.05 – 0.1 mL min^{-1}, equating to t_{Res} range of 9 – 18 s. The temperature was maintained at 30 °C for the duration. Fractions were collected every 30 – 60 min, however, some fractions were collated before analysis by NMR.


(a)
Conversion / %
Time / h
0
10
20
30
40
50
60
70
80
90
100


(b)
Specific Activity / U mg-1
Time / h
0
1
2
3
4
5
6
10
20
30
40
50

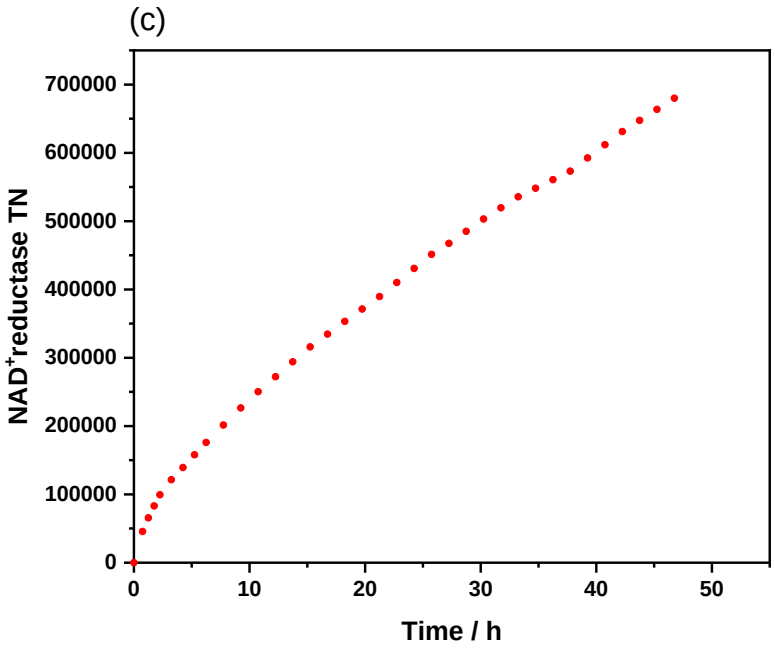


Figure 8-4. Extended run of SH+Hyd1+LDH/C in the H-Cube flow reactor to monitor the deactivation of the catalytic system under strain, for the conversion of pyruvate to lactate. (a) Conversion of pyruvate to lactate over time. t_{Res} ■ = 9 s (liquid flow rate = 0.1 mL min^{-1}, H_2 flow rate = 1.2 mL min^{-1}), ● = 18 s (liquid flow rate = 0.05 mL min^{-1}, H_2 flow rate = 0.6 mL min^{-1}). (b) Specific activity of the NAD^+ reductase module in the SH over time. (c) Cumulative turnover of the NAD^+ reductase module in the SH over time. Under the reaction conditions of sodium pyruvate (20 mM) NAD^+ (1 mM), Tris-HCl (50 mM, pH 8.0), SH (0.25 mg), Hyd1 (0.18 mg) LDH (3 mg), activated charcoal (30 mg), 30 °C.

The results in Figure 8-4(a) show that the conversion of 20 mM pyruvate to lactate peaked at 73% with the liquid flow rate at 0.1 mL min^{-1} and the H_2 flow rate at 1.2 mL min^{-1} (t_{Res} = 9 s). Under the same conditions, the conversion declines over the subsequent 90 min to 39%. The reaction was left overnight; to decrease reagent waste the liquid flow rate was changed to 0.05 mL min^{-1} and the H_2 flow rate to 0.6 mL min^{-1} (t_{Res} = 18 s). At the increased residence time, the conversion increased to 53%. The conversion steadily declined to 26% over the subsequent 43.5 h. Slight fluctuations in the conversion were throughout the final 30 h of the experiment, which can be explained by the subtle differences in reaction solution concentrations, as more fresh reaction solutions had to be

prepared than anticipated. In general, the system appeared to remain stable at 22-30% conversion for the final 33 h of the experiment. Owing to time restraints in the laboratory, the reaction was ended after 48.5 h, however, the chart indicates that the system might have remained active for a longer period of time. Along with the conversion of pyruvate to lactate over time, Figure 8-4(b) shows that the specific activity of the NAD^+ reductase module of the SH/C maintains a performance of >1 U mg^{-1}, throughout the experiment. The highest specific activity of the SH (batch-56) immobilised onto the carbon recorded was 5.95 U mg^{-1}. In Figure 8-4(c) the cumulative turnover number of the immobilised SH batch-56 is shown to reach 679,900 over the experiment, displaying a maximum TOF of 1,013 min^{-1}. A total 108 mg lactate was synthesised, corresponding to a reaction productivity of 444 $g_{lactate}$ g_{SH}^{-1}. These metrics would have improved further if the experiment had been able to run for longer.

Table 8-1: Comparison of lifetime experiments performed with the immobilised SH+LDH system against the immobilised SH+Hyd1+LDH system for conversion of NAD^+ to NADH

Figure	Enzyme(s)	Reactor Volumes	Peak specific activity[a] / U mg^{-1}	Final specific activity[a] / U mg^{-1}	SH productivity / $g_{lactate}$ g_{SH}^{-1}	SH TTN[a]
Figure 8-3	SH+LDH	5070	5.06	0.16	102	156500
Figure 8-4	SH, Hyd1 & LDH	9555	5.95	1.06	444	679900

[a]NAD^+ reductase module of the SH

In comparison to the lifetime experiment of SH+LDH/C performed in Section 8.2.3, the SH+Hyd1+LDH/C has displayed a far longer enzyme activity period >1 U mg^{-1} (SH+ LDH/C = 3 h, SH+Hyd1+LDH/C = 26 h). The SH+Hyd1+LDH/C also exhibited an increase TTN (SH and Hyd1= 156,497; SH, Hyd1 and LDH = 679,900). This confirms

that the Hyd1 is supplementing the NAD^+ reductase module with electrons by conduction through the activated charcoal, thereby boosting the activity lifetime of the system.

8.2.5 Closed loop, multi pass continuous flow with SH+Hyd1+LDH/C for the conversion of pyruvate to lactate in the H-Cube

After assessing and comparing different combinations of the H_2-driven system in the H-Cube, it was clear that the SH+Hyd1+LDH/C was performing very well with respect to activity lifetime and TTN. This could be a benefit of the increased H_2 availability, high enzyme-to-substrate ratio, and short t_{Res} in the H-Cube. If the conversions of the system were to be improved, an option would be to increase the catalyst bed volume, however, this would present a requirement for increased enzyme loadings, and currently the SH and Hyd1 are both produced at laboratory scale. Therefore, a closed loop reactor set-up was explored in which the reaction solution is recirculated through the hydrogenation flow reactor over multiple passes, from a single reaction solution vessel. The conversion of the reaction solution as a whole was then measured periodically over time, by aliquoting samples from the reaction solution vessel. This system offers the benefits of flow in the H-Cube, such as increased H_2 availability and higher catalyst to substrate ratio, as well as a path towards achieving higher conversions.

To establish whether the closed loop, multi-pass continuous hydrogenation system would work well, the reaction conditions were intensified to perform a gram scale transformation of pyruvate to lactate. A CatCart cartridge was loaded with SH batch-56 (1.26 mg), Hyd1 (0.9 mg) and LDH (5 mg) immobilised onto activated charcoal (60 mg). A 100 mL reaction solution containing sodium pyruvate (92 mM) and NAD^+ (1.7 mM) in Tris-HCl buffer was pumped through the H-Cube Pro reactor at 0.5 mL min^{-1}, with the H_2 switched on from the H-Cube electrolyser and fixed at ~12 mL min^{-1}. This equates

to a t_{Res} of 1 s. The temperature was maintained at 30 °C for the duration. The reaction solution was continuously recirculated through the reactor and analysed regularly for conversion.

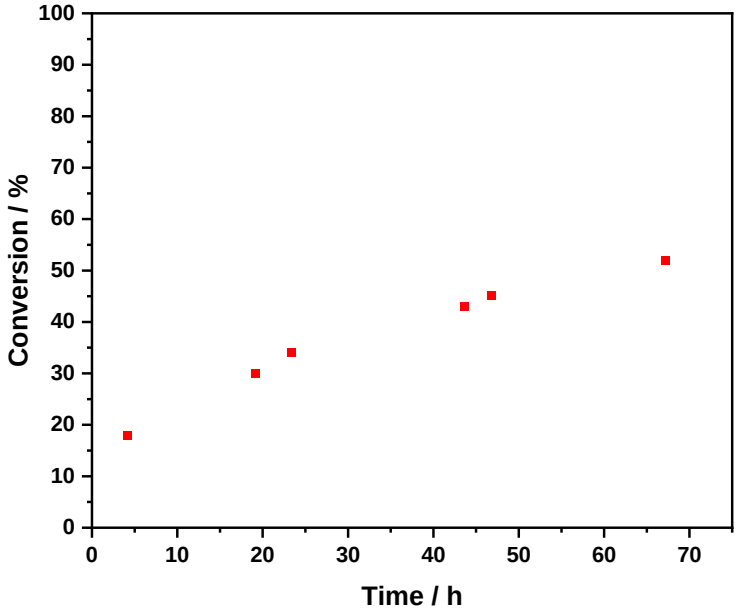


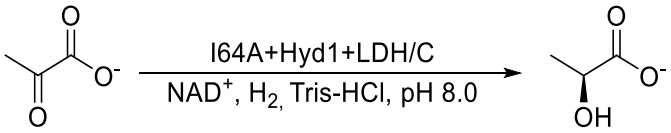
Figure 8-5: Attempted scale-up for H_2-driven biocatalytic conversion of pyruvate to lactate under semi-continuous flow conditions. A 100 mL solution of pyruvate and NAD^+ was repeatedly cycled through the H-Cube containing a 30 mm CatCart loaded with SH+Hyd1+LDH/C. The reaction solution conversion was monitored over time. Under the reaction conditions of sodium pyruvate (92 mM) NAD^+ (1.7 mM), Tris-HCl (50 mM, pH 8.0), SH (1.26 mg), Hyd1 (0.9 mg) LDH (5 mg), activated charcoal (60 mg), 30 °C, liquid flow rate = 0.5 mL min^{-1}, H_2 flow rate = ~12 mL min^{-1}.

The results in Figure 8-5 show that a 52% conversion of pyruvate to lactate was achieved, equating to 0.53 g of lactate. The highest specific activity of the NAD^+ reductase module on the SH was recorded at the first time point of 6.24 U mg^{-1} (TOF = 1061 min^{-1}). Overall an SH TTN of 766,133 was achieved. To increase the conversion of the reaction further, the catalyst loading could be increased by using a larger sized CatCart column.

8.2.6 Preliminary test of I64A+Hyd1+LDH/C for the conversion of pyruvate to lactate in the H-Cube

In Section 7.4.5, the I64A (NAD^+ reductase) and Hyd1 were combined to perform cofactor regeneration. Here, a preliminary experiment was performed to see whether the addition of an NADH dependent enzyme would boost the activity of the system in flow. The I64A (1 mg), Hyd1 (0.6mg) and LDH (2 mg) were co-immobilised onto activated charcoal in a CatCart cartridge and were tested in the H-Cube reactor for conversion of 20 mM pyruvate to lactate (Scheme 8-3).

Scheme 8-3: NADH-dependent biocatalytic conversion of pyruvate to lactate, employing a I64A+Hyd1+LDH/C catalyst, in the H-Cube reactor.



A liquid flow rate 0.1 mL min^{-1} and a H_2 flow rate 1 mL min^{-1} were used in the experiment, giving a t_{Res} of 11 s. The temperature was maintained at 30 °C for the duration. Each data point was collected every 10 – 60 min. Some product fractions were collated before analysis.

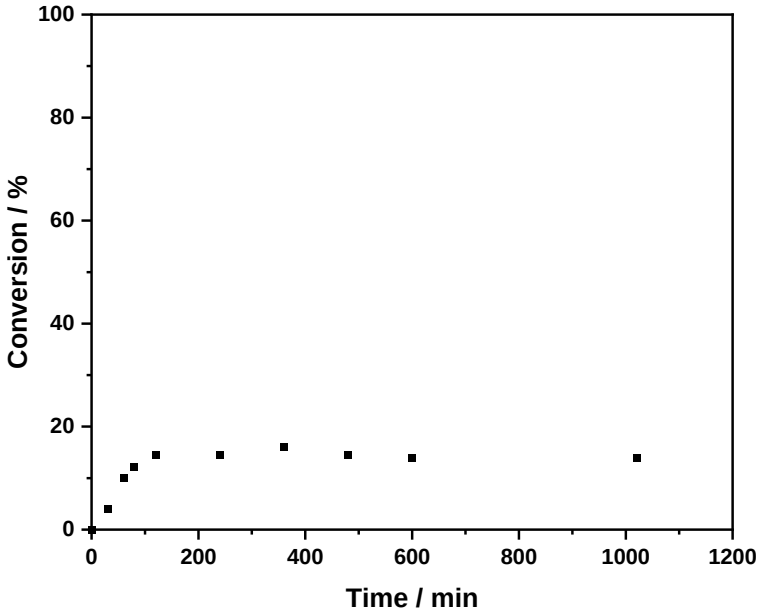


Figure 8-6: Conversion achieved of pyruvate to lactate in continuous flow with I64A+Hyd1+LDH/C in a 30 mm CatCart, performed at reaction solution flow rate of 0.1 mL min^{-1} Under the reaction conditions of sodium pyruvate (20 mM), NAD^+ (1 mM), Tris-HCl (50 mM, pH 8), I64A (1 mg), Hyd1 (0.6 mg), LDH (2 mg), activated charcoal (35 mg), 25 °C. Reactor Volume = 0.3 mL, liquid flow rate = 0.1 mL min^{-1}, H_2 flow rate = 1 mL min^{-1}, t_{Res} = 1.7 s,

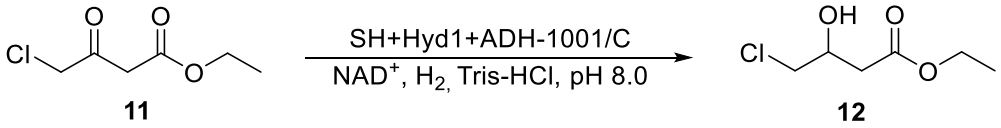
The results in Figure 8-6 show that after a reaction time of 120 min under the initial liquid flow rate of 0.1 mL min^{-1} and H_2 flow rate of 1 mL min^{-1} the I64A+Hyd1+LDH/C reached a steady state conversion of 14.5% pyruvate to lactate, following an activation period, typical to what had been seen with the I64A and Hyd1 in Section 7.4.5. The system remained at a steady state for 900 min, demonstrating an I64A specific activity of 0.16 U mg^{-1} and TTN of 8,100.

8.3 Biocatalytic ketone reduction of ethyl 4-chloroacetoacetate with H_2-driven cofactor recycling by ADH-1001 in the H-Cube

In this section, the transformation of **11** to **12**, which had previously been studied with substrate-coupled cofactor recycling in Chapter 5, was investigated in the H-Cube reactor with H_2-driven cofactor recycling (Scheme 8-4). The system was studied with the SH,

Hyd1 and ADH-1001 co-immobilised onto activated charcoal (SH+Hyd1+ADH-1001/C). This would enable further comparison with the substrate-coupled recycling approach developed in Chapter 5.

Scheme 8-4: NADH-dependent biocatalytic conversion of **11** to **12**, employing a SH+Hyd1+ADH-1001/C catalyst, in the H-Cube reactor.



To establish whether the SH+Hyd1+ADH-1001/C system would display activity for the conversion of **11** to **12** a flow experiment was performed in the H-Cube reactor. A CatCart cartridge was loaded with SH batch-56 (0.28 mg), Hyd1 (0.2 mg) and ADH-1001 (6.5 mg) co-immobilised onto activated charcoal (40 mg). A single liquid feed containing **11** (30 mM), NAD^+ (1 mM) and DMSO (3 v/v%) in Tris-HCl buffer was pumped through the H-Cube reactor. The H_2 flow rate was 0.6 mL min^{-1} and the liquid flow rate was 0.05 mL min^{-1}, equating to t_{Res} of 18 s. The temperature was maintained at 30 °C for the duration. The total reaction solution volume was 20 mL. Fractions were collected every 20 min, until one full pass of the reaction solution over the PBR had been achieved (Figure 8-7(a)). After this point, the fractions were combined and recirculated through the system in the manner of the closed loop set-up developed in Section 8.2.5. The conversion of the reaction solution was monitored once after being combined and then after 20 h, 24 h and 48 h (Figure 8-7(b)). The conversion was monitored by using GC.

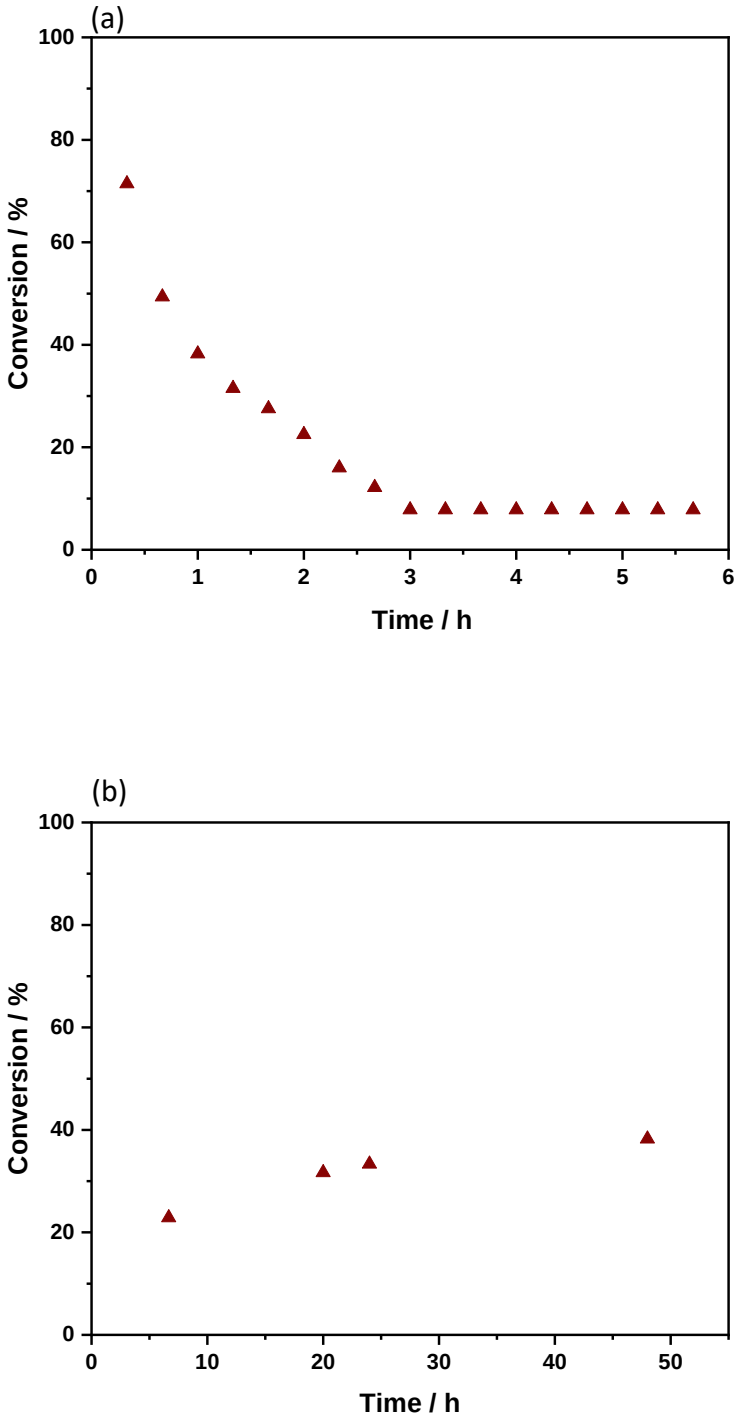


Figure 8-7: SH+Hyd1+ADH-1001/C in the H-Cube flow reactor for the conversion of **11** to **12**. (a) Conversion of each fraction collected every 20 min, during the first full pass of reaction solution b) Conversion over time of reaction solution in the closed-loop multi-pass system. Performed under the reaction conditions of ethyl 4-chloroacetoacetate (30 mM) NAD^+ (1 mM), DMSO (3 v/v%), Tris-HCl (50 mM, pH 8.0), SH (0.28 mg), Hyd1 (0.120 mg), ADH-1001 (6.5 mg), activated charcoal (40 mg), 30 °C.

The results in Figure 8-7(a), which displays the conversion of the fractions collected during the first reaction solution pass, show that the system achieved an initial 71% conversion of **11** to **12**, with the NAD^+ reductase module of the SH operating at a specific activity of 3.8 U mg^{-1}. The conversion steadily drops over 3 h to a steady-state of 8%, operating at a specific activity of 0.4 U mg^{-1}. It is possible that the presence of DMSO (3 v/v%) in the reaction solution had a deactivating effect on the SH and Hyd1. The results in Figure 8-7(b) show that after the fractions were combined and recirculated through the reactor in the closed-loop set-up, a 38% conversion was achieved at 48 h. The catalyst appears to remain active throughout the 48 h experiment, with the NAD^+ reductase module of the SH achieving a TTN of 138,400 and a productivity of 135 $g_{product}\ g_{SH}^{-1}$. This process demonstrated the potential of the SH+Hyd1+ADH-1001/C for the continuous production of chiral pharmaceutical compounds with H_2-driven cofactor recycling in the H-Cube reactor.

8.4 Summary

In this chapter, the H_2-driven carbon-supported biocatalyst developed in Chapter 7 for NAD^+ reduction in the H-Cube hydrogenation reactor was successfully applied to ketone reduction reactions with H_2-driven cofactor recycling by the addition of a keto-reductase enzyme to the carbon-supported biocatalyst.

The SH+Hyd1+LDH/C catalyst displayed a peak SH specific activity of 5.95 U mg^{-1}, a productivity of 444 $g_{lactate}\ g_{SH}^{-1}$ and a SH TTN of 679,900. This system outperformed the SH+LDH/C and also demonstrated greatly improved metrics against the SH+Hyd1/C for NAD^+ reduction owing to the increased driving force from the NADH-dependent LDH.

Intensification of the system in a closed loop, multi-pass flow set-up with SH+Hyd1+LDH/C gave 0.5 g product using the model pyruvate to lactate reaction.

The potential of this H_2-driven H-Cube set-up was demonstrated for the continuous production of pharmaceutical compounds when the SH, Hyd1 and ADH-1001 were co-immobilised onto activated charcoal achieved conversion of **11** to **12**.

Overall H_2-powered biocatalysis performed in the H-Cube reactor, using simply-prepared enzyme-modified activated charcoal catalyst CatCart cartridges, is shown to give comparable catalyst TOF to supported metal transfer hydrogenation catalyst columns.[112] The immobilisation of the biocatalysts onto a commercial carbon support used in a commercial hydrogenation flow reactors illustrates how this clean H_2-driven biocatalytic set-up could be slotted into existing reactor infrastructure. Furthermore, a wide-range of keto-reductase enzymes are commercially available for catalysis of a multitude of different ketone reductions, which could be applied to the system developed here, thereby simplifying the adoption of NADH-dependent biocatalysis for asymmetric synthesis in flow.

9 Summary and Comparison

In this Thesis, carbon particles have been used as a simple and widely available biocatalyst support for performing continuous flow biocatalytic ketone reductions with cofactor recycling in a PBR. Two traditional cofactor recycling systems (FDH–formate and ADH–IPA) were developed and translated into flow, highlighting the ease of transferring reactions from batch to flow biocatalysis without having to change the cofactor recycling system. The benefits of these continuous flow systems included improved an *E* factor and STY over their batch counterparts, and taking away the requirement for an enzyme separation step. Next, carbon-supported H_2-driven biocatalysis systems (such as HydRegen) were translated into a commercial hydrogenation flow reactor (H-Cube). The system developed displayed a range of benefits compared with the existing enzymatic approaches, including a higher STY and TTN, and a lower *E* factor. The H_2-driven flow system also demonstrated a similar TOF to a metal hydrogenation system.

In Chapter 3 carbon particles were applied as a biocatalyst support for the enzymes FDH and LDH, for the continuous conversion of pyruvate to lactate in a continuous PBR with FDH–formate cofactor recycling. Optimisation studies were carried out for conversion, STY and *E* factor, and the system was shown to operate at high conversion over a >30 h period. In Chapter 4, the immobilised FDH–formate cofactor recycling flow system presented in Chapter 3 was extended by co-immobilising a suite of different NADH-dependent enzymes onto the carbon particles alongside the FDH for the synthesis of industrially relevant molecules in continuous flow.

In Chapter 5, carbon particles were applied as a biocatalyst support for ADH-101 and ADH-105 for continuous ketone reduction in a continuous PBR with substrate-coupled IPA-driven cofactor recycling. The systems were first studied in batch, comparing the performance of immobilised ADH against ADH free in solution, before being translated into flow. The two systems achieved low conversions of their target substrates in continuous flow, probably because of a poor retention of enzyme activity after immobilisation, and future studies could look to elucidate why this is occurring. In Chapter 6, the substrate-coupled IPA-driven cofactor recycling investigated by the immobilisation of ADH-1001 onto activated charcoal for the continuous synthesis of a molecule relevant to the industrial partner. The system achieved high steady-state conversion of up to 100 mM substrate and achieved a cofactor turnover number of 1,000 in a t_{Res} of 12 min. Furthermore, an exciting real-time analysis approach was examined using in-line benchtop flow NMR to determine the conversion of each reactor volume.

Chapters 7 and 8 translated the H_2-driven cofactor recycling system into a commercially available hydrogenation flow reactor called the H-Cube. Initial studies focused on performing the conversion of NAD^+ to NADH to help to determine the stability of the cofactor regeneration technique in continuous flow. These studies discovered that SH+Hyd1 that was immobilised onto activated charcoal showed improved stability over the SH immobilised onto activated charcoal. Subsequently, the immobilised SH+Hyd1 H_2-driven system was demonstrated for ketone reduction by the co-immobilisation of an NADH-dependent enzyme (LDH) alongside the cofactor-recycling enzyme(s) onto a carbon particle support. Here, the NAD^+ reductase module of the SH exhibited a TTN of 766,100 over a 67 h operational period. Finally, the system was extended towards the synthesis of an industrially relevant molecule.

This chapter compares the TOF, TTN, STY and *E* factor of the three systems developed in this Thesis with a selection of systems described in the literature that use common industry cofactor recycling techniques in batch and continuous flow, and also with H_2-driven cofactor recycling in batch (Table 9-1).

Entry 1 was discussed in Section 1.4 as a way of using GDH–glucose cofactor recycling alongside KRED-101 to generate a chemokine receptor inhibitor precursor in batch. Entry 2 was discussed in Section 1.9.1 as a way of generating secondary aryl amines with an immobilised GDH and reductive amininase. Entry 3 was discussed in Section 1.9.2 as a way of generating a chiral amine with an immobilised FDH and amine dehydrogenase in continuous flow. Entry 4 was discussed in Section 1.9.3 as a way of generating (*R*)-phenylethanol with an immobilised ADH (substrate-coupled cofactor recycling) in continuous flow. Entry 5 is the case of using the HydRegen H_2-driven cofactor recycling system in batch, discussed in Section 1.5. Entries 6, 7 and 8 are results from the three systems developed in this Thesis. All metrics in the table were calculated using data from the available literature. Missing data points occurred in cases without sufficient data available to make the calculation.

Table 9-1: Comparison of the biocatalytic cofactor regeneration characteristics of selected literature biosynthesis systems with the continuous flow systems developed in this Thesis.

Entry	System	Duration / h	TOF / min^{-1}	TTN	STY / $g\ L^{-1}\ h^{-1}$	*E* factor
1	GDH in batch[187]	4.6	186	285 800	11	6
2	GDH in flow[227]	132	-	-	103	-
3	FDH in flow[230]	6	-	-	24	-
4	ADH in flow[234]	32	10	12 000	117	5.8
5	HydRegen in batch	21.5	84.6	135 000	1.34	2
6	This work (Chapter 3 and 4)	35	2.1	4 490	22.9	2.5
7	This work (Chapter 6)	32	10	12 000	83	4.5
8	This work (Chapter 7 and 8)	48	236	679 900	2500	0.9

The work in this Thesis in Chapters 3 and 4 (entry 6), in which FDH–formate cofactor recycling was implemented in continuous flow, showed similar STY values compared to the FDH–formate flow system in entry 3, indicating that the activity of FDH was a limitation of both systems. However, the work in Chapters 3 and 4 demonstrates an almost sixfold longer run-time in continuous flow, highlighting its improved stability over entry 3. Furthermore, entry 3 used 10 equivalents of formate versus 3–5 equivalents in entry 6, leading to much lower carbon-based waste generation for the latter. When entry 6 is compared to the GDH in batch (entry 1) and flow (entry 2), it is clear that the GDH–glucose cofactor recycling system has the ability to outperform the FDH–formate flow system with respect to TTN and STY. However, this could be expected based on the high known activity of GDH compared to FDH, and a major benefit of FDH–formate

cofactor recycling is the generation of CO_2, which can be easily removed from the system, unlike the gluconic acid generated by the GDH–glucose system.

The work in this Thesis in Chapters 5 and 6 (entry 7), in which ADH–IPA substrate-coupled cofactor recycling was implemented in continuous flow, showed very similar TTN and STY values over the same flow reactor operational period compared to the ADH in flow literature example (entry 4)—a promising result. The STY of entry 7 is lower than entry 4; however, the *E* factor of entry 7 is better. This is probably because entry 4 achieves 92% in a shorter t_{Res} compared with entry 7, which achieves full conversion. Thus, entry 4 produces product at a faster rate but also produces more waste materials compared with entry 7. The ADH–IPA continuous flow system developed in this Thesis (entry 7) does not require modification of the enzyme or an expensive modified support, in contrast entry 4, which implements the HaloTag immobilisation technique. This could make entry 7 a more appealing ADH–IPA cofactor recycling prospect for uptake into industry compared with entry 4.

The work in this Thesis in Chapters 7 and 8 (entry 8), in which H_2-driven cofactor recycling was implemented in continuous flow, showed the highest TOF, TTN and STY values over the longest flow reactor operational period out of all the entries, indicating that the system regenerates NADH very efficiently. Promisingly, the results showed a good improvement in TOF and STY over the HydRegen particles used in batch conditions, indicating that the technology readiness level of the HydRegen cofactor regeneration system has progressed from early developmental stages. It is also promising that entry 8 outperforms the metrics of the GDH systems in batch and flow, as GDH–glucose is the most established cofactor recycling technique. The results from the H_2-driven system in entry 8 compare well to the chiral iridium catalyst (Ir-SpiroPAP)

discussed in Section 1.1.4, which achieved a TTN and TOF of 5×10^6 and 231 min^{-1}, respectively, over a 360 h reaction period.[118] Although entry 8 achieved a lower TTN than the metal catalyst, the TOF achieved is very similar to the chiral iridium catalyst. The demonstration of the H_2-driven biocatalytic hydrogenation system, producing metrics comparable to metal hydrogenation in a commercial hydrogenation flow reactor, could help to introduce the possibility of flow biocatalysis to a new field of academic and industry scientists.

10 Outlook and Future Work

Chapters 3 and 4

Although the FDH did not show a high retention of activity after immobilisation onto BP2000 particles, the technology could prove to be useful and future work could investigate the transferal into flow and scale-up of an industrially relevant process that currently uses FDH in batch. The FDH–formate flow system could be beneficial over batch in scenarios in which faster reaction times are required, such as if the product racemises over time or if the substrate/product degrades. Alternatively, if a multi-step synthesis was being designed to be performed wholly in flow, the use of this system would alleviate the requirement to separate the enzyme from the product solution in-line.

Chapters 5 and 6

In the future, collaboration could continue with the industrial partner to apply the immobilised ADH-1001 to the chemical transformation that it is currently applied to in-house and compared with their current system. If successful, the system could be applied at a larger scale. Further investigations could implement a cofactor separation and recirculation method to further increase the overall cofactor turnover number, and/or increase the substrate concentration. The ADH-1001 was very successfully transferred into flow with the carbon particle support and this reveals the possibility of implementing other industrially used ADHs into flow with this approach.

Chapters 7 and 8

Similar to the ADH system, future work could explore a cofactor separation and recirculation method to further increase the overall cofactor turnover number, and/or

increase the substrate concentration. Moreover, studies could scale-up by increasing catalyst and substrate loadings with the aim of achieving higher conversions over a single pass. Once more, there are a multitude of NADH-dependent enzymes and industrially relevant substrates that further work could be focused on exploring, thereby simplifying the adoption of these biocatalysts for highly selective synthesis in continuous flow. In 2021, HydRegen Ltd. spun-out from the University of Oxford and it promises that it has plans to continue research and development with the H-Cube and begin to distribute H-Cube 'Bio-CatCarts' to other laboratories; these could be used in a 'plug and play'-style hydrogenation set-up. The continuous H_2-driven biocatalytic system developed in this Thesis presents a viable alternative or replacement to traditional cofactor regeneration systems. However, ultimately, this hybrid approach between metal-modified carbon hydrogenations and traditional biocatalysis has the potential to enable many more chemists to use the H-Cube reactor to perform flow hydrogenation biocatalysis, which could lead to a step-change in biocatalysis.

References

1 C. Jiménez-González, P. Poechlauer, Q. B. Broxterman, B.-S. S. Yang, D. am Ende, J. Baird, C. Bertsch, R. E. Hannah, P. Dell'Orco, H. Noorman, S. Yee, R. Reintjens, A. Wells, V. Massonneau, J. Manley, P. Dell'Orco, H. Noorman, S. Yee, R. Reintjens, A. Wells, V. Massonneau and J. Manley, *Org. Process Res. Dev.*, 2011, **15**, 900–911.

2 W. H. Brooks, W. C. Guida and K. G. Daniel, *Curr. Top. Med. Chem.*, 2011, **11**, 760–770.

3 L. A. Nguyen, H. He and C. Pham-Huy, *Int. J. Biomed. Sci.*, 2006, **2**, 85–100.

4 J. Panten and H. Surburg, in *Ullmann's Encyclopedia of Industrial Chemistry*, American Cancer Society, 2015, pp. 1–9.

5 D. J. Pollard and J. M. Woodley, *Trends Biotechnol.*, 2007, **25**, 66–73.

6 R. N. Patel, A. Banerjee and L. J. Szarka, *J. Am. Oil Chem. Soc.*, 1995, **72**, 1247–1264.

7 J. H. Kim and A. R. Scialli, 2011, **122**, 1–6.

8 A. Calcaterra and I. D'Acquarica, *J. Pharm. Biomed. Anal.*, 2018, **147**, 323–340.

9 R. N. Patel, *Coord. Chem. Rev.*, 2008, **252**, 659–701.

10 R. N. Patel, *Biomolecules*, 2013, **3**, 741—777.

11 R. N. Patel, *Curr. Opin. Biotechnol.*, 2001, **12**, 587–604.

12 S. W. May and S. R. Padgette, *Bio/Technology*, 1983, **1**, 677–686.

13 A. S. Bommarius, M. Schwarm and K. Drauz, *J. Mol. Catal. B Enzym.*, 1998, **5**, 1–11.

14 B. M. Nestl, S. C. Hammer, B. A. Nebel and B. Hauer, *Angew. Chem. Int. Ed.*, 2014, **53**, 3070–3095.

15 A. Wells and H.-P. Meyer, *ChemCatChem*, 2014, **6**, 918–920.

16 P. N. Devine, R. M. Howard, R. Kumar, M. P. Thompson, M. D. Truppo and N. J. Turner, *Nat. Rev. Chem.*, 2018, **2**, 409–421.

17 Q. Wu, C.-X. Chen, L.-L. Du and X.-F. Lin, *Appl. Biochem. Biotechnol.*, 2010, **160**, 2026–2035.

18 R. Xue and J. M. Woodley, *Bioresour. Technol.*, 2012, **115**, 183–195.

19 G. Matcham and A. S. Bowen, *Chim. Oggi-chemistry Today*, 1996, **14**, 20–24.

20 K. Q. Chen and F. H. Arnold, *Biotechnology. (N. Y).*, 1991, **9**, 1073–1077.

21 K. Chen and F. H. Arnold, *Proc. Natl. Acad. Sci. U. S. A.*, 1993, **90**, 5618–5622.

22 F. H. Arnold, *Curr. Opin. Biotechnol.*, 1993, **4**, 450–455.

23 R. E. Cobb, R. Chao and H. Zhao, *AIChE J.*, 2013, **59**, 1432–1440.

24 F. Cheng, L. Zhu and U. Schwaneberg, *Chem. Commun.*, 2015, **51**, 9760–9772.

25 N. L. Wagner, J. A. Greco, M. J. Ranaghan and R. R. Birge, *J. R. Soc. Interface*, 2013, **10**, 20130197.

26 F. Cheng, L. Zhu, H. Lue, J. Bernhagen and U. Schwaneberg, *Appl. Microbiol. Biotechnol.*, 2015,

99, 1237–1247.

27 F. Cheng, T. Kardashliev, C. Pitzler, A. Shehzad, H. Lue, J. Bernhagen, L. Zhu and U. Schwaneberg, *ACS Synth. Biol.*, 2015, **4**, 768–775.

28 P. A. Romero, E. Stone, C. Lamb, L. Chantranupong, A. Krause, A. E. Miklos, R. A. Hughes, B. Fechtel, A. D. Ellington, F. H. Arnold and G. Georgiou, *ACS Synth. Biol.*, 2012, **1**, 221–228.

29 G. Güven, R. Prodanovic and U. Schwaneberg, *Electroanalysis*, 2010, **22**, 765–775.

30 N. J. Turner, *Nat. Chem. Biol.*, 2009, **5**, 567–573.

31 F. H. Arnold, *Q. Rev. Biophys.*, 2015, **48**, 404–410.

32 J. C. Moore, H. M. Jin, O. Kuchner and F. H. Arnold, *J. Mol. Biol.*, 1997, **272**, 336–347.

33 H. Zhao and F. H. Arnold, *Proc. Natl. Acad. Sci. U. S. A.*, 1997, **94**, 7997–8000.

34 L. Giver, A. Gershenson, P.-O. Freskgard and F. H. Arnold, *Proc. Natl. Acad. Sci.*, 1998, **95**, 12809–12813.

35 O. May, P. T. Nguyen and F. H. Arnold, *Nat. Biotechnol.*, 2000, **18**, 317–320.

36 J. D. Bloom, C. O. Wilke, F. H. Arnold and C. Adami, *Biophys. J.*, 2004, **86**, 2758–2764.

37 J. D. Bloom, P. A. Romero, Z. Lu and F. H. Arnold, *Biol. Direct*, 2007, **2**, 17.

38 S. Bastian, X. Liu, J. T. Meyerowitz, C. D. Snow, M. M. Y. Chen and F. H. Arnold, *Metab. Eng.*, 2011, **13**, 345–352.

39 C. K. Prier, T. K. Hyster, C. C. Farwell, A. Huang and F. H. Arnold, *Angew. Chem. Int. Ed.*, 2016, **55**, 4711–4715.

40 M. A. Fischbach, J. R. Lai, E. D. Roche, C. T. Walsh and D. R. Liu, *Proc. Natl. Acad. Sci.*, 2007, **104**, 11951–11956.

41 W. R. Jarvis, J. C. Colbeck, A. Krebber, F. J. Fleitz and J. Brands, *Science*, 2010, **329**, 305–310.

42 A. A. Desai, *Angew. Chem. Int. Ed.*, 2011, **50**, 1974–1976.

43 C. K. Savile, J. M. Janey, E. C. Mundorff, J. C. Moore, S. Tam, W. R. Jarvis, J. C. Colbeck, A. Krebber, F. J. Fleitz, J. Brands, P. N. Devine, G. W. Huisman and G. J. Hughes, *Science*, 2010, **329**, 305–309.

44 M. D. Truppo, *ACS Med. Chem. Lett.*, 2017, **8**, 476–480.

45 M. P. P. Thompson, I. Peñafiel, S. C. Cosgrove, N. J. Turner, I. Penafiel, S. C. Cosgrove and N. J. Turner, *Org. Process Res. Dev.*, 2018, **23**, 9–18.

46 M. B. Plutschack, B. Pieber, K. Gilmore and P. H. Seeberger, *Chem. Rev.*, 2017, **117**, 11796–11893.

47 M. Baumann and I. R. Baxendale, *Beilstein J. Org. Chem.*, 2015, **11**, 1194–1219.

48 M. Baumann, T. S. Moody, M. Smyth, S. Wharry, T. S. Moody, M. Smyth and S. Wharry, DOI:10.1021/acs.oprd.9b00524.

49 B. Gutmann, D. Cantillo and C. O. Kappe, *Angew. Chem. Int. Ed.*, 2015, **54**, 6688–6728.

50 D. Dallinger and C. O. Kappe, *Curr. Opin. Green Sustain. Chem.*, 2017, **7**, 6–12.

51 R. Ciriminna, M. Pagliaro and R. Luque, *Green Energy Environ.*, 2020, **6**, 161–166.

52 R. Porta, M. Benaglia and A. Puglisi, *Org. Process Res. Dev.*, 2016, **20**, 2–25.

53 D. L. Hughes, *Org. Process Res. Dev.*, 2020, **24**, 1850–1860.

54 M. C. Bryan, P. J. Dunn, D. Entwistle, F. Gallou, S. G. Koenig, J. D. Hayler, M. R. Hickey, S. Hughes, M. E. Kopach, G. Moine, P. Richardson, F. Roschangar, A. Steven and F. J. Weiberth, *Green Chem.*, 2018, **20**, 5082–5103.

55 C. A. Shukla and A. A. Kulkarni, *Beilstein J. Org. Chem.*, 2017, **13**, 960–987.

56 C. Mateos, M. J. Nieves-Remacha and J. A. Rincón, *React. Chem. Eng.*, 2019, **4**, 1536–1544.

57 P. P. Plehiers, C. W. Coley, H. Gao, F. H. Vermeire, M. R. Dobbelaere, C. V Stevens, K. M. Van Geem and W. H. Green, *Front. Chem. Eng.*, 2020, **2**, 5.

58 A. Adamo, R. L. Beingessner, M. Behnam, J. Chen, T. F. Jamison, K. F. Jensen, J. C. M. Monbaliu, A. S. Myerson, E. M. Revalor, D. R. Snead, T. Stelzer, N. Weeranoppanant, S. Y. Wong and P. Zhang, *Science (80-.).*, 2016, **352**, 61–67.

59 M. P. Thompson, I. Peñafiel, S. C. Cosgrove and N. J. Turner, *Org. Process Res. Dev.*, 2019, **23**, 9–18.

60 L. Tamborini, P. Fernandes, F. Paradisi and F. Molinari, *Trends Biotechnol.*, 2018, **36**, 73–88.

61 J. Britton, S. Majumdar and G. A. Weiss, *Chem. Soc. Rev.*, 2018, **47**, 5891–5918.

62 S. Velasco-Lozano, S. Silva, J. Llop, L. Fernando, E. S. da Silva, J. Llop and F. López-Gallego, *ChemBioChem*, 2018, **19**, 395–403.

63 M. Santi, L. Sancineto, V. Nascimento, J. Braun Azeredo, E. V. M. Orozco, L. H. Andrade, H. Gröger and C. Santi, *Int. J. Mol. Sci.*, 2021, **22**, 1–32.

64 P. De Santis, L.-E. Meyer and S. Kara, *React. Chem. Eng.*, 2020, **5**, 2155–2184.

65 J. I. Ramsden, S. C. Cosgrove and N. J. Turner, *Chem. Sci.*, 2020, **11**, 11104–11112.

66 R. A. Sheldon and S. van Pelt, *Chem. Soc. Rev.*, 2013, **42**, 6223–6235.

67 R. C. Rodrigues, C. Ortiz, Á. Berenguer-Murcia, R. Torres and R. Fernández-Lafuente, *Chem. Soc. Rev.*, 2013, **42**, 6290–6307.

68 A. Liese and L. Hilterhaus, *Chem. Soc. Rev.*, 2013, **42**, 6236–6249.

69 J. Döbber and M. Pohl, *J. Biotechnol.*, 2017, **241**, 170–174.

70 M. L. Contente, F. Dall'Oglio, L. Tamborini, F. Molinari and F. Paradisi, *ChemCatChem*, 2017, **9**, 3843–3848.

71 F. Dall'Oglio, M. L. Contente, P. Conti, F. Molinari, D. Monfredi, A. Pinto, D. Romano, D. Ubiali, L. Tamborini and I. Serra, *Catal. Commun.*, 2017, **93**, 29–32.

72 T. Peschke, M. Skoupi, T. Burgahn, S. Gallus, I. Ahmed, K. S. Rabe and C. M. Niemeyer, *ACS Catal.*, 2017, **7**, 7866–7872.

73 D. Roura Padrosa, A. I. Benítez-Mateos, L. Calvey and F. Paradisi, *Green Chem.*, 2020, **22**, 5310–5316.

74 R. A. Sheldon, *Green Chem.*, 2017, **19**, 18–43.

75 F. Nerozzi, *Platin. Met. Rev.*, 2012, **56**, 236–241.

76 S. Werkmeister, K. Junge and M. Beller, *Green Chem.*, 2012, **14**, 2371.

77 H.-U. Blaser, C. Malan, B. Pugin, F. Spindler, H. Steiner and M. Studer, *Adv. Synth. Catal.*, 2003, **345**, 103–151.

78 L. Bonomo, L. Kermorvan and P. Dupau, *ChemCatChem*, 2015, **7**, 907–910.

79 H. Grünewald, *Angew. Chem.*, 1968, **80**, 52.

80 B. D. Vineyard, W. S. Knowles, M. J. Sabacky, G. L. Bachman and D. J. Weinkauff, *J. Am. Chem. Soc.*, 1977, **99**, 5946–5952.

81 O. C. Reactions, *Colacot, Thomas J.*, 2002, **46**, 2001–2002.

82 A. Mengel and O. Reiser, *Chem. Rev.*, 1999, **99**, 1191–1224.

83 S. Caron, R. W. Dugger, S. G. Ruggeri, J. A. Ragan and D. H. B. Ripin, *Chem. Rev.*, 2006, **106**, 2943–2989.

84 J. Magano and J. R. Dunetz, *Org. Process Res. Dev.*, 2012, **16**, 1156–1184.

85 L. A. Saudan, *Acc. Chem. Res.*, 2007, **40**, 1309–1319.

86 P. Mäki-Arvela, J. Hájek, T. Salmi and D. Y. Murzin, *Appl. Catal. A Gen.*, 2005, **292**, 1–49.

87 M. V. de Souza and T. R. Alves Vasconcelos, *Appl. Organomet. Chem.*, 2006, **20**, 798–810.

88 M. R. Johnson and B. Rickborn, *J. Org. Chem.*, 1970, **35**, 1041–1045.

89 K. Ralphs, É. McCourt, C. Ormandy, T. A. Carneiro de Souza, P. Nockemann, J. Jacquemin and H. G. Manyar, *ChemistrySelect*, 2018, **3**, 11706–11711.

90 M. Periasamy and M. Thirumalaikumar, *J. Organomet. Chem.*, 2000, **609**, 137–151.

91 A. Giannis and K. Sandhoff, *Angew. Chem. Int. Ed. English*, 1989, **28**, 218–220.

92 B. Jiang, Y. Feng and J. Zheng, *Tetrahedron Lett.*, 2000, **41**, 10281–10283.

93 J. V. B. Kanth and M. Periasamy, *J. Org. Chem.*, 1991, **56**, 5964–5965.

94 J. K. Nelson, B. Twamley, T. J. Villalobos and N. R. Natale, *Tetrahedron Lett.*, 2008, **49**, 5957–5960.

95 Y. Suseela and M. Periasamy, *Tetrahedron*, 1992, **48**, 371–376.

96 R. H. Tale, K. M. Patil and S. E. Dapurkar, *Tetrahedron Lett.*, 2003, **44**, 3427–3428.

97 J. Z. Saavedra, A. Resendez, A. Rovira, S. Eagon, D. Haddenham and B. Singaram, *J. Org. Chem.*, 2012, **77**, 221–228.

98 E. J. Corey, R. K. Bakshi and S. Shibata, *J. Am. Chem. Soc.*, 1987, **109**, 5551–5553.

99 E. J. Corey, R. K. Bakshi, S. Shibata, C. P. Chen and V. K. Singh, *J. Am. Chem. Soc.*, 1987, **109**, 7925–7926.

100 A. Hirao, S. Itsuno, S. Nakahama and N. Yamazaki, *Chem. Commun.*, 1981, 315–317.

101 S. Itsuno, K. Ito, A. Hirao and S. Nakahama, *Chem. Commun.*, 1983, 469–470.

102 C. F. Lane, *Chem. Rev.*, 1976, **76**, 773–799.

103 E. R. Burkhardt and K. Matos, *Chem. Rev.*, 2006, **106**, 2617–2650.

104 W. J. Atkins, E. R. Burkhardt and K. Matos, *Org. Process Res. Dev.*, 2006, **10**, 1292–1295.

105 Y. Zhou, G. Gao, H. Li and J. Qu, *Tetrahedron Lett.*, 2008, **49**, 3260–3263.

106 Y. Zhou, G. Gao, Y. Song and J. Qu, *Synth. Commun.*, 2014, **44**, 1515–1520.

107 B. T. Cho, *Chem. Soc. Rev.*, 2009, **38**, 443–452.

108 E. J. Corey and C. J. Helal, *Angew. Chem. Int. Ed. Engl.*, 1998, **37**, 1986–2012.

109 E. J. Corey and C. J. Helal, *Tetrahedron Lett.*, 1996, **37**, 5675–5678.

110 F. Meemken and A. Baiker, *Chem. Rev.*, 2017, **117**, 11522–11569.

111 Y. Liu, X. Yue, C. Luo, L. Zhang and M. Lei, *Energy & Environ. Mater.*, 2019, **2**, 292–312.

112 B. Štefane and F. Požgan, *Top. Curr. Chem.*, 2016, **374**, 1–67.

113 W. V. O. N. E. Doering and R. W. Young, *J. Am. Chem. Soc.*, 1950, **72**, 631.

114 H. Meerwein and R. Schmidt, *Justus Liebigs Ann. Chem.*, 1925, **444**, 221–238.

115 T. Ohkuma, M. Koizumi, K. Muñiz, G. Hilt, C. Kabuto and R. Noyori, *J. Am. Chem. Soc.*, 2002, **124**, 6508–6509.

116 R. Noyori, *Angew. Chem. Int. Ed.*, 2002, **41**, 2008–2022.

117 K. Matsumura, N. Arai, K. Hori, T. Saito, N. Sayo and T. Ohkuma, *J. Am. Chem. Soc.*, 2011, **133**, 10696–10699.

118 J.-H. Xie, X.-Y. Liu, J.-B. Xie, L.-X. Wang and Q.-L. Zhou, *Angew. Chem. Int. Ed.*, 2011, **50**, 7329–7332.

119 W. Wu, S. Liu, M. Duan, X. Tan, C. Chen, Y. Xie, Y. Lan, X.-Q. Dong and X. Zhang, *Org. Lett.*, 2016, **18**, 2938–2941.

120 A. Zanotti-Gerosa, W. Hems, M. Groarke and F. Hancock, *Platin. Met. Rev.*, 2005, **49**, 158–165.

121 D. J. Bayston, C. B. Travers and M. E. C. Polywka, *Tetrahedron: Asymmetry*, 1998, **9**, 2015–2018.

122 R. Noyori and S. Hashiguchi, *Acc. Chem. Res.*, 1997, **30**, 97–102.

123 S. Hashiguchi, A. Fujii, J. Takehara, T. Ikariya and R. Noyori, *J. Am. Chem. Soc.*, 1995, **117**, 7562–7563.

124 J. Takehara, S. Hashiguchi, A. Fujii, S. Inoue, T. Ikariya and R. Noyori, *Chem. Commun.*, 1996, 233–234.

125 P. A. Dub and J. C. Gordon, *Dalt. Trans.*, 2016, **45**, 6756–6781.

126 J. Hannedouche, G. J. Clarkson and M. Wills, *J. Am. Chem. Soc.*, 2004, **126**, 986–987.

127 A. M. Hayes, D. J. Morris, G. J. Clarkson and M. Wills, *J. Am. Chem. Soc.*, 2005, **127**, 7318–7319.

128 W. Baratta, F. Benedetti, A. Del Zotto, L. Fanfoni, F. Felluga, S. Magnolia, E. Putignano and P. Rigo, *Organometallics*, 2010, **29**, 3563–3570.

129 P.-N. Liu, P.-M. Gu, J.-G. Deng, Y.-Q. Tu and Y.-P. Ma, *European J. Org. Chem.*, 2005, **2005**, 3221–3227.

130 T.-Y. Cheng, J.-L. Zhuang, H. Yao, H.-S. Zhang and G.-H. Liu, *Chinese Chem. Lett.*, 2014, **25**, 613–616.

131 X. Zhang, Y. Zhao, J. Peng and Q. Yang, *Green Chem.*, 2015, **17**, 1899–1906.

132 X. Li, X. Wu, W. Chen, F. E. Hancock, F. King and J. Xiao, *Org. Lett.*, 2004, **6**, 3321–3324.

133 J. F. Sonnenberg and R. H. Morris, *Catal. Sci. Technol.*, 2014, **4**, 3426–3438.

134 F. Michalek, A. Lagunas, C. Jimeno and M. A. Pericàs, *J. Mater. Chem.*, 2008, **18**, 4692–4697.

135 a Tungler, T. Tarnai and L. Hegedus, *Platin. Met. Rev.*, 1998, **42**, 108–115.

136 T. Mallat, E. Orglmeister and A. Baiker, *Chem. Rev.*, 2007, **107**, 4863–4890.

137 K. Kacprzak and J. Gawroński, *Synthesis (Stuttg).*, 2004, **2001**, 961–998.

138 Y. Orito, S. Imai and S. Niwa, *J. Chem. Soc. Jpn.*, 1979, 1118–1120.

139 H.-U. Blaser and M. Studer, *Acc. Chem. Res.*, 2007, **40**, 1348–1356.

140 S. Hübner, J. G. de Vries and V. Farina, *Adv. Synth. & Catal.*, 2016, **358**, 3–25.

141 F. Agbossou-Niedercorn and C. Michon, *Coord. Chem. Rev.*, 2020, **425**, 213523.

142 W. Zuo, A. J. Lough, Y. F. Li and R. H. Morris, *Science*, 2013, **342**, 1080–1083.

143 G. Zhang and S. K. Hanson, *Chem. Commun.*, 2013, **49**, 10151–10153.

144 P. T. Anastas and J. C. Warner, *Green Chemistry: Theory and Practice*, Oxford University Press, 1st edn., 1998.

145 F. Hollmann, D. J. Opperman and C. E. Paul, *Angew. Chem. Int. Ed.*, 2021, **60**, 5644–5665.

146 B. M. Trost, *Angew. Chem. Int. Ed. English*, 1995, **34**, 259–281.

147 R. A. Sheldon, *Pure Appl. Chem.*, 2000, **72**, 1233–1246.

148 R. A. Sheldon, *Chem. Ind.(London)*, 1992, 903–906.

149 R. A. Sheldon, *Green Chem.*, 2007, **9**, 1273–1283.

150 R. A. Sheldon, *ACS Sustain. Chem. Eng.*, 2018, **6**, 32–48.

151 C. Capello, U. Fischer and K. Hungerbühler, *Green Chem.*, 2007, **9**, 927–934.

152 C. J. Clarke, W.-C. Tu, O. Levers, A. Bröhl and J. P. Hallett, *Chem. Rev.*, 2018, **118**, 747–800.

153 C. Aranda and G. de Gonzalo, *Molecules*, 2020, **25**, 3016.

154 J. M. Woodley, *Trends Biotechnol.*, 2008, **26**, 321–327.

155 C. K. Winkler, J. H. Schrittwieser and W. Kroutil, *ACS Cent. Sci.*, 2021, **7**, 55–71.

156 Y. Ni, D. Holtmann and F. Hollmann, *ChemCatChem*, 2014, **6**, 930–943.

157 F. Hollmann, I. W. C. E. Arends and D. Holtmann, *Green Chem.*, 2011, **13**, 2285–2314.

158 H. Zhao and W. A. van der Donk, *Curr. Opin. Biotechnol.*, 2003, **14**, 583–589.

159 S. Wu and Z. Li, *ChemCatChem*, 2018, 2164–2178.

160 S. Siedler, S. Bringer and M. Bott, *Appl. Microbiol. Biotechnol.*, 2011, **92**, 929–937.

161 K. Goldberg, K. Schroer, S. Lütz and A. Liese, *Appl. Microbiol. Biotechnol.*, 2007, **76**, 249–255.

162 G. W. Huisman, J. Liang and A. Krebber, *Curr. Opin. Chem. Biol.*, 2010, **14**, 122–129.

163 M. M. Musa and R. S. Phillips, *Catal. Sci. Technol.*, 2011, **1**, 1311–1323.

164 Grand View Research, *Enzymes Market Size, Share & Trends Analysis Report By Application (Industrial Enzymes, Specialty Enzymes), By Product (Carbohydrase, Proteases, Lipases), By Source, By Region, And Segment Forecasts, 2020 - 2027*, 2020.

165 P. Tufvesson, J. Lima-Ramos, M. Nordblad and J. M. Woodley, *Org. Process Res. Dev.*, 2011, **15**, 266–274.

166 P. Tufvesson, W. Fu, J. S. Jensen and J. M. Woodley, *Food Bioprod. Process.*, 2010, **88**, 3–11.

167 S. K. Ma, J. Gruber, C. Davis, L. Newman, D. Gray, A. Wang, J. Grate, G. W. Huisman and R. A. Sheldon, *Green Chem.*, 2010, **12**, 81–86.

168 R. A. Sheldon, *Adv. Synth. Catal.*, 2007, **349**, 1289–1307.

169 H. Gröger, E. Capan, A. Barthuber and K.-D. Vorlop, *Org. Lett.*, 2001, **3**, 1969–1972.

170 V. I. Lozinsky and F. M. Plieva, *Enzyme Microb. Technol.*, 1998, **23**, 227–242.

171 S. Velasco-Lozano, F. López-Gallego, J. C. Mateos-Díaz and E. Favela-Torres, *Biocatalysis*, 2016, **1**, 166–177.

172 P. Ferraboschi, M. De Mieri and F. Galimberti, *Tetrahedron: Asymmetry*, 2010, **21**, 2136–2141.

173 L. Cao, in *Carrier-bound Immobilized Enzymes*, John Wiley & Sons, Ltd, 2006, pp. 53–168.

174 A. B.-M. and R. Fernandez-Lafuente, *Curr. Org. Chem.*, 2010, 14, 1000–1021.

175 L. Sellés Vidal, C. L. Kelly, P. M. Mordaka and J. T. Heap, *Biochim. Biophys. Acta - Proteins Proteomics*, 2018, **1866**, 327–347.

176 J. Liu, S. Wu and Z. Li, *Curr. Opin. Chem. Biol.*, 2018, **43**, 77–86.

177 G. Grogan, *Curr. Opin. Chem. Biol.*, 2018, **43**, 15–22.

178 H. Schägger, W. A. Cramer and G. von Jagow, *Anal. Biochem.*, 1994, **217**, 220–230.

179 C. Auriol, G. Bestel-Corre, J.-B. Claude, P. Soucaille and I. Meynial-Salles, *Proc. Natl. Acad. Sci.*, 2011, **108**, 1278–1283.

180 X. Wang, T. Saba, H. H. P. Yiu, R. F. Howe, J. A. Anderson and J. Shi, *Chem*, 2017, **2**, 621–654.

181 W. Liu and P. Wang, *Biotechnol. Adv.*, 2007, **25**, 369–384.

182 Y. Ni, C.-X. X. Li, J. Zhang, N.-D. D. Shen, U. T. Bornscheuer and J.-H. H. Xu, *Adv. Synth. Catal.*, 2011, **353**, 1213–1217.

183 N. Richter and W. Hummel, *Enzyme Microb. Technol.*, 2011, **48**, 472–479.

184 S. Q. Pham, P. Gao and Z. Li, *Biotechnol. Bioeng.*, 2013, **110**, 363–373.

185 L. J. Wang, C. X. Li, Y. Ni, J. Zhang, X. Liu and J. H. Xu, *Bioresour. Technol.*, 2011, **102**, 7023–7028.

186 S. Janocha and R. Bernhardt, *Appl. Microbiol. Biotechnol.*, 2013, **97**, 7639–7649.

187 B. Kosjek, J. Nti-Gyabaah, K. Telari, L. Dunne and J. C. Moore, *Org. Process Res. Dev.*, 2008, **12**, 584–588.

188 W. Kroutil, H. Mang, K. Edegger and K. Faber, *Curr. Opin. Chem. Biol.*, 2004, **8**, 120–126.

189 J. Zdarta, M. Pinelo, T. Jesionowski and A. S. Meyer, *ChemCatChem*, 2018, 5164–5173.

190 C. Ning, E. Su, Y. Tian and D. Wei, *J. Biotechnol.*, 2014, **184**, 7–10.

191 K. Seelbach, B. Riebel, W. Hummel, M.-R. Kula, V. I. Tishkov, A. M. Egorov, C. Wandrey and U. Kragl, *Tetrahedron Lett.*, 1996, **37**, 1377–1380.

192 W. Wu, D. Zhu and L. Hua, *J. Mol. Catal. B Enzym.*, 2009, **61**, 157–161.

193 G. Dong and U. Ryde, *JBIC J. Biol. Inorg. Chem.*, 2018, **23**, 1243–1254.

194 Z. Shaked and G. M. Whitesides, *J. Am. Chem. Soc.*, 1980, **102**, 7104–7105.

195 Y. Zhu, L. Shao, A. Jian, Z. Huang, Q. Chen, Q. Wu, X. Huang, P. So, Z. Yao, Y. Jia, Z. Li, W. Yu, Y. Yang, S. Sang, W. Zhang and X. Zhang, 2019, 1–9.

196 L. Lauterbach, O. Lenz and K. A. Vincent, *FEBS J.*, 2013, **280**, 3058–3068.

197 J. Ratzka, L. Lauterbach, O. Lenz and M. B. Ansorge-Schumacher, *J. Mol. Catal. B Enzym.*, 2012, **74**, 219–223.

198 J. Ratzka, L. Lauterbach, O. Lenz and M. B. Ansorge-Schumacher, *Biocatal. Biotransformation*, 2011, **29**, 246–252.

199 R. Mertens, L. Greiner, E. C. D. van den Ban, H. B. C. M. Haaker and A. Liese, *J. Mol. Catal. B Enzym.*, 2003, **24**–**25**, 39–52.

200 H. A. Reeve, L. Lauterbach, P. A. Ash, O. Lenz and K. A. Vincent, *Chem. Commun.*, 2012, **48**, 1589–1591.

201 H. A. Reeve, L. Lauterbach, O. Lenz and K. A. Vincent, *ChemCatChem*, 2015, **7**, 3480–3487.

202 H. A. Reeve, P. A. Ash, H. S. Park, A. Huang, M. Posidias, C. Tomlinson, O. Lenz and K. A. Vincent, *Biochem. J.*, 2017, **474**, 215–230.

203 J. Britton and T. F. Jamison, *Nat. Protoc.*, 2017, **12**, 2423.

204 A. C. Bédard, A. R. Longstreet, J. Britton, Y. Wang, H. Moriguchi, R. W. Hicklin, W. H. Green and T. F. Jamison, *Bioorganic Med. Chem.*, 2017, **25**, 6233–6241.

205 C. Wiles and P. Watts, *Green Chem.*, 2012, **14**, 38–54.

206 C. Wiles and P. Watts, *Green Chem.*, 2014, **16**, 55–62.

207 P. T. Anastas and M. M. Kirchhoff, *Acc. Chem. Res.*, 2002, **35**, 686–694.

208 S. V. Ley, *Tetrahedron*, 2010, **66**, 6270–6292.

209 I. R. Baxendale, J. Deeley, C. M. Griffiths-Jones, S. V Ley, S. Saaby and G. K. Tranmer, *Chem. Commun.*, 2006, 2566–2568.

210 C. A. Correia, K. Gilmore, D. T. McQuade and P. H. Seeberger, *Angew. Chem. - Int. Ed.*, 2015, **54**, 4945–4948.

211 Z. Amara, J. F. B. Bellamy, R. Horvath, S. J. Miller, A. Beeby, A. Burgard, K. Rossen, M. Poliakoff and M. W. George, *Nat. Chem.*, 2015, **7**, 489–495.

212 R. Yuryev, S. Strompen and A. Liese, *Beilstein J. Org. Chem.*, 2011, **7**, 1449–1467.

213 B. Tomaszewski, R. C. Lloyd, A. J. Warr, K. Buehler and A. Schmid, *ChemCatChem*, 2014, **6**,

2567–2576.

214 J. Lutz, V. V Mozhaev, Y. . Khmelnitsky, B. Witholt and A. Schmid, *J. Mol. Catal. B Enzym.*, 2002, **19**–**20**, 177–187.

215 R. V. Jones, L. Godorhazy, N. Varga, D. Szalay, L. Urge and F. Darvas, *J. Comb. Chem.*, 2006, **8**, 110–116.

216 J. Britton, S. Majumdar and G. A. Weiss, *Chem. Soc. Rev.*, 2018, **47**, 5891–5918.

217 S. Ghannadi, H. Abdizadeh, M. Miroliaei and A. A. Saboury, *Ind. Eng. Chem. Res.*, , DOI:10.1021/acs.iecr.9b01370.

218 M. Heidlindemann, G. Rulli, A. Berkessel, W. Hummel and H. Gröger, *ACS Catal.*, DOI:10.1021/cs4010387.

219 M. Zezzi Do Valle Gomes and A. E. C. Palmqvist, *New J. Chem.*, , DOI:10.1039/c7nj02028g.

220 L. Tamborini, P. Fernandes, F. Paradisi and F. Molinari, *Trends Biotechnol.*, 2018, **36**, 73–88.

221 P. De Santis, L. E. Meyer and S. Kara, *React. Chem. Eng.*, 2020, **5**, 2155–2184.

222 A. I. Benítez-Mateos, M. L. Contente, D. Roura Padrosa and F. Paradisi, *React. Chem. Eng.*, 2021, **6**, 599–611.

223 A. Naramittanakul, S. Buttranon, A. Petchsuk, P. Chaiyen and N. Weeranoppanant, *React. Chem. Eng.*, , DOI:10.1039/d1re00189b.

224 T. Peschke, P. Bitterwolf, S. Hansen, J. Gasmi, K. S. Rabe and C. M. Niemeyer, *Catalysis*, 2019, **9**, 164.

225 T. Peschke, P. Bitterwolf, S. Gallus, Y. Hu, C. Oelschlaeger, N. Willenbacher, K. S. Rabe and C. M. Niemeyer, *Angew. Chem. Int. Ed.*, 2018, **57**, 17028–17032.

226 N. Adebar and H. Gröger, *Bioengineering*, 2019, **6**, 99.

227 W. Finnigan, J. Citoler, S. C. Cosgrove and N. J. Turner, *Org. Process Res. Dev.*, 2020, **24**, 1969–1977.

228 B. Tomaszewski, A. Schmid and K. Buehler, *Org. Process Res. Dev.*, 2014, **18**, 1516–1526.

229 R. D. Franklin, J. A. Whitley, A. A. Caparco, B. R. Bommarius, J. A. Champion and A. S. Bommarius, *Chem. Eng. J.*, 2021, **407**, 127065.

230 M. P. Thompson, S. R. Derrington, R. S. Heath, J. L. Porter, J. Mangas-Sanchez, P. N. Devine, M. D. Truppo and N. J. Turner, *Tetrahedron*, 2019, **75**, 327–334.

231 H. Li, J. Moncecchi and M. D. Truppo, *Org. Process Res. Dev.*, 2015, **19**, 695–700.

232 J. Döbber, M. Pohl, S. V. Ley and B. Musio, *React. Chem. Eng.*, , DOI:10.1039/C7RE00173H.

233 J. Döbber, T. Gerlach, H. Offermann, D. Rother and M. Pohl, *Green Chem.*, 2018, **20**, 544–552.

234 B. Baumer, T. Classen, M. Pohl and J. Pietruszka, *Adv. Synth. Catal.*, 2020, **362**, 2894–2901.

235 C. J. Mallia and I. R. Baxendale, *Org. Process Res. Dev.*, 2016, **20**, 327–360.

236 H. A. Reeve, P. A. Ash, H. Park, A. Huang, M. Posidias, C. Tomlinson, O. Lenz and K. A. Vincent, *Biochem. J.*, 2017, **474**, 215–230.

237 A. Al-Shameri, M.-C. Petrich, K. junge Puring, U.-P. Apfel, B. Nestl and L. Lauterbach, *Angew. Chem. Int. Ed.*, DOI:10.1002/anie.202001302.

238 B. Rodriguez-Colinas, L. Fernandez-Arrojo, P. Santos-Moriano, A. Ballesteros and F. Plou, *Catalysts*, 2016, **6**, 189.

239 E. Hald, P. Lehmann and J. Ziegenhorn, *Clin. Chem.*, 1975, **21**, 884–887.

240 T. Burgdorf, A. L. De Lacey and B. Friedrich, *J. Bacteriol.*, 2002, **184**, 6280–6288.

241 J. Quinson, R. Hidalgo, P. A. Ash, F. Dillon, N. Grobert and K. A. Vincent, *Faraday Discuss.*, 2014, **172**, 473–496.

242 M. Irfan, T. N. Glasnov and C. O. Kappe, *ChemSusChem*, 2011, **4**, 300–316.

243 P. J. Cossar, L. Hizartzidis, M. I. Simone, A. McCluskey and C. P. Gordon, *Org. Biomol. Chem.*, 2015, **13**, 7119–7130.

244 C. C. Russell, J. R. Baker, P. J. Cossar and A. McCluskey, in *New Advances in Hydrogenation Processes - Fundamentals and Applications*, InTech, 2017.

245 K. A. Vincent, X. Li, C. F. Blanford, N. a Belsey, J. H. Weiner and F. a Armstrong, *Nat. Chem. Biol.*, 2007, **3**, 761–762.

246 M. Thompson, I. Penafiel, S. C. Cosgrove and N. J. Turner, *Org. Process Res. Dev.*, 2018, **23**, 9–18.

247 R. A. Sheldon, *Chem. Commun.*, 2008, 3352–3365.

248 M. D. Argyle and C. H. Bartholomew, *Catalysts*, 2015, **5**, 145–269.

249 B. Tomaszewski, R. C. Lloyd, A. J. Warr, K. Buehler and A. Schmid, *ChemCatChem*, 2014, **6**, 2567–2576.

250 R. Karande, A. Schmid and K. Buehler, *Adv. Synth. Catal.*, 2011, **353**, 2511–2521.

251 V. De Vitis, D. Oglio, A. Pinto, C. De Micheli, F. Molinari, P. Conti, D. Romano and L. Tamborini, 2017, 668–673.

252 A. I. Benítez-Mateos, E. San Sebastian, N. Ríos-Lombardía, F. Morís, J. González-Sabín and F. López-Gallego, *Chem. – A Eur. J.*, 2017, **23**, 16843–16852.

253 M. L. Contente and F. Paradisi, *Nat. Catal.*, 2018, **1**, 452–459.

254 L. Wallentin, R. C. Becker, A. Budaj, C. P. Cannon, H. Emanuelsson, C. Held, J. Horrow, S. Husted, S. James, H. Katus, K. W. Mahaffey, B. M. Scirica, A. Skene, P. G. Steg, R. F. Storey and R. A. Harrington, *N. Engl. J. Med.*, 2009, **361**, 1045–1057.

255 S. Husted and J. J. J. Van Giezen, *Cardiovasc. Ther.*, 2009, **27**, 259–274.

256 T. M. Dando and C. M. Perry, *Drugs*, 2004, **64**, 777–794.

257 A. Duval and L. Dubertret, *N. Engl. J. Med.*, 2009, **361**, 1415–1416.

258 D. Dascier, S. Kambourakis, L. Hua, J. David Rozzell and J. D. Stewart, *Org. Process Res. Dev.*, , DOI:10.1021/op400312n.

259 D. Pollard, M. Truppo, J. Pollard, C. Chen and J. Moore, *Tetrahedron: Asymmetry*, 2006, **17**, 554–559.

260 L. A. Thompson, J. S. Rowbotham, J. H. Nicholson, M. A. Ramirez, C. Zor, H. A. Reeve, N. Grobert and K. A. Vincent, *ChemCatChem*, 2020, **12**, 3913–3918.

261 A. Radman Kastelic, R. Odžak, I. Pezdirc, K. Sović, T. Hrenar, A. Čipak Gašparović, M. Skočibušić and I. Primožič, *Mol.* , 2019, 24.

262 M. Hall and A. S. Bommarius, *Chem. Rev.*, 2011, **111**, 4088–4110.

263 O. W. Gooding, R. Voladri, A. Bautista, T. Hopkins, G. Huisman, S. Jenne, S. Ma, E. C. Mundorff, M. M. Savile, S. J. Truesdell and J. W. Wong, *Org. Process Res. Dev.*, 2010, **14**, 119–126.

264 S. J. Calvin, D. Mangan, I. Miskelly, T. S. Moody and P. J. Stevenson, *Org. Process Res. Dev.*, 2012, **16**, 82–86.

265 G. Brown, D. Mangan, I. Miskelly and T. S. Moody, *Org. Process Res. Dev.*, 2011, **15**, 1036–1039.

266 J. Pan, G. W. Zheng, Q. Ye and J. H. Xu, *Org. Process Res. Dev.*, 2014, **18**, 739–743.

267 S. García-Cerrada, L. Redondo-Gallego, F. Martínez-Olid, J. A. Rincón and P. García-Losada, *Org. Process Res. Dev.*, 2017, **21**, 779–784.

268 B. Kosjek, W. Stampfer, M. Pogorevc, W. Goessler, K. Faber and W. Kroutil, *Biotechnol. Bioeng.*, DOI:10.1002/bit.20004.

269 J. Solé, J. Brummund, G. Caminal, M. Schürman, G. Álvaro and M. Guillén, *ChemCatChem*, , DOI:10.1002/cctc.201901090.

270 J. Döbber, M. Pohl, S. V. Ley and B. Musio, *React. Chem. Eng.*, , DOI:10.1039/c7re00173h.

271 M. Cortes-Clerget, N. Akporji, J. Zhou, F. Gao, P. Guo, M. Parmentier, F. Gallou, J.-Y. Berthon and B. H. Lipshutz, *Nat. Commun.*, 2019, **10**, 2169.

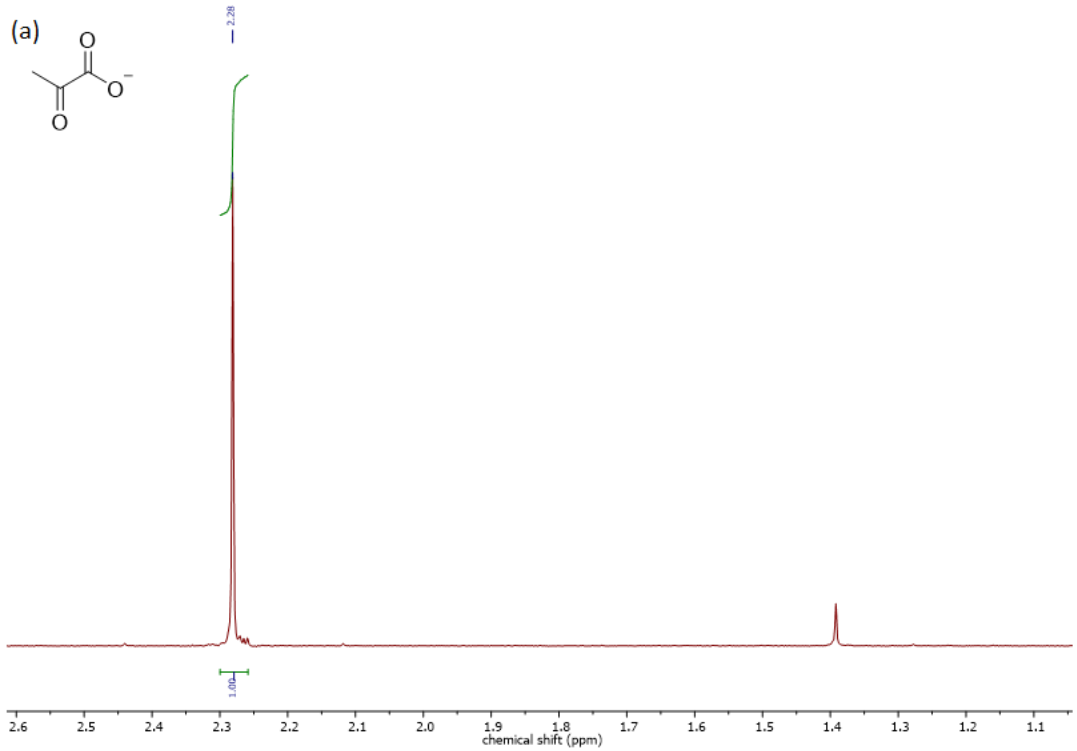
272 K. A. J. Walsh, R. M. Daniel and H. W. Morgan, *Biochem. J.*, 1983, **209**, 427–433.

273 H. A. Reeve, D.Phil Thesis, University of Oxford, 2014.

274 S. Joseph Srinivasan, S. E. Cleary, M. Ramirez, H. Reeve, C. Paul and K. A. Vincent, *Angew. Chem. Int. Ed.*, 2021, anie.202101186.

Appendices

A. NMR spectra for pyruvate to lactate



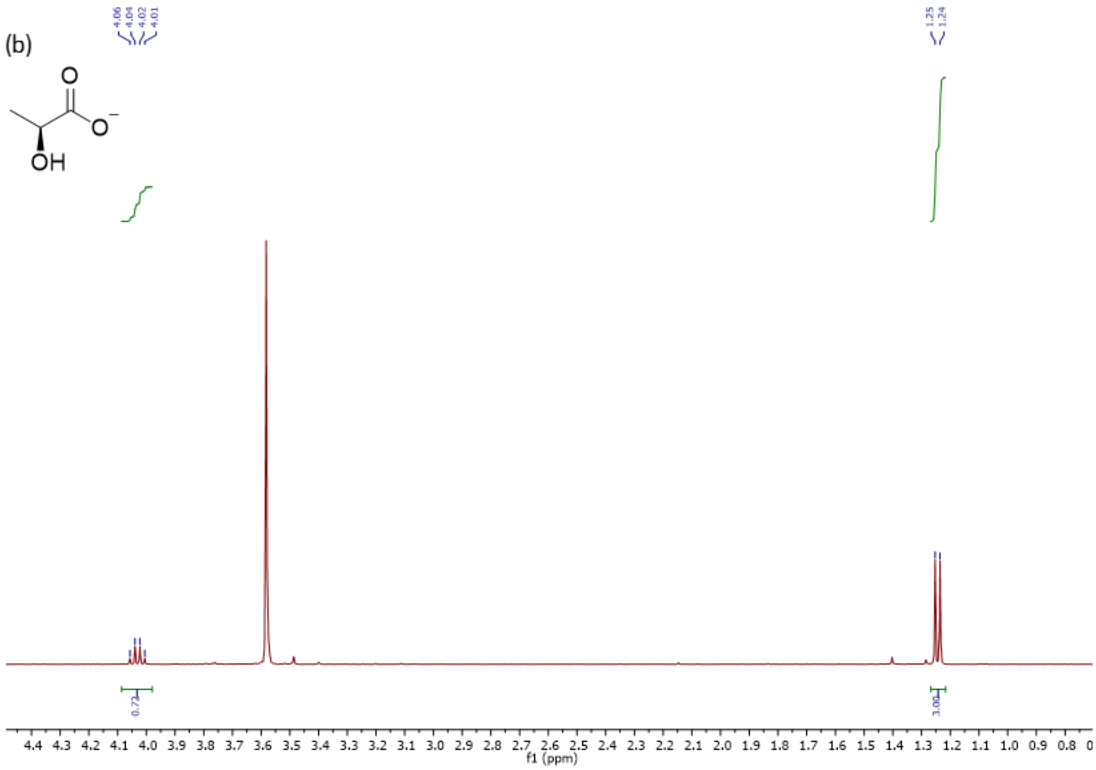


Figure A-1: Typical ^{1}H NMR spectra recorded for (a) pyruvate and (b) L-lactate. Performed using a Bruker Avance III HD nanobay (400 MHz), with the addition of 10% D_2O to all samples.

B. GC traces

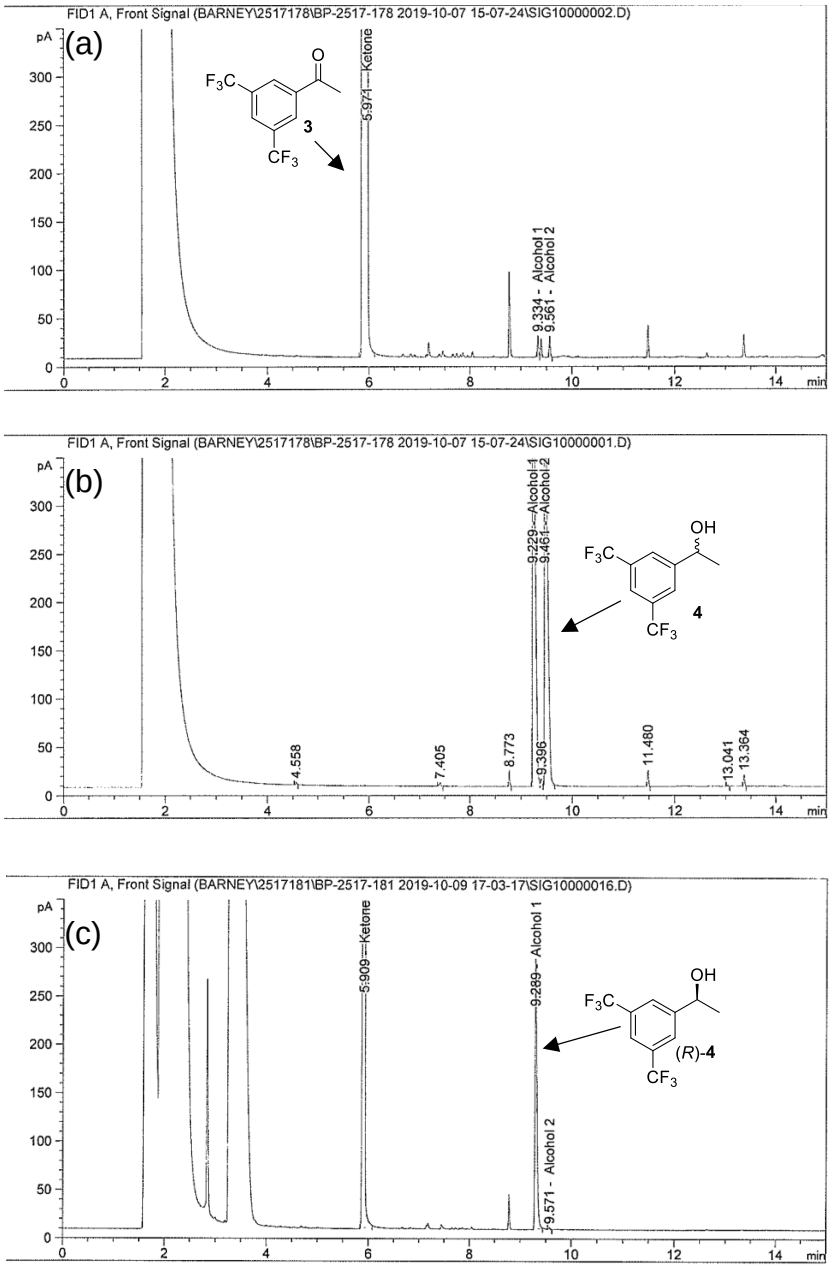


Figure B-1: Chiral gas chromatograms of (a) **3** standard, (b) **4** standard, (c) typical final reaction solution sample from Figure 4-2 in Section 4.2.7 containing **3** and (*R*)-**4**.

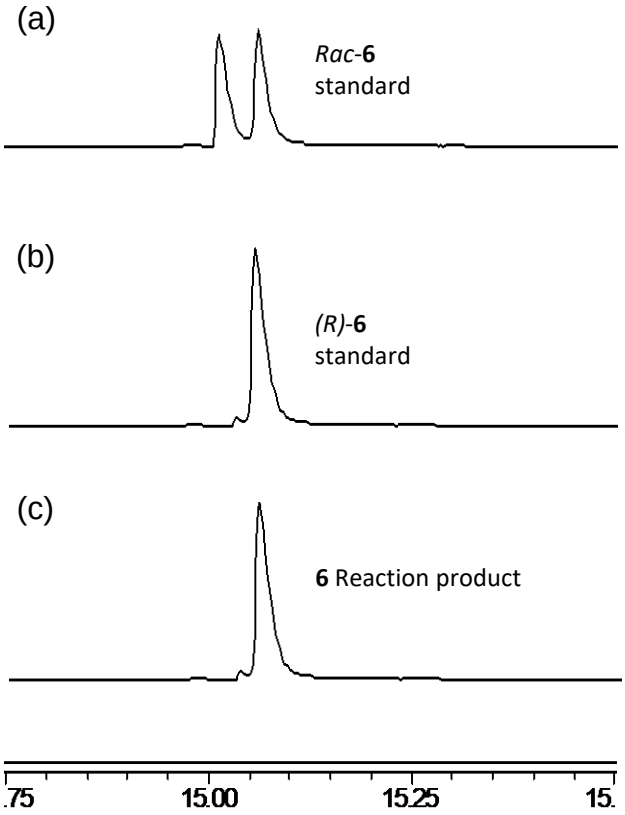


Figure B-2: Chiral gas chromatograms of (a) *rac*-***6*** standard, (b) (*R*)-**6** standard, (c) **6** reaction product from Section 4.3, Figure 4-3.

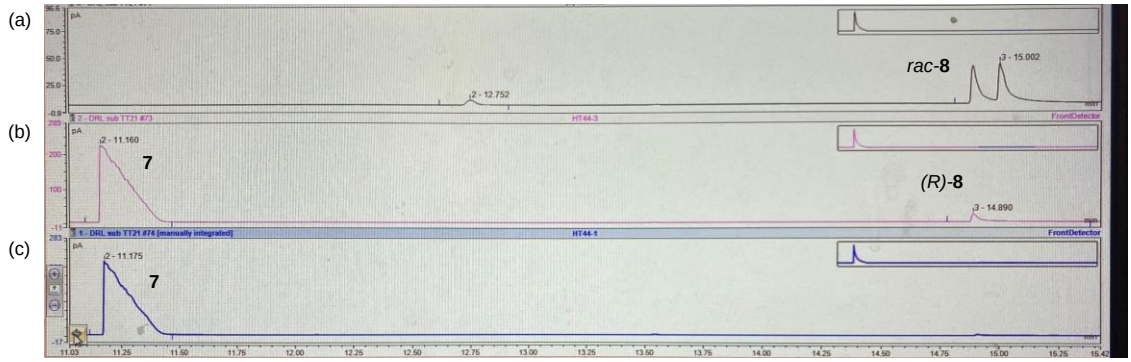


Figure B-3: Chiral gas chromatograms of (a) *rac*-**8** standard, (b) typical final reaction solution sample from Figure 5-9 in Section 5.5.1, (c) **7** standard. The lab did not have access to a pure sample of the chiral; alcohol product.

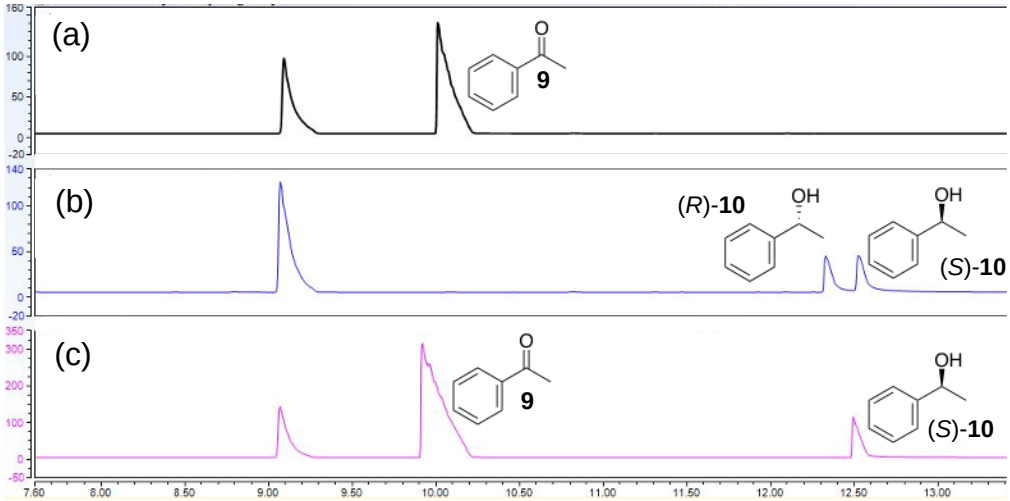


Figure B-4: Chiral gas chromatograms of (a) **9** standard, (b) **10** standard, (c) typical final reaction solution sample from Figure 5-11 in Section 5.5.1 containing **9** and (*S*)-**10**.

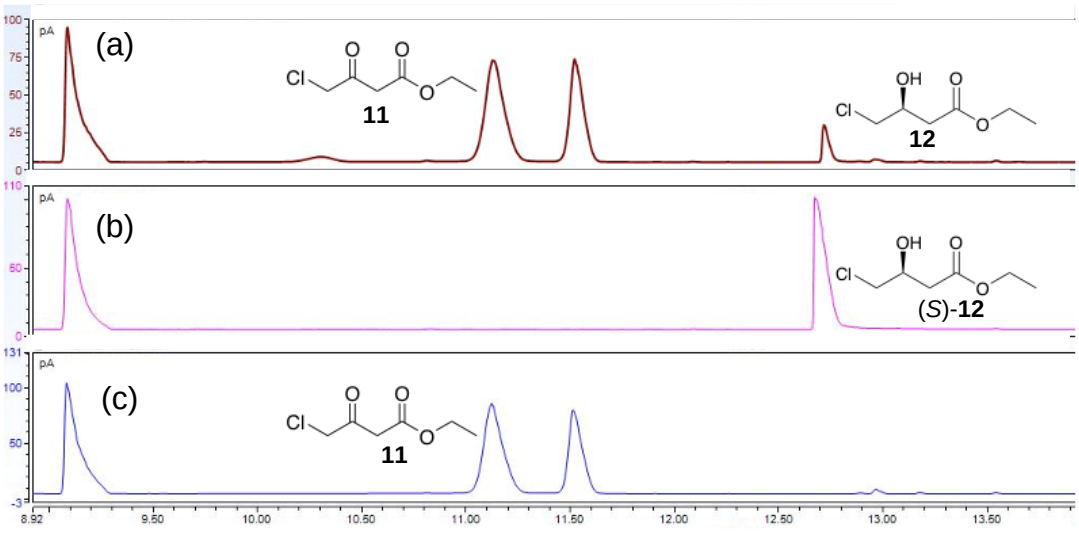


Figure B-5: Chiral gas chromatograms of (a) typical final reaction solution sample from Figure 6-5 in Section 6.4 containing **11** and **12**, (b) (*S*)-**12** standard, (c) **11** standard.

C. GC calibration curves

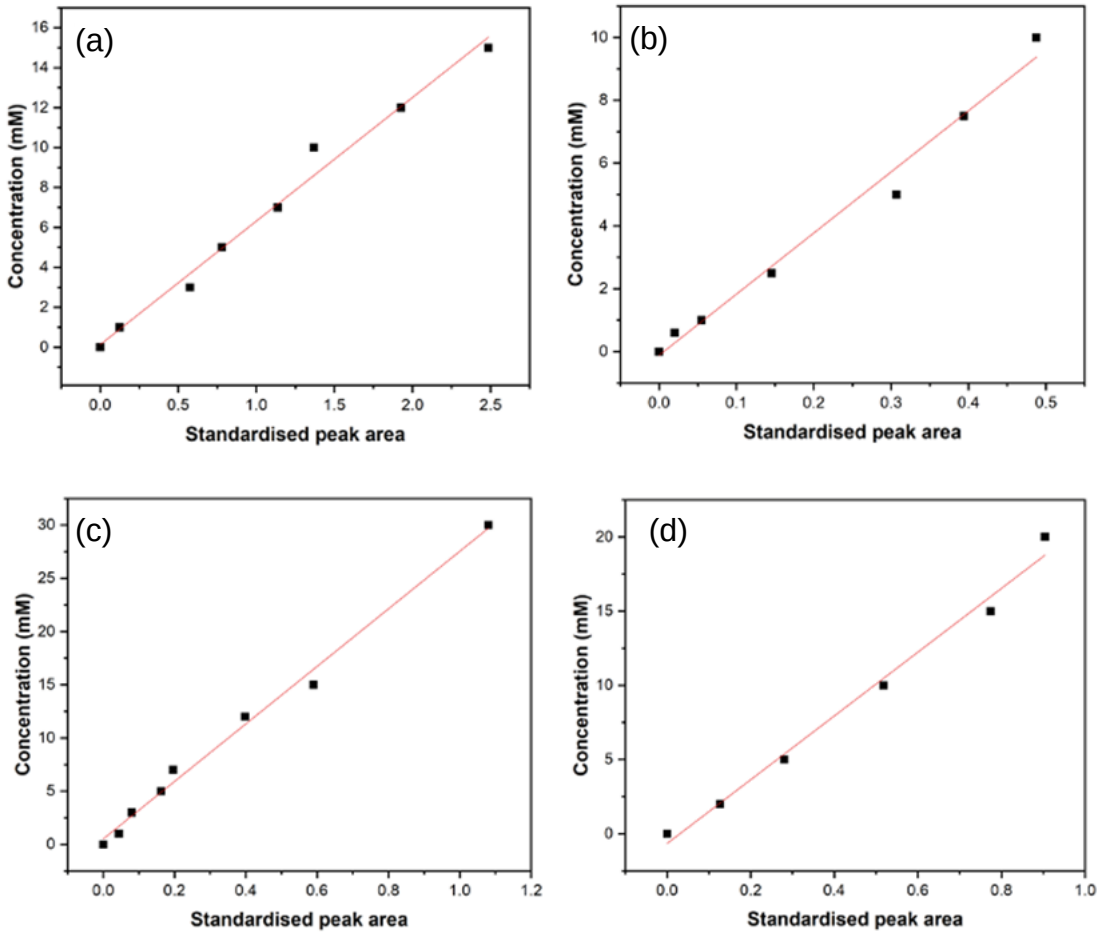


Figure C-1: Chiral GC calibration curves for (a) **9**, (b) (*S*)-**10**, (c) **11** (d) (*S*)-**12**. Determined by the preparation of standard GC samples at concentrations from 0–30 mM. For other reagents and products used in this Thesis the ratio of raw peak area was used to determine the reaction conversion.

D. HPLC traces

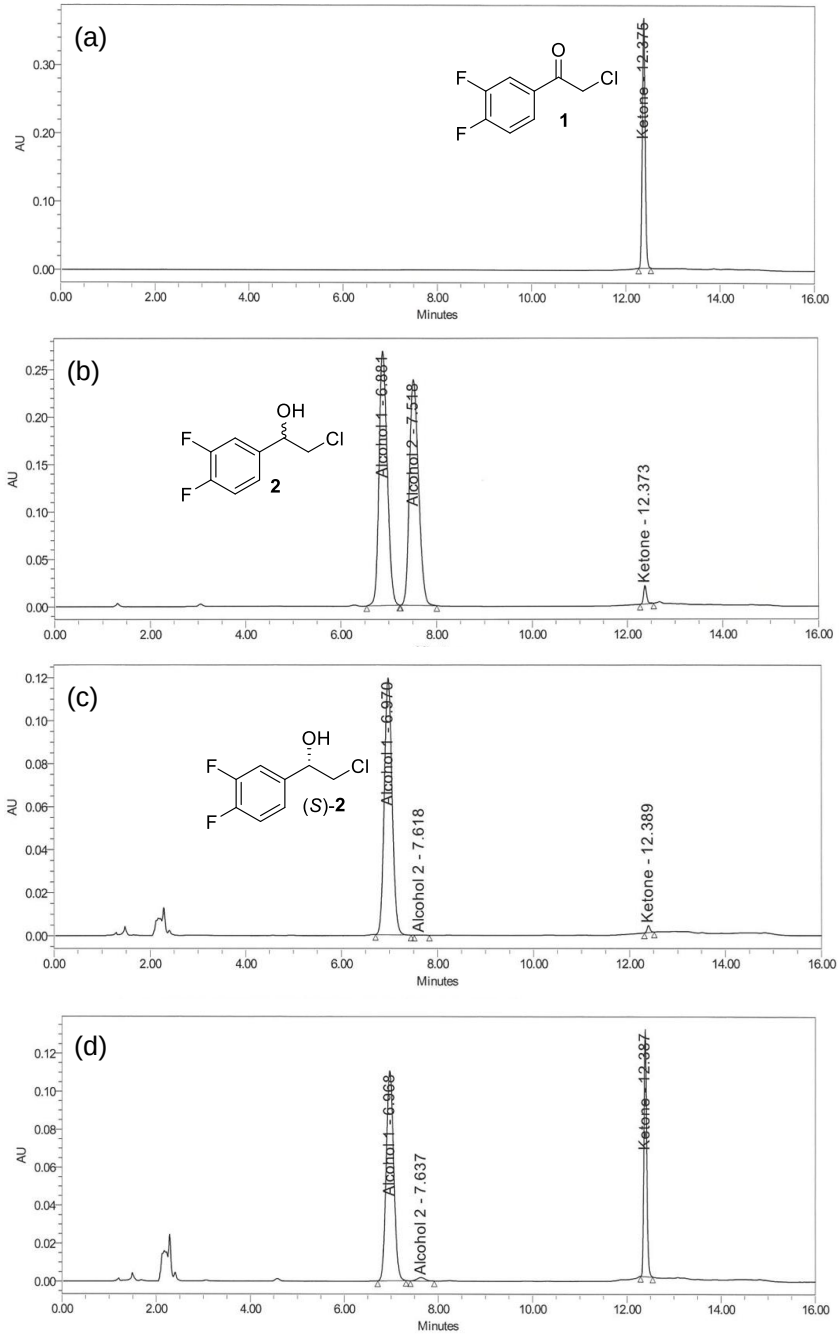
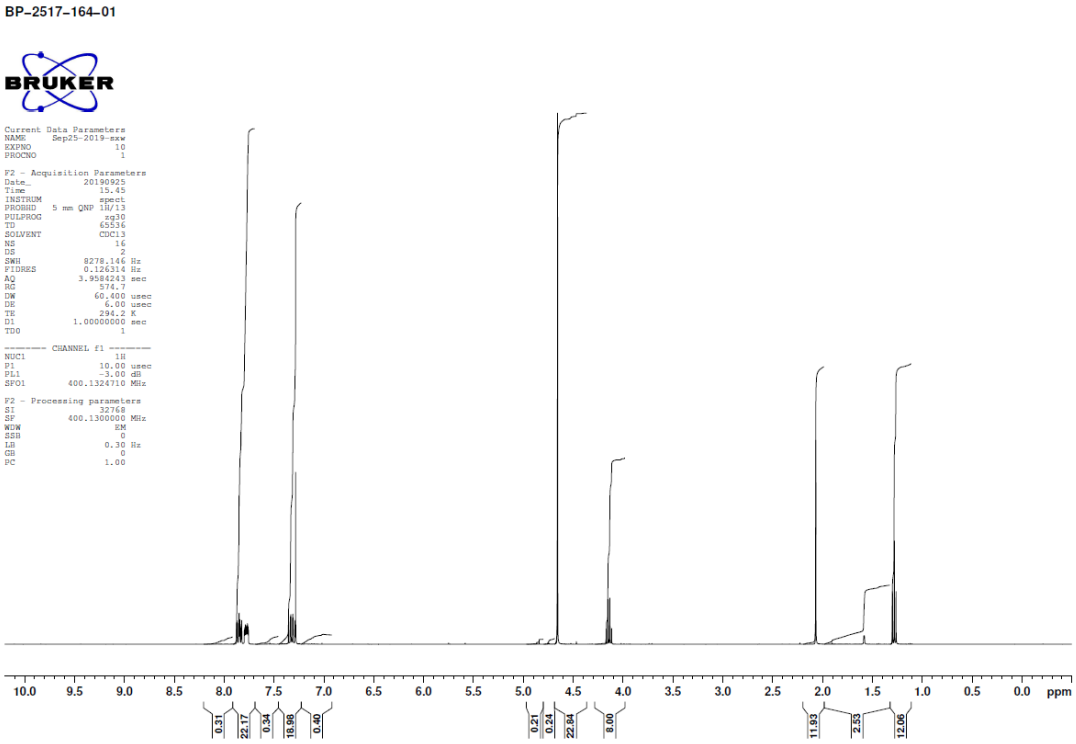


Figure D-1: The HPLC traces for (a) **1** (standard), (b) **2** (standard)**,** (c) (*S*)-**2** (standard) (d) typical final reaction solution sample from Table 4-1 in Section 4.2.3 containing **1** and (*S*)-**2**.

E. Friedel-Crafts preparation of 2-chloro-1-(3,4-difluorophenyl)ethan-1-one in Section 4.2.2

1,2-Difluorobenzene (9.0 g, 79 mmol) was placed under N_2 in a two-necked round bottomed flask (250 mL) for 1 h. Aluminium chloride (9.4 g, 71 mmol) was added over the course of 5 min and the mixture was heated to 55 °C. Choroacetyl chloride (6.25 mL, 78 mmol) was added with a syringe pump over the course of 1 h at 55–61 °C. The reaction was stirred at 55 °C for a further 1 h and then allowed to cool to 35 °C. The reaction mixture was then mixed with iced water (500 mL), in an ice bath (5 °C) and then concentrated HCl (75 mL) was slowly added, followed by ethyl acetate (250 mL). The resulting mixture was stirred for 15 min and the organic layer was removed. The aqueous layer was extracted with ethyl acetate (250 mL). The organic layers were combined, washed with saturated $NaHCO_3$ solution (2 x 250 mL), and dried over $MgSO_4$. The solvent was removed under reduced pressure to yield the crude product as a yellow crystallised solid (10.43 g, 84%).

^{1}H NMR (400 MHz, Chloroform-*d*) δ 7.94 − 7.66 (m, 2H), 7.44 − 7.20 (m, 1H), 4.66 (s, 2H). HPLC: see Figure D1 for comparison of 2-chloro-1-(3,4-difluorophenyl)ethan-1-one (**1**) used as a starting material in a reaction against a standard sample of **1**.



F. Benchtop NMR spectra and calibration curves

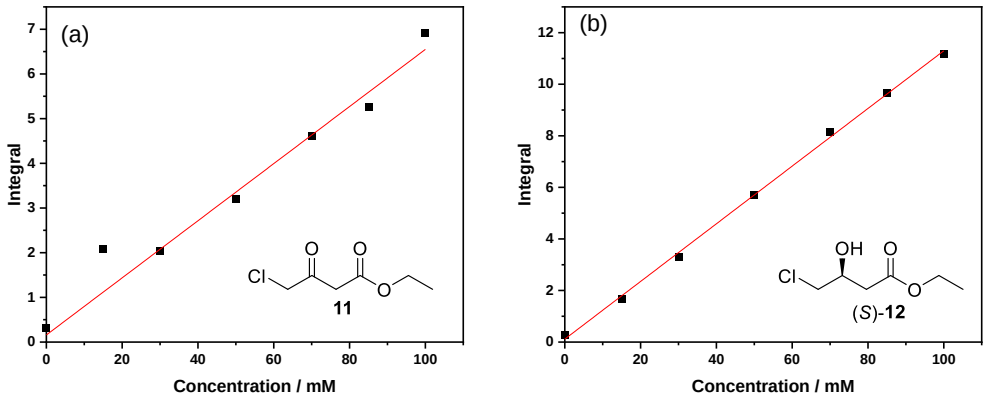


Figure F-1: Benchtop NMR calibration curves for (a) **11** diagnostic signal at 2.92 ppm (b) (*S*)-**12** diagnostic signal at 2.78 ppm. Determined by the preparation of standard NMR samples at concentrations from 0–100 mM.

G. Protein concentration calibration curves

Protein concentration calibration curves were produced for each enzyme used in this chapter according to the procedure outlined in Section 2.2.2. A calibration curve was produced for LDH between the concentration range of 0 to 64 μg mL^{-1}, shown in Figure G-1(a). A calibration curve was produced for FDH between the concentration range of 0 to 1 mg mL^{-1}, shown in Figure G-1(b). A calibration curve was produced for ADH-105 between the concentration range of 0 to 0.45 mg mL^{-1}, shown in Figure G-1(c). A calibration curve was produced for ADH-101 between the concentration range of 0 to 0.85 mg mL^{-1}, shown in Figure G-1(d). A calibration curve was produced for ADH-1001 between the concentration range of 0 to 0.80 mg mL^{-1}, shown in Figure G-1(e). A calibration curve was produced for SH between the concentration range of 0 to 0.38mg mL^{-1}, shown in Figure G-1(f). A calibration curve was produced for Hyd1 between the concentration range of 0 to 0.13mg mL^{-1}, shown in Figure G-1(g). A calibration curve was produced for I64A between the concentration range of 0 to 0.80mg mL^{-1}, shown in Figure G-1(h).

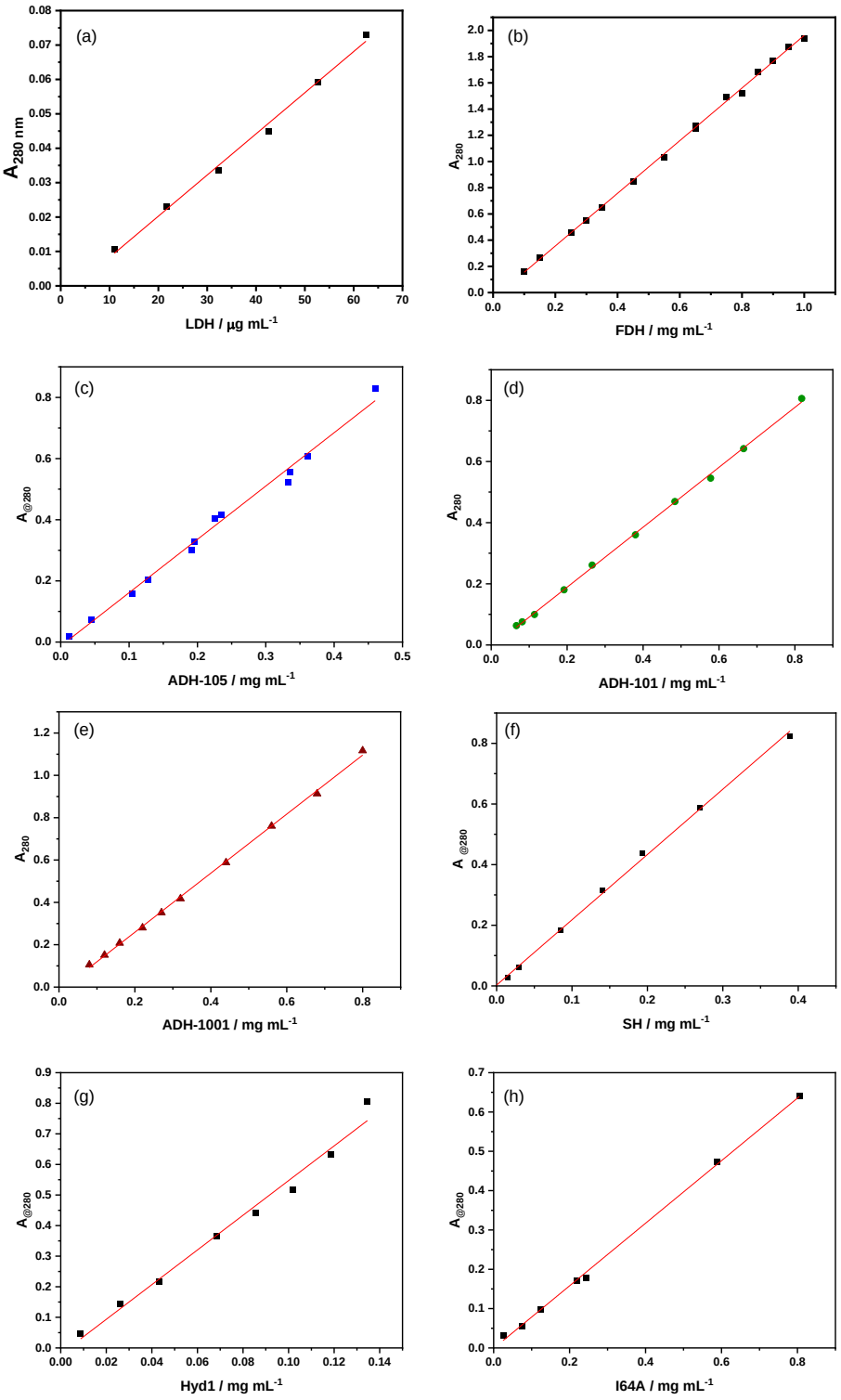


Figure G-1: Protein concentration calibration curves for (a) LDH, (b) FDH, (c) ADH-105, (d) ADH-101, (e) ADH-1001, (f) SH, (g) Hyd1, (h) I64A.